ELECTRON CORRELATION EFFECTS

IN

SOME S AND P STATES

OF

HELIUM AND LITHIUM

Paul Kenneth Youngman

ABSTRACT

In Section (I), the origins and nature of the correlation problem are discussed, and two approaches to its solution are outlined. Some of the methods by which correlation effects in the ground state of helium have been analysed in the past are briefly reviewed.

In Section (II.1), position-space correlation effects in the 2^1S, 2^3S, 2^1P and 2^3P states of helium are studied. The investigation is performed by examining the effects of correlation on various radial, angular and interparticle distribution functions and expectation values; where possible, comparisons are made with the ground state. For each of the four excited states studied, it was found that correlation causes a significant inward movement of electron density from the outer regions of the atom, due to a reduction in nuclear shielding.

In the light of the results obtained in position space, a parallel momentum-space investigation of the 2^3S, 2^1P and 2^3P states was performed, and the results are presented in Section (II.2). Differences between the interparticle correlation properties of the three states were rationalised by considering the varying interactions between the radial and angular components of correlation in each instance. For 2^3S and 2^1P, as for the ground state, radial and angular correlation have opposing effects on the interparticle momentum distributions; for 2^3P, on the other hand, the two effects act together.

In Section (III), a partitioning technique used previously to examine correlation effects in individual electron pairs within many-electron atoms is applied to a momentum-space study of the $(1s^2 2s)^2S$ and $(1s^2 2p)^2P$ states of lithium. For both states, the effects of correlation observed in the K-shell electron pairs show a strong resemblance to those found in Li^+. As for the excited states of helium, the rationalisation of the behaviour of, and differences between, the interparticle correlation properties of the intershell electron pairs was achieved by considering the varying interactions between the radial and angular components of correlation in each instance.

ELECTRON CORRELATION EFFECTS

IN

SOME S AND P STATES

OF

HELIUM AND LITHIUM

by

Paul Kenneth Youngman

A thesis submitted to the

University of Leicester

for the degree of

Doctor of Philosophy

in the

Faculty of Science

1986

UMI Number: U360071

UMI

Dissertation Publishing

ProQuest

TO

My Parents

--for everything

If you cannot - in the long run - tell
everyone what you have been doing, your
doing has been worthless.

E. Schrödinger

ACKNOWLEDGEMENTS

CONTENTS

CONTENTS (continued)

III   MOMENTUM-SPACE CORRELATION EFFECTS IN THE
$2^2 S$ AND $2^2 P$ STATES OF LITHIUM

ELECTRON CORRELATION EFFECTS

IN

SOME S AND P STATES

OF

HELIUM AND LITHIUM

Paul Kenneth Youngman

ABSTRACT

In Section (I), the origins and nature of the correlation problem are discussed, and two approaches to its solution are outlined. Some of the methods by which correlation effects in the ground state of helium have been analysed in the past are briefly reviewed.

In Section (II.1), position-space correlation effects in the 2^1S, 2^3S, 2^1P and 2^3P states of helium are studied. The investigation is performed by examining the effects of correlation on various radial, angular and interparticle distribution functions and expectation values; where possible, comparisons are made with the ground state. For each of the four excited states studied, it was found that correlation causes a significant inward movement of electron density from the outer regions of the atom, due to a reduction in nuclear shielding.

In the light of the results obtained in position space, a parallel <u>momentum-space</u> investigation of the 2^3S, 2^1P and 2^3P states was performed, and the results are presented in Section (II.2). Differences between the interparticle correlation properties of the three states were rationalised by considering the varying interactions between the radial and angular components of correlation in each instance. For 2^3S and 2^1P, as for the ground state, radial and angular correlation have opposing effects on the interparticle momentum distributions; for 2^3P, on the other hand, the two effects act together.

In Section (III), a partitioning technique used previously to examine correlation effects in individual electron pairs within many-electron atoms is applied to a momentum-space study of the $(1s^2 2s)^2S$ and $(1s^2 2p)^2P$ states of lithium. For both states, the effects of correlation observed in the K-shell electron pairs show a strong resemblance to those found in Li^+. As for the excited states of helium, the rationalisation of the behaviour of, and differences between, the interparticle correlation properties of the intershell electron pairs was achieved by considering the varying interactions between the radial and angular components of correlation in each instance.

SECTION (I)

GENERAL INTRODUCTION

CHAPTER (I.1.1)

THE CORRELATION PROBLEM

The predictive and explanative abilities of quantum mechanics are embodied in the mathematics of the Schrödinger[1] equation, which relates the energy of an atomic or molecular system to its wavefunction. For an N-electron atom of atomic number Z, the non-relativistic, fixed-nucleus, time-independent Schrödinger equation has the form

$$[-1/2 \sum_{i=1}^{N} \nabla_i^2 - Z \sum_{i=1}^{N} (1/r_i) + \sum_{i<j}^{N} (1/r_{ij})] \Psi = E \Psi , \qquad (I.1)$$

where Ψ is the system wavefunction, E is the energy, r_i is the radial separation of the i'th electron from the nucleus and r_{ij} is the distance between electrons i and j. (Atomic units are used[1].) Unfortunately, the presence of the term

$$\sum_{i<j}^{N} (1/r_{ij}) ,$$

which describes the Coulombic repulsion between the electrons, means that Equation (I.1) cannot be solved exactly for any system containing more than one electron. Consequently, for neutral atoms a precise analytic solution to the Schrödinger equation can be obtained only for

---

[1]The atomic unit (a.u.) of length is the Bohr radius, 0.52918×10^{-10}m, the atomic unit of momentum is 0.19926×10^{-23}Ns and the atomic unit of energy is 27.210eV. For a more complete discussion see Pilar[2].

hydrogen; for all other atoms, recourse must be made to approximate methods.

One of the earliest attempts to obtain an approximate solution to the Schrödinger equation of a 'many-electron' atom was that by Hartree[3]. In Hartree's method, it is assumed that each electron moves in a central field, which is computed from the nuclear charge and the spherically averaged charge distribution of all the other electrons. Hartree's idea was almost entirely intuitive in its origin; the first steps in fitting it into the broader picture of quantum mechanics were taken approximately simultaneously, but independently, by Gaunt[4] and Slater[5]. These authors were able to show that the equations derived by Hartree are the conditions which optimise an approximate solution to Equation (I.1) having the form

$$\Psi(\underline{x}_1,\underline{x}_2,\underline{x}_3\cdots\underline{x}_N) = \varphi_1(\underline{x}_1)\ \varphi_2(\underline{x}_2)\ \varphi_3(\underline{x}_3)\ \cdot\ \cdot\ \varphi_N(\underline{x}_N)\ , \quad (I.2)$$

where $\underline{x}_i$ represents the space and spin coordinates of the i'th electron, and the one-electron functions φ_i are known as space-spin <u>orbitals</u> -- an expression first used by Mulliken[6].

It is clear that when Ψ is expressed in this way, it neither obeys the Pauli exclusion principle[7], nor takes into account the indistinguishability of the electrons. Both of these defects may be rectified by expressing Ψ in the following form

$$\Psi = (N!)^{-1/2} \begin{vmatrix} \varphi_1(\underline{x}_1) & \varphi_2(\underline{x}_1) & \varphi_3(\underline{x}_1) & \cdot & \cdot & \varphi_N(\underline{x}_1) \\ \varphi_1(\underline{x}_2) & \varphi_2(\underline{x}_2) & \varphi_3(\underline{x}_2) & \cdot & \cdot & \varphi_N(\underline{x}_2) \\ \varphi_1(\underline{x}_3) & \varphi_2(\underline{x}_3) & \varphi_3(\underline{x}_3) & \cdot & \cdot & \varphi_N(\underline{x}_3) \\ \cdot & \cdot & \cdot & & \cdot & \\ \cdot & \cdot & \cdot & & \cdot & \\ \varphi_1(\underline{x}_N) & \varphi_2(\underline{x}_N) & \varphi_3(\underline{x}_N) & \cdot & \cdot & \varphi_N(\underline{x}_N) \end{vmatrix} \qquad (I.3)$$

This form of wavefunction was suggested originally by Heisenberg[8] and Dirac[9], and then applied to the many-electron problem by Slater[10], with the result that Equation (I.3) is usually referred to as a Slater determinant. The optimisation of any approximate wavefunction may be obtained by application of the variation principle[11]. The conditions for optimising a determinantal wavefunction in this way were derived by Slater[12] and independently by Fock[13]. When Ψ is constructed from the resulting N 'best-possible' spin-orbital functions φ_i, it is known as the Hartree-Fock (HF) wavefunction.

One of the principal assumptions of the Hartree-Fock method is that the interelectronic potential energy of an electron, located at some point in space, depends only on the averaged positions of all the other electrons. It is, however, intuitively obvious that two electrons, repelling each other by virtue of the Coulombic forces which exist between them, will be less likely to be found at the same point in space than at points separated from each other. The determinantal form of the HF wavefunction means that the probability of finding two electrons with parallel spins

occupying the _same point_ in space is zero. Since a fundamental requirement of quantum mechanics is that the wavefunction be smooth and continuous, it follows that the wavefunction (and hence the probability density associated with it) will _tend_ to zero as two electrons with parallel spins _approach_ each other in space. As a result, it is said that each electron is surrounded by a 'Fermi hole' -- a region of space in which electrons with parallel spins are less likely to be found than those with antiparallel spins. From this, it is seen that the Hartree-Fock method describes the motions of electrons with _parallel_ spins rather more realistically than it does those of electrons whose spins are opposed. Clearly, any attempt to improve on the accuracy of the Hartree-Fock method must take into account the effects of the "correlation" between the motions of electrons with antiparallel spins.

Some idea of the extent to which the HF wavefunction of an atom is in error may be obtained by calculating the _correlation energy_ of the system. Since the term was first used in 1934 by Wigner[14], a number of different definitions of the correlation energy have been suggested in the literature[15]; today, the most widely used is that of Löwdin[16]:

> "The correlation energy for a certain state with respect to a specified Hamiltonian is the difference between the exact eigenvalue of the Hamiltonian and its expectation value in the Hartree-Fock approximation for the state under consideration."

4

Of course, the exact eigenvalue of the non-relativistic Hamiltonian is not known, and in practice it is necessary to calculate this quantity by making relativistic corrections[17] to experimental data[18]. Hartree-Fock calculations for light atoms indicate that the correlation energy is usually of the order of 1% of the exact value. Initially, therefore, it would appear that there is quite good agreement between the HF and ´exact´ energies of an atom. However, it must be recalled that total energies *per se* are generally of little significance in the problems of physics and chemistry. Instead, the quantity of interest is usually an energy difference -- for example, the energy difference between two spectroscopic states. Unfortunately, these energy differences themselves are often of the order of 1% of the total energy of either state, and small absolute errors in the total energies may easily lead to large relative errors in their differences. As a result, there is considerable interest in quantum-mechanical calculations which yield energies better than those predicted by the Hartree-Fock method.

Not surprisingly, most early attempts to construct correlated wavefunctions concentrated on the ground state of the helium atom, since this system forms a ´bridge´ between the exactly soluble problem of the hydrogen atom, and that of the more complicated many-electron systems. As early as 1929, Hylleraas[19] noted that the wavefunction for the ground state of helium can be regarded as a function of only three variables: r_1, r_2, the distances of the two electrons from the nucleus, and r_{12}, the distance between

the two electrons. It is the dependence on r_{12} which introduces correlation into the description of the system. Hylleraas suggested handling this dependence by a procedure which, in its simplest form, amounts to including in the wavefunction a multiplicative factor, such as $(1 + br_{12})$, which causes the wavefunction to increase with r_{12}. By expanding this 'correlating factor' to a more complicated form, involving powers of r_1, r_2 and r_{12}, Hylleraas was able to secure excellent agreement with the experimentally observed energy of helium.

The central idea of Hylleraas's method is the re-expression of the problem in terms of the elliptic coordinates

$$s = r_1 + r_2$$
$$t = r_2 - r_1$$
$$\text{and} \quad u = r_{12} \quad .$$

In 1958, Pekeris[20] suggested using instead the perimetric coordinates

$$x = (r_2 + r_{12} - r_1) / 2$$
$$y = (r_1 + r_{12} - r_2) / 2$$
$$z = (r_1 + r_2 - r_{12}) / 2 \quad ,$$

and began a series of calculations on helium which have remained virtually unsurpassed in accuracy until the present day. Unfortunately, attempts to extend the methods of Hylleraas and Pekeris to heavier atoms have met with little

success. There are two principal reasons for this. Firstly, the number of terms that must be handled increases rapidly with the number of electrons in the system. Secondly, elliptic and perimetric coordinate systems cannot be set up for three or more electrons[21], and integrals involving powers and functions of r_{12} are much more difficult to evaluate in other coordinate systems. In view of these difficulties, it is fortunate indeed that Hylleraas[22] had earlier suggested another technique by which correlation effects may be included in an atomic wavefunction; this method has come to be known as that of Configuration Interaction (CI).

In the method of Configuration Interaction, the wavefunction is expanded as a linear combination of Slater determinants

$$\Psi = \sum_i c_i \; \phi_i (\underline{x}_1, \underline{x}_2, \underline{x}_3 \cdots \underline{x}_N) \; , \qquad (I.4)$$

where each of the ϕ's (configurations) is an antisymmetrised product of one-electron spin orbitals, and the coefficients c_i are taken as those which minimise the total energy according to the variation principle. The major advantage of this technique is that if the set of configurations is allowed to become infinitely large, the trial wavefunction Ψ will approach the exact wavefunction of the system. In practice, of course, there is a restriction on the number of configurations that can be conveniently handled; the more terms that can be accomodated, the better the calculated energy becomes. The principal disadvantages of the method

are that the energy convergence of a CI expansion is often extremely slow, and it is by no means obvious which configurations will be most effective in lowering the energy. These difficulties, once considered almost insuperable, should now be viewed in the light of the considerable improvements in computer hardware design, computational procedures and theoretical techniques that have occurred over the last three decades. Taking these factors into consideration, it seems that Configuration Interaction is the most likely method by which accurate wavefunctions for small- and medium-size atomic systems may be obtained.

The majority of the early attempts to produce atomic wavefunctions more accurate than the Hartree-Fock function were concerned principally with calculating the best possible value for the _energy_ of the system. Since the energy of an atom could be measured experimentally with great precision, it was possible to tell how good a wavefunction was on an _absolute_ scale by simply comparing the calculated energy with experimental results. Furthermore, the variation principle afforded a method by which the accuracy of any two wavefunctions could be compared on a _relative_ scale by simply determining which function produced the lowest energy. Consequently, the almost exclusive preoccupation with the effects of correlation on the energy seems, at first sight, to be quite reasonable. However, it is clear from Equation (I.1) that the exact energy of an atom is related directly to the interelectronic separation r_{12}, and it seems somewhat

surprising that it was not until 1961 that Coulson and Neilson[23] first computed the electron-electron distribution function $f(r_{12})$ from a quantum-mechanical wavefunction. By analogy with the correlation energy, these authors defined the _Coulomb hole_, $\Delta f(r_{12})$, (_cf_ the Fermi hole, discussed earlier) as the difference between the values of $f(r_{12})$ when evaluated from a correlated wavefunction and the corresponding Hartree-Fock function. This definition provides a simple physical picture of the average extent to which electronic charge is repelled from an electron as a result of its instantaneous (as opposed to averaged) interaction with other electrons. For any given value of r_{12}, $\Delta f(r_{12})$ will be negative if the probability of two electrons being separated by that distance is reduced by the introduction of correlation, and positive if the probability is increased. For the ground state of helium, Coulson and Neilson found that $\Delta f(r_{12})$ is negative for all r_{12} less than 1.1 a.u. and positive for all r_{12} greater than this; they concluded that the radius of the Coulomb hole for this system is 1.1 a.u. Since 1961, at least two other definitions of the Coulomb hole have been proposed. Gilbert[24] has suggested that $\Delta f(r_{12})$ should be weighted by a factor of r_{12}^{-1}, thereby providing a better indication of the relationship between the correlation energy and the size of the Coulomb hole; Tatewaki and Tanaka[25], on the other hand, claim that $\Delta f(r_{12})r_{12}^{-2}$ is a more appropriate quantity for investigation, since the resulting hole shows how the density per unit volume of the interelectronic separation probability decreases following the introduction of correlation. Neither of these two alternative definitions

appears to have found much favour in the literature, possibly due to the fact that both lack some of the conceptual simplicity of the original suggestion.

As early as 1952, Taylor and Parr[26] had shown that correlation effects in an atom may be considered as the sum of _radial_ and _angular_ components. In the radial sense, electrons tend to occupy regions of space which are at different _distances_ from the nucleus, whereas from an angular point of view, the propensity of the electrons is to be on opposite _sides_ of the nucleus. Clearly, by its very nature, the Coulomb hole will be sensitive to both the radial and angular components of correlation contained within a wavefunction. As a result, it became of interest to study the effects of correlation on the radial and angular distributions of the electrons in an atom. In 1969 Baker and Banyard[27] analysed radial effects in the isoelectronic series H^- to O^{6+} by examining the two-particle radial density function and a number of one- and two-particle expectation values at both the correlated and Hartree-Fock levels. More recently, Boyd[28] and Gupta and Boyd[29] have analysed the effects of correlation on the one-electron radial density function for a number of He-like ions. The effects of correlation on the angular distribution of electrons have been studied by Banyard and Ellis[30], and also by Tatum[31]. Banyard and Ellis defined a distribution function for the angle between the electron position vectors, and then studied correlation effects in the ground state of He by evaluating 'angular holes'. Tatum, on the other hand, derived an expression for the

cosine of the interelectronic angle as a function of the radial locations of the two electrons. It should be noted, however, that Tatum's work considered only correlated wavefunctions, without reference to the corresponding Hartree-Fock results. As a consequence, his analysis cannot be said to constitute a correlation study in the same spirit as, for example, Coulson and Neilson's study of the Coulomb hole[23].

Naturally, these studies of the ground state of the helium atom were only able to provide information about the effects of correlation on the interaction of 1s electrons with other 1s electrons. Intuitively, it is to be expected that in a system where the electrons are described at the HF level by orbitals with different principal quantum numbers or different symmetries, the introduction of correlation will produce effects somewhat different from those encountered in $(1s)^2$ systems. Therefore, in an effort to compare helium with a more complicated atom, Banyard and Mashat[32] analysed electron correlation effects in beryllium, using the partitioning technique of Sinanoglu[33] to factorise the problem into a number of two-electron interactions. Their study revealed a number of interesting effects, not the least of which was the inversion of the Coulomb holes for the intershell electron pairs by comparison with the intrashell curves. Recently, Al-Bayati[34] has used a similar approach to analyse correlation effects in the lithium isoelectronic sequence, and has produced results of similar complexity.

Aims of the Present Work

Investigations such as those discussed above indicate that conclusions drawn from a study of correlation effects in the ground state of helium suffer from a lack of generality, and show that there exists an obvious need for further investigation of systems in which electron-electron interactions other than 1s:1s occur. The simplest systems of this type are the excited states of helium, and in Section (II.1) we present a study of correlation effects in the 2^1S, 2^3S, 2^1P and 2^3P states of helium.

During recent years, there has been a growing interest in the study of correlation effects in momentum space, where it has been shown that radial and angular correlation can have opposing effects, with radial correlation reducing the probability of the two electrons having equal values of scalar momenta and angular correlation increasing the angle between the momentum vectors. Accordingly, in Section (II.2) we analyse the effects of correlation on the momentum distributions of three of the states investigated in Section (II.1).

In Section (III) we investigate momentum-space correlation effects in two low-lying states of lithium. This study not only complements the position-space work of Al-Bayati[34] mentioned earlier, but also permits comparison with the momentum-space results for the excited states of He, presented in Section (II.2).

REFERENCES - SECTION (I)

REFERENCES - SECTION (I)

1) a) E. Schrödinger, Ann. der Physik <u>79</u> 361, 489, 734 (1926)

   b) E. Schrödinger, Ann. der Physik <u>81</u> 109 (1926)

   c) E. Schrödinger, Phys. Rev. <u>28</u> 1049 (1926)

2) F.L. Pilar, 'Elementary Quantum Chemistry', McGraw-Hill Book Company : New York (1968)

3) D.R. Hartree, Proc. Camb. Phil. Soc. <u>24</u> 89, 111 (1928)

4) J.A. Gaunt, Proc. Camb. Phil. Soc. <u>24</u> 328 (1928)

5) J.C. Slater, Phys. Rev. <u>32</u> 339 (1928)

6) R.S. Mulliken, Phys. Rev. <u>41</u> 49 (1932)

7) W. Pauli,Jr., Z. Physik <u>43</u> 601 (1927)

8) a) W. Heisenberg, Z. Physik <u>38</u> 411 (1926)

   b) W. Heisenberg, Z. Physik <u>39</u> 499 (1926)

   c) W. Heisenberg, Z. Physik <u>41</u> 239 (1927)

9) P.A.M. Dirac, Proc. Roy. Soc. (London) <u>A112</u> 661 (1926)

10) J.C. Slater, Phys. Rev. <u>34</u> 1293 (1929)

11) C.E. Eckart, Phys. Rev. <u>36</u> 878 (1930)

12) J.C. Slater, Phys. Rev. <u>35</u> 210 (1930)

13) V. Fock, Z. Physik <u>61</u> 126 (1930)

14) E. Wigner, Phys. Rev. <u>46</u> 1002 (1934)

15) a) D. Pines, Solid State Physics <u>1</u> 368 1955

    b) J.C. Slater, Rev. Mod. Phys. <u>25</u> 199 (1953)

16) P.O. Löwdin, Advan. Chem. Phys. <u>2</u> 207 (1959)

17) A. Fröman, Phys. Rev. <u>112</u> 870 (1958)

18) a) A. Fröman, Rev. Mod. Phys. <u>32</u> 317 (1960)

    b) E. Clementi, J. Chem. Phys. <u>38</u> 2248 (1963)

    c) E. Clementi, J. Chem. Phys. <u>39</u> 175 (1963)

    d) E. Clementi, J. Chem. Phys. <u>42</u> 2783 (1965)

19) E. Hylleraas, Z. Physik <u>54</u> 347 (1929)

20) C.L. Pekeris, Phys. Rev. 112 1649 (1958)

21) P. Wang, J. Chem. Phys. 47 2229 (1967)

22) E. Hylleraas, Z. Physik 48 469 (1928)

23) C.A. Coulson and A.H. Neilson, Proc. Phys. Soc. (London) 78 813 (1961)

24) T.L. Gilbert, Rev. Mod. Phys. 35 491 (1963)

25) H. Tatewaki and K. Tanaka, J. Chem. Phys. 60 601 (1974)

26) G.R. Taylor and R.G. Parr, Proc. Natl. Acad. Sci. U.S. 38 154 (1952)

27) K.E. Banyard and C.C. Baker, J. Chem. Phys. 51 2680 (1969)

28) R.J. Boyd, Chem. Phys. Lett. 44 363 (1976)

29) A. Gupta and R.J. Boyd, J. Chem. Phys. 68 1951 (1978)

30) K.E. Banyard and D.J. Ellis, Mol. Phys. 24 1291 (1972)

31) J.P. Tatum, Int. J. Quant. Chem. 10 967 (1976)

32) K.E. Banyard and M.M Mashat, J. Chem. Phys. 67 1405 (1977)

33) O. Sinanoglu, Rev. Mod. Phys. 35 517 (1963)

34) K.H. Al-Bayati, Ph.D. Thesis, 'Electron Correlation in the $(1s^2 2s)^2 S$ and $(1s^2 2p)^2 P$ States of the Lithium Isoelectronic Sequence in Position and Momentum Space', University of Leicester, 1984

SECTION (II)

A STUDY OF ELECTRON CORRELATION EFFECTS IN
SOME EXCITED S AND P STATES OF HELIUM

(II.1) POSITION-SPACE CORRELATION EFFECTS IN THE
2^1S, 2^3S, 2^1P AND 2^3P STATES OF HELIUM

(II.2) MOMENTUM-SPACE CORRELATION EFFECTS IN THE
2^3S, 2^1P AND 2^3P STATES OF HELIUM

(II.1) POSITION-SPACE CORRELATION EFFECTS IN THE 2^1S, 2^3S, 2^1P AND 2^3P STATES OF HELIUM

CHAPTER (II.1.1)

INTRODUCTION

One of the first investigations of the effects of correlation in excited states was that of Brickstock and Pople[1] in 1952. Using methods which had been applied earlier to the ground state of He by Lennard-Jones and Pople[2], they analysed the consequences of introducing correlation into various singlet and triplet P states of He and Be. Although their discussion was largely qualitative, they measured the effects of angular correlation on θ_{12}, the angle subtended at the nucleus by the position vectors of the two electrons. In particular, they calculated numerical values for $\langle(\cos\theta_{12});r_1,r_2\rangle$ and $\langle\cos\theta_{12}\rangle$, where the former quantity is used to denote the average value of $\cos\theta_{12}$ for a given pair of values (r_1,r_2). Unfortunately, Brickstock and Pople used the term 'correlation' in the statistical rather than quantum-mechanical sense, and the conclusions drawn by them must be viewed in the light of such a distinction. In particular, they claimed that for the 2^1P and 2^3P states of He, the average angle between the electron position vectors would, in the absence of correlation, be 90°. For two _statistically_ uncorrelated particles, this would indeed be the case, since all angles between 0° and 180° would be equally likely, yielding 90° as the mean value. For two electrons described by a 2^1P and 2^3P Hartree-Fock function however, such a statement is demonstrably incorrect, despite the fact that the electrons are then described as _quantum-mechanically_ uncorrelated. Such confusion was by no means uncommon, but fortunately, in 1959, the matter was largely

resolved when Löwdin's[3] definition of the correlation energy provided a quantity by analogy with which all other correlation properties could be defined. However, the resolution of this one difficulty did little to overcome the wide-spread pre-occupation with the ground state problem, and interest in excited states virtually ceased for well over a decade.

In 1973, Boyd and Coulson[4] analysed correlation effects in the 2^1S and 2^3S states of He using Coulomb holes, partial Coulomb holes and various expectation values. Of particular interest was their discovery that in these states, the Coulomb hole is more complicated than in the ground state; in addition to the expected reduction in probability of _small_ values of r_{12}, correlation also produces a reduction in probability of _large_ values of this variable, with the result that the expectation values $\langle r_{12}^{-1} \rangle$ and $\langle r_{12} \rangle$ are _both_ reduced. A year later, in response to the obvious need for further investigation, Boyd and Katriel[5] evaluated the Coulomb hole for the 2^3S state of a series of He-like ions. The most striking feature of their results was that the neutral atom was the only system in the series for which the Coulomb hole was found to display a reduction in probability of large r_{12} values. All the other ions possessed curves which resembled the shape previously found for the ground state. In 1977 Moiseyev, Katriel and Boyd[6] examined the corresponding problem in the 2^1S state of the same iso-electronic series. Interestingly, they found that for this state the discontinuity in results between He and Li^+ was much less pronounced than in 2^3S and

16

that although the Coulomb hole for the neutral atom was noticeably different from the curves for the other ions, the changes with increasing atomic charge were more gradual than in the triplet state.

Interest in states with non-zero total angular momentum was even more limited than that in the S states. In 1974, Ellis[7] extended an earlier ground-state analysis[8] to examine the behaviour of the interelectronic angular distribution function $p(\theta_{12})$ for a number of excited states of neutral He. For the 2^3S, 2^1P and 2^3P states he evaluated the 'angular holes' $\Delta p(\theta_{12})$ and found that despite certain differences in characteristics between the Hartree-Fock $p(\theta_{12})$ curves for the P states, the holes for all three excited states were of the same general shape and roughly the same width as that obtained for the ground state. A year later, Moiseyev and Katriel[9] examined the correlation corrections to a number of interparticle expectation values for the same three excited states of the helium iso-electronic series. They confirmed the findings of Boyd and Katriel[5] with regard to the correlation induced changes in $\langle r_{12}^{-1} \rangle$ and $\langle r_{12} \rangle$ for the 2^3S state and also found that for the neutral atom, correlation increases $\langle r_{12}^{-1} \rangle$ in both the P states.

Since the early days of quantum mechanics, it had been argued that the introduction of correlation would cause electrons to avoid each other in a more efficient manner, with a consequent reduction in the interelectronic repulsion and an increase in the average distance $\langle r_{12} \rangle$ between the

electrons; evidence in support of such an argument had been found in studies of the H_2 molecule[10] and the ground state of the He-like ions[11-13]. The results for the excited S and P states, discussed above, demonstrated the inadequacy of such a simple minded approach to the problem and provided much of the motivation for the present study.

In Section (II.1) we present a comprehensive investigation of position-space correlation effects in the 2^1S, 2^3S and 2^1P and 2^3P states of He. Previous studies of these states have tended to concentrate on one aspect or another of the electron distribution, thereby preventing an overall view of the consequences of correlation from being obtained. In an attempt to overcome this, our analysis is performed using a wide variety of one- and two-particle distribution functions and expectation values. In particular, we shall consider the way in which changes in interparticle properties can be rationalised in terms of the combined changes in radial and angular properties. The correlated and Hartree-Fock wavefunctions used in our investigation are described in Chapter (II.1.2).

Atomic units are used throughout this work.[1]

---

[1]See the footnote on page 1, or for a more complete discussion see Pilar[14].

One of the reasons for the apparent lack of interest in excited states is the relative paucity of appropriate wavefunctions by which such systems can be described at either the correlated or Hartree-Fock level. For the present investigation, the number of suitable wavefunctions from which a choice could be made was reduced further by the requirement that the correlated wavefunctions should not contain explicit reference to the interelectronic distance r_{12}. This constraint on the nature of the wavefunction was a result of our intention to extend the analysis of correlation effects by examining the corresponding properties in momentum space.

For the description of the 2^3S, 2^1P and 2^3P states of He at the correlated level we chose the wavefunctions of Tweed[15]. These functions have been used previously by Ellis[7] to study 'angular holes'. The functional form of each configuration $\varphi(\underline{r}_1,\underline{r}_2)$ in the Tweed functions is as follows:

$$\varphi(\underline{r}_1,\underline{r}_2) = \sum_{m_1 m_2} C_{m1\,m2\,M}^{l1\,l2\,L} \{ r_1^m r_2^n e^{-\varepsilon1\,r1} e^{-\varepsilon2\,r2} Y_{l1\,m1}(\theta_1,\varphi_1) Y_{l2\,m2}(\theta_2,\varphi_2)$$

$$+ (-1)^S r_1^n r_2^m e^{-\varepsilon2\,r1} e^{-\varepsilon1\,r2} Y_{l2\,m2}(\theta_1,\varphi_1) Y_{l1\,m1}(\theta_2,\varphi_2) \}, \quad (II.1.1)$$

where the summation is over the allowed values of m_1 and m_2 and the quantum numbers L, M and S refer to the angular momentum, azimuthal angular momentum and the total spin,

respectively. The spin parts of the wavefunction are separable and normalise to unity. The $C_{m1\,m2\,M}^{l1\,l2\,L}$ are Clebsch-Gordan coefficients which weight the orbital products so that their linear combinations are correct eigenfunctions -- for the state in question -- of the angular momentum operators[16]. Thus, the wavefunctions contain configurations formed from the basic angular term supplemented by configurations containing basis terms of a different behaviour but coupled to provide the same angular momentum. The states differing in M are degenerate, so for simplicity the states with M=0 were examined.

For the 2^3S state, we repeated the calculations using the CI wavefunctions of Weiss[17], and selected results are included here for the purposes of comparison. The form of the Weiss function is

$$\phi(\underline{r}_1,\underline{r}_2) = [1s,2s,3s,1s',2s'] + [2p,3p,2p',3p'] +$$
$$[3d,4d,3d']\qquad,$$

$$(II.1.2)$$

where the square bracket notation is shorthand for a linear combination of all possible ^3S combinations of the enclosed orbitals. The form of the configurations used is then

$$(\varphi\chi) = [2D_\lambda]^{-1/2}\ \times$$
$$\sum_\mu \{|\varphi^*_{\lambda\mu}(1)\alpha(1)\chi_{\lambda\mu}(2)\beta(2)| - |\chi^*_{\lambda\mu}(1)\alpha(1)\varphi_{\lambda\mu}(2)\beta(2)|\},$$

$$(II.1.3)$$

where the symmetry species of each orbital is labelled by λ, the degeneracy by D_λ and the subspecies by μ. Summing over

this latter quantity from $-\lambda$ to $+\lambda$ yields the S state required. The basis set of one-electron functions used by Weiss consisted of the normalised Slater type orbitals defined by

$$\phi_{nlm} = (((2\alpha)^{n+1/2})/([(2n)!]^{1/2}))\ r^{n-1}\ e^{-\alpha r}\ Y_{l,m}(\theta,\varphi).$$

$$(II.1.4)$$

Ideally, it would have been desirable to extend the full analysis of correlation effects to the 2^1S state. Unfortunately, no Tweed wavefunction exists for this state, and no other comparable wavefunction was available. For completeness, therefore, we include in Chapter (II.1.4) some of the results obtained by Boyd and Coulson[4] using the explicitly-correlated wavefunction of Perkins[18].

For each of the states examined, the description at Hartree-Fock level was given by the wavefunctions of Davidson[19]. These single-configuration functions have the form

$$\phi(\underline{r}_1,\underline{r}_2) = 2^{-1/2}\ [\varphi_1(\underline{r}_1)\varphi_2(\underline{r}_2) \pm \varphi_2(\underline{r}_1)\varphi_1(\underline{r}_2)],\qquad (II.1.5)$$

where the orbitals φ are constructed from linear combinations of primitive functions. In Equation (II.1.5), the upper sign corresponds to the singlet state and the lower to the triplet state. The normalised spin components have been separated out of the description. The correlated and Hartree-Fock functions are summarised in Table (II.1.1).

In Chapter (II.1.3) we define and discuss the various distribution functions and expectation values which we have used to analyse the effects of correlation.

CHAPTER (II.1.3)

EVALUATION OF CORRELATION PROPERTIES.

The theoretical study of the electron distribution in an atomic or molecular system is greatly facilitated by the use of density functions[20], which reduce significantly the number of variables to be considered. We begin this Chapter by defining the functions from which all one- and two-particle properties can be derived. In the analysis that follows, we shall adopt the convention that unless otherwise stated, integrations are performed over all possible values of the specified variables.

For any N-electron wavefunction $\phi(\underline{x}_1, \underline{x}_2 \ldots \underline{x}_N)$, normalised to unity, we may define the spinless one-particle probability density function $\varrho_i(\underline{r}_i)$ as

$$\varrho_i(\underline{r}_i) = \int \phi^*(\underline{x}_1, \underline{x}_2 \ldots \underline{x}_N) \, \phi(\underline{x}_1, \underline{x}_2 \ldots \underline{x}_N) \times$$

$$d\underline{r}_1 d\underline{r}_2 \ldots d\underline{r}_{i-1} \, d\underline{r}_{i+1} \ldots d\underline{r}_N \, d\underline{s}_1 \, d\underline{s}_2 \ldots d\underline{s}_i \ldots d\underline{s}_N , \qquad (II.1.6)$$

where $\underline{x}_i$ denotes the usual space $(\underline{r}_i)$ and spin $(\underline{s}_i)$ variables collectively. $\varrho_i(\underline{r}_i)$ is then the probability density of finding the i'th electron at position $\underline{r}_i$, irrespective of its spin. When defined by Equation (II.1.6), $\varrho_i(\underline{r}_i)$ is clearly normalised to unity.

In an entirely analogous fashion, we can define the spinless two-particle probability density $\varrho_{ij}(\underline{r}_i, \underline{r}_j)$ by

$$\varrho_{ij}(\underline{r}_i, \underline{r}_j) = \int \phi^*(\underline{x}_1, \underline{x}_2 \cdots \underline{x}_N) \; \phi(\underline{x}_1, \underline{x}_2 \cdots \underline{x}_N) \times$$

$$d\underline{r}_1 d\underline{r}_2 \cdots d\underline{r}_{i-1} d\underline{r}_{i+1} \cdots d\underline{r}_{j-1} d\underline{r}_{j+1} \cdots d\underline{r}_N \; d\underline{s}_1 d\underline{s}_2 \cdots d\underline{s}_i \cdots d\underline{s}_j \cdots d\underline{s}_N .$$

$$(II.1.7)$$

$\varrho_{ij}(\underline{r}_i, \underline{r}_j)$ is then the probability density of finding, simultaneously, electrons i and j at positions $\underline{r}_i$ and $\underline{r}_j$, irrespective of their spins. Once again, $\varrho_{ij}(\underline{r}_i, \underline{r}_j)$ is normalised to unity. Since the quantities defined in Equations (II.1.6) and (II.1.7) refer to the specific electrons i and j, we may use the fact that $\phi^*\phi$ is completely symmetric in the variables of the N electrons and so define two related __electron__ densities by

$$\varrho(\underline{r}) = N\varrho_i(\underline{r}_i) \qquad\qquad (II.1.8)$$

and $\quad \pi(\underline{r},\underline{r}') = N(N-1)\varrho_{ij}(\underline{r}_i,\underline{r}_j) \qquad (II.1.9)$

where $\varrho(\underline{r})$ is the probability density of finding __any__ electron at position $\underline{r}$ and $\pi(\underline{r},\underline{r}')$ is the probability density of finding simultaneously __any two__ electrons at position $\underline{r}$ and $\underline{r}'$. We note that $\varrho(\underline{r})$ is normalised to the total number of electron pairs. The factor N(N-1) in Equation (II.1.9), represents the total number of pairs, whereas the number of distinct pairs is N(N-1)/2.

The effects of correlation on the probability densities defined above can be analysed by examining various inter-particle, radial and angular properties derived from them. We shall now define each of the properties used in the

present study. The results of our investigations are discussed in Chapter (II.1.4).

Interparticle Properties

A quantity which is particularly sensitive to the effects of correlation is the electron-electron distribution function, $f(r_{12})$. Physically, $f(r_{12})dr_{12}$ is interpreted as the probability that the distance separating two electrons lies between r_{12} and $r_{12} + dr_{12}$. The function was initially used by Coulson and Neilson[11] in their study of correlation effects in the ground state of helium. For this spherically symmetric system it was shown that since $\phi^*\phi$ is effectively a function of r_1, r_2 and r_{12} only, $f(r_{12})$ has a particularly simple form, expressed by

$$f(r_{12}) = 8\pi^2 r_{12} \int \phi^2 (r_1, r_2) \, r_1 r_2 \, dr_1 dr_2 . \qquad (II.1.10)$$

In Equation (II.1.10), r_1 and r_2 are allowed all values compatible with a given value of r_{12}, and the factor $8\pi^2$ occurs as a result of integrating over the angular variables. Many systems, of course, are not spherically symmetric, in which case Equation (II.1.10) no longer applies. For this reason, the original definition by Coulson and Neilson has since been generalised[21] to yield an expression for $f(r_{12})$ for any N-electron system in terms of the appropriate two-particle density function, thus:-

$$f(r_{12}) = \int \varrho_{12}(\underline{r}_1, \underline{r}_2) \, d\underline{r}_1 . d\underline{r}_2 / dr_{12} . \qquad (II.1.11)$$

We have assessed the effects of correlation on $f(r_{12})$ by

evaluating the Coulomb hole, $\Delta f(r_{12})$, defined by

$$\Delta f(r_{12}) = f^{corr}(r_{12}) - f^{HF}(r_{12}). \qquad (II.1.12)$$

In Equation (II.1.12), f^{corr} is the electron-electron distribution function calculated from Equation (II.1.11) using a correlated wavefunction and f^{HF} is the same quantity evaluated at the Hartree-Fock level.

In his study of the generalised definition of $f(r_{12})$, Benesch[21] observed that in those cases where the wavefunction is expressed as a linear sum of one or more Slater-type determinants, the derivation of $f(r_{12})$ is reduced to the problem of solving a number of integrals of the general form [1]

$$I = \int u_1(r_1)\, u_2(r_1)\, u_3(r_2)\, u_4(r_2) \quad \times$$

$$Y_{l_1 m_1}^{*}(\theta_1, \varphi_1)\, Y_{l_2 m_2}(\theta_2, \varphi_2) \quad \times$$

$$Y_{l_3 m_3}^{*}(\theta_2, \varphi_2)\, Y_{l_4 m_4}(\theta_1, \varphi_1)\, d\underline{r}_1 \cdot d\underline{r}_2\, /dr_{12} \quad , (II.1.13)$$

where the subscripts on the $u(r)$ terms signify the collection of appropriate quantum numbers. Throughout this work, angular integrals such as those occurring in Equation (II.1.13) were evaluated analytically using expressions derived by Calais and Löwdin[22]. (Details of the solution of these integrals have since been recorded

---

[1]There is an obvious misprint in Equation (22) of Reference [21].

elsewhere - see Reed[23]). The calculations of the radial integrals, on the other hand, were performed numerically by computer, using the NAG[24] library of algorithms. The NAG library is a set of independent sub-programs, stored in compiled form, which can be called upon to perform various numerical tasks such as integration, differentiation, interpolation etc. The double integrals over the radial variables necessitate the use of some form of quadrature for their evaluation, and the NAG routine which was used for this purpose is based on a technique described by Patterson[25]. Essentially, the method improves the economy of a Gaussian formula by augmenting it with a set of points in such a way that the accuracy of a numerical integration can be considerably improved without wasting integrand evaluations at the Gaussian abscissae.

The magnitude of a Coulomb hole can be expressed in terms of the percentage Y of the $f^{HF}(r_{12})$ distribution function which is redistributed as a result of the introduction of correlation; we have evaluated Y for each of the Coulomb holes presented here.

From the theory of probability and statistics it is well known that distribution functions can be characterised by a number of moments[26] derived from them. For a general distribution function of a single variable, these moments are defined by

$$\langle x^n \rangle = \int f(x) \, x^n dx \qquad \text{(II.1.14)}$$

where different regions of $f(x)$ are emphasised by the function x^n for each value of n. The moment $\langle x^1 \rangle$ is known as the mean or expectation of x, and in quantum mechanics this latter name has been generalised so that all moments are referred to as <u>expectation values.</u> We have gained insight into the nature of the various $f(r_{12})$ curves by calculating from each the expectation values

$$\langle r_{12}^n \rangle = \int f(r_{12}) \; r_{12}^n \; dr_{12} \qquad\qquad (II.1.15)$$

for n = -1, 0, +1 and +2. The expectation value $\langle r_{12}^0 \rangle$ is simply the normalisation of $f(r_{12})$, which, from the definition of $\varrho_{12}(\underline{r}_1, \underline{r}_2)$, is unity. This observation therefore offers a useful, but by no means conclusive, check on the calculated distributions. The value $\langle r_{12}^{-1} \rangle$ is of additional importance since it gives directly the electron-electron repulsion energy. The discrepancy which exists at the Hartree-Fock level in this energy term accounts for a large fraction of the correlation energy and so $\langle r_{12}^{-1} \rangle$ is expected to be particularly sensitive to correlation[27].

A useful concept for quantifying the spread of the general function $f(x)$ is the standard deviation[26], defined by

$$\sigma(x) = \sqrt{[\langle x^2 \rangle - \langle x \rangle^2]} \qquad , \qquad\qquad (II.1.16)$$

and we have evaluated $\sigma(r_{12})$ for each $f(r_{12})$ function. It is interesting to note that the use of the standard deviation applied to electron densities dates back to the

1940's, when statistical theory was applied to the results of X-ray crystallography experiments in an attempt to assess their accuracy[28].

The distribution function $f(r_{12})$ is, of course, obtained by averaging over all positions of the electrons. To investigate the nature of the interelectronic distribution when one electron (the _test_ electron) is at a specified distance r_1 from the nucleus, one can define a new distribution function, $g(r_{12}, r_1)$. The original definition of this function by Boyd and Coulson[4] was applicable only to the S-states of He, so, by analogy with Equation (II.1.11), we have generalised the definition to be

$$g(r_{12}, r_1) = \int \rho_{12}(\underline{r}_1, \underline{r}_2) \; d\underline{r}_1 . d\underline{r}_2 / dr_{12} dr_1 . \qquad \text{(II.1.17)}$$

From Equation (II.1.17) it is seen that

$$\int g(r_{12}, r_1) dr_1 = f(r_{12}) \qquad \text{(II.1.18)}$$

which again offers a useful check on the calculated distributions. The existence of $g(r_{12}, r_1)$ leads naturally to the concept of the _partial_ Coulomb hole, and we have evaluated

$$\Delta g(r_{12}, r_1) = g^{corr}(r_{12}, r_1) - g^{HF}(r_{12}, r_1) . \qquad \text{(II.1.19)}$$

In the past, the visual representation of functions of two variables has been limited either to the use of contour diagrams or to the depiction of sections through the surface

29

defined by the function at fixed values of one or other of the variables. Recently, however, advances in computer graphics software have led to the possibility of producing computer-drawn isometric projections of three-dimensional objects such as these surfaces. The routines used for the preparation of the surface diagrams presented in this work are part of the GHOST[29] graphical package. Like the NAG[24] library, GHOST is a collection of pre-compiled programs which can be called from other programs to perform various specialised tasks -- in this case, all related to graph-plotting. Essentially, to draw the surface defined by $f(x,y)$, one evaluates $f(x,y)$ at regular intervals in the x and y directions, and stores the results in a data file. This file is then used as the input data for a plotting program which calls various GHOST routines. For most of the surfaces presented here, this was a relatively straight-forward procedure. For the 2^1S state, however, the partial Coulomb hole was constructed using the $g^{corr}(r_{12},r_1)$ values provided by Boyd[30]. This data was not available on a regular grid of r_{12} and r_1 values and considerable numerical manipulation was required to obtain an accurate representation of the 2^1S $\Delta g(r_{12},r_1)$ surface. The function g^{HF} was evaluated at all the required grid coordinates (r_{12},r_1) and if the corresponding g^{corr} value was also available, the appropriate value of $\Delta g(r_{12},r_1)$ was calculated. Interpolation routines from both the NAG and GHOST libraries were then used to evaluate $\Delta g(r_{12},r_1)$ at all those coordinates where g^{corr} data was not available. The resulting grid of values was then plotted in the normal way.

For those systems which possess an axis of symmetry, such as the 2^1P and 2^3P states of helium, the position of the test electron can be described in more detail than given by Equation (II.1.17). Specifically, we can define a distribution function

$$g(r_{12},r_1;\theta_1) = \int \varrho_{12}(\underline{r}_1,\underline{r}_2)\ d\underline{r}_1 \cdot d\underline{r}_2/dr_{12}dr_1\ \sin\theta_1 d\theta_1,$$

$$(II.1.20)$$

where θ_1 is the angle between the position vector of the test electron and the symmetry axis. Within this definition it is seen that

$$\int\int g(r_{12},r_1;\theta_1)\sin\theta_1 d\theta_1 dr_1 = \int g(r_{12},r_1)dr_1 = f(r_{12}),\quad(II.1.21)$$

once again allowing the calculated densities to be verified against each other. To investigate how the effects of correlation change as the angular orientation of the test electron changes we have, where appropriate, evaluated the partial Coulomb hole defined by

$$\Delta g(r_{12},r_1;\theta_1) = g^{corr}(r_{12},r_1;\theta_1) - g^{HF}(r_{12},r_1;\theta_1)\quad(II.1.22)$$

for the values $\theta_1 = 0°$, $30°$, $60°$ and $90°$.

Radial Properties

To investigate the radial distribution of electrons, irrespective of their angular orientation, it is necessary to eliminate from the two-particle probability density all reference to the angular variables. From Equation (II.1.7)

one can define the joint radial probability density $D_{ij}(r_i, r_j)$ by

$$D_{ij}(r_i, r_j) = \int \varrho_{ij}(\underline{r}_i, \underline{r}_j) \, r_i^2 r_j^2 \, d\Omega_i d\Omega_j \quad , \qquad (II.1.23)$$

where Ω_i and Ω_j refer to the collective angular variables of electrons i and j respectively. Within this definition, $D_{ij}(r_i, r_j)$ is normalised so that

$$\int D_{ij}(r_i, r_j) \, dr_i dr_j = 1 \quad . \qquad (II.1.24)$$

In order to gain insight into the effects of correlation on $D_{ij}(r_i, r_j)$ we have, where possible, calculated the two-particle 'radial hole' $\Delta D_{12}(r_1, r_2)$ defined by

$$\Delta D_{12}(r_1, r_2) = D_{12}^{corr}(r_1, r_2) - D_{12}^{HF}(r_1, r_2) \quad , \qquad (II.1.25)$$

where $D_{12}(r_1, r_2)$ is derived at the correlated and Hartree-Fock levels, respectively. We have also analysed the concomitant changes which occur in the related expectation values

$$\langle r_1^n r_2^n \rangle = \int D_{12}(r_1, r_2) \, r_1^n r_2^n dr_1 dr_2 \qquad (II.1.26)$$

for n = -2, -1, +1 and +2. By analogy with the $\langle r_{12}^n \rangle$ values discussed earlier, these expectation values allow us to compare the correlated and uncorrelated two-particle distribution functions in different regions of (r_1, r_2) space.

The radial behaviour of <u>one</u> electron, irrespective of the position of the other, is described by the one-electron radial probability density $D_i(r_i)$ and the associated expectation values $\langle r_i^n \rangle$ defined by

$$D_i(r_i) = \int \varrho_i(r_i) r_i^2 d\Omega_i \qquad \qquad (II.1.27)$$

$$\text{and} \quad \langle r_i^n \rangle = \int D_i(r_i) r_i^n dr_i \quad , \qquad \qquad (II.1.28)$$

respectively. From these definitions it can be seen that

$$\iint D_{ij}(r_i, r_j) \, dr_j \, dr_i = \int D_i(r_i) dr_i = 1 \; . \qquad (II.1.29)$$

To investigate the effects of correlation on the one-particle radial density we have used Equation (II.1.27) to evaluate $D_1(r_1)$ at both the correlated and Hartree-Fock levels, thereby producing the one-particle 'radial hole',

$$\Delta D_1(r_1) = D_1^{corr}(r_1) - D_1^{HF}(r_1) \; . \qquad (II.1.30)$$

We have also calculated the expectation values $\langle r_i^n \rangle$ for $n = -2, -1, +1$ and $+2$. The expectation values for <u>both</u> electrons may be obtained by using Equation (II.1.8):

$$\langle r^n \rangle = \int D_1(r_1) r_1^n dr_1 + \int D_2(r_2) r_2^n dr_2 = \langle r_1^n \rangle + \langle r_2^n \rangle$$

$$= 2 \int D_i(r_i) r_i^n dr_i = 2 \langle r_i^n \rangle \; . \qquad (II.1.31)$$

A number of the expectation values defined by Equation (II.1.31) are of some practical interest. In

33

addition to being directly related to the electron-nuclear potential energy of the system, $\langle r^{-1} \rangle$ occurs in the definition of the nuclear diamagnetic shielding factor[31]. This quantity is a measure of the extent to which the effective magnetic field acting on a nucleus differs from some externally applied field (the change is due to the shielding effect induced by the Larmor precession[32] of the electron). Similarly, the magnetic moment induced within a system by an external magnetic field is related to the intensity of the field by the diamagnetic susceptibility[33], which is a function of $\langle r^2 \rangle$. We have already pointed out the usefulness of the standard deviation (defined in Equation (II.1.16)) in assessing the diffuseness of a distribution about its mean. Accordingly, we have evaluated $\sigma(r_1)$ at both levels of approximation to enable us to examine the effects of correlation on the shape of the radial distribution function, $D_1(r_1)$.

Angular Properties

The effects of correlation on the angular distribution of the electrons have been investigated by calculating the expectation values

$$\langle \underline{r}_1 \cdot \underline{r}_2 / r_1^n r_2^n \rangle = \int \varrho_{12}(\underline{r}_1, \underline{r}_2)(\underline{r}_1 \cdot \underline{r}_2 / r_1^n r_2^n) \, d\underline{r}_1 \, d\underline{r}_2$$

$$(II.1.32)$$

for n=0, +1 and +2 at the correlated and Hartree-Fock levels. Each of the quantities evaluated using Equation (II.1.32) involves the term $\cos\theta_{12}$. Since

$$\cos\theta_{12} = (4\pi/3) \sum_m Y_{1m}(\theta_1,\varphi_1) \, Y^*_{1m}(\theta_2,\varphi_2) \qquad (II.1.33)$$

the angular integrals occurring in Equation (II.1.32) all have the general form

$$J = \int Y_{l_1 m_1}(\theta,\varphi) \, Y_{l_2 m_2}(\theta,\varphi) \, Y^*_{l_3 m_3}(\theta,\varphi) \sin\theta \, d\theta \, d\varphi \qquad (II.1.34)$$

and from Rose[16], J is found to have the solution

$$J = [(2l_1+1)(2l_2+1) \, / \, 4\pi(2l_3+1)]^{1/2} \, C^{l_1 \, l_2 \, l_3}_{m_1 \, m_2 \, m_3} \, C^{l_1 \, l_2 \, l_3}_{0 \ \ 0 \ \ 0},$$
$$(II.1.35)$$

where the C's are the usual Clebsch-Gordan coefficients. We note that, according to the cosine rule,

$$\langle r^2_{12} \rangle = \langle r^2_1 \rangle + \langle r^2_2 \rangle - 2\langle \underline{r}_1 \cdot \underline{r}_2 \rangle \, . \qquad (II.1.36)$$

The use of Equations (II.1.36), (II.1.15), (II.1.28) and (II.1.32) therefore provides an extremely valuable check on the consistency of the results obtained for each quantity. For n=1, Equation (II.1.32) yields the expectation value $\langle \cos\theta_{12} \rangle$, which is the average of the cosine of the angle between the position vectors of the electrons. The expectation value $\langle \underline{r}_1 \cdot \underline{r}_2 \rangle$, obtained from Equation (II.1.32) with n=0, is of some practical importance since it occurs in the definition of the atomic dipole polarisability[34]. This quantity relates the dipole moment induced in an atom to the magnitude of an externally applied field.

Presentation of Results

In Figure (II.1.1) we present the uncorrelated interparticle distribution functions $f^{HF}(r_{12})$ for the 2^1S, 2^3S, 2^1P and 2^3P states of helium. The effects of correlation on these distributions are seen in the corresponding Coulomb holes, $\Delta f(r_{12})$, shown in Figure (II.1.2). The Hartree-Fock and correlated expectation values $\langle r_{12}^n \rangle$ are shown in Table (II.1.2); also given in this table is the standard deviation, $\sigma(r_{12})$, of each of the $f(r_{12})$ distributions, as well as the value of Y for each Coulomb hole. In Figure (II.1.3) we present the uncorrelated distributions $g^{HF}(r_{12}, r_1)$ as surfaces. As an aid to the understanding of the structure of these surfaces, we show in Figure (II.1.4) a single-contour representation of the $g^{HF}(r_{12}, r_1)$ distribution for the 2^1S state. In Figure (II.1.5) we present for each state the partial Coulomb hole $\Delta g(r_{12}, r_1)$, again in the form of a surface; alternative views of these surfaces are shown in Figure (II.1.6). For the 2^1S state, $\Delta g(r_{12}, r_1)$ was calculated using results derived from the correlated wavefunction of Perkins[18]; for the other three states, the partial Coulomb hole was derived from the energetically better Tweed[15] function in each instance. Figure (II.1.7) shows the uncorrelated distributions $g^{HF}(r_{12}, r_1; \theta_1)$ for the two P states; surfaces for $\theta_1 = 0°$, $30°$, $60°$ and $90°$ are presented. The corresponding partial Coulomb holes, $\Delta g(r_{12}, r_1; \theta_1)$, for the energetically better Tweed functions are shown in Figure (II.1.8).

In Figure (II.1.9) we show the uncorrelated one-particle radial distribution, $D_1^{HF}(r_1)$, for the 2^1S, 2^3S, 2^1P and 2^3P

states.   The corresponding radial holes, $\Delta D_1(r_1)$, are seen in Figure (II.1.10). The hole for 2^1S was calculated using results derived from the correlated wavefunction of Perkins; the $\Delta D_1(r_1)$ curves for the other states are for the energetically better Tweed function in each instance. The Hartree-Fock and correlated one-particle radial expectation values, $\langle r_1^n \rangle$, are presented in Table (II.1.3); also given in this table is the standard deviation, $\sigma(r_1)$, of each of the $D_1(r_1)$ distributions.   In Figure (II.1.11) we present the uncorrelated two-particle radial distribution functions, $D_{12}^{HF}(r_1, r_2)$,   for   the 2^3S, 2^1P and 2^3P states.   The corresponding two-particle radial holes, $\Delta D_{12}(r_1, r_2)$, for the energetically better Tweed wavefunctions are seen in Figure (II.1.12).   The two-particle radial expectation values, $\langle r_1^n r_2^n \rangle$, are given in Table (II.1.4).

Finally,   in Table (II.1.5) we present the angular expectation values $\langle \underline{r}_1 \cdot \underline{r}_2 / r_1^n r_2^n \rangle$ for $n=0$, 1 and 2 for each state.

CHAPTER (II.1.4)

DISCUSSION

Comparisons between Figure (II.1.2) and the results of Coulson and Neilson[11] reveal that the Coulomb holes for the (1s,nl) excited states studied here are more complicated than that for the ground state. We begin by examining the excited S states.

In order to discuss the effects of correlation, it will be useful to consider first the distribution of electrons as described by the Hartree-Fock (HF) wavefunctions. In this way, we may construct a theoretical 'model' of each system at the uncorrelated level, and then analyse the changes which occur in that model as a result of introducing correlation into the description. As we might anticipate, the $D_1^{HF}(r_1)$ curves shown in Figure (II.1.9a) both possess two maxima, corresponding to the most probable radial locations of the two electrons. The sharp peak at small r_1 corresponds to the tightly-bound core electron, while the second, relatively diffuse, peak at larger r_1 is attributable to the outer electron. For the purposes of discussion, we shall refer to the values of r_1 at which these two maxima in $D_1^{HF}(r_1)$ occur as r_K and r_L; electrons at radial locations close to these values will be described as being in the K and L shells respectively.

We consider next the $g^{HF}(r_{12},r_1)$ surfaces, presented in Figure (II.1.3a,b). We shall analyse the 2^1S surface in some detail and make comments on the 2^3S surface only when

38

it differs substantially from that for the singlet state. To aid our discussion, it will be useful to refer to Figure (II.1.4), which illustrates, by the use of a single contour, the relative locations of the principal features of the $g^{HF}(r_{12}, r_1)$ surface for 2^1S. It is seen that there are three main regions of probability density:

Region (A) - in the small (r_{12}, r_1) region,

Region (B) - at small r_1, parallel to the r_{12} axis

and Region (C) - along the $(r_{12}=r_1)$ diagonal axis.

We now discuss the significance of each of these features in turn.

Consider a test electron located somewhere in the K-shell region, such that $r_1 \approx r_K$. The changes in the shape of $g^{HF}(r_{12}, r_1)$ with changing r_{12} should then illustrate the behaviour of the second electron. As we increase r_{12} from zero, keeping r_1 constant, we encounter Region (A) at small values of r_{12}. This region of probability density results from the situation in which the radial location of the second electron is <u>also</u> close to r_K, and hence corresponds to a double occupancy of the K-shell region. Now, at the HF level, the most probable angle between the position vectors of the two electrons is 90°, and hence the maximum in Region (A) occurs when $r_1 = r_K$ and $r_{12} = \sqrt{(2r_K^2)}$. This corresponds to the two electrons both being at a distance r_K from the nucleus, with their position vectors orthogonal to each other.

As r_{12} is increased further, we encounter Region (B), which arises from the more probable situation of the second

electron being located somewhere in the L-shell region. That Region (B) is so extensive in the r_{12} - direction merely reflects the diffuse nature of the L shell, which, with the test electron confined to the K shell, gives rise to a large spread of probable r_{12} values. (By a similar argument, the relatively small spread of Regions (A) and (B) in the r_1 direction indicates the localised nature of the K shell and hence the restricted range of probable locations for a test electron at small r_1). The maximum in Region (B) occurs when $r_1 = r_K$ and $r_{12} = \surd(r_K^2 + r_L^2)$, corresponding to electrons at distances r_K and r_L from the nucleus, with their position vectors again orthogonal to each other.

To understand the origin of Region (C), we must consider a test electron somewhere in the L-shell. The change in shape of $g^{HF}(r_{12}, r_1)$ with increasing r_{12} is then determined by the behaviour of the tightly bound K-shell electron, which explains the relatively small spread of probable r_{12} values for any given r_1. The maximum in Region (C) appears to be located on the $(r_{12} = r_1)$ diagonal axis, but in fact occurs when $r_1 = r_L$ and $r_{12} = \surd(r_K^2 + r_L^2)$. The data grid from which the $g^{HF}(r_{12}, r_1)$ surface is plotted is not sufficiently detailed to allow such a distinction to be made visually. Clearly, the maxima in Regions (B) and (C) both correspond to the same relative orientation of the two electrons, but seen from different 'viewpoints'.

Inspection of the $g^{HF}(r_{12}, r_1)$ surface for 2^3S reveals that it is broadly similar to that for 2^1S except that the structure seen at small (r_{12}, r_1) in the singlet state is

absent from the triplet. This is a result of the Fermi effect in 2^3S restricting the two electrons from approaching each other too closely, thereby preventing the double occupancy of the K shell.

As we have seen in Chapter (II.1.3), the $f^{HF}(r_{12})$ curves in Figure (II.1.1) are obtained by integrating the corresponding $g^{HF}(r_{12},r_1)$ functions with respect to r_1. For both S states, $f^{HF}(r_{12})$ is seen to possess a maximum located at a value of $r_{12} = \sqrt{(r_K^2 + r_L^2)}$. The difference in the location of this maximum between the two states is due to the different radial locations of the L shell in each system, since r_K is effectively the same in 2^1S and 2^3S. In keeping with our earlier comments regarding the $g^{HF}(r_{12},r_1)$ surface for 2^1S, the $f^{HF}(r_{12})$ curve for the singlet state displays a local maximum at $r_{12} = \sqrt{(2r^2_K)}$. This feature is absent from the 2^3S curve.

Having thus established the nature of the uncorrelated electron distributions for the S states, we now examine the effects of correlation in 2^1S and 2^3S, and begin by considering in more detail the Coulomb holes presented in Figure (II.1.2a). The balance between the positive and negative contributions in each $\Delta f(r_{12})$ curve is, of course, a consequence of the normalisation conditions on f^{corr} and f^{HF}, but the magnitude and, in particular, the location of each extremum in a Coulomb hole can be rationalised in terms of changes which occur in the HF 'model' discussed above.

Inspection of the Boyd and Coulson[4] Coulomb hole for

2^1S reveals that at large values of r_{12}, correlation causes a significant reduction in $f(r_{12})$, while at intermediate r_{12} there is an enhancement of probability of roughly the same magnitude. At **small** r_{12} (that is, $0 < r_{12} < 2$), $\Delta f(r_{12})$ possesses a shape similar to that of the Coulomb hole in the ground state. The first zero in $\Delta f(r_{12})$ is almost coincident with the value of r_{12} which locates the first maximum in $f^{HF}(r_{12})$ for 2^1S, indicating that at small r_{12} the structure of $\Delta f(r_{12})$ is determined by the effects of correlation on the double occupancy of the K shell. Without additional information, it is not possible to explain the shape of the remainder of the curve. Accordingly, to gain further insight into the effects of correlation, we turn our attention to the $\Delta g(r_{12}, r_1)$ surface for 2^1S presented in Figure (II.1.5a). An alternative view of this surface is shown in Figure (II.1.6a).

The partial Coulomb hole $\Delta g(r_{12}, r_1)$ shows the change in behaviour of the Coulomb hole as the position of the test electron is varied. It follows from our earlier discussion of the $g^{HF}(r_{12}, r_1)$ surface that when r_1 is small, and the test electron is thus located in the K shell, the corresponding Δg **vs** r_{12} behaviour should illustrate the effects of correlation on the L-shell electron. On the other hand, when the test electron is located somewhere in the L shell, the Δg **vs** r_{12} characteristics are largely a result of correlation effects within the K shell.

For a test electron located in the L-shell region, Figures (II.1.5a) and (II.1.6a) reveal that the main

features in Δg occur about the diagonal $(r_{12}=r_1)$ axis. These features, which extend over quite a large range of r_1 values, indicate a density decrease on the near side of the nucleus $(r_{12}<r_1)$. From this, it would appear that correlation causes the average angle between the position vectors to be increased. Confirmation of such an increase in θ_{12} is provided by a comparison of the HF and correlated values for $\langle\cos\theta_{12}\rangle$, presented in Table (II.1.5). Now, in the uncorrelated description of this state, the outer electron experiences a high degree of nuclear shielding, due to the spherically symmetric nature of the K shell. Following the introduction of correlation, and the consequent increase in the angular separation of the electrons, the nuclear shielding is seen to be reduced. Comparison of the radial holes, $\Delta D_1(r_1)$, shown in Figure (II.1.10a), with the $D_1^{HF}(r_1)$ curves in Figure (II.1.9a) reveals that correlation then causes a large shift in probability from the outer to the inner regions of the loosely bound L shell, thereby minimising the energy of the system. The magnitude of $\Delta D_1(r_1)$ at small r_1 is, by comparison, relatively insignificant, indicating that correlation induces only a minimal change in the radial location of the more tightly bound K-shell electron. From the foregoing, it is seen that the reduction in probability of large interelectronic separations seen in $\Delta f(r_{12})$ is a result of the <u>reduction</u> in the <u>radial</u> separation of the two shells, which is itself a consequence of the <u>increase</u> in the <u>angular</u> separation of the two electrons.

In keeping with our earlier comment concerning the shape

of $\Delta f(r_{12})$ at small r_{12}, examination of $\Delta g(r_{12}, r_1)$ for 2^1S in the region $0 < (r_{12}, r_1) < 2$ reveals that the surface possesses characteristics which are almost identical to those of the ground-state surface obtained by Banyard and Reed[35]. Finally for the 2^1S state, we note that the $\Delta g(r_{12}, r_1)$ surface as a whole is remarkably similar in shape to the 2^1S intershell surface in Be[36], again in keeping with a comparison between the corresponding $\Delta f(r_{12})$ curves.

We consider now the effects of correlation in the 2^3S state. Inspection of Figure (II.1.2a) reveals that at large and intermediate values of r_{12}, the Coulomb hole for 2^3S displays the same sort of structure as that found in the singlet curve. However, whereas in 2^1S the increase in probability at intermediate r_{12} was approximately commensurate with the decrease at large r_{12}, in the triplet state the enhancement at intermediate r_{12} is only partially accounted for by the reduction at large r_{12}. At very small values of r_{12}, the Fermi effect in 2^3S causes $f^{HF}(r_{12})$, $f^{corr}(r_{12})$ and hence $\Delta f(r_{12})$ to be vanishingly small. As r_{12} is increased, $\Delta f(r_{12})$ becomes increasingly more negative and it is the reduction in probability here which balances the larger part of the probability increase at intermediate r_{12}. The Y values, presented in Table (II.1.2), reflect quite clearly the differences in magnitude between the Coulomb holes for the 2^1S and 2^3S states.

For 2^3S, the Δg surface in Figures (II.1.5b) and (II.1.6b) possesses maxima and minima which are smaller than the 2^1S values. However, except at small (r_{12}, r_1), the

surface is very similar in _shape_ to that for the singlet state. The absence of structure in the 2^3S surface when $0 < (r_{12}, r_1) < 2$ is obviously the result of the Fermi effect in the triplet state obviating the need for Coulomb correlation at small r_{12}. For a test electron located in the L-shell region, the main characteristics of the 2^3S surface occur, as for the singlet state, about the $(r_{12}=r_1)$ diagonal axis. It is seen that there is a density decrease when $r_{12} < r_1$, and an increase when $r_{12} > r_1$. The deepest minimum and highest maximum in this region both occur at the same value of r_1. This value is found to be the same as that which locates the maximum in the corresponding $\Delta D_1(r_1)$ curve. Furthermore, the principal diagonal features in the $\Delta g(r_{12}, r_1)$ surface are separated in their r_{12}-coordinates by a value equal to $2r_K$, where, it will be recalled, r_K is the most likely radial location of the K-shell electron at the HF level. From Figure (II.1.10a) it is seen that this inner electron experiences a relatively insignificant radial movement following the introduction of correlation. Consequently, for a test electron located at a large value of r_1, the reduction in density on the near $(r_{12} < r_1)$ side of the nucleus can only occur as the result of the angular component of correlation. Inspection of the HF and correlated values for $\langle \cos\theta_{12} \rangle$ in Table (II.1.5) confirms that correlation does indeed produce an increase in the average angular separation of the position vectors of the two electrons.

The $\Delta D_1(r_1)$ curve in Figure (II.1.10a) reveals that, as for 2^1S, correlation produces a shift of probability from

the outer to the inner regions of the L shell. However, for 2^3S the change in the radial distribution is considerably smaller than that in the singlet state. To understand this difference it is useful to consider again the $D_1^{HF}(r_1)$ curves in Figure (II.1.9). At the uncorrelated level, Fermi correlation lowers the energy of the triplet state relative to the corresponding singlet by a more subtle and economic packing of the electron density. As we noted earlier, the principal difference between the $D_1^{HF}(r_1)$ curves for the 2^1S and 2^3S states occurs in the L-shell region; at small values of r_1, the two curves are nearly coincident. Inspection of the uncorrelated expectation values in Table (II.1.3) reveals that as we progress from the singlet to the triplet state, $\langle r_1^2 \rangle$ and $\sigma(r_1)$ are decreased by 30.1% and 18.1%, respectively, while $\langle r_1^{-1} \rangle$, which emphasizes the K-shell region, experiences an increase of about 1.75%. Thus, for the radial density, the main effect of introducing Fermi correlation is to produce a contraction of the L-shell charge cloud. It is then hardly surprising that the subsequent L-shell contraction caused by the introduction of Coulomb correlation should be smaller in 2^3S than in 2^1S.

Although it is not immediately obvious from either of the presented views of the $\Delta g(r_{12},r_1)$ surface for 2^3S, there is a deep minimum when $r_{12} \approx 1.75$ and $r_1 \approx 1.0$. From Figure (II.1.10a) it is seen that $\Delta D_1(r_1 \approx 1.0)$ is very small, indicating a minimal change in the radial position of an electron located at this value of r_1. It therefore seems that the deep negative region in the 2^3S surface arises from the increase in the angular separation of the electrons when

the <u>decrease</u> in the <u>radial</u> separation is very small. Furthermore it would appear that it is this feature, combined with the negative region on the $(r_{12} < r_1)$ side of the diagonal axis, which gives rise to the principal minimum in the corresponding $\Delta f(r_{12})$ curve.

Finally for the 2^3S state, inspection of Figure (II.1.2) and the expectation values in Tables (II.1.2) to (II.1.5) reveals that the various wavefunctions used for the correlated description exhibit similar correlation characteristics, thus helping to substantiate our physical interpretation of the Coulomb holes.

We now examine the effects of correlation in the P states. As before, it is useful to consider first the nature of the electron distribution as described by the HF wavefunctions. For both P states we can, from Figure (II.1.9), identify two maxima in $D_1^{HF}(r_1)$, located at r_1 values which, for obvious reasons and future convenience, will again be referred to as r_K and r_L. As in the S states, the value of r_K is effectively the same in both singlet and triplet. In contrast to this, we note that $r_L(2^1P) > r_L(2^3P)$, thus indicating that once again the main effect of Fermi correlation is to cause a contraction of the L shell towards the nucleus. That this effect should be so much smaller in the P states than in the S states may be understood by inspection of the analytical form of the HF wavefunctions. For the 2^3S state, Fermi correlation gives a zero value for the two-particle density whenever $|\underline{r}_1| = |\underline{r}_2|$, whereas for 2^3P the density is zero only for the more

47

limited condition represented by $\underline{r}_1 = \underline{r}_2$; consequently Fermi correlation is less powerful in the P states than in the S states.

In a study of the distribution function of the interelectronic angle θ_{12}, Ellis[7] has shown that at the HF level, the most probable value of θ_{12} in 2^1P is less than 90°, while in 2^3P it is greater than 90°. Thus, in the uncorrelated description of the singlet state, the electrons tend to be located on the same side of the nucleus, while in the triplet state they favour opposite sides. This difference in the angular orientation of the electrons between the singlet and triplet P states is also revealed by examining an angular expectation value, such as $\langle \cos\theta_{12} \rangle$. The HF results for both S states are, of course, identically zero, but Table (II.1.5) shows that, as expected, the uncorrelated values of $\langle \cos\theta_{12} \rangle$ for 2^1P and 2^3P differ in both magnitude and sign. These differences can be accounted for by examining the corresponding two-particle densities when expressed in terms of their component orbitals ´1s´ and ´2p´. A non-zero contribution to $\langle \cos\theta_{12} \rangle$ arises only from the cross term in the HF density and therefore the sign of this expectation value follows that of the appropriate exchange term. The magnitude of $\langle \cos\theta_{12} \rangle$ depends on the overlap of the <u>radial</u> parts of the 1s and 2p oribitals and, since Fermi correlation produces a contracted L shell, the 2^3P state will yield the larger value.

The $g^{HF}(r_{12}, r_1)$ surfaces in Figure (II.1.3c,d) display features parallel to the r_{12} axis and along the $(r_{12} = r_1)$

diagonal axis which are similar to those seen in the S-state surfaces. However, there is one obvious point of contrast between the surfaces for 2^1S and 2^1P. In the P state, the difference in symmetry between the K- and L-shell orbitals means that when both electrons are in the vicinity of the nucleus, the system does not bear any resemblance to the ground state. As a consequence, the structure seen in the 2^1S surface in the region $0 < (r_{12}, r_1) < 2$ is not found in the surface for 2^1P. Naturally, this difference between the singlet S and P states is also reflected in the $f^{HF}(r_{12})$ curves in Figure (II.1.1).

Having established the differences between 2^1P and 2^3P at the HF level, we now consider the effects of Coulomb correlation in both states. An examination of the Coulomb holes in Figure (II.1.2b) reveals an overall similarity between the $\Delta f(r_{12})$ characteristics for the singlet and triplet P states, which is in marked contrast to the comparison between the ^1S and ^3S curves. A further point of contrast is that for the P states the Coulomb holes for the triplet are larger than for the singlet; this difference is reflected in the $\langle r_{12}^n \rangle$ values presented in Table (II.1.2). The reversal in the relative magnitudes of correlation effects in the singlet and triplet states as one progresses from S to P states has also been noted by Moiseyev and Katriel[9]. Figure (II.1.2b) also reveals that, as for the 2^3S state, an energy improvement in the Tweed description of the P states produces a slightly deeper Coulomb hole in each instance; a similar effect occurs in the ground state of He[37]. Interestingly, the Y values, also presented in Table (II.1.2), indicate that the effects of Coulomb

49

correlation are approximately three times greater in 2^3P than in 2^3S. This is consistent with our earlier observation that the effects of _Fermi_ correlation are greater in the S state.

A comparison of the $\Delta g(r_{12}, r_1)$ surfaces for the 2^1P and 2^3P states in Figures (II.1.5c,d) and (II.1.6c,d) shows them to be broadly similar. However, the 2^3P surface is more negative in the 'small (r_{12}, r_1)' region, which accounts for the greater depth of $\Delta f(r_{12})$ at small r_{12} in the triplet state. Furthermore, for the _singlet_ state, the maximum which occurs in $\Delta g(r_{12}, r_1)$ when $r_1 \approx 0.5$ is quite distinct from that at $r_1 \approx 2.25$, whereas for 2^3P the two maxima merge together. Such an effect was also observed, to a much lesser extent, in the $g^{HF}(r_{12}, r_1)$ surfaces, but from the orientation of those surfaces in Figure (II.1.3) the effect is barely noticeable. At the uncorrelated level, the overlapping of the K- and L-shell contributions to $g^{HF}(r_{12}, r_1)$ in the triplet state is a result of Fermi correlation allowing a more subtle interaction between the two electrons, thereby producing a more compact two-particle density. Naturally, this effect is also present in the partial Coulomb holes, but the degree of merging seen in the 2^3P $\Delta g(r_{12}, r_1)$ surface indicates that it is _Coulomb_, rather than Fermi, correlation which is principally responsible for the infilling which occurs as we progress from the singlet to the triplet state. We shall return to this point in due course.

For both P states, the shape of the $\Delta g(r_{12}, r_1)$ surface

about the $(r_{12}=r_1)$ diagonal indicates that, as for the S states, correlation causes an increase in the interelectronic angle θ_{12} -- see also the expectation values in Table (II.1.5). The subsequent reduction in nuclear shielding by the inner electron again causes a contraction of the L shell, as indicated by the $\Delta D_1(r_1)$ curves in Figure (II.1.10b). Although the radial holes for the P states appear to possess the same general characteristics of shape as those for the S states, closer inspection reveals a number of significant differences, especially when the $\Delta D_1(r_1)$ curves are compared with the corresponding HF distribution. For the S states, the minimum in $\Delta D_1(r_1)$ at large r_1 in the singlet state is considerably deeper than that in the triplet. In contrast to this, for $r_1 > 6.0$, the 2^3P radial hole is remarkably similar to that for 2^1P, with the triplet curve being <u>marginally</u> deeper than that for the singlet. For both P states, the value of r_1 at which the principal minimum in $\Delta D_1(r_1)$ occurs is noticeably larger than the value at which the same feature occurs in the corresponding S state. Inspection of the $D_1^{HF}(r_1)$ curves in Figure (II.1.9) shows that this difference between the radial holes is not simply due to a dissimilarity at the uncorrelated level, and indicates that Coulomb correlation acts on different regions of the L shell in the S and P states.

For values of $r_1 < 6.0$, the $\Delta D_1(r_1)$ curves for 2^1P and 2^3P display differences in shape and magnitude which contrast strongly with the near coincidence of the curves at larger r_1. Referring once again to the $D_1^{HF}(r_1)$ curves in

Figure (II.1.9b), we see that for both P states, the principal maximum in $\Delta D_1(r_1)$ occurs very close to the corresponding 'intershell' minimum in $D_1^{HF}(r_1)$. In the singlet state, the enhancement of probability is spread over a larger r_1 range than in the triplet, and new insight into this difference between the 2^1P and 2^3P radial holes is obtained by considering the $D_{12}^{HF}(r_1,r_2)$ and $\Delta D_{12}(r_1,r_2)$ surfaces in Figures (II.1.11) and (II.1.12) respectively. Although the uncorrelated distributions for 2^1P and 2^3P are very similar, the shapes of the $\Delta D_{12}(r_1,r_2)$ surfaces are quite different. In the singlet surface, the principal maxima occur when the radial locations of the two electrons are different, indicating that correlation tends to maintain the K/L structure of the HF model, while producing a contraction of the L shell towards the nucleus. In contrast to this, the surface for 2^3P demonstrates that correlation produces the greatest enhancement of probability when $r_1 = r_2$, thereby producing a <u>reduction</u> in the 'split-shell' structure of the system. This difference between the $\Delta D_{12}(r_1,r_2)$ surfaces for the singlet and triplet P states is consistent with the previously mentioned differences in the partial Coulomb holes; in particular, the maximum in $\Delta D_{12}(r_1,r_2)$ for 2^3P accounts for the merging together of the features in the corresponding $\Delta g(r_{12},r_1)$ surface. Furthermore, for 2^3P it is seen that there is a reduction in $D_{12}(r_1,r_2)$ at small (r_1,r_2), the local minimum again occurring when the two electrons are located at the same radial distance from the nucleus. This feature is in keeping with the previously observed negative region at small (r_{12},r_1) seen in the 2^3P partial Coulomb hole.

Interestingly, in $\Delta D_{12}(r_1, r_2)$ both of the features found on the $(r_1 = r_2)$ diagonal axis for the 2^3P state are absent from the corresponding S state surface, reflecting, no doubt, the difference between the Fermi effect in the S and P states.

Finally for the P states, the $g^{HF}(r_{12}, r_1; \theta_1)$ and $\Delta g(r_{12}, r_1; \theta_1)$ surfaces, shown in Figures (II.1.7) and (II.1.8), respectively, demonstrate the effect of varying the angular orientation of the position vector of the test electron with respect to the symmetry axis of the p orbital. For both P states, it is seen that when $\theta_1 = 0°$, the g^{HF} and Δg surfaces display the same general characteristics of shape as do their angularly integrated counterparts. As θ_1 increases from $0°$, the components of the surfaces which lie parallel to the r_{12} axis remain approximately constant in magnitude, while those in the region of the $(r_{12} = r_1)$ diagonal become progressively less significant, until they disappear completely when $\theta_1 = 90°$. This behaviour is most easily explained by noting that a test electron at small r_1 (that is, in the K shell) is most likely to be described by contributions to the two-particle density from the spherically symmetric s orbital, and will be relatively unaffected by changes in θ_1; on the other hand, a test electron which is at a <u>large</u> value of r_1 is more likely to be described by contributions from the angle-dependent p orbital. When $\theta_1 = 90°$, the test electron lies in the nodal plane of the p orbital and is therefore described solely by the K-shell distribution, which rapidly becomes very small as r_1 is increased beyond r_K. As a consequence, for this value of θ_1, the diagonal features, which arise from a test

electron located at large r_1, are absent from the $g^{HF}(r_{12}, r_1)$ and $\Delta g(r_{12}, r_1)$ surfaces of both P states.

We conclude our discussion by noting that the expectation values presented in Tables (II.1.2) to (II.1.5) support our interpretation of the correlation effects in all four states. Of particular interest are the interparticle properties, such as $\langle r_{12} \rangle$. At the HF level, we have seen that as we progress from 2^1S to 2^3S, the principal effect of Fermi correlation is to cause the L-shell electron to approach the nucleus, and hence the K-shell electron. As a consequence, we anticipate that $\langle r_{12} \rangle^{HF}(2^1S) > \langle r_{12} \rangle^{HF}(2^3S)$ and this is confirmed by inspection of Table (II.1.2). When we make the transition from 2^1P to 2^3P, the changes in the radial and angular properties produce opposing effects, but the common radial contraction of the L shell more than compensates for the increase in the angle θ_{12}, with the result that $\langle r_{12} \rangle^{HF}(2^1P) > \langle r_{12} \rangle^{HF}(2^3P)$. Since the effects of Fermi correlation are so much greater than those of Coulomb correlation, the same ordering also holds at the correlated level. Similar comments may also be made with regard to the $\sigma(r_{12})$ values, also presented in Table (II.1.2).

The introduction of Coulomb correlation causes the interelectronic angle to increase in all four states, and this is reflected, as we have seen, in the angular expectation values presented in Table (II.1.5). In the absence of any other effect, such a change in the orientation of the electrons would cause $\langle r_{12} \rangle$ to be

increased. However, in each state the subsequent reduction in the _radial_ separation of the K and L shells actually produces a _reduction_ in $\langle r_{12} \rangle$.

In Table (II.1.4), we present the two-particle radial expectation values $\langle r_1^n r_2^n \rangle$ for 2^3S, 2^1P and 2^3P (results for 2^1S are not available). For all three states, correlation causes $\langle r_1 r_2 \rangle$ and $\langle r_1^2 r_2^2 \rangle$ to be reduced. Such a change also occurs in these expectation values in the ground state[38], and without additional information it would be tempting to assume a common change in the corresponding radial densities. However, for the 1^1S state it has been shown[39] that correlation reduces the two-particle radial density $D_{12}(r_1, r_2)$ along the $(r_1 = r_2)$ axis, where it is a _maximum_ at the uncorrelated level, and increases the density in the off-diagonal regions, thereby producing the usual 'in-out' radial correlation effect, and the observed reduction in $\langle r_1^n r_2^n \rangle$ for n=1,2. In contrast to this, Figure (II.1.11) shows that in the excited states the value of $D_{12}^{HF}(r_1, r_2)$ along the $(r_1 = r_2)$ diagonal is either identically zero or very small, and correlation reduces $\langle r_1 r_2 \rangle$ and $\langle r_1^2 r_2^2 \rangle$ by producing the previously discussed increase in θ_{12} and inward shift of the L-shell density. This contraction of the outer shell, seen clearly in the $\Delta D_{12}(r_1, r_2)$ surfaces in Figure (II.1.12), produces an _increase_ in $\langle r_1^{-1} r_2^{-1} \rangle$; in the 2^3S and 2^1P states, $\langle r_1^{-2} r_2^{-2} \rangle$ is also increased, but in 2^3P the minimum in $\Delta D_{12}(r_1, r_2)$ at small (r_1, r_2) causes a _decrease_ in this expectation value.

CHAPTER (II.1.5)

SUMMARY

Electron correlation effects in the 2^1S, 2^3S, 2^1P and 2^3P states of He have been analysed in terms of a number of electron density distributions and expectation values.

Examination of the expectation values $\langle \underline{r}_1 \cdot \underline{r}_2 / r_1^n r_2^n \rangle$ showed that the principal angular effect of correlation in all four states is an increase in the interelectronic angle, θ_{12}, which reduces the degree of nuclear shielding provided by the K-shell electron. As a result of such a reduction, the major radial effect of correlation in each state is a contraction of the outer-orbital electron density towards the nucleus, as may be seen from the shape of the one- and two-particle radial holes ($\Delta D_1(r_1)$ and $\Delta D_{12}(r_1, r_2)$, respectively). The combination of the radial and angular effects was found to produce a significant reduction in the probability of large interparticle separations, as illustrated by the shape of the Coulomb holes, $\Delta f(r_{12})$, at large values of r_{12}. The maximum in each $\Delta f(r_{12})$ curve at _intermediate_ values of r_{12} is largely associated with the inner- and outer-orbital electrons being located on opposite sides of the nucleus. In particular, it was noted that the effects of Coulomb correlation in 2^3S are smaller than in 2^1S--a result which is not unreasonable in view of the Fermi correlation present in the triplet state. Such reasoning does not, however, carry over to the P states, where electron correlation in the triplet was found to be noticeably _larger_ than in the singlet.

The use of _partial_ Coulomb holes facilitated the examination, individually, of the effects of correlation in the K and L shells. When presented in the form of surfaces, these partial holes are especially useful in understanding the mechanisms by which overall correlation effects come about. Close to the nucleus, the $\Delta g(r_{12}, r_1)$ surface for $2^1 S$ shows characteristics similar to those for the ground state, indicating a partially doubly-occupied K shell. Such a feature is not present in the $2^1 P$ surface because of the symmetry difference between the two shells.

Examination of the radial two-particle expectation values revealed trends similar to those already observed for the ground state. Interestingly, it was found that the corresponding changes in the appropriate two-particle densities were completely dissimilar. The differences were, nevertheless, found to be quite compatible with our understanding of the Coulomb holes.

FIGURES AND TABLES - SECTION (II.1)
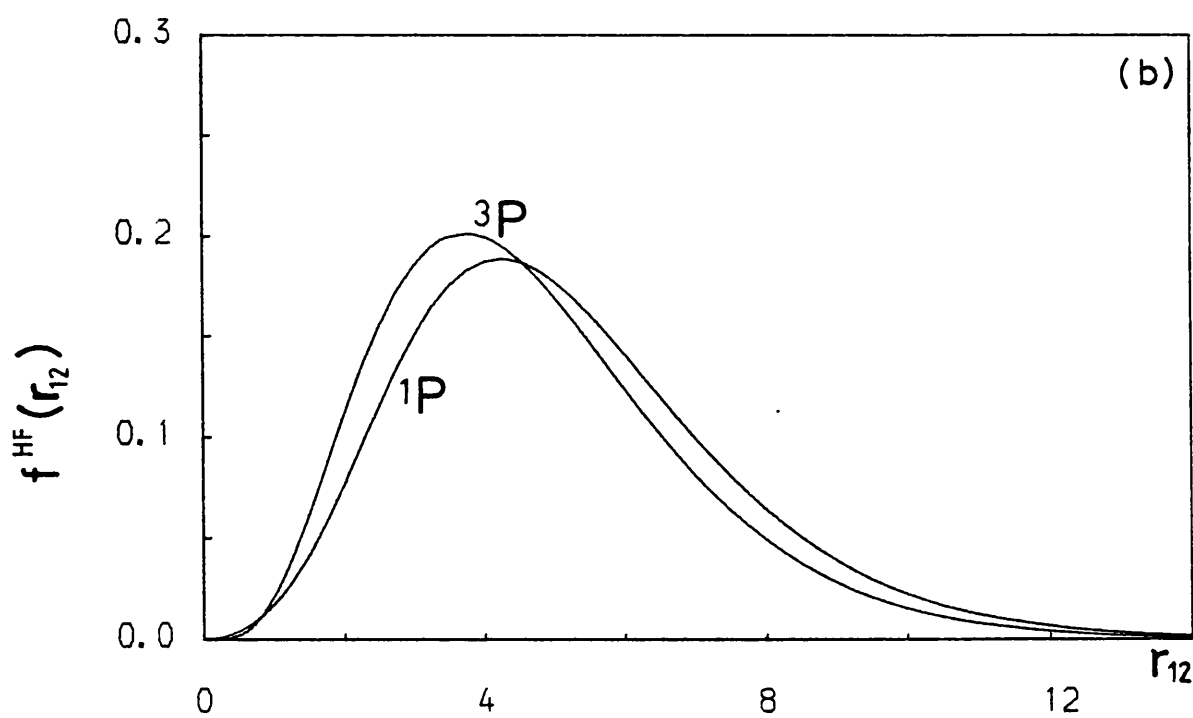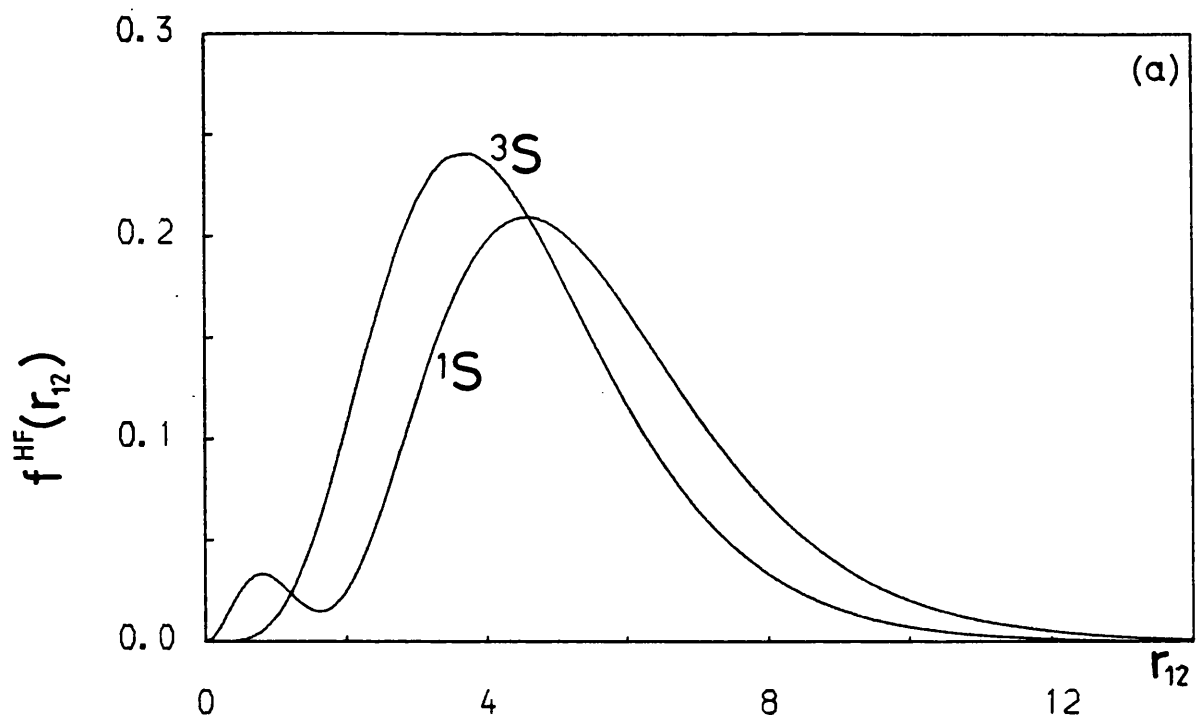
Figure (II.1.1)

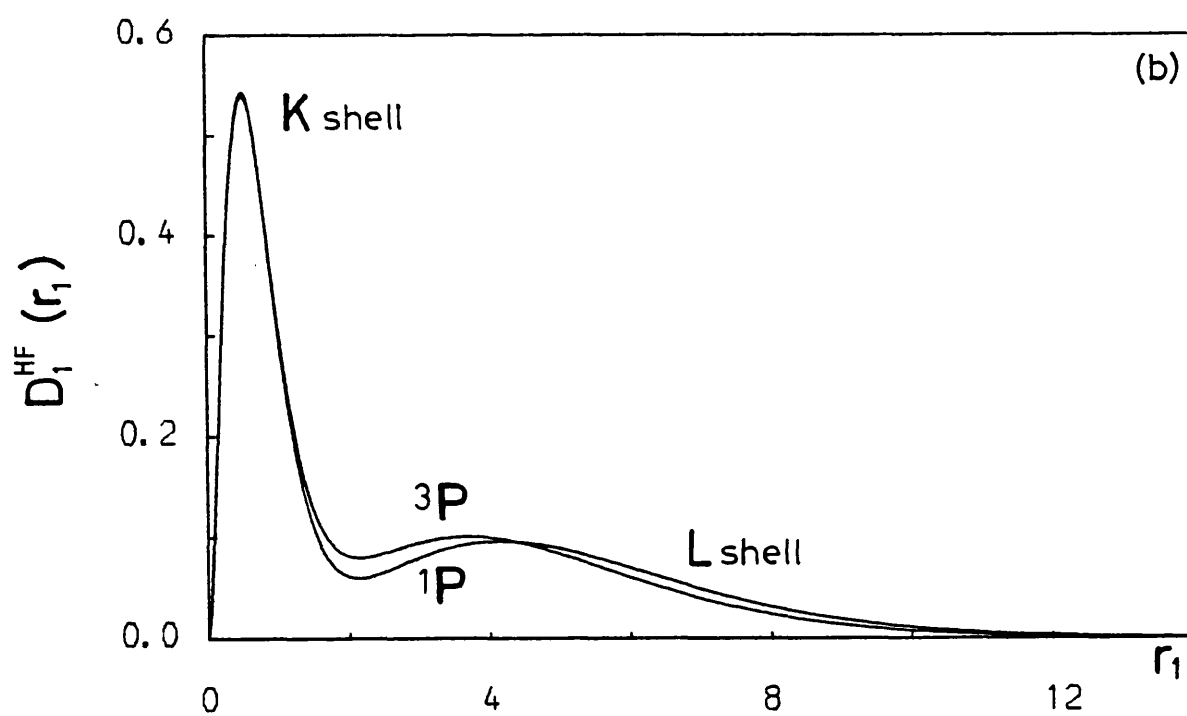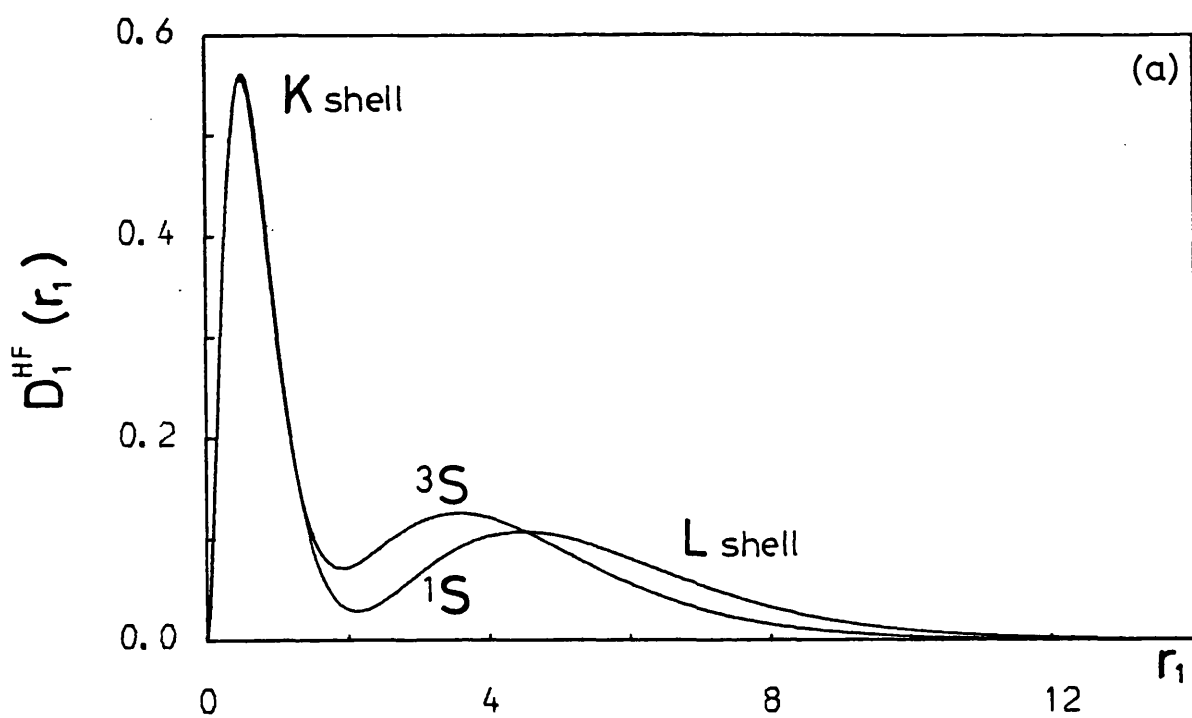The $f^{HF}(r_{12})$ distributions for the (a) 2^1S and 2^3S
and (b) 2^1P and 2^3P states of He.
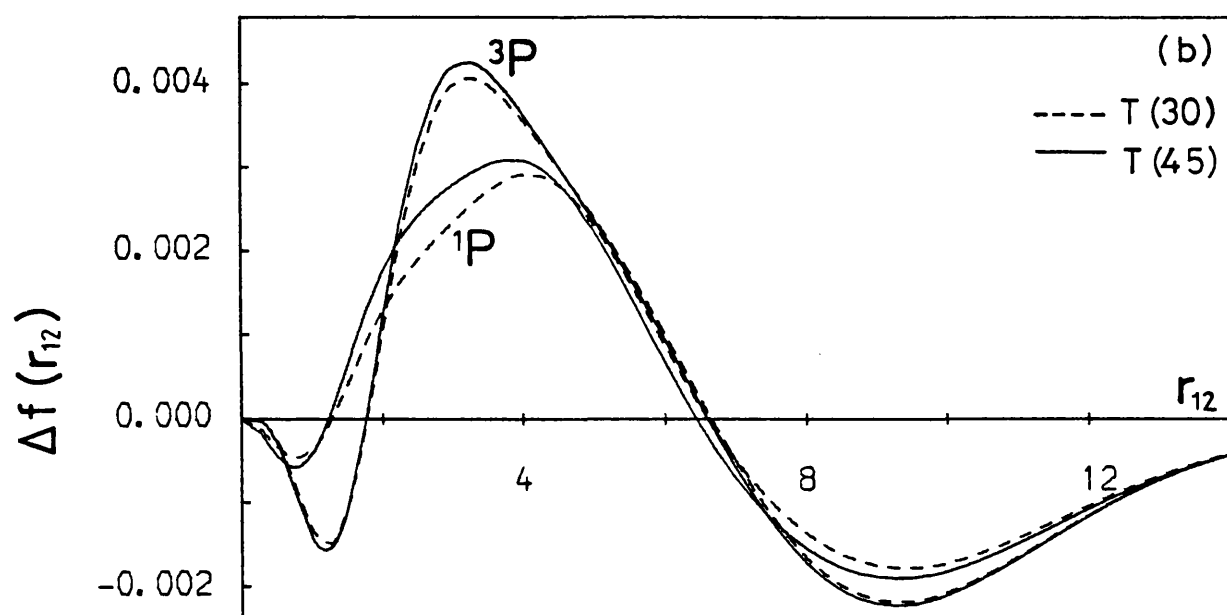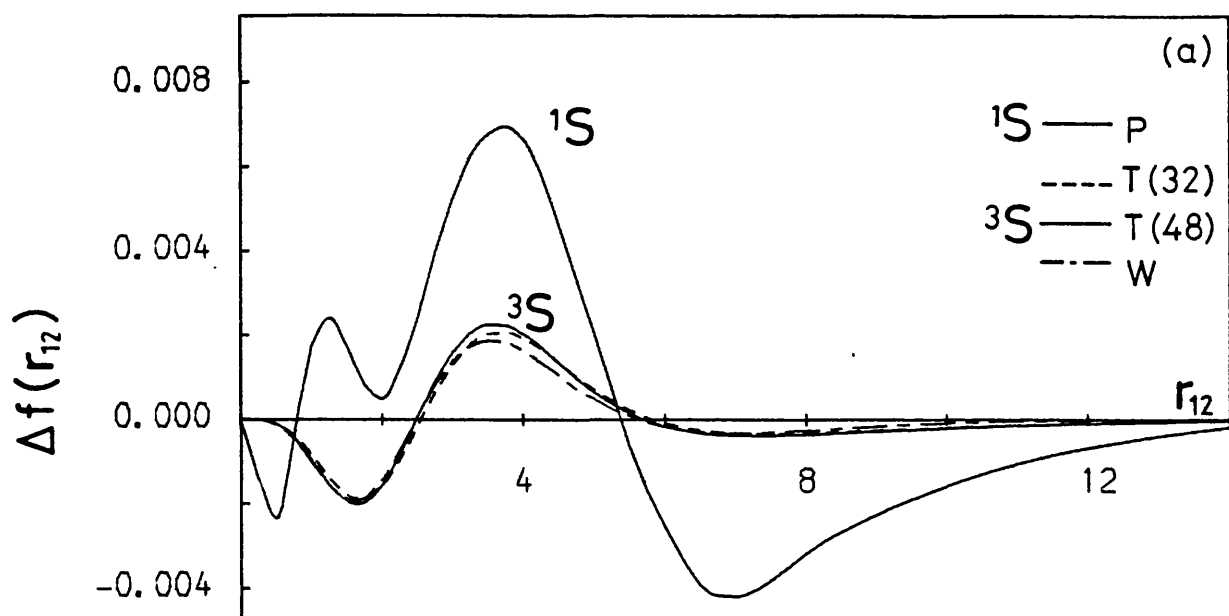
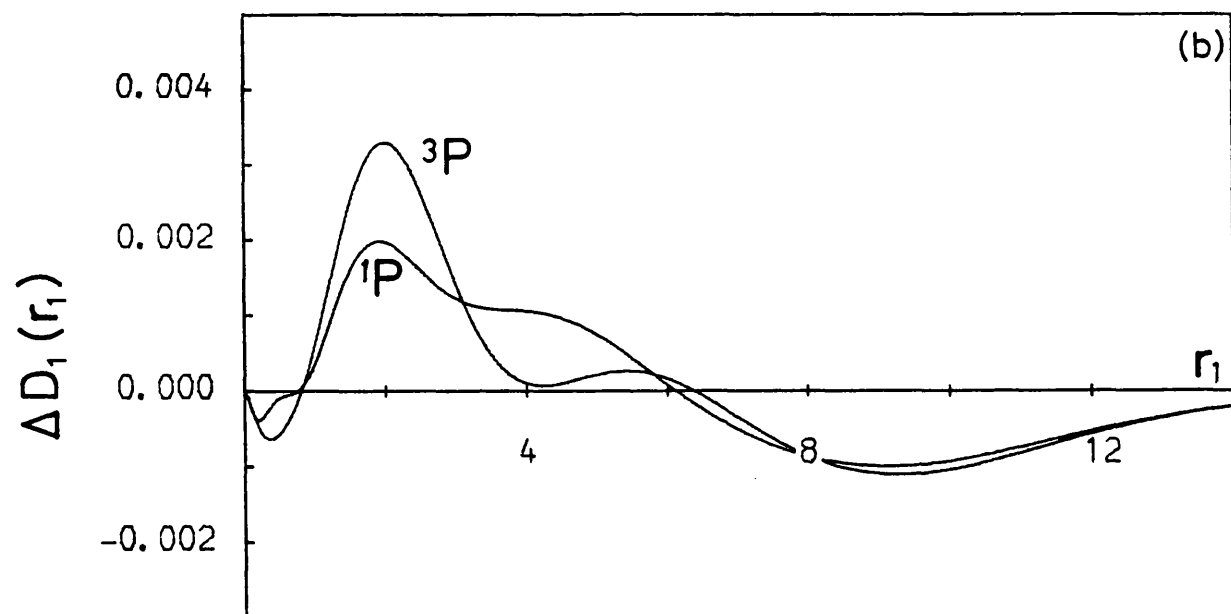**Figure (II.1.2)**

The Coulomb holes $\Delta f(r_{12})$ for the (a) 2^1S and 2^3S and (b) 2^1P and 2^3P states of He.

Figure (II.1.3)

(see over)

(a) $2\,^1S$ (b) $2\,^3S$ (c) $2\,^1P$ (d) $2\,^3P$

$g^{HF}(r_{12}, r_1)$

Figure (II.1.4)

A single-contour representation of the $g^{HF}(r_{12}, r_1)$ distribution for the 2^1S state of He.

Figure (II.1.5)

(see over)

Figure (II.1.5)

The partial Coulomb holes $\Delta g(r_{12}, r_1)$ for the

(a) 2^1S, (b) 2^3S, (c) 2^1P and (d) 2^3P states of He.

(a) $2\,^1S$

(b) $2\,^3S$

(c) $2\,^1P$

(d) $2\,^3P$

$\Delta g(r_{12}, r_1)$ 0.004

(c) $2\,^1P$

$\Delta g(r_{12}, r_1)$ 0.004

(d) $2\,^3P$

$\Delta g(r_{12}, r_1)$ 0.004

(a) $2\,^1S$

$\Delta g(r_{12}, r_1)$ 0.004
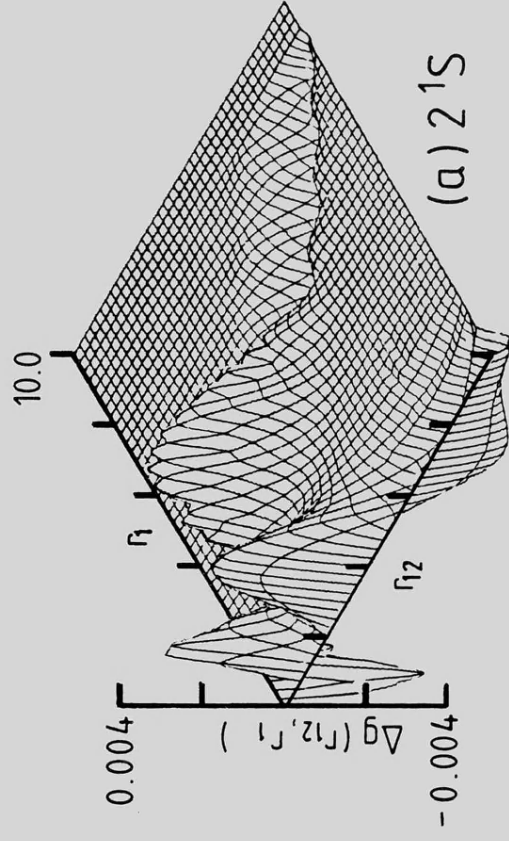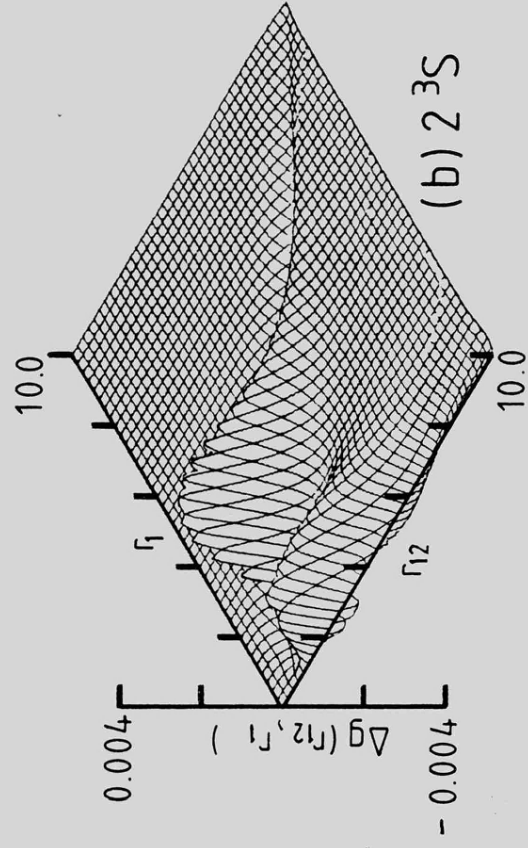
(b) $2\,^3S$
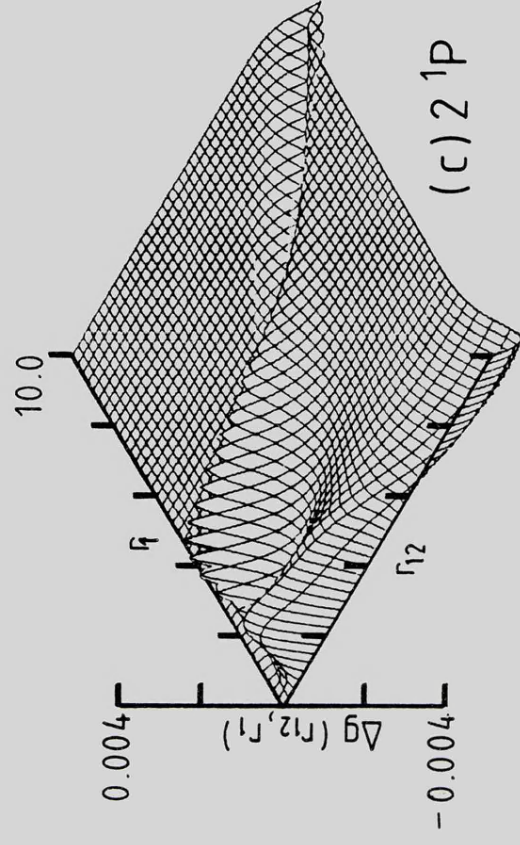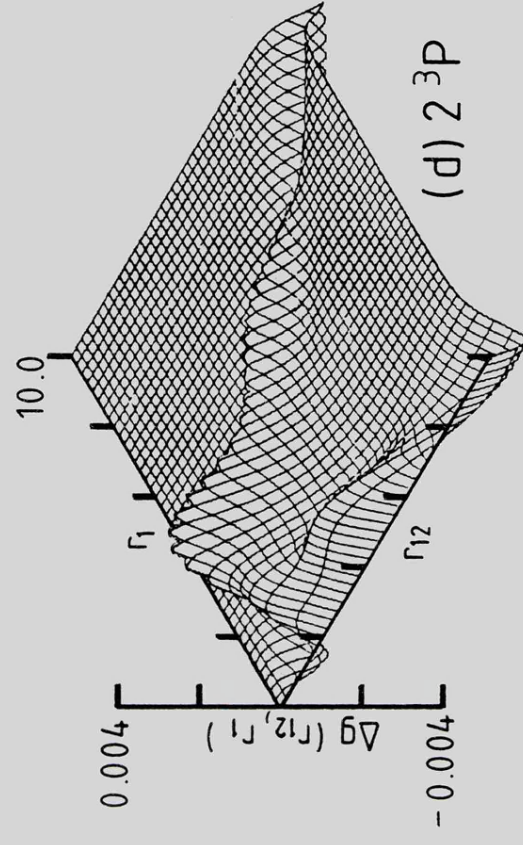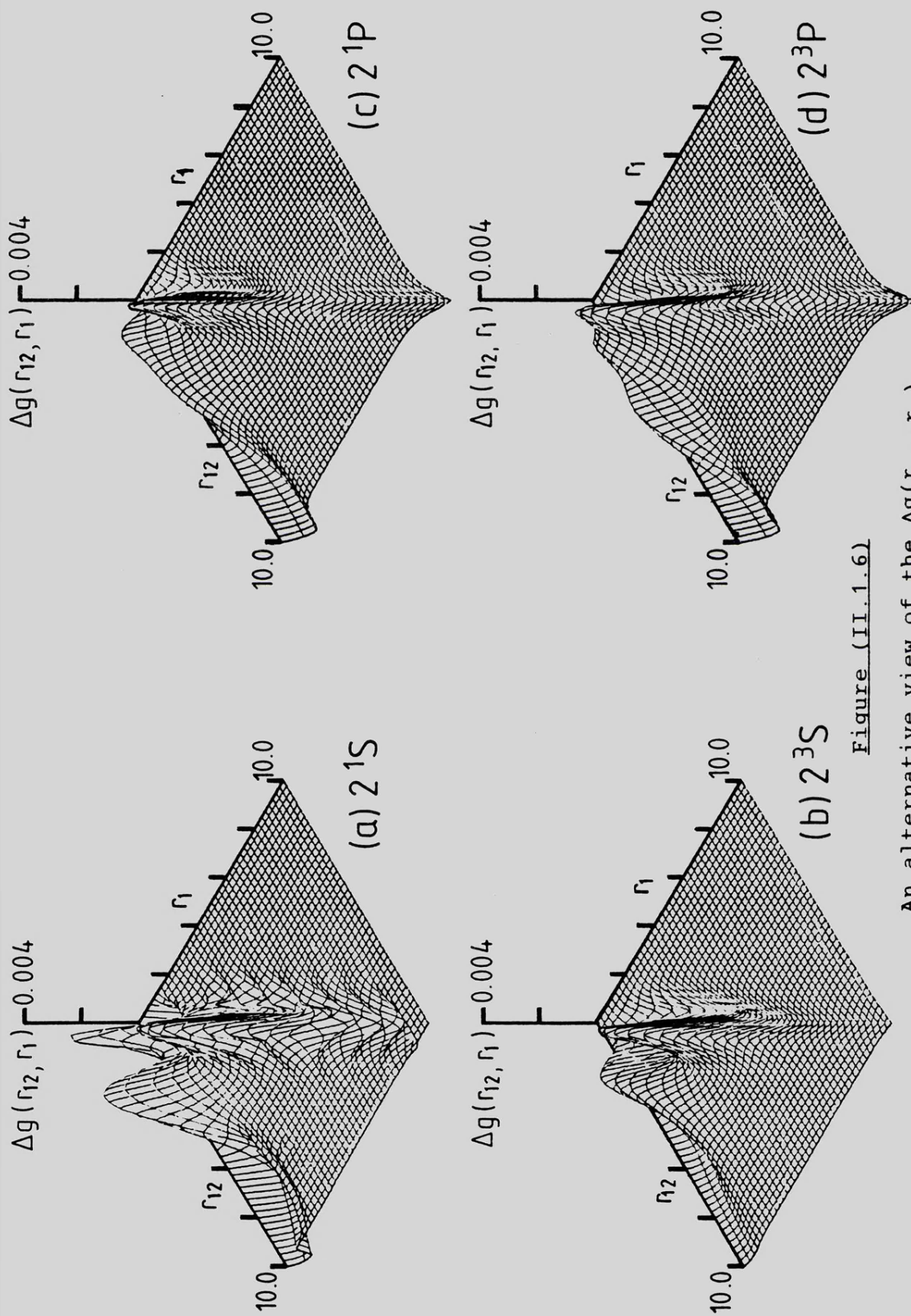
Figure (II.1.6)

An alternative view of the $\Delta g(r_{12}, r_1)$ surfaces presented in Figure (II.1.5).

63

Figure (II.1.7)

(see over)

<u>Figure (II.1.7)</u>

The $g^{HF}(r_{12}, r_1 ; \theta_1)$ distributions for the

a)2^1P and b)2^3P states of He.

$\theta_1 = 0°$

$\theta_1 = 30°$

$\theta_1 = 60°$

$\theta_1 = 90°$
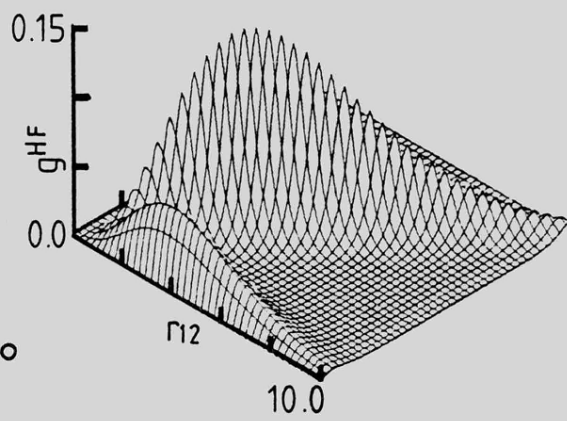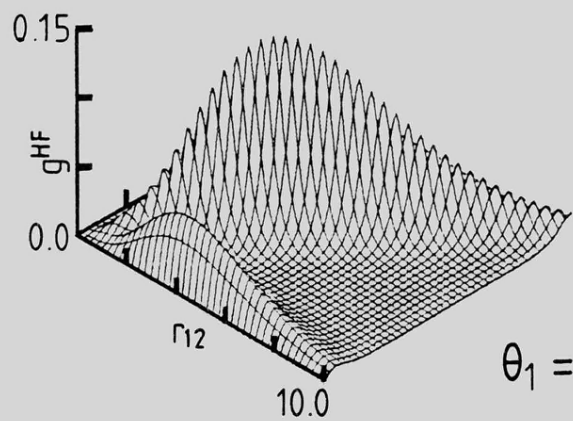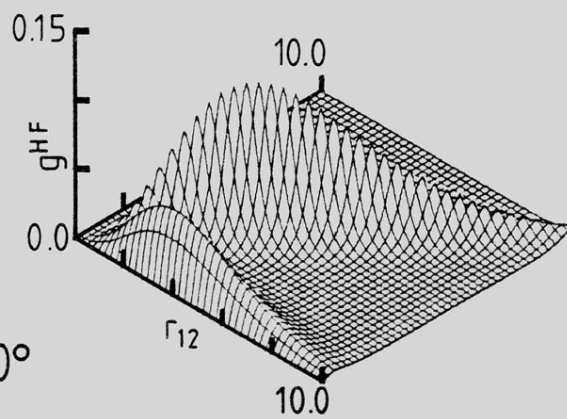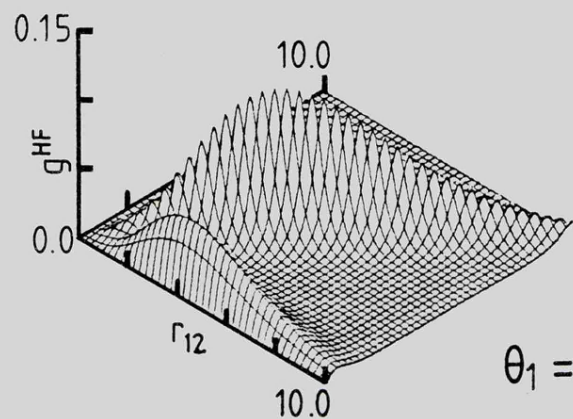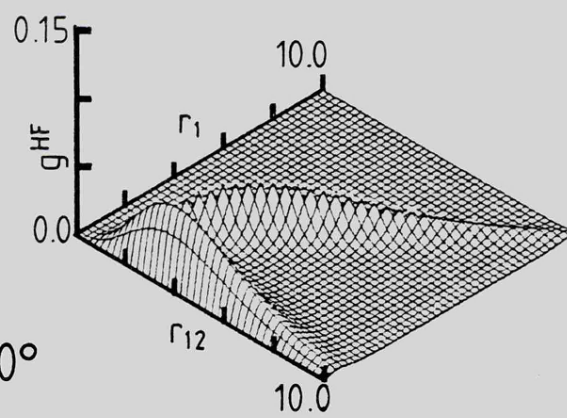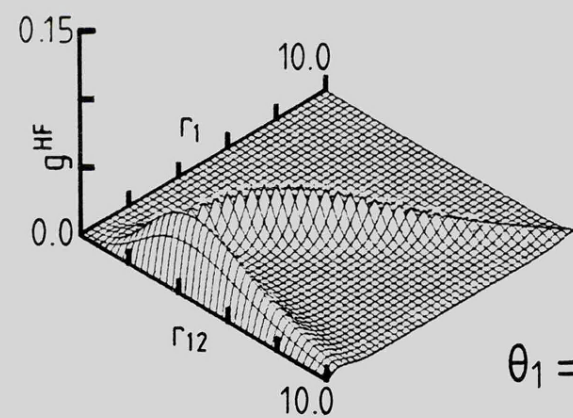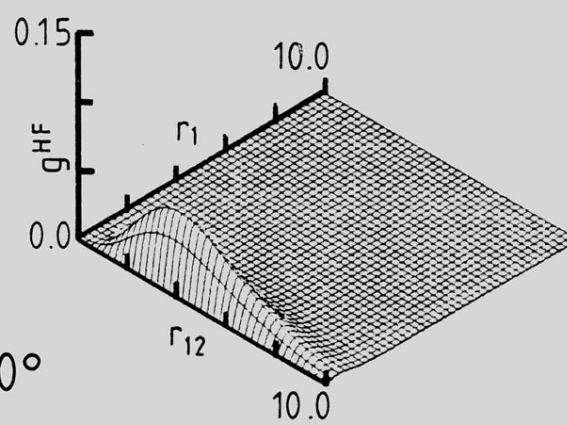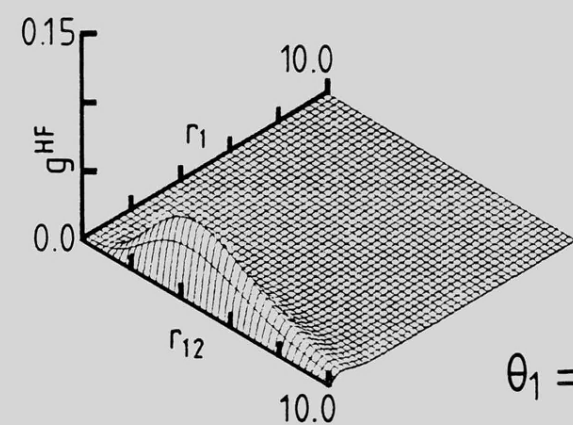
(a) $2\,^1P$

(b) $2\,^3P$

Figure (II.1.8)

(see over)

Figure (II.1.8)

The partial Coulomb holes $\Delta g(r_{12}, r_1; \theta_1)$ for the

a) 2^1P and b) 2^3P states of He.

$\theta_1 = 0°$

$\theta_1 = 30°$

$\theta_1 = 60°$

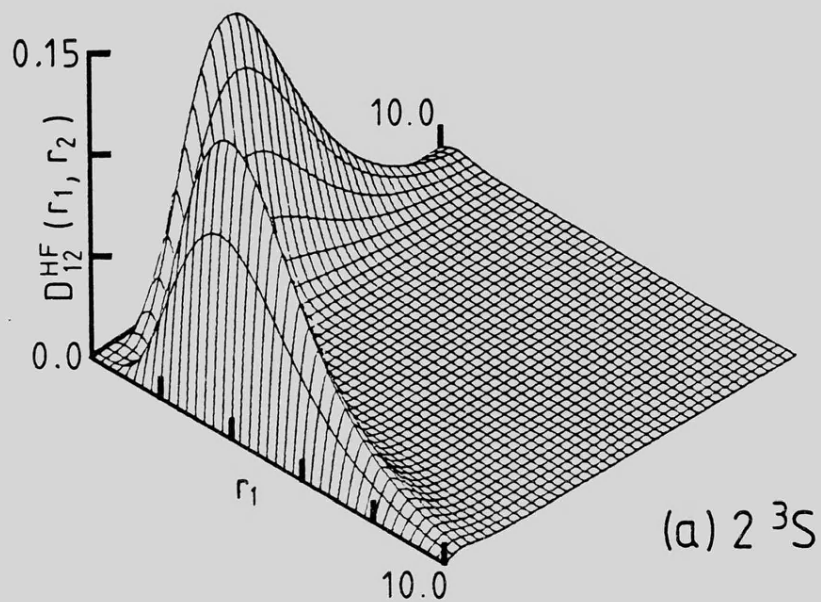$\theta_1 = 90°$
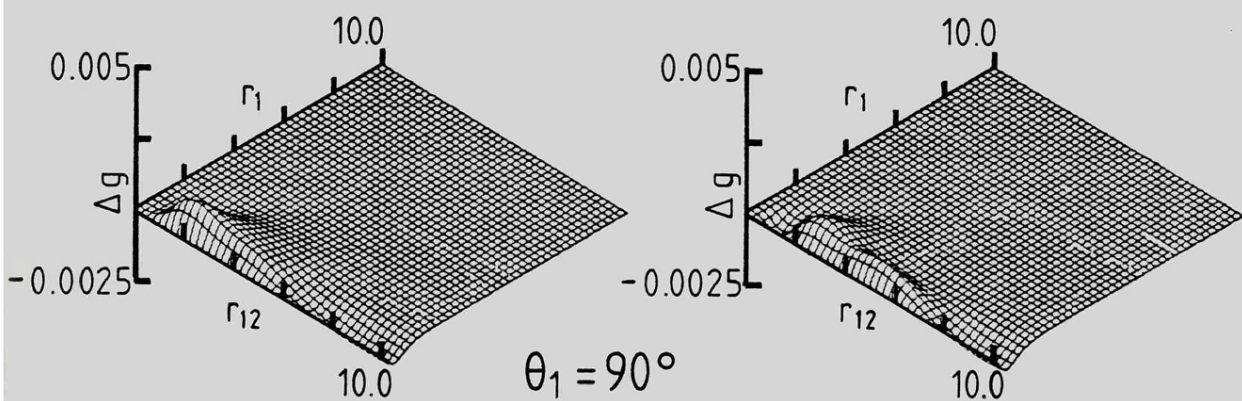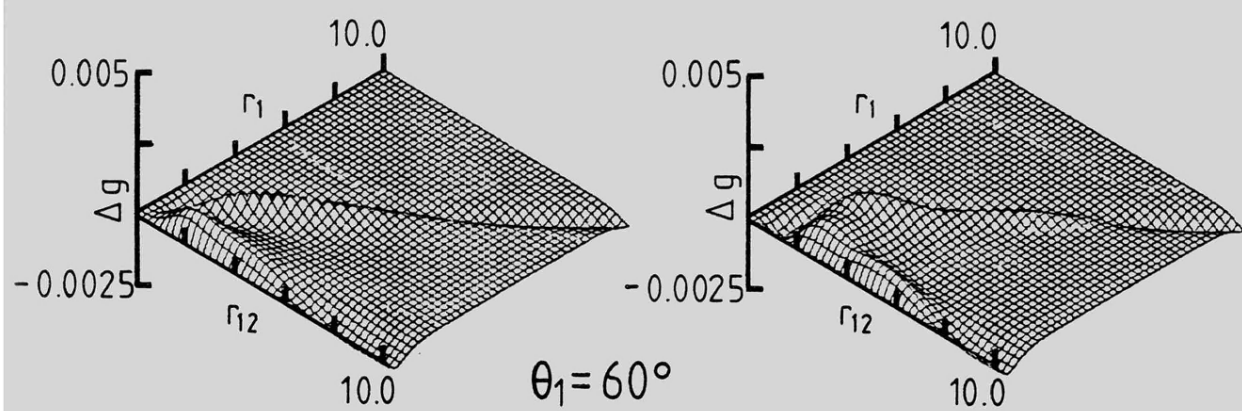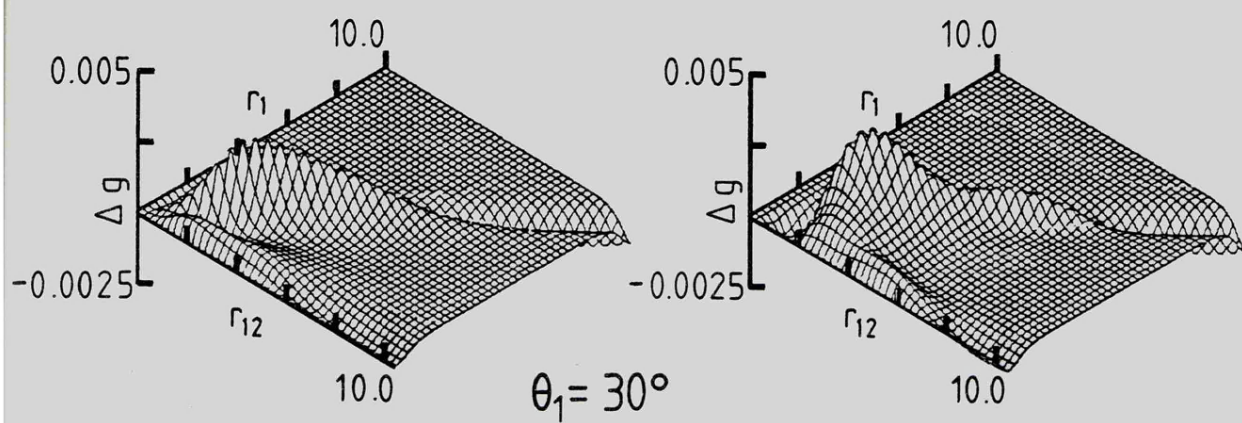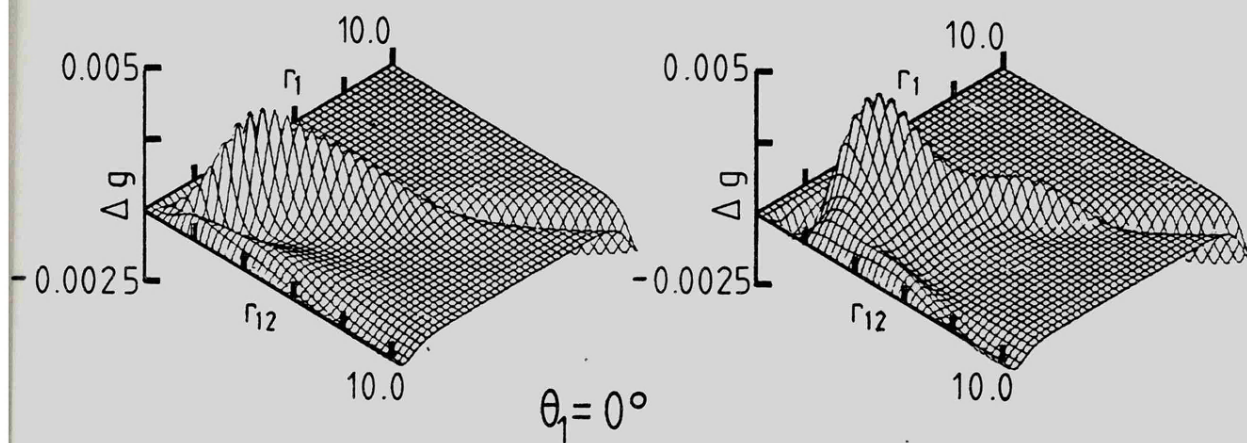
(a) $2\,^1P$ (b) $2\,^3P$

Figure (II.1.9)

The $D_1^{HF}(r_1)$ distributions for the (a) 2^1S and 2^3S and (b) 2^1P and 2^3P states of He.
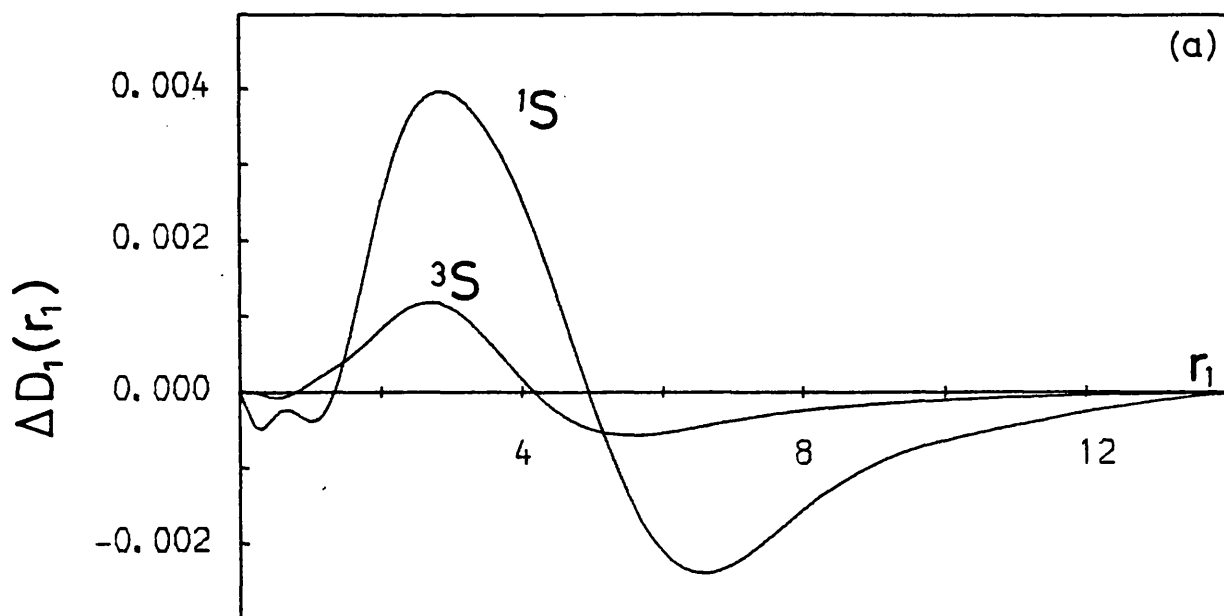
Figure (II.1.10)

The one-particle radial holes $\Delta D_1(r_1)$ for the

(a) 2^1S and 2^3S and (b) 2^1P and 2^3P states of He.
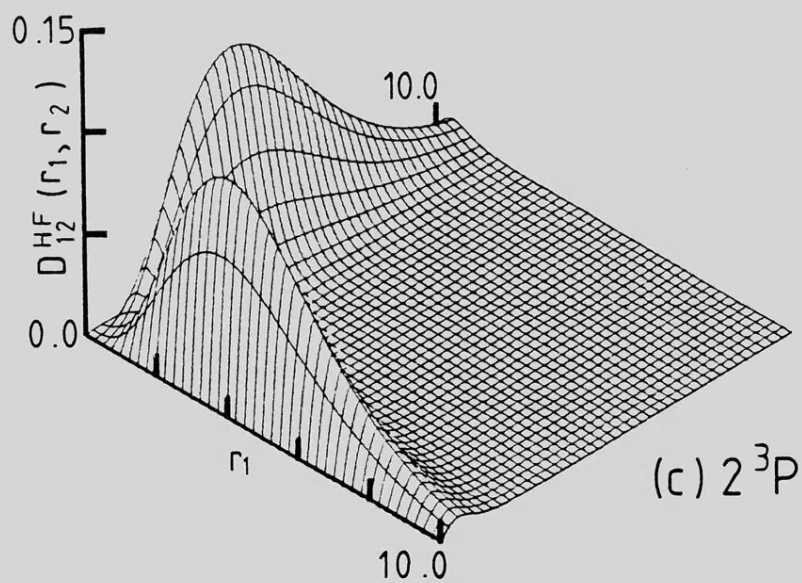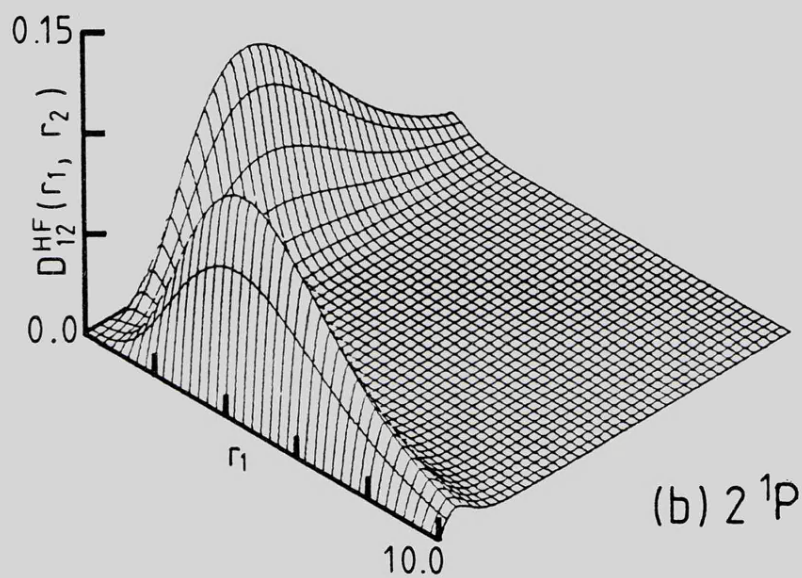
Figure (II.1.11)

The $D_{12}^{HF}(r_1, r_2)$ distributions for the
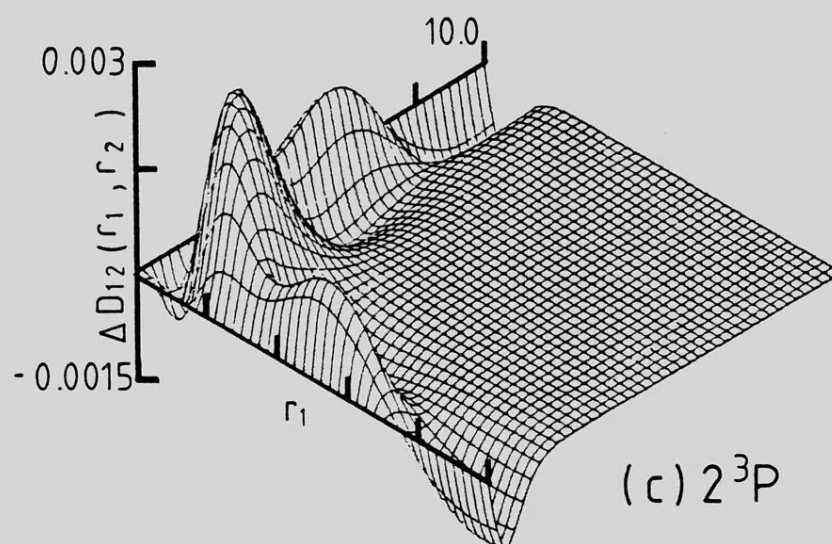
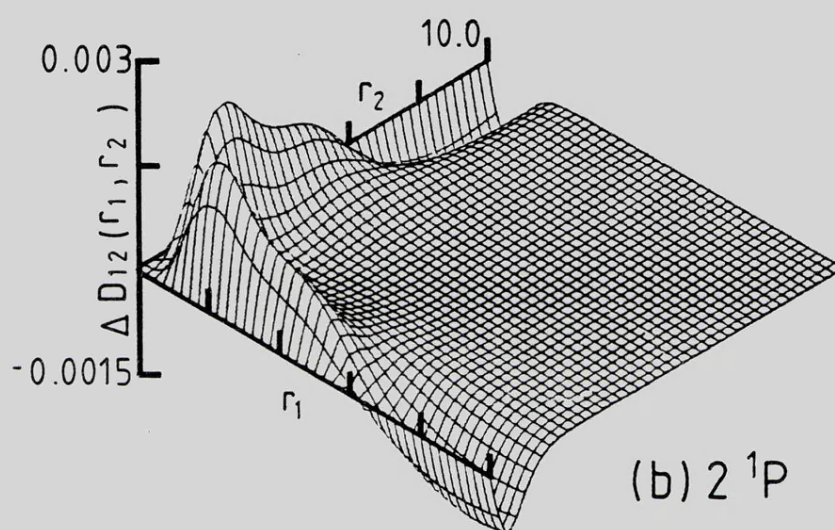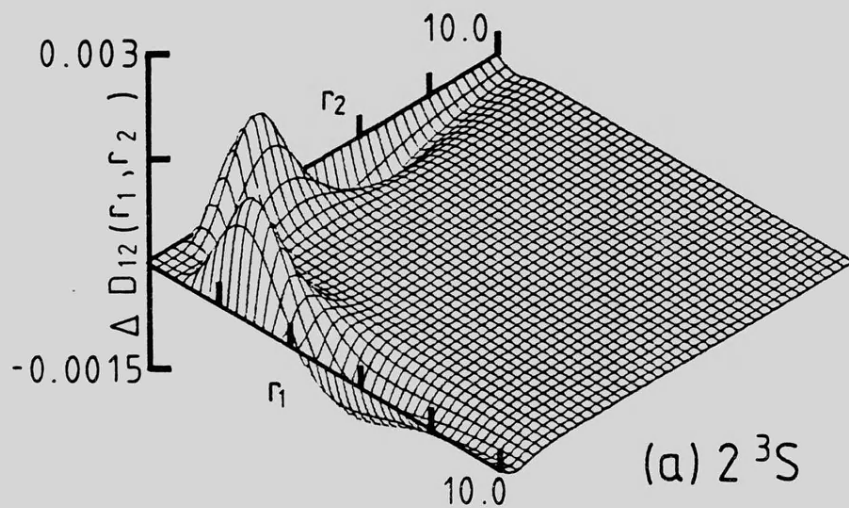(a) 2^3S, (b) 2^1P and (c) 2^3P states of He.

Figure (II.1.12)

The two-particle radial holes $\Delta D_{12}(r_1, r_2)$ for the
(a) 2^3S, (b) 2^1P and (c) 2^3P states of He.

State	Wavefunction		Number of Terms	Orbital Configuration Types	Energy	`Exact´ Energy
2^1S	Perkins	(P)	–	–	-2.14589	-2.14597
	Davidson	(D)	1 (HF)	ss	-2.14344	
2^3S	Tweed	(T)	32	ss/pp	-2.17516	-2.17523
	Tweed	(T)	48	ss/pp/dd	-2.17520	
	Weiss	(W)	19	ss/pp/dd	-2.17521	
	Davidson	(D)	1 (HF)	ss	-2.17425	
2^1P	Tweed	(T)	30	sp/pd	-2.12346	-2.12384
	Tweed	(T)	45	sp/pd/df	-2.12355	
	Davidson	(D)	1 (HF)	sp	-2.12246	
2^3P	Tweed	(T)	30	sp/pd	-2.13276	-2.13316
	Tweed	(T)	45	sp/pd/df	-2.13279	
	Davidson	(D)	1 (HF)	sp	-2.13143	

<u>Table (II.1.1)</u>

A summary of the wavefunctions used in the correlation analysis presented in Section (II). The `exact´ energy for each state was taken from Accad, Pekeris and Schiff[40]. Atomic units are used.

State	ϕ	$\langle r_{12}^{-1}\rangle$	$\langle r_{12}\rangle$	$\langle r_{12}^{2}\rangle$	$\sigma(r_{12})$	$Y(\%)$
$2^{1}S$	P^{*}	0.24950^{0}	0.52733^{1}	0.32330^{2}	0.21266^{1}	1.61
	$D(HF)$	0.24971^{0}	0.53340^{1}	0.33075^{2}	0.21503^{1}	$-$
$2^{3}S$	$T(32)$	0.26740^{0}	0.44478^{1}	0.23041^{2}	0.18049^{1}	0.38
	$T(48)$	0.26872^{0}	0.44470^{1}	0.23030^{2}	0.18040^{1}	0.41
	W	0.26810^{0}	0.44483^{1}	0.23095^{2}	0.18186^{1}	0.34
	$D(HF)$	0.26898^{0}	0.44506^{1}	0.23122^{2}	0.18205^{1}	$-$
$2^{1}P$	$T(30)$	0.24492^{0}	0.51311^{1}	0.31350^{2}	0.22411^{1}	0.97
	$T(45)$	0.24506^{0}	0.51256^{1}	0.31286^{2}	0.22392^{1}	1.05
	$D(HF)$	0.24365^{0}	0.51913^{1}	0.32262^{2}	0.23049^{1}	$-$
$2^{3}P$	$T(30)$	0.26716^{0}	0.46775^{1}	0.26199^{2}	0.20788^{1}	1.20
	$T(45)$	0.26718^{0}	0.46759^{1}	0.26181^{2}	0.20777^{1}	1.23
	$D(HF)$	0.26613^{0}	0.47433^{1}	0.27202^{2}	0.21686^{1}	$-$

* Taken from Boyd and Coulson[4]

Table (II.1.2)

Values of $\langle r_{12}^{n}\rangle$ when $n = -1$, $+1$ and $+2$, the standard deviation, $\sigma(r_{12})$, and Y, the percentage of $f(r_{12})$ redistributed by correlation, for the $2^{1}S$, $2^{3}S$, $2^{1}P$ and $2^{3}P$ states of He. The superscripts denote the power of ten by which each entry is to be multiplied.

State	ϕ	$\langle r_1^{-2} \rangle$	$\langle r_1^{-1} \rangle$	$\langle r_1 \rangle$	$\langle r_1^2 \rangle$	$\sigma(r_1)$
2^1S	P*	-	0.11353^1	0.29748^1	0.16106^2	0.26938^1
	D(HF)	0.38787^1	0.11344^1	0.30130^1	0.16538^2	0.27312^1
2^3S	T(32)	0.41686^1	0.11544^1	0.25507^1	0.11461^2	0.22259^1
	T(48)	0.41713^1	0.11548^1	0.25502^1	0.11456^2	0.22255^1
	W	0.41703^1	0.11546^1	0.25525^1	0.11491^2	0.22306^1
	D(HF)	0.41711^1	0.11543^1	0.25599^1	0.11561^2	0.22378^1
2^1P	T(30)	0.40421^1	0.11230^1	0.29089^1	0.15659^2	0.26828^1
	T(45)	0.40419^1	0.11230^1	0.29062^1	0.15628^2	0.26799^1
	D(HF)	0.40474^1	0.11220^1	0.29444^1	0.16153^2	0.27356^1
2^3P	T(30)	0.40139^1	0.11332^1	0.26645^1	0.13006^2	0.24302^1
	T(45)	0.40138^1	0.11332^1	0.26637^1	0.12996^2	0.24292^1
	D(HF)	0.40189^1	0.11320^1	0.27064^1	0.13560^2	0.24971^1

*Supplied by Boyd[41]

Table (II.1.3)

The one-particle radial expectation values $\langle r_1^n \rangle$ when $n = -2$, -1, $+1$ and $+2$, and the standard deviation, $\sigma(r_1)$, for the 2^1S, 2^3S, 2^1P and 2^3P states of He. The superscripts denote the power of ten by which each entry is to be multiplied.

State	ϕ	$\langle r_1^{-2} r_2^{-2} \rangle$	$\langle r_1^{-1} r_2^{-1} \rangle$	$\langle r_1 r_2 \rangle$	$\langle r_1^2 r_2^2 \rangle$
$2^1 S$ *	D(HF)	0.29492^1	0.55778^0	0.39790^1	0.24514^2
$2^3 S$	T(32)	0.78658^0	0.56047^0	0.32315^1	0.16366^2
	T(48)	0.78719^0	0.56073^0	0.32298^1	0.16348^2
	W	0.78730^0	0.56045^0	0.32337^1	0.16407^2
	D(HF)	0.77957^0	0.55812^0	0.32430^1	0.16489^2
$2^1 P$	T(30)	0.63612^0	0.48990^0	0.37997^1	0.22915^2
	T(45)	0.63771^0	0.49045^0	0.37959^1	0.22869^2
	D(HF)	0.61549^0	0.48333^0	0.38463^1	0.23521^2
$2^3 P$	T(30)	0.82586^0	0.55028^0	0.34459^1	0.19112^2
	T(45)	0.82642^0	0.55046^0	0.34447^1	0.19099^2
	D(HF)	0.83309^0	0.54643^0	0.35218^1	0.20177^2

* Results at the correlated level are not available.

Table (II.1.4)

The two-particle radial expectation values $\langle r_1^n r_2^n \rangle$ when n = -2, -1, +1 and +2, for the $2^1 S$, $2^3 S$, $2^1 P$ and $2^3 P$ states of He. The superscripts denote the power of ten by which each entry is to be multiplied.

State	ϕ	$\langle \underline{r}_1 \cdot \underline{r}_2 / r_1^2 r_2^2 \rangle$	$\langle \cos \theta_{12} \rangle$	$\langle \underline{r}_1 \cdot \underline{r}_2 \rangle$
2^1S	TS*	–	-0.14659^{-1}	–
	D(HF)	0.0	0.0	0.0
2^3S	T(32)	-0.70051^{-2}	-0.16025^{-1}	-0.59539^{-1}
	T(48)	-0.69532^{-2}	-0.15879^{-1}	-0.58908^{-1}
	W	-0.68971^{-2}	-0.15534^{-1}	-0.56237^{-1}
	D(HF)	0.0	0.0	0.0
2^1P	T(30)	0.11293^{-2}	-0.15153^{-2}	-0.15975^{-1}
	T(45)	0.12551^{-2}	-0.12691^{-2}	-0.15091^{-1}
	D(HF)	0.58804^{-2}	0.86393^{-2}	0.22367^{-1}
2^3P	T(30)	-0.21313^{-1}	-0.33050^{-1}	-0.94470^{-1}
	T(45)	-0.21290^{-1}	-0.32968^{-1}	-0.94056^{-1}
	D(HF)	-0.13345^{-1}	-0.17129^{-1}	-0.41018^{-1}

*Taken from Thakkar and Smith[42]

Table (II.1.5)

Values of $\langle \underline{r}_1 \cdot \underline{r}_2 / r_1^n r_2^n \rangle$ when n = 2, 1 and 0, for the 2^1S, 2^3S, 2^1P and 2^3P states of He. The superscripts denote the power of ten by which each entry is to be multiplied.

(II.2) MOMENTUM-SPACE CORRELATION EFFECTS IN THE

2^3S, 2^1P AND 2^3P STATES OF HELIUM

CHAPTER (II.2.1)

MOMENTUM SPACE

The primary effort in quantum-mechanical calculations is directed towards the determination of the appropriate wavefunction for a given system. Usually, this function is defined with respect to the positions of the constituent particles of the system, but such a representation is by no means unique. For example, given an N-electron atom, it is equally possible to discuss the behaviour of the electrons in terms of their momenta. Instead of describing the electrons in a space whose coordinates are the distances from some fixed spatial origin (usually a nucleus), we can consider them in a space where the coordinates are the components of momentum of an electron, and the origin corresponds to a particle at rest. More formally, we can consider the problem of evaluating the system wavefunction not in position space but in momentum space. Recently, a number of studies have shown that momentum-space calculations can provide valuable new insight into the effects of electron correlation in atoms and molecules. A full appreciation of the advantages afforded by this new investigative technique requires at least some knowledge of the history of the determination of electron momentum distributions. Accordingly, we present here a relatively brief, and necessarily simplified, account of a story which spans more than three quarters of a century. (For a more detailed description of the curious and disjointed historical development of this subject, see the excellent review by Williams[43]).

In a series of γ-ray scattering experiments conducted in 1904, Eve[44] found that for a number of different target materials, the scattered radiation was much less penetrating (softer) than the original beam. At the time, not only the nature of the scattering process, but even the very nature of γ-rays was barely understood, and Eve was unable to provide an explanation of his observations. Over the next few years, Eve's findings were investigated by a number of other workers, most notably Bragg[45], Florance[46] and Gray[47], and following the invention of the Bragg spectrometer and the Coolidge X-ray tube, the experiments were extended to X-rays. During one such experiment performed in 1920, Gray[48] established that when X-rays are scattered by matter, they experience an increase in wavelength; he also found that the magnitude of the increase is dependent on the scattering angle but independent of the nature of the scatterer. An explanation of this phenomenon, together with experimental evidence, was provided by Compton[49] in 1922; a more rigorous mathematical treatment was published in the following year[50]. Compton's formulation of the scattering process was expressed in terms of the conservation of energy and linear momentum during the inelastic scattering of a photon by an electron. The theory, which considers the electron to be initially free and stationary, predicts that a wavelength λ will experience an increase $\Delta\lambda$ upon scattering, defined by

$$\Delta\lambda = (4\pi/c) \sin^2(\varphi/2) \quad , \qquad \qquad \text{(II.2.1)}$$

where φ is the angle of scattering and c is the velocity of light (atomic units are used). Compton continued to pursue his experimental investigations and, in 1923[51], noted that the 'Compton scattered' line in his spectrum appeared to be broader than could be explained by the known inhomogeneity in the scattering angle or in the imperfect resolution of the spectrometer. The following year, Jauncey[52] explained the broadening by pointing out that electrons are <u>not</u> stationary, and that the magnitude of the Compton shift should depend on the initial momentum of the scattering electron. In 1929, Dumond[53] showed that the effect of the electron's motion on the Compton scattering process could be described as a Doppler broadening process which is independent of the precise atomic model chosen for the analysis. Mathematically, the result of Dumond's work was to introduce a second term into Compton's scattering equation (Equation (II.2.1)), thus:

$$\Delta\lambda = \lambda' - \lambda = (4\pi/c) \sin^2(\varphi/2) - (2\lambda p_z/c) \sin(\varphi/2) \ , \quad (II.2.2)$$

where p_z is the component of the electron momentum along the scattering vector. The interpretation of Equation (II.2.2) is that photons emerging from the scattering process with a wavelength λ' will have been scattered by electrons whose z-component of momentum is p_z. Since it is reasonable to assume that the probability of a photon interacting with any particular electron is independent of the value of p_z for that electron, the intensity of scattered radiation at wavelength λ' should be proportional to the distribution function $J(p_z)$ for the momentum component p_z. For an array

of electrons with a momentum distribution $\varrho(\underline{p})$ = $\varrho(p_x, p_y, p_z)$, the probability that an electron has a particular value of p_z is given by

$$J(p_z) = \iint \varrho(p_x, p_y, p_z) \, dp_x \, dp_y \quad . \tag{II.2.3}$$

This quantity is known as the <u>directional Compton profile</u>, and is simply the projection of the three-dimensional electron momentum density onto the scattering direction. Together, Equations (II.2.2) and (II.2.3) represent a method by which direct access to the full momentum distributions of electrons in atoms and molecules may be achieved. To obtain such a distribution one need only, in principle at least, measure the spectrum of the scattered radiation, relate the wavelengths to momenta and then invert Equation (II.2.3). The complexity of this inversion process depends to a large extent on the physical state of the sample being examined.

The problem of inverting Equation (II.2.3) can be avoided completely by calculating $\varrho(\underline{p})$ and then comparing the <u>theoretical</u> Compton profile derived from it with the <u>measured</u> line shape. The momentum density $\varrho(\underline{p})$ is, of course, directly related to the momentum-space wavefunction of the system, and it is appropriate at this point to consider how such a function may be obtained.

There are two distinct approaches to the determination of momentum-space wavefunctions. One can either formulate, and attempt to solve, the Schrödinger Equation <u>directly</u> in momentum space, or one can solve it at some level of

approximation in position space and then <u>transform</u> the results to momentum space. Despite the complementarity which exists between the position and momentum representations, there is a striking asymmetry between the relative degrees of success obtained using these two methods. We shall consider the 'direct' approach first.

For the one-dimensional problem, the language of classical mechanics may be transformed into that of the quantum-mechanical position representation by substitution of the multiplicative operator 'x' for position and the differential operator '-i ∂/∂x' for momentum. In a similar manner, we can transfer from classical mechanics to the momentum representation of quantum mechanics by substituting 'i ∂/∂p' for position and 'p' for momentum; in this case the Schrödinger Equation takes the form of a differential equation in momentum space. Unfortunately, the potentials encountered in atomic and molecular systems are generally dependent on position rather than momentum, and this approach has consequently met with very little success.[1] An alternative 'direct' method of obtaining wavefunctions in momentum space is to perform a Fourier transform of the complete Schrödinger Equation, which converts it from a differential equation in position space to an <u>integral</u> equation in momentum space. For the one-particle problem we find

---

[1]This method has, however, been used by Hylleraas[54] to obtain the momentum space wavefunctions for the discrete spectrum of hydrogen.

$$(p^2/2) \, \Psi(\underline{p}) + [u(\underline{p}) - E]\Psi(\underline{p}) = 0 \qquad\qquad (II.2.4)$$

where $\Psi(\underline{p})$ is the wavefunction and $u(\underline{p})$ is related to the Fourier transform of the position-space potential energy term $V(\underline{r})$. For the case of the hydrogen atom, Equation (II.2.4) has been solved exactly by Fock[55], but for more complicated systems, the results have been disappointing. In 1945, Svartholm[56] developed an iterative method for solving integral equations in momentum space, while working on the problem of evaluating the binding energies of light nuclei. Four years later, McWeeny and Coulson[57] attempted to use the same technique to solve the N-electron analogue of Equation (II.2.4) for a chemical system, but found that the calculation of successive iterants was exceedingly difficult. Starting from a simple product wavefunction for the helium atom they were able to obtain a first, but not a second, iterative correction; similarly disappointing results were obtained by McWeeny[58] for the hydrogen molecular ion and the hydrogen molecule. As a result of the computational difficulties that they encountered, McWeeny and Coulson concluded that their method was impracticable for larger systems. In 1951 a related, but more general, approach to the solution of Equation (II.2.4) was proposed by Levy[59]. Unfortunately, his treatment, like the iterative technique developed by Salpeter[60] at about the same time, appears useful only for problems involving a single particle experiencing a central potential; such a limitation is clearly more restrictive in chemical problems than it is in those problems of nuclear

physics to which these methods have been applied with some success[61].

In view of the difficulties experienced in these varied attempts to solve the Schrödinger Equation directly in momentum space, it is fortunate indeed that a second, considerably easier, approach to the problem exists. The basis of this alternative method is the expansion of the single-particle position-space wavefunction $\phi(\underline{r})$ in terms of the continuous set of momentum eigenfunctions, $u(\underline{r}) = (2\pi)^{-3/2} e^{i\underline{p}\cdot\underline{r}}$, such that

$$\phi(\underline{r}) = (2\pi)^{-3/2} \int \Psi(\underline{p}) e^{i\underline{p}\cdot\underline{r}} d\underline{p} \quad , \qquad (II.2.5)$$

where the integral is understood to be performed over all possible values of $\underline{p}$ (that is, over all momentum space). The expansion coefficients $\Psi(\underline{p})$ are a continuous function of $\underline{p}$ and are given by the projection of the eigenfunction $u(\underline{r})$ on the state function $\phi(\underline{r})$. We have then

$$\Psi(\underline{p}) = (2\pi)^{-3/2} \int \phi(\underline{r}) e^{-i\underline{p}\cdot\underline{r}} d\underline{r} \quad , \qquad (II.2.6)$$

where, in this instance, the integral is performed over all position-space. Examination of Equations (II.2.5) and (II.2.6) reveals that $\phi(\underline{r})$ and $\Psi(\underline{p})$ are Fourier transforms of one another, and it is obvious that $\Psi(\underline{p})$ is the momentum-space analogue of the original position-space wavefunction $\phi(\underline{r})$. The application of transformation theory to the problems of quantum mechanics was considered first by Dirac[62], and for that reason, Equations (II.2.5) and

(II.2.6) are known as 'Dirac transforms'. For an N-electron atomic system, Equation (II.2.11) takes the form

$$\Psi(\underline{p}_1,\underline{p}_2,\ldots,\underline{p}_N) = (2\pi)^{-3N/2} \int \Phi(\underline{r}_1,\underline{r}_2,\ldots,\underline{r}_N) \times$$

$$\prod_{j=1,N} e^{-i\underline{p}_j\cdot\underline{r}_j} \, d\underline{r}_1 d\underline{r}_2\ldots d\underline{r}_N \quad . \quad (II.2.7)$$

Perhaps the most attractive feature of the transformation defined by Equation (II.2.7) is that it preserves the _form_ of the wavefunction. Thus, if $\Phi(\underline{r}_1,\underline{r}_2,\ldots,\underline{r}_N)$ is a single Slater determinant or a multiconfiguration sum of such terms, each involving a number of orbitals $\varphi(\underline{r})$, then the momentum space wavefunction $\Psi(\underline{p}_1,\underline{p}_2,\ldots,\underline{p}_N)$ is obtained by _replacing_ the individual position space orbitals $\varphi(\underline{r})$ by their momentum-space counterparts, $\psi(\underline{p})$. Interestingly, it is found that for position-space orbitals of the form

$$\varphi(\underline{r}) = f_{nl}(r) \, Y_{lm}(\theta_r,\varphi_r) \quad ,$$

where θ_r and φ_r are the angular variables in position space, the angular dependence of the corresponding momentum-space orbitals is the same, so that

$$\psi(\underline{p}) = u_{nl}(p) \, Y_{lm}(\theta_p,\varphi_p) \quad ,$$

where θ_p and φ_p are the angular variables in momentum space. Furthermore, Parseval's theorem[63] may be used to show that normalisation and overlap integrals are also invariant under the transformation. In a comprehensive study, Kaijser and Smith[64] have derived the $u_{nl}(p)$ terms corresponding to

82

those forms of $f_{nl}(r)$ most commonly used in the construction of atomic and molecular wavefunctions.

Considering the vast array of methods available for the computation of wavefunctions in position space, it is hardly surprising that the Dirac transform approach to momentum-space wavefunctions has been far more widely applied and considerably more successful than the ´direct´ methods considered earlier. Within months of Dumond´s[53] explanation of the Compton scattering process, Podolsky and Pauling[65] used Equation (II.2.7) to calculate the momentum wavefunctions of the hydrogen atom. However, the first quantitative comparisons between theory and experiment did not occur until 1937, when Hicks[66] calculated the Compton profiles of helium and molecular hydrogen from the momentum-space transforms of a number of different wavefunctions. The measurements of Dumond and Kirkpatrick[67] on helium were in excellent agreement with Hicks´s predictions, but the hydrogen profile obtained by Kirkpatrick and Dumond[68] was considerably broader than the calculated one -- a discrepancy which seems to have resulted from deficiencies in the wavefunction.

The years 1941 and 1942 saw a new and important development in the theoretical study of electron momentum distributions. In a series of interesting and innovative analyses, Coulson and Duncanson[69] examined the changes which occur in momentum distributions when a chemical bond is formed. The fundamental principle on which their investigations were largely based is most conveniently

explained with reference to the Gaussian or 'normal' distribution function, defined by

$$g(x) = (2\pi\sigma^2)^{-1/2} \exp(-x^2/2\sigma^2) \quad .$$

It is found that $g(x)$ has a full width at half maximum (FWHM)[2] of $2\sqrt{(2\log_e 2)}\sigma$. In contrast to this, the Fourier transform of $g(x)$ has the form

$$G(k) = (2\pi/\sigma^2)^{-1/2} \exp(-k^2\sigma^2/2) \quad ,$$

which has a FWHM of $2\sqrt{(2\log_e 2)}\sigma^{-1}$. Although the similarity of the analytical forms for $g(x)$ and $G(k)$ is a feature peculiar to this particular distribution, the qualitative conclusion is completely general: the Fourier (Dirac) transform of a narrow function is a broad one and _vice versa_. In chemical terms, this implies that inner orbitals, which are usually highly localised, will have broad, relatively flat momentum distributions, while the more diffuse outer orbitals will be sharply peaked in momentum space. A study of Compton profiles reveals that the principal features of the line shape are effectively governed by the behaviour of the _outer_ electrons; the core electrons merely provide a relatively slowly varying background contribution. As a result, electron momentum distributions provide an effective means of studying the

---

[2]For an even function $f(x)$ possessing a single maximum at $x=0$ such that $f(x=0) = f_o$, the full width at half maximum is defined as $2x_H$, where $f(x=x_H) = (f_o/2)$.

behaviour of the valence electrons, which are, of course, precisely those electrons which are responsible for chemical bonding. By studying simple systems like H_2 and H_2^+ , as well as a series of hydro-carbon gases, Coulson and Duncanson derived considerable insight into the chemically significant aspects of electron momentum distributions. Interestingly, they also found that improvements in the wavefunction often resulted in a broader calculated Compton profile and momentum distribution.

With the exception of the aforementioned attempts by McWeeny and Coulson to calculate wavefunctions directly in momentum space, the next few years saw relatively little interest in the theoretical study of electron momentum distributions. After this period of almost complete inactivity on the part of theoreticians and experimentalists alike, the mid-1960s then saw a resurgence of interest in the subject. With this revival of interest came changes in technology which brought, in turn, significant improvements in experimental accuracy. Taking advantage of this increased accuracy, the experimentalists began to point to the shortcomings of the theory as the reason for the discrepancies between the measured and calculated momentum distributions. In particular, Weiss[70] suggested that electron correlation effects could account for the fact that experimental Compton profiles frequently display a greater intensity at larger momenta than do those line shapes calculated from Self Consistent Field or more approximate wavefunctions. Physically, it was argued that electrons must speed up to avoid each other, thereby giving rise to

the enhancement in the high momentum region of the profile. Of course, a converse argument could be that electron correlation should lead to a more diffuse charge cloud which, as a consequence of the Fourier transformation, would predict a _narrower_ momentum density and Compton profile. Since some experiments[71] did give results which supported this latter argument, the situation regarding correlation was rather confused.

In an attempt to clarify matters, Benesch, Smith and Brown[72-77] used an elegant formalism involving the natural orbital representation of the momentum density matrix to calculate the electron momentum distributions of He, Li^+, Li, Be, H_2 and Ne. They concluded that correlation effects produce a significant improvement in the description of open-shell systems, but make only very minor contributions to closed-shell systems. With regard to Compton profiles, their results showed that, in general, correlation produces _no_ high momentum tail. In 1976, Ahlberg and Lindner[78] examined the effects of Fermi correlation in Be, Ne, Ar and Zn. They concluded that the rules governing this type of correlation in momentum space are the same as in position space. Two years later, Banyard and Moore[79] investigated the effects of electron correlation on the Compton profiles of the iso-electronic systems H^-, He and Li^+. Contrary to the findings of Benesch _et al_, they found that correlation _does_ cause an increase in the probability that an electron has a high momentum. In the same study, Banyard and Moore calculated a number of momentum expectation values and correlation coefficients.[80] In contrast to the findings

of an earlier _position-space_ analysis[81], they discovered that for these systems, the radial and angular components of correlation create opposite trends in momentum space; radial correlation causes a negative effect (as in position space), whereas angular correlation causes a positive effect and therefore tends to _align_ the momentum vectors.

In 1978, Banyard and Reed[35] defined the momentum-space Coulomb 'shift', $\Delta f(p_{12})$, by analogy with Coulson and Neilson's[11] definition of the Coulomb hole in position space. For the ground states of H^-, He and Li^+, Banyard and Reed found that, relative to the HF description, radial correlation increases the probability of a large momentum separation $p_{12} = |\underline{p}_1 - \underline{p}_2|$ and decreases the occurrence of smaller values of p_{12}. Conversely, the effect of introducing angular-based configurations is to produce, on average, an enhanced alignment between the momentum vectors $\underline{p}_1$ and $\underline{p}_2$. As anticipated by Moore[82], the two types of correlation combine to produce changes in $f(p_{12})$ which are considerably more complex than those which arise in the corresponding position-space function $f(r_{12})$. In 1979, Doggett[83] examined the distribution of electron momenta in the H_2, LiH and BH molecules. By analogy with an earlier position-space analysis[84], he showed that partial integration of the two-electron momentum density functions for these systems yields longitudinal and transverse distribution functions which can be used to construct coresponding 'holes' in momentum space. More recently, Mobbs and Banyard[85] have studied momentum-space correlation effects in Be. To examine the Coulomb shift in

specific electronic shells, they used the Many-Electron Theory of Sinanoglu[86] to partition the two-particle density-difference function from which $\Delta f(p_{12})$ is calculated. In keeping with the results of Banyard and Reed[35], they found that the structure of the Coulomb shift in any given shell reflects the nature of the dominant correlation component for that shell.

The complementary nature of the information obtained from the position and momentum representations suggests that a full understanding of electron correlation effects requires the analysis to be performed in both spaces. In accordance with this, we have extended our earlier analysis of correlation in excited states of helium by examining the corresponding problem in momentum space. Specifically, we have studied momentum-space correlation effects in the 2^3S, 2^1P and 2^3P states of helium. In Section (II.1), the position-space results for 2^1S provided by Boyd[87] were based on Hylleraas-type wavefunctions, which contain explicitly the interelectronic coordinate r_{12}. For such functions, the transformation defined by Equation (II.2.7) is extremely difficult to evaluate, and in 1979, Benesch and Thomas[88] concluded that Hylleraas-type wavefunctions are not suited to momentum-space calculations. As a result, no attempt has been made to study the 2^1S state in momentum space.

In Chapter (II.1.2) we make brief comments regarding the Dirac transformation of the relevant Hartree-Fock and correlated wavefunctions, and also discuss the methods by

which we have analysed correlation effects in momentum space. Atomic units are used throughout this work.

CHAPTER (II.2.2)

WAVEFUNCTIONS AND CORRELATION PROPERTIES

IN MOMENTUM SPACE

To study momentum-space correlation effects in the 2^3S, 2^1P and 2^3P states of helium we have used the same correlated and Hartree-Fock wavefunctions that were employed in the position-space analysis presented in Section (II.1) (see Chapter (II.1.2) and Table (II.1.1)). In each case, the momentum-space function was obtained by evaluating the Dirac transform of each orbital or primitive function used in the formation of the position-space wavefunction.

The Weiss[17] wavefunction for the 2^3S state is constructed from a basis set of Slater-type orbitals; the method by which these orbitals were converted to momentum space has since been described in some detail by Reed[23], and we merely quote the result here. A position-space Slater-type orbital having the form

$$u_{n,1,m}(r,\theta_r,\varphi_r) = N \; r^{n-1} \; e^{-\alpha r} \; Y_{1,m}(\theta_r,\varphi_r) \; , \quad (II.2.8a)$$

where N is the normalisation constant, transforms to the momentum-space function

$$v_{n,1,m}(p,\theta_p,\varphi_p) = (-1)^n \; N \; (2pi)^1 \; (1!) \; \sqrt{(2/\pi)} \; \times$$

$$\partial^{n-1}/\alpha^{n-1} [(\alpha^2+p^2)^{-(1+1)}] Y_{l,m}(\theta_p,\phi_p) \quad (II.2.8b)$$

In this instance, subscripts on the angular arguments

emphasize the different spaces in which the angles are
measured. After trivial changes of variables, the Tweed[15]
orbitals and the primitive terms used to construct the
Davidson[19] Hartree-Fock orbitals were transformed by
similar techniques.

The isomorphism of the transform which links
Equation (II.2.8a) to Equation (II.2.8b) implies that the
investigation of correlation effects in momentum space may
be accomplished by using the same analytical techniques that
were used in position space. Accordingly, we have studied a
number of radial, angular and interparticle distribution
functions, each of which is defined by analogy with its
position-space counterpart. Since the definitions and
properties of the position-space distributions were
considered in some detail in Chapter (II.1.3), we present
here only a comparatively brief description of the
corresponding momentum functions. To avoid the confusion of
introducing a complete new nomenclature for the
momentum-space analysis, we shall adopt the convention that,
unless otherwise stated, the space to which a given
distribution function applies is defined by the argument(s)
of that function. Thus, for example, $D_1(r_1)$ is understood
to be a one-particle radial distribution function in
position space, while $D_1(p_1)$ is the analogous function in
momentum space. As before, it is assumed that integrations
are performed over all possible values of the specified
variables.

Given an N-electron momentum-space wavefunction

$\Psi(\underline{q}_1, \underline{q}_2 \cdots \underline{q}_n)$, where $\underline{q}_i$ denotes the collective momentum-space $\underline{p}_i$ and spin $\underline{\sigma}_i$ coordinates of the i'th electron and Ψ is normalised to unity, we can define the spinless one- and two-particle momentum distributions $\varrho_i(\underline{p}_i)$ and $\varrho_{ij}(\underline{p}_i, \underline{p}_j)$ by

$$\varrho_i(\underline{p}_i) = \int \Psi^*(\underline{q}_1, \underline{q}_2 \cdots \underline{q}_n) \; \Psi(\underline{q}_1, \underline{q}_2 \cdots \underline{q}_n) \times$$

$$d\underline{p}_1 d\underline{p}_2 \cdots d\underline{p}_{i-1} d\underline{p}_{i+1} \cdots d\underline{p}_n \; d\underline{\sigma}_1 d\underline{\sigma}_2 \cdots d\underline{\sigma}_i \cdots d\underline{\sigma}_n \qquad (II.2.9)$$

and

$$\varrho_{ij}(\underline{p}_i, \underline{p}_j) = \int \Psi^*(\underline{q}_1, \underline{q}_2 \cdots \underline{q}_n) \; \Psi(\underline{q}_1, \underline{q}_2 \cdots \underline{q}_n) \times$$

$$d\underline{p}_1 d\underline{p}_2 \cdots d\underline{p}_{i-1} d\underline{p}_{i+1} \cdots d\underline{p}_{j-1} d\underline{p}_{j+1} \cdots d\underline{p}_n \; d\underline{\sigma}_1 d\underline{\sigma}_2 \cdots d\underline{\sigma}_i \cdots d\underline{\sigma}_j \cdots d\underline{\sigma}_n.$$

$$(II.2.10)$$

Both $\varrho_i(\underline{p}_i)$ and $\varrho_{ij}(\underline{p}_i, \underline{p}_j)$ are normalised to unity; $\varrho_i(\underline{p}_i)$ is the probability density of finding the i'th electron with a momentum $\underline{p}_i$, while $\varrho_{ij}(\underline{p}_i, \underline{p}_j)$ is the probability of finding, simultaneously, a pair of electrons i and j with momenta $\underline{p}_i$ and $\underline{p}_j$.

Despite the similarities between Equations (II.2.9) and (II.1.6) and Equations (II.2.10) and (II.1.7), there is an important practical difference between the subsequent derivations of distribution functions in the two spaces. In <u>position space</u>, the radial components of atomic orbitals are always real, and hence the complex conjugation of the total wavefunction affects only the angular term of each orbital.

Inspection of Equation (II.2.8) reveals that in momentum space, the radial term can be imaginary and therefore the conjugation must be applied to each <u>complete</u> orbital. One further point of practical interest makes use of the fact, noted earlier, that the Dirac transformation leaves overlap integrals unchanged; in deriving Equation (II.1.9) from Equation (II.1.10), the overlap integrals which arise have precisely the same values that were calculated in the position-space analysis, and need not, therefore, be evaluated again in momentum space.

Radial Properties

To investigate the changes in the radial distribution, we have studied the joint radial momentum density, $D_{12}(p_1, p_2)$, defined by

$$D_{12}(p_1, p_2) = \int \rho_{12}(\underline{p}_1, \underline{p}_2) p_1^2 p_2^2 \, d\Omega_1 d\Omega_2 , \qquad (II.2.11)$$

and the associated density difference $\Delta D_{12}(p_1, p_2)$, defined by

$$\Delta D_{12}(p_1, p_2) = D_{12}^{corr}(p_1, p_2) - D_{12}^{HF}(p_1, p_2) . \qquad (II.2.12)$$

In Equation (II.2.11) Ω_1 and Ω_2 refer to the collective angular variables of electrons 1 and 2. We have also calculated the expectation values $\langle p_1^n p_2^n \rangle$ defined by

$$\langle p_1^n p_2^n \rangle = \int D_{12}(p_1, p_2) \, p_1^n p_2^n dp_1 dp_2 \qquad (II.2.13)$$

for $n = -2, -1, 0, +1$ and $+2$. As a result of the form of

the momentum-space orbitals, the integrations occurring in Equation (II.2.13) were evaluated numerically by computer; once again, the expectation value $\langle p_1^0 p_2^0 \rangle$ was a valuable check on the accuracy of the integration techniques.

Although one-particle densities and expectation values are less sensitive to correlation than two-particle properties, they are, nevertheless, conceptually easier to visualise. Accordingly, we have studied the one-particle radial momentum density, $D_1(p_1)$ defined by

$$D_1(p_1) = \int \varrho_1(\underline{p}_1) \, p_1^2 \, d\Omega_1 \quad , \qquad (II.2.14)$$

and the associated 'radial shift' $\Delta D_1(p_1)$ defined by

$$\Delta D_1(p_1) = D_1^{corr}(p_1) - D_1^{HF}(p_1) \quad . \qquad (II.2.15)$$

For each wavefunction a number of one-particle radial expectation values $\langle p_1^n \rangle$ have also been obtained using

$$\langle p_1^n \rangle = \int D_1(p_1) p_1^n dp_1 \qquad (II.2.16)$$

with $n = -2, -1, 0, +1,$ and $+2$. Expectation values for both electrons are defined by

$$\langle p^n \rangle = \langle p_1^n \rangle + \langle p_2^n \rangle = \int D_1(p_1) p_1^n dp_1 + \int D_2(p_2) p_2^n dp_2$$

$$= 2\int D_i(p_i) p_i^n dp_i \quad . \qquad (II.2.17)$$

Like their position-space counterparts, the $\langle p^n \rangle$ values are

of some practical importance. It may be shown[89] that $\langle p^{-1} \rangle$ is equal to twice the maximum height of the spherically-averaged Compton profile, while for n=0, Equation (II.2.17) is simply equal to the number of electrons in the system. Epstein[90] believes that it may be possible to relate $\langle p \rangle$ to a molecular property such as the nuclear magnetic resonance spectrum, but such a connection has yet to be established. The expectation value $\langle p^2 \rangle$ is simply twice the kinetic energy of the system when expressed in atomic units.

It is interesting to note that it may be shown[89] that

$$\langle p^n \rangle = 2(n+1) \int_0^{\infty} q^n J(q) dq \quad , \qquad (II.2.18)$$

where $J(q)$ is the spherical average of the directional Compton profile, $J(p_z)$. In 1973, Epstein[91] investigated the possibility of using Equation (II.2.18) to obtain $\langle p^n \rangle$ values from _experimental_ Compton profiles. He considered both the effects of a finite momentum range[1] and of experimental error, and concluded that, although values of $\langle p^0 \rangle$ could easily be obtained under the standard experimental conditions of the time, reasonably accurate determination of $\langle p \rangle$ stood at the limit of available techniques. The accurate evaluation of $\langle p^2 \rangle$ (and hence, by the virial theorem, the total energy of the system) by Compton scattering experiments required vast improvements in experimental accuracy at high values of q, -- an opinion borne out by Gadre and Narasimhan[92], who in 1975 attempted

---

[1]The profile is only measured to some finite q^{max}.

to use experimental Compton profiles to evaluate the total energies of He, Ne, H_2, N_2 and O_2 with only limited success. However, since 1976, a number of improvements in experimental accuracy have taken place, thereby increasing the reliability of experimental data to the point where useful estimates of the energy might be obtained.

Angular Properties

To study the effects of correlation on the angular distribution of the electron momenta, we have evaluated the expectation values defined by

$$\langle \underline{p}_1 \cdot \underline{p}_2 / p_1^n p_2^n \rangle = \int \varrho_{12}(\underline{p}_1, \underline{p}_2)(\underline{p}_1 \cdot \underline{p}_2 / p_1^n p_2^n) \, d\underline{p}_1 \, d\underline{p}_2 \qquad (II.2.19)$$

for $n = 0$, $+1$ and $+2$, at both the correlated and Hartree-Fock levels. The quantity $\langle \underline{p}_1 \cdot \underline{p}_2 \rangle$ is of some practical importance because, except for a constant factor, it is the so-called mass-polarisation correction to the total energy[93].

To obtain additional insight into the angular effects of correlation momentum space, we have examined the distribution function $P(\gamma)$, defined by

$$P(\gamma) = \int \varrho_{12}(\underline{p}_1, \underline{p}_2) \, d\underline{p}_1 \cdot d\underline{p}_2 / d\gamma \quad , \qquad (II.2.20)$$

and the `angular shift' $\Delta P(\gamma)$, defined by

$$\Delta P(\gamma) = P^{corr}(\gamma) - P^{HF}(\gamma) \quad , \qquad (II.2.21)$$

where γ is the angle between the momentum vectors of the two electrons and $P(\gamma)$ is evaluated at the correlated and HF levels, respectively. The definition of $P(\gamma)$ in Equation (II.2.20) is broadly similar to that of the distribution function $p(\theta_{12})$ used by Ellis[7] in his study of position-space 'angular holes'. However, it should be noted that the definition of $P(\gamma)$ includes the factor 'sin(γ)', so that the normalisation of $P(\gamma)$ is expressed by

$$\int P(\gamma) \, d\gamma = 1, \qquad (II.2.22)$$

whereas Ellis arbitrarily defined $p(\theta_{12})$ such that

$$\int p(\theta_{12}) \, \sin \theta_{12} \, d\theta_{12} = (1/2\pi) \quad .$$

In the present work, the change in the average relative angular orientation of the electron momentum vectors was obtained, for each state, by calculating the expectation value $\langle \gamma \rangle$, defined by

$$\langle \gamma \rangle = \int P(\gamma) \, \gamma \, d\gamma, \qquad (II.2.23)$$

at both the correlated and Hartree-Fock level. It is interesting to note that for n=1, Equation (II.2.19) yields the expectation value $\langle \cos\gamma \rangle$; this quantity can also be obtained from

$$\langle \cos\gamma \rangle = \int P(\gamma) \, \cos\gamma \, d\gamma, \qquad (II.2.24)$$

which provides yet another check on the consistency of the

results obtained.

Interparticle Properties

Following Banyard and Reed[35], we define the interparticle momentum distribution $f(p_{12})$ by

$$f(p_{12}) = \int \varrho_{12}(\underline{p}_1, \underline{p}_2) \, d\underline{p}_1 \cdot d\underline{p}_2 / \, dp_{12} \, , \qquad (II.2.25)$$

where p_{12} is the momentum difference $|\underline{p}_1 - \underline{p}_2|$. For each state, we measured the effects of correlation on $f(p_{12})$ by evaluating the quantity $\Delta f(p_{12})$, defined by

$$\Delta f(p_{12}) = f^{corr}(p_{12}) - f^{HF}(p_{12}) \, , \qquad (II.2.26)$$

where $f(p_{12})$ is evaluated at the correlated and Hartree-Fock levels, respectively. Clearly, $\Delta f(p_{12})$ is the momentum-space analogue of the Coulomb hole, and Banyard and Reed referred to it as the Coulomb `shift´ -- partly to avoid confusion with the position-space quantity and partly because the complicated shape of $\Delta f(p_{12})$ for $1^1 S$ He is less easily recognised as a `hole´. We have adopted the same terminology as Banyard and Reed throughout this work. To gain some insight into the relative magnitudes of the various Coulomb shifts, we have evaluated for each $\Delta f(p_{12})$ curve the fraction Y of the $f^{HF}(p_{12})$ distribution which has been redistributed as a result of the introduction of correlation.

For each wavefunction, the expectation values $\langle p_{12}^n \rangle$ were calculated from

$$\langle p_{12}^n \rangle = \int f(p_{12}) \, p_{12}^n \, dp_{12} \qquad \text{(II.2.27)}$$

with $n = -1$, 0, $+1$ and $+2$, together with the standard deviation $\sigma(p_{12})$, defined by

$$\sigma(p_{12}) = \sqrt{(\langle p_{12}^2 \rangle - \langle p_{12} \rangle^2)} \, . \qquad \text{(II.2.28)}$$

Although lacking the obvious `physical´ significance of the corresponding quantities in position-space, the $\langle p_{12}^n \rangle$ values help to characterise different regions of the $f(p_{12})$ curves; in addition, $\langle p_{12}^0 \rangle$ and $\langle p_{12}^2 \rangle$ provide necessary (but not sufficient) checks on the accuracy of the calculated distributions. The former value is just the normalisation of the wavefunction, while the latter quantity can be obtained independently by combining two other expectation values, defined above. According to the cosine rule we have

$$\langle p_{12}^2 \rangle = \langle p_1^2 \rangle + \langle p_2^2 \rangle - 2\langle \underline{p}_1 \cdot \underline{p}_2 \rangle \, , \qquad \text{(II.2.29)}$$

which provides, as in position space, a check on the accuracy and consistency of the calculated distributions and expectation values. Inspection of Equation (II.2.29) reveals that for a wavefunction not possessing angular terms of any type, such as the HF description of an S state, $\langle p_{12}^2 \rangle$ is exactly equal to the kinetic energy term, $\langle p^2 \rangle$, since $\langle \underline{p}_1 \cdot \underline{p}_2 \rangle$ is identically zero for such a function.

Since $\Delta f(p_{12})$ is obtained from two `averaged´

distributions, it is of interest to investigate the shape of the `shift´ when electron 1, say, has a specific momentum. Thus, again following Banyard and Reed, we have examined the <u>partial</u> Coulomb shift, $\Delta g(p_{12},p_1)$, defined such that

$$\int \Delta g(p_{12},p_1)dp_1 = \int g^{corr}(p_{12},p_1)dp_1 - \int g^{HF}(p_{12},p_1)dp_1$$

$$= \Delta f(p_{12}) \ . \qquad\qquad (II.2.30)$$

For the P states, we have also studied the angle-dependent partial Coulomb shift, $\Delta g(p_{12},p_1;\theta_1)$, for $\theta_1 = 0°$, $30°$, $60°$ and $90°$, where

$$\int \Delta g(p_{12},p_1;\theta_1) \ \sin\theta_1 d\theta_1 = \Delta g(p_{12},p_1), \qquad (II.2.31)$$

and θ_1 is the angle, measured in momentum space, between the test-electron momentum vector and the symmetry axis of the system. The angular integrals which occur in the definitions of the Coulomb shift and partial Coulomb shifts are of the same type as those that occur in the corresponding position-space expressions, and were evaluated in the same way. The radial integrals were once again evaluated numerically, but as a result of the more complicated nature of the orbital expressions in momentum space, the computing time required to evaluate the Coulomb shifts was found to be considerably greater than that required to evaluate the position-space `holes´.

Presentation of Results

In Figure (II.2.1) we present the uncorrelated one-particle radial momentum distribution functions, $D_1^{HF}(p_1)$, for the 2^3S, 2^1P and 2^3P states of helium. The effects of correlation on these distributions are shown in the corresponding radial shifts, $\Delta D_1(p_1)$, presented in Figure (II.2.2). The two-particle radial momentum distributions, $D_{12}^{HF}(p_1,p_2)$, are shown as surfaces in Figure (II.2.3), and the associated radial shifts, $\Delta D_{12}(p_1,p_2)$, are similarly displayed in Figure (II.2.4). In Figure (II.2.5) we present cross-sections of the $D_{12}^{HF}(p_1,p_2)$ and $\Delta D_{12}(p_1,p_2)$ surfaces when $p_1 = p_2$, for both the P states. For all three states, the one- and two-particle radial shifts presented here are those for the energetically better Tweed wavefunction in each instance. The one- and two-particle expectation values, $\langle p_1^n \rangle$ and $\langle p_1^n p_2^n \rangle$, derived from the Hartree-Fock and correlated radial distributions are presented in Tables (II.2.1) and (II.2.2), respectively.

The angular distributions of the electron momenta are illustrated by the $P^{HF}(\gamma)$ curves shown in Figure (II.2.6); the effects of correlation on these distributions are shown by the angular shifts, $\Delta P(\gamma)$, presented in Figure (II.2.7). Once again, the energetically better Tweed function was used for the correlated description of each state. In Table (II.2.3) we present the Hartree-Fock and correlated angular expectation values $\langle \underline{p}_1 \cdot \underline{p}_2 / p_1^n p_2^n \rangle$ and $\langle \gamma \rangle$.

The uncorrelated interparticle momentum distributions $f^{HF}(p_{12})$ are shown in Figure (II.2.8); the effects of

correlation on these distributions are seen in the associated Coulomb shifts, $\Delta f(p_{12})$, presented in Figure (II.2.9). In Table (II.2.4), the Hartree-Fock and correlated expectation values $\langle p_{12}^n \rangle$ are presented; also given in this table is the standard deviation $\sigma(p_{12})$, of each of the various $f(p_{12})$ distributions, as well as the value of Y for each Coulomb shift. The uncorrelated distribution functions $g^{HF}(p_{12}, p_1)$ are shown as surfaces in Figure (II.2.10); alternative views of these surfaces are provided in Figure (II.2.11). Two views of the corresponding partial Coulomb shifts, $\Delta g(p_{12}, p_1)$, are presented in Figures (II.2.12) and (II.2.13), respectively. In Figures (II.2.14) and (II.2.15) we show, for the two P states, two different aspects of the uncorrelated distributions $g^{HF}(p_{12}, p_1; \theta_1)$ for $\theta_1 = 0°$, $30°$, $60°$ and $90°$; the corresponding views of the associated θ_1-dependent partial Coulomb shifts, $\Delta g(p_{12}, p_1; \theta_1)$, are presented in Figures (II.2.16) and (II.2.17). For the partial Coulomb holes, the energetically better Tweed function is used for the correlated description in each instance.

Finally, to aid our discussion, we present in Figure (II.2.18) a purely schematic, 2-D representation of the electron distributions in 1s2s and 1s2p states of helium in both position and momentum space.

CHAPTER II.2.3

DISCUSSION

One of the principal problems encountered when attempting to describe atoms or molecules in momentum space is that of disorientation. Since physical reality seems so firmly rooted in <u>position</u> space, it is often extremely difficult to visualise even the simplest system when it is described in the momentum representation. Accordingly, in an attempt to compensate for this lack of familiarity, we shall preface our discussion of momentum-space correlation effects with a thorough analysis of the corresponding Hartree-Fock properties; where possible we shall also relate these properties to those already studied in position space. As before, we shall attempt to combine all the various facets of the Hartree-Fock description into a consistent 'model', and then examine how the various effects of correlation in momentum space combine to change that model. We begin by studying the uncorrelated momentum-space description of the 2^3S state.

The $D_1^{HF}(p_1)$ curve for 2^3S, shown in Figure (II.2.1), reveals two distinct regions, corresponding to the two shells in the system. From the nature of the Dirac[62] transform which relates the position and momentum representations, it is clear that the larger, localised peak at small p_1 corresponds to the momentum distribution of the L shell, while the much more diffuse region at large p_1 corresponds to the K shell. For later convenience we shall

denote the values of p_1 which locate the maxima in $D_1^{HF}(p_1)$ for the K and L shells by p_K and p_L, respectively. Not surprisingly, the two-shell nature of the momentum distribution is also clearly visible in $D_{12}^{HF}(p_1, p_2)$, shown in Figure (II.2.3). For this surface, it is seen that there are two principal regions of probability density, each corresponding to one electron being in the K shell and the other in the L shell. Interestingly, although it is not obvious from the orientation of the surface shown in Figure (II.2.3), the two-particle radial momentum distribution function, like its position-space counterpart, is identically zero along the leading diagonal. In <u>position</u> space, the zero probability when $r_1 = r_2$ is the result of the Fermi effect preventing two electrons from being the same distance from the nucleus. Since the Dirac transform preserves the determinantal form of the Hartree-Fock wavefunction, the Fermi effect manifests itself in momentum space by preventing the two electron <u>momenta</u> from having the same magnitude.

In Chapter (II.2.1) we saw that the angular nature of an orbital is unchanged by transformation to the momentum representation, and consequently at the HF level the 2^3S state is spherically symmetric in momentum space, as it was in position space. As a result of this symmetry, the shape of the angular distribution function, $P^{HF}(\gamma)$, shown in Figure (II.2.6), depends solely on the 'sin γ' term included in the definition. This curve is included primarily for later comparison with the corresponding functions for the P states; as expected, $P^{HF}(\gamma)$ for 2^3S is symmetric about

$\gamma=90°$, where the function is a maximum, and consequently $\langle\gamma\rangle=90°$.

Naturally, the radial and angular properties of the system influence the interparticle distributions. The $f^{HF}(p_{12})$ curve for 2^3S, shown in Figure (II.2.8), displays a single maximum, the location of which is related to p_K and p_L by Pythagoras's Theorem, as was the case in position space. For comparative purposes, we have also calculated the $f^{HF}(p_{12})$ distribution for the 2^1S state, and this function is included as the 'chain' curve in Figure (II.2.8). It is interesting to note that for 2^3S, $f^{HF}(p_{12})$ is vanishingly small for very small values of p_{12}, with the result that near to the origin the triplet curve displays a distinct 'flatness' which is absent from the 2^1S curve. A similar contrast between the interparticle distribution curves for the 2^1S and 2^3S states was also observed in position space. In the latter representation, the flatness of $f^{HF}(r_{12})$ near to the origin was attributed to the action of Fermi correlation, which prevents electrons of like spin from achieving very small interelectronic separations. The existence of a similar effect in momentum space, together with our earlier comments regarding the behaviour of $D_{12}^{HF}(p_1,p_2)$ on the $(p_1=p_2)$ diagonal, appears to confirm the findings of Ahlberg and Lindner[78], who claimed that the same rules govern the effects of Fermi correlation in momentum space as in position space. However, for 2^3S the behaviour of $f^{HF}(r_{12})$ at small r_{12} was found to be primarily the result of the Fermi effect preventing both electrons from occupying the K shell. Examination of the

$D_1^{HF}(p_1)$ curve in Figure (II.2.1) reveals that in <u>momentum</u> space, a double occupancy of the K shell would be characterised by both electron momenta being large. Since the momentum vectors are, on average, orthogonal to each other at the uncorrelated level, it is clear that both electrons being located in the K shell would give rise to <u>large</u> values of p_{12}. Consequently, it might be expected that any differences between the 2^1S and 2^3S $f^{HF}(r_{12})$ curves at small r_{12} should manifest themselves in $f^{HF}(p_{12})$ at <u>large</u>, not small, values of p_{12}. Given the average angular orientation of the momentum vectors, it seems likely that small values of p_{12} will be achieved only when p_1 and p_2 are themselves both <u>small</u>. Consequently, for 2^3S the behaviour of $f^{HF}(p_{12})$ as p_{12} approaches zero would appear to be the result of the Fermi effect preventing the electrons from both occupying the <u>L shell</u>. Of course, in reality the Fermi effect prevents the double occupancy of both shells in both representations. However, the diffuse nature of the K shell in momentum space leads to such a wide range of large p_1 values that in order to prevent both electrons being in the K shell, Fermi correlation must be effective over large ranges of p_{12}. As a result, the effects of Fermi correlation in the K shell are spread out more than in the L shell, and are consequently less easily observed. Naturally, these arguments apply equally well to other spherically symmetric systems in which Fermi correlation occurs. For example, it has been shown that the uncorrelated interelectronic distribution functions for the ^1S and ^3S electron pairs in the ground state of Be display the same differences in the two representations as the

singlet and triplet states of He discussed above.

We conclude our examination of the uncorrelated description of the 2^3S state of He by examining the $g^{HF}(p_{12},p_1)$ distribution function, shown in Figure (II.2.10); an alternative view of this surface is given in Figure (II.2.11). This distribution, like its position-space counterpart, displays two principal features: a region of probability density lying parallel to the p_{12} axis at small values of p_1, and a second region, located along the $(p_{12}=p_1)$ diagonal axis. For convenience, we shall refer to these as the ´parallel´ and ´diagonal´ features respectively. To aid our understanding of the $g^{HF}(p_{12},p_1)$ surface for 2^3S we present in Figure (II.2.18) a purely schematic representation of the 2^3S state in position and momentum space. Since this system is spherically symmetric in both spaces, the principal difference between the appearance of the 2^3S state in the two representations is simply the radial ordering of the two shells. As a consequence of this, the appearance of the system in momentum space should bear a strong resemblance to its appearance in position space. Previously, we were able to rationalise the shape of the $g^{HF}(r_{12},r_1)$ surface by examining the system from a viewpoint located in each shell in turn; the same procedure should now be equally applicable in momentum space.

Consider a test electron in the L shell. Since the radial momentum distribution of that shell is highly localised, the range of momenta that such a test electron

can have is quite restricted, and consequently p_1 is quite small and close in value to p_L. On the other hand, the relatively diffuse nature of the K shell gives rise to a large range of possible p_{12} values for the two electrons. This view of the system therefore gives rise to the 'parallel' feature in $g^{HF}(p_{12},p_1)$. Consider now a test electron located somewhere in the K shell, so that p_1 is now somewhat larger than its earlier value. The diffuse form of the K shell in momentum space gives rise to a wide range of possible p_1 values, while the compact nature of the L shell results in a more restricted band of possible p_2 values for the second electron. The most probable value of p_{12} for a given choice of p_1 is then obtained by averaging over all possible angular orientations of the two electron momentum vectors. The interparticle separation in momentum space therefore ranges from $p_{12} = (p_1 + p_2)$, which corresponds to the two electrons moving parallel to each other, to $p_{12} = (p_1 - p_2)$, which results from the electrons moving in opposite directions. Recalling the spherically symmetric nature of the two shells, the mean value of p_{12} is then simply the average of the two extreme orientations, whereupon $p_{12} = p_1$. Clearly, this view of the system gives rise to the 'diagonal' feature on the $g^{HF}(p_{12},p_1)$ surface. Not surprisingly, both of the principal regions of probability density possess a maximum at the same value of p_{12}, since both maxima correspond to the same, most probable, orientation of the two electrons, simply viewed from different shells.

Having thus described the nature of the Hartree-Fock

momentum distributions for the 2^3S state, we now consider the effects of introducing correlation into the description, and begin by studying the $\Delta D_1(p_1)$ curve, shown in Figure (II.2.2). The most obvious characteristic of this curve is that at small values of p_1, correlation has caused a shift to higher momenta. The first zero in $\Delta D_1(p_1)$ occurs at a value of p_1 close to p_L, which indicates that this movement of probability density is an L-shell correlation effect. This is consistent with our findings in position space, where we saw that correlation causes the L-shell electron to approach the nucleus; such a movement would, of course, cause an increase in the momentum of the electron. The existence of a second, very much less significant, negative/positive feature in $\Delta D_1(p_1)$ at larger values of p_1 suggests that the K-shell electron has also undergone a shift to higher momentum. Since the negative region located between $p_1 \approx 0.8$ and $p_1 \approx 1.0$ is obviously not comparable in magnitude to the positive region which exists beyond 1.0, it seems likely that the K- and L-shell correlation effects actually overlap, so that the probability enhancement in the high-p_1 region of the L shell offsets the probability reduction in the low-p_1 region of the K shell.

The $\Delta D_{12}(p_1,p_2)$ surface shown in Figure (II.2.4) appears to confirm that <u>both</u> electrons do indeed experience a shift to higher momentum; if we consider the positive feature located parallel to the p_1 axis, the coordinates at which the maximum for this region occurs are greater, in both directions, than the coordinates of the corresponding maximum in the $D_{12}^{HF}(p_1,p_2)$ surface. In keeping with the

109

observed changes in the radial distribution of the electrons, it is seen from Tables (II.2.1) and (II.2.2), respectively, that the expectation values $\langle p_1^n \rangle$ and $\langle p_1^n p_2^n \rangle$ are increased for $n > 0$ and decreased for $n < 0$; the standard deviation $\sigma(p_1)$, presented in Table (II.2.1), is also decreased, indicating a 'tightening up' of the $D_1(p_1)$ distribution about its mean, $\langle p_1 \rangle$. Similar changes in the one- and two-particle expectation values have been noted for the ^3S inter-shell electron pair in the ground state of $Be^{[85]}$, and also for the ground state of $He^{[79]}$. This latter observation is quite surprising, since a comparison between the $\Delta D_{12}(p_1, p_2)$ surfaces for the ground[35] and 2^3S states reveals them to be quite different; it will be recalled that a similar effect was also observed in position space.

We consider now the effects of correlation on the relative angular orientation of the two momentum vectors. Inspection of the $\Delta P(\gamma)$ curve in Figure (II.2.7) reveals that the introduction of correlation reduces the probability of large values of γ and increases the probability of small values; the zero of $\Delta P(\gamma)$ occurs very close to $90°$, which was, of course, the most probable value of γ at the HF level. The reduction of the average angle between the momentum vectors is reflected in the changes in the angular expectation values given in Table (II.2.3), and contrasts strongly with the corresponding situation in position space, where it has been shown that correlation causes the angle between $\underline{r}_1$ and $\underline{r}_2$ to increase; see for example, the $\Delta p(\theta_{12})$ curves of Ellis[7], or the $\langle \cos \theta_{12} \rangle$ values quoted in

Table (II.1.5). This difference between the angular effects of correlation when analysed in the position and momentum representations, which has also been observed in the ground state of $He^{(82)}$ and in the various intra- and inter-shell electron pairs of $Be^{(85)}$, can be rationalised by means of the following model. At the Hartree-Fock level, the two electrons in the 2^3S state of He are described by orbitals with zero angular momentum, and consequently the momentum vector $\underline{p}_i$ of each electron must be parallel or antiparallel to its position vector $\underline{r}_i$. Furthermore, as we have already noted, the HF description indicates that the average angle between the electronic vectors is 90° in both spaces. If the two electrons are thought of as oscillating about the nucleus along a pair of perpendicular axes, it is reasonable -- from the point of view of minimising the electron-electron repulsion energy -- to assume that there is a phase difference of $\pi/2$ between their motions. Thus, for example, as the 2s electron starts to approach the nucleus, the 1s electron moves away from the nucleus along a line orthogonal to the direction of motion of the 2s electron. Simple geometrical arguments then dictate that any increase in the angle between the position vectors of the electrons must be accompanied by a corresponding decrease in the angular separation of the momentum vectors.

Having discussed the effects of correlation on the radial and angular distributions of the electron momenta, we can consider now how these effects combine to change the interparticle momentum distributions, and we begin by examining the $\Delta g(p_{12}, p_1)$ surface shown in Figure (II.2.12);

an alternative view of this surface is presented in Figure (II.2.13). For $0 < p_1 < p_L$, it is seen that correlation reduces $g(p_{12}, p_1)$ for all values of p_{12}. As p_1 is increased through p_L, the surface shows an enhancement of probability -- again for all p_{12}. This behaviour clearly illustrates the increase in the momentum of the L-shell electron. It is interesting to note that if we denote the value of p_1 at which the two maxima in $\Delta D_1 (p_1)$ occur as p_L^{max} and p_K^{max}, then the coordinates of the maximum in the 'parallel' feature of $\Delta g(p_{12}, p_1)$ are found to be very close to $p_{12} = p_K^{max} - p_L^{max}$ and $p_1 = p_L^{max}$. Thus, the principal enhancement of probability in the 'parallel' feature occurs when the K- and L-shell electrons have momenta p_K^{max} and p_L^{max}, respectively, <u>and</u> are both moving in the same direction. This is in keeping with our earlier observation that correlation causes an increase in the probability of small angles between the momentum vectors.

As we increase p_1 still further, we find that for a given value of p_1, $\Delta g(p_{12}, p_1)$ is initially positive and then negative as p_{12} is increased from zero. The alternative view of the surface shown in Figure (II.2.13) reveals that the zero contour between the maxima and minima in this region is almost exactly coincident with the $(p_{12} = p_1)$ diagonal. This structure, with an increase in probability when $p_{12} < p_1$ and a decrease when $p_{12} > p_1$, illustrates once again the reduction of the angle between the momentum vectors.

Finally in our discussion of correlation effects in the

2^3S state, we consider the Coulomb shifts, presented in Figure (II.2.9). The three correlated wavefunctions produce $\Delta f(p_{12})$ curves which are similar in shape and magnitude, the principal characteristic of all the curves being a general shift from large to small values of p_{12}. At very small p_{12}, the $\Delta f(p_{12})$ curves are all 'flat' -- the result of the Fermi effect causing both the Hartree-Fock and correlated distributions to be vanishingly small near to the origin. The $\sigma(p_{12})$ values, presented in Table (II.2.4), reveal no definite trend with the introduction of correlation. However, in keeping with the shape of the Coulomb shifts, inspection of the $\langle p_{12}^n \rangle$ expectation values reveals that $\langle p_{12}^{-1} \rangle$ is increased by correlation, while $\langle p_{12} \rangle$ and $\langle p_{12}^2 \rangle$ are both reduced. The Y values, also presented in Table (II.2.4), give an indication of the relative magnitudes of the Coulomb shifts produced by the three correlated wavefunctions. Interestingly, the 32-term Tweed wavefunction gives rise to a marginally deeper Coulomb shift than the energetically better 48 term function; this is in contrast to the results in position space, which showed that the larger wavefunction produces a slightly deeper Coulomb hole.

A comparison of the Coulomb shifts for 2^3S with the $\Delta f(p_{12})$ curve for the ^3S inter-shell electron pair in the ground state of Be[85] reveals that the two shifts are inverted with respect to each other; a similar inversion was also found when comparing the corresponding Coulomb holes. As we have already noted, in momentum space the principal radial effect of correlation is the same in both of these

systems, producing an increase in the momentum of the L-shell electron. In the absence of any other effect, it is clear that this radial change would lead to an overall _increase_ in p_{12}. Furthermore, the angular effect is also the same for both electron pairs, and results in the reduction of the angular separation of the momentum vectors. Taken in isolation, this change would produce an overall _reduction_ in p_{12}. From the different behaviour of the Coulomb shifts for He and Be, we may conclude that the relative magnitudes of the radial and angular effects are different in the two systems, with the angular effect being dominant in He, and the radial change being more powerful in Be. Evidence in support of this is found in a comparison of the changes due to correlation in the various radial and angular expectation values for the two systems. Thus, for example, as a fraction of the Hartree - Fock value $\langle p_1^2 \rangle^{HF}$, the correlation change in $\langle p_1^2 \rangle$ is found to be more than eight times greater for the Be ^{3}S inter-shell electron pair than for the 2^3S state of He, while the corresponding change in $\langle \gamma \rangle$ is nearly three times smaller[1]. It should be noted, of course, that for Be, intershell correlation effects are influenced by those in the closed K and L shells.

We now turn our attention to a consideration of the 2^1P and 2^3P states and, as before, we begin our discussion by examining the uncorrelated radial momentum distributions. For the P states, the $D_1^{HF}(p_1)$ curves, presented in

---

[1]For Be, the change was evaluated from [arc cos($\Delta\tau''$)] -- see Reference (85) for the definition of $\Delta\tau''$.

Figure (II.2.1), display considerably less shell structure than the corresponding distribution in the 2^3S state; this is also reflected in the uncorrelated $\sigma(p_1)$ values given in Table (II.2.1). In <u>position</u> space, the radial distributions for all three states possessed a local minimum, corresponding to the intershell region, whereas in momentum space, such a feature is found only in the S state. Careful inspection of the $D_1^{HF}(p_1)$ curve for 2^1P reveals that there is a slight change of slope at large p_1, where a K-shell maximum might be anticipated, but the 2^3P curve displays no such structure, and the most probable radial momentum of the K-shell electron cannot be predicted. Differences between the shell structure of a system when described in the position and momentum representations have also been noted by Gadre, Chakravorty and Pathak[94], who have concluded that the number of discernible shells in an atom in momentum space is not necessarily equal to that in its position-space description. Returning to Figure (II.2.1), we see that all three $D_1^{HF}(p_1)$ curves are very similar at large p_1, and that the lack of shell structure in the P state is due primarily to the differences in the location and spread of the peak in $D_1^{HF}(p_1)$ at small p_1. In the P states, this peak not only occurs at slightly higher momentum values than in the S states, but it is also more diffuse. This latter observation is in keeping with the findings of Duncanson and Coulson[95], who noted a similar difference between the momentum distributions of 's' and 'p' electrons. In the present work, the similarities and differences among the $D_1^{HF}(p_1)$ curves are particularly well illustrated by comparison of the uncorrelated one-particle radial

expectation values for the three states. Thus, for example, $\cdot\langle p_1^2 \rangle$, which emphasizes large values of p_1, shows relatively little variation among the three states, whereas the value of $\langle p_1^{-2} \rangle$, which emphasizes very small values of p_1, is some three times larger for 2^3S than for either of the P states. These observations are, of course, consistent with our findings in position space, where it was seen that the principal variation among the $D_1^{HF}(r_1)$ curves occurred at large values of r_1.

As a result of the degree of overlap between the contributions from the K- and L-shell electrons to the $D_1^{HF}(p_1)$ curves for the P states, it is difficult to obtain a value for p_K, the most probable momentum of an electron in the K shell. Since the two basis orbitals for the P states are orthogonal in their angular terms, $D_1^{HF}(p_1)$ could be decomposed into contributions from the ´1s´ and ´2p´ orbitals, thereby allowing the location of the maximum in the ´2p´ component to be determined. However, inspection of the $D_{12}^{HF}(p_1,p_2)$ surfaces for the P states, shown in Figure (II.2.3), reveals that this is not necessary. The surfaces for both P states each display two principal regions of probability density, and from the location of the maximum in these two regions, it is possible to obtain good approximations to p_L and p_K. From Figure (II.2.5a), it is seen that, in contrast to the corresponding surface for 2^3S, which is identically zero for all $p_1 = p_2$, the $D_{12}^{HF}(p_1,p_2)$ surfaces for the P states both display non-zero probabilities on the $(p_1=p_2)$ diagonal axis. A similar observation also holds in position space, of course, and in

both instances, this is a result of the Fermi effect being more powerful in S states than in P states. However, in $D_{12}^{HF}(r_1,r_2)$ for 2^1P, for example, the ratio of the maximum height on the diagonal to the maximum height in one of the off-diagonal probability regions was of the order of 13.1:1, whereas in momentum space the corresponding ratio is closer to 1.52:1. This is consistent with the different behaviour of the $D_1^{HF}(r_1)$ and $D_1^{HF}(p_1)$ curves, discussed earlier. Further inspection of Figure (II.2.5a) also reveals that except at small p_1 and p_2, the height of the 2^3P $D_{12}^{HF}(p_1,p_2)$ surface on the ($p_1=p_2$) diagonal is _greater_ than that of the singlet. This is somewhat surprising when one recalls that in the triplet state, the Fermi effect is known to prevent the condition that $\underline{p}_1= \underline{p}_2$. In the light of this, we anticipate that the angular distributions of the electron momenta will be different in the 2^1P and 2^3P states, such that the electrons in the 2^3P state are less likely to be located in the same angular regions of space; inspection of the $P^{HF}(\gamma)$ curves in Figure (II.2.6) reveals that this is indeed so.

By comparison with the symmetrical distribution for the 2^3S state, it is seen from Figure (II.2.6) that the $P^{HF}(\gamma)$ curve for 2^1P is skewed towards $\gamma=0°$, so that small angles have a higher probability of occurrence than larger ones. Physically, this corresponds to the two electrons having a greater probability of moving in the same direction. The $P^{HF}(\gamma)$ curve for 2^3P, on the other hand, is skewed towards $\gamma=180°$, so that the two electrons are more likely to be moving in _opposite_ directions. This difference between the

angular distributions of the electron momenta in the two states is, of course, also shown in the uncorrelated angular expectation values, listed in Table (II.2.3); for example, for 2^1P we find $\langle\gamma\rangle^{HF} = 85.824°$, while for 2^3P, $\langle\gamma\rangle^{HF} = 95.855°$. Of particular interest are the values of $\langle\cos\gamma\rangle^{HF}$ which, although having the same sign as the corresponding $\langle\cos\theta_{12}\rangle^{HF}$ values, are significantly larger (numerically) than their position-space counterparts. In Chapter (II.1.4) we noted that for these 2P states, the sign of $\langle\cos\theta_{12}\rangle^{HF}$ follows that of the exchange term in the appropriate two-particle density, whereas the magnitude of this expectation value is directly related to the degree of radial overlap which exists between the ´1s´ and ´2p´ orbitals. Since the analytical form of the two-particle density is unchanged in momentum space, it follows that $\langle\cos\gamma\rangle^{HF}$ must necessarily have the same sign as $\langle\cos\theta_{12}\rangle^{HF}$. Furthermore, the greater numerical magnitude of the momentum-space values is seen to be a direct consequence of the greater degree of intershell overlap exhibited by $D_1^{HF}(p_1)$ when compared to $D_1^{HF}(r_1)$ for a given state.

We conclude our discussion of the uncorrelated description of the P states by considering the various interparticle distributions. Inspection of Figure (II.2.8) reveals that the principal difference between the $f^{HF}(p_{12})$ curves for the 2^1P and 2^3P states occurs at very small p_{12}. In this region, the triplet curve exhibits the same ´flatness´ that was seen in the 2^3S curve, and this feature is once again attributable to the effects of Fermi correlation. This behaviour near to the origin, together

with the greater degree of radial overlap exhibited by the two shells, causes the 2^3P $f^{HF}(p_{12})$ as a whole to be slightly more compact than the corresponding singlet curve -- as evidenced by a comparison of the $\sigma(p_{12})$ values for the two states (see Table (II.2.4)). As before, the value of p_{12} at which each $f^{HF}(p_{12})$ curve is a maximum can be related to the corresponding values of p_K, p_L and γ^{MAX}, where the latter quantity is the most probable angle between the two momentum vectors and is obtained from $P^{HF}(\gamma)$ for each state.

For the 2^3S state, we have seen that there is some degree of correspondence between the appearance of the system in the position and momentum representations -- in both spaces the atom appears to consist of two concentric spherical shells. For the 2^1P and 2^3P states, on the other hand, the lack of spherical symmetry introduced by the ´2p´ orbital results in a quite different appearance in the two spaces, as seen from the position- and momentum-space representations of a 2P state shown in Figure (II.2.18). Once again, these are two-dimensional, <u>purely schematic</u> depictions, and we have deliberately not specified whether the system illustrated is a singlet or triplet state. Since the angular description of the system is invariant under the Dirac transformation which links the two spaces, the ´shape´ of the momentum distribution of the ´2p´ orbital has the same general form as that of the corresponding position distribution. However, as we have already noted, the ´1s´ orbital is characterised by large momenta, while the ´2p´ orbital displays a more compact distribution at smaller momentum values, and therefore appears ´inside´ the ´1s´

orbital in momentum space. Evidence in support of this view of the P states is provided by the $g^{HF}(p_{12}, p_1; \theta_1)$ surfaces displayed in Figure (II.2.14). When $\theta_1 = 0°$, the momentum surfaces for both P states bear a strong resemblance to their position-space counterparts. As θ_1 is increased, the 'diagonal' feature remains virtually constant in magnitude, while the 'parallel' feature reduces in height, until it disappears entirely when $\theta_1 = 90°$. This behaviour is in contrast to that observed in position space, where it was the 'diagonal' feature which became less significant as θ_1 was increased. Inspection of the alternative view of the $g^{HF}(p_{12}, p_1; \theta_1)$ surface given in Figure (II.2.15) reveals a further difference between the position and momentum space θ_1-dependent surfaces. For $\theta_1 = 0°$, it is seen that the 'diagonal' feature in the $g^{HF}(p_{12}, p_1; \theta_1)$ distribution of both P states actually displays a local <u>minimum</u> along the exact $(p_{12} = p_1)$ diagonal. Of the two regions which flank this minimum, the maximum on the $(p_{12} < p_1)$ side of the diagonal is the greater in magnitude in 2^1P, while in 2^3P, it is the feature on the $(p_{12} < p_1)$ side which is greater. As θ_1 is increased, the local minimum in both states becomes less noticeable and then disappears altogether.

To explain the behaviour of the $g^{HF}(p_{12}, p_1; \theta_1)$ surfaces, we shall concern ourselves specifically with the 2^1P state, and shall discuss the 2^3P state only where it differs substantially from the singlet. For $\theta_1 = 0°$, consider a test electron with a small value of p_1, which corresponds to the electron being located on the symmetry axis of the system and in the L shell. The compact L-shell distribution

in momentum space means that the range of small p_1 values that such a test electron can possess is quite restricted, whereas the diffuse nature of the K shell produces a wide range of p_{12} values. Clearly, this situation gives rise to the ´parallel´ feature in the $g^{HF}(p_{12}, p_1; \theta_1)$ surface. If we now retain the same small p_1 value, but allow θ_1 to increase, the locus of probable locations for the test electron intersects smaller and smaller fractions of the L-shell distributions, with the result that the ´parallel´ feature decreases in magnitude. When $\theta_1 = 90°$, the test electron lies in the nodal plane of the ´2p´ orbital. The only possibility that the test electron has a small momentum p_1 and is also situated in the nodal plane is that it is now located (in position space) in the far outer regions of the K shell, where the probability density is vanishingly small. Consequently, as θ_1 approaches $90°$ the parallel feature in the $g^{HF}(p_{12}, p_1; \theta_1)$ surface disappears.

Let us now consider a test electron with a somewhat larger value of p_1, such that it is located in the K shell. The diffuse nature of this shell in momentum space gives rise to a wide range of possible p_1 values for the test electron. In contrast to this, the localised nature of the L shell means that the range of momentum values displayed by the second electron is quite restricted. Furthermore, since the L shell is not spherically symmetric, its ´appearance´ to a test electron located at large p_1 will depend on that part of the K shell from which it is viewed, and will consequently be strongly dependent on θ_1. Consider again the schematic representation of the 2P state shown in

Figure (II.2.18). When $\theta_1 = 0°$, the test electron is located on the symmetry axis of the system. The momentum distribution of the second electron corresponds to the familiar lobes of the ´2p´ orbital, which appear on the $g^{HF}(p_{12}, p_1; \theta_1)$ surface as the two maxima lying parallel to the $(p_{12} = p_1)$ diagonal. The positive lobe of the orbital gives rise to values of $p_{12} < p_1$. The local minimum, which lies exactly along the diagonal, corresponds to the nodal plane of the ´2p´ orbital, where an electron with small momentum has a relatively small probability of being located. To explain the difference in height between the two maxima which flank the diagonal, we need only recall that in 2^1P, values of γ close to $0°$ are more probable than those close to $180°$. As a consequence, when $\theta_1 = 0°$ a test electron at large p_1 will detect a greater probability distribution from the positive lobe of the ´2p´ orbital than from the negative, with the result that in 2^1P, $p_{12} < p_1$ will be found to have a greater probability than $p_{12} > p_1$. In the triplet state, on the other hand, the presence of the Fermi effect means that values of γ closer to $180°$ are now more likely, and this gives rise to the maximum on the $(p_{12} > p_1)$ side having the greater height. If we now maintain the test electron at the same large value of p_1 and allow θ_1 to increase, similar arguments still hold, but the difference between the contributions to $g^{HF}(p_{12}, p_1; \theta_1)$ from the two lobes of the ´2p´ orbitals becomes progressively smaller. When $\theta_1 = 90°$, both lobes of the orbital ´appear´ the same to the test electron, with the result that both $g^{HF}(p_{12}, p_1; \theta_1 = 90°)$ surfaces display only one maximum, located very close to the diagonal.

The $g^{HF}(p_{12}, p_1)$ surfaces for the 2^1P and 2^3P states are presented in Figure (II.2.10), and are seen to bear a strong resemblance to the corresponding surface for the 2^3S state. In the alternative view of these surfaces provided in Figure (II.2.11), the different degrees of radial overlap in the three states are revealed by the extent to which the parallel and diagonal features in each surface are merged together. Interestingly, the different angular distributions which occur in the three states are not so easily observed.

We can now discuss the effects of correlation on the momentum distributions of the 2P states. Inspection of the $\Delta D_1(p_1)$ curves presented in Figure (II.2.2) reveals that in the small p_1 region, both the 2^1P and 2^3P states display a shift to higher momentum. The first zero in both $\Delta D_1(p_1)$ curves occurs, as for the 2^3S state, quite close to the corresponding value of p_L, indicating that this shift of probability density is once again an L-shell correlation effect; this is, of course, consistent with the inward radial shift of the '2p' electron seen in position space. At large values of p_1, there are slight differences between the $\Delta D_1(p_1)$ curves for the two states. Although it is difficult to associate these changes with any specific relocation of the electrons, it is interesting to note that the radial momentum shift for the 2^3P state displays a local minimum at $p_1 = 0.85$, which imparts to the $\Delta D_1(p_1)$ curve a very slight 'two-shell' structure. This is particularly surprising in view of the complete <u>lack</u> of distinction

between the K- and L-shell contributions to the corresponding $D_1^{HF}(p_1)$ curve. The changes in $\Delta D_1(p_1)$ are reflected in the one-particle radial expectation values presented in Table (II.2.1). For both states, it is seen that correlation reduces $\langle p_1^n \rangle$ for $n < 0$ and increases it for $n > 0$. The $\sigma(p_1)$ values, also shown in that Table, indicate that correlation causes the $D_1(p_1)$ distributions for both states to be 'sharpened up' about their respective means.

Further insight into the radial effects of correlation is afforded by an examination of the $\Delta D_{12}(p_1, p_2)$ surfaces, shown in Figure (II.2.4). In the regions parallel to the axes, the surfaces for both states display structures which are consistent with the increase in momentum of the L-shell electron. Elsewhere on these surfaces, however, there are significant differences between the two 2P states -- particularly in the region of the $(p_1 = p_2)$ diagonal. In particular, for 2^1P, $\Delta D_{12}(p_1, p_2)$ displays a single maximum, which occurs when both electrons have the same momentum; in contrast to this, the principal enhancement of probability in the triplet state occurs when the electron momenta are different -- as seen from the two off-diagonal peaks in the 2^3P surface. These effects differ strongly from our findings in position space, where we saw that the $\Delta D_{12}(r_1, r_2)$ surface for the singlet state displayed two off-diagonal maxima, while that for the triplet possessed a single enhancement of probability when $r_1 = r_2$. A comparison of the coordinates of the principal maxima in the $\Delta D_{12}(p_1, p_2)$ surfaces with the positions of maximum probability in the corresponding $D_{12}^{HF}(p_1, p_2)$ surfaces shows

that for 2^1P, the L-shell electron has its momentum increased by correlation and the K-shell electron has its momentum reduced. A similar comparison for 2^3P reveals that for this state, correlation produces an increase in the momentum of <u>both</u> electrons. The nature of each $\Delta D_{12}(p_1,p_2)$ surface is, to some extent, reflected in the associated two-particle radial expectation values, presented in Table (II.2.2). Thus, for both P states it is seen that $\langle p_1^n p_2^n \rangle$ is reduced by correlation when $n<0$. Interestingly, in 2^1P, $\langle p_1^2 p_2^2 \rangle$ and $\langle p_1 p_2 \rangle$ are both increased, whereas in 2^3P, $\langle p_1 p_2 \rangle$ is increased but $\langle p_1^2 p_2^2 \rangle$ is marginally <u>reduced</u>. Such observations illustrate once again the difficulty of predicting correlation effects from expectation values alone.

To illustrate the behaviour of $\Delta D_{12}(p_1,p_2)$ in the region of the leading diagonal, we present in Figure (II.2.5b) a section through both of the P state surfaces when $p_1=p_2$. In passing, we note that the curve for 2^1P displays a local minimum when $p_1=p_2 \approx 0.85$, which is the same as the value of p_1 at which a similar minimum occurred in the <u>one</u> - particle radial shift $\Delta D_1(p_1)$ for 2^3P. When p_1 and $p_2 \approx$ 2.0, the section through the 2^3P surface is seen to be slightly negative, and this offers an explanation of the reduction by correlation of the $\langle p_1^2 p_2^2 \rangle$ expectation value for this state. Inspection of the $\Delta D_{12}(p_1,p_2)$ data for 2^3P has revealed that for <u>all</u> large (p_1,p_2), $\Delta D_{12}(p_1,p_2)$ is slightly reduced by correlation, and it is <u>this</u> feature which produces the observed change in $\langle p_1^2 p_2^2 \rangle$.

We now turn our attention to the $\Delta P(\gamma)$ curves presented in Figure (II.2.7). It is seen that the angular effects of correlation in the 2^1P state are quite different to those in 2^3P. The $\Delta P(\gamma)$ curve for the singlet state reveals an increase in probability at small angles of γ, a reduction at large values and then a second, relatively insignificant, increase in probability as γ approaches 180°. The curve for 2^3P, on the other hand, shows a reduction in probability at small values of γ, an enhancement at larger values and a minor reduction as γ approaches 180°. In the 2^3S state, we saw that the single zero in $\Delta P(\gamma)$ occurred at a value of γ very close to 90°, which is where the $P^{HF}(\gamma)$ curve is a maximum. For the 2^1P state, the first zero in $\Delta P(\gamma)$ also occurs quite close to the value of γ which locates the peak of the singlet $P^{HF}(\gamma)$ curve. In contrast to this, the first zero in the $\Delta P(\gamma)$ curve for 2^3P, although close to the corresponding point in the singlet angular shift, does not appear to relate to any significant point in the $P^{HF}(\gamma)$ for the triplet state. However, it is interesting to note that the principal <u>maximum</u> in the $\Delta P(\gamma)$ curve for 2^3P occurs very close to the value at which the peak in the corresponding $P^{HF}(\gamma)$ curve is located.

The differences between the angular effects of correlation in the 2^1P and 2^3P states are also seen in the expectation values in Table (II.2.3). In particular, we note that for 2^1P, the average angle between the momentum vectors, $\langle\gamma\rangle$, is less than 90° at the HF level, and correlation <u>reduces</u> the angle still further. In the triplet state, the uncorrelated value of $\langle\gamma\rangle$ is greater than 90°,

and correlation <u>increases</u> this expectation value. In keeping with the uncorrelated values of $\langle \gamma \rangle$, the expectation value $\langle \underline{p}_1 . \underline{p}_2 \rangle^{HF}$ for 2^1P is seen to be positive, while the corresponding quantity for 2^3P is negative. However, for this expectation value, the introduction of correlation causes an increase (in the absolute sense) in <u>both</u> P states. In Chapter (II.2.2) we noted that this expectation value is related to the mass polarisation correction, ε_m. Values of ε_m have been evaluated for the 2^1P and 2^3P states of He by Accad, Pekeris and Schiff[40], who used highly accurate, explicitly correlated wavefunctions for their calculations; for both P states, the $\langle \underline{p}_1 . \underline{p}_2 \rangle$ values derived from those ε_m terms also show an increase relative to the Hartree-Fock results.

We now consider the ways in which the radial and angular effects of correlation change the interparticle distribution for the 2P states, and we begin by examining the partial Coulomb shifts presented in Figure (II.2.12). The surfaces for both P states display their principal features parallel to the p_{12} axis at small p_1, and in the region of the $(p_{12}=p_1)$ diagonal; as before, these 'parallel' and 'diagonal' features can be identified with test electrons located in the L and K shells, respectively. The 'parallel' features in both $\Delta g(p_{12},p_1)$ surfaces are quite similar to that seen in the 2^3S surface, and reflect the previously noted shift to higher momentum of the L-shell electron in each state. In contrast to this similarity, the 'diagonal' features for the two P states display significant differences, which are best illustrated by the alternative

view of the $\Delta g(p_{12}, p_1)$ surfaces, provided in Figure (II.2.13). For 2^1P, we see that when p_{12} and p_1 are both greater than approximately 1.0, there is a negative region along the exact $(p_{12}=p_1)$ axis, bounded on each side by a local maximum lying parallel to the diagonal. At smaller values of p_{12} and p_1, the 'parallel' and 'diagonal' features merge together, resulting in a single maximum. This merging is consistent with the shape of the corresponding $\Delta D_{12}(p_1, p_2)$ surface, which, as we have already noted, indicates that for this state, the greatest enhancement of probability occurs when both electron momenta have the same magnitude. For the 2^3P state, on the other hand, when p_{12} and p_1 are both greater than approximately 1.5, the 'diagonal' feature consists of positive and negative regions parallel to the diagonal on the $(p_{12}<p_1)$ side, and a significantly larger positive region, also parallel to the $(p_{12}=p_1)$ axis, on the $(p_{12}>p_1)$ side; the correlation change on the exact diagonal is quite small. In contrast to the singlet state, the maxima associated with the 'parallel' and 'diagonal' features in the 2^3P surface are quite distinct from one another. This observation is in accord with the shape of the $\Delta D_{12}(p_1, p_2)$ surface for this state, from which we surmised that the greatest enhancement of probability in 2^3P occurs when the two electron momenta have different magnitudes.

To gain some understanding of the differences which exist between the $\Delta g(p_{12}, p_1)$ surfaces for these two states, we now turn to the $\Delta g(p_{12}, p_1; \theta_1)$ surfaces, presented in Figure (II.2.16), and begin by considering the 2^1P state.

When $\theta_1 = 0°$, the 'parallel' feature in the $\Delta g(p_{12}, p_1; \theta_1)$ surface is quite similar to that in the corresponding $\Delta g(p_{12}, p_1)$ surface, and clearly results from the correlation-induced shift to higher momentum of the L-shell electron. As θ_1 is increased, this feature becomes progressively smaller, disappearing completely when $\theta_1 = 90°$. Such behaviour is consistent with that seen in the 'parallel' feature in the $g^{HF}(p_{12}, p_1; \theta_1)$ surfaces, and simply reflects the fact that at both levels of approximation, the probability of an electron having a small momentum and being located in the nodal plane of the '2p' orbital is vanishingly small.

The form of the 'diagonal' feature in $\Delta g(p_{12}, p_1; \theta_1)$ is best illustrated by the alternative view of the surfaces presented in Figure (II.2.17). When $\theta_1 = 0°$, the 'diagonal' feature is quite complicated, and consists of negative, and then positive, regions flanking the diagonal on each side, with minimal change along the exact $(p_{12} = p_1)$ axis. To understand this structure, we recall the explanation of the shape of the 'diagonal' feature in the corresponding $g^{HF}(p_{12}, p_1; \theta_1)$ surface. At the uncorrelated level, this feature of the $g(p_{12}, p_1; \theta_1)$ distribution is characterised by two local maxima, one on each side of the exact diagonal, with a local minimum along the $(p_{12} = p_1)$ axis. These maxima are attributed to the average effects of the two lobes of the '2p' orbital as they 'appear' to a test electron on the symmetry axis at large p_1 (see Figure (II.2.18)). As we have already noted, the principal radial effect of correlation in this state is to increase the momentum of the '2p' electron,

and this causes an expansion of the two lobes of the orbital away from the origin. In the $\Delta g(p_{12}, p_1; \theta_1)$ surface, this expansion manifests itself as a reduction, and then an increase, in probability on both sides of the diagonal as we move away from the $(p_{12}=p_1)$ axis. The difference in magnitude between the two positive regions which then flank the diagonal in $\Delta g(p_{12}, p_1; \theta_1)$ may be explained by noting that, in addition to the radial effect described above, correlation also produces an increase in probability of small angles between the momentum vectors. As a consequence, there is an enhancement of probability when $p_{12} < p_1$ and a reduction when $p_{12} > p_1$. The behaviour of the $\Delta g(p_{12}, p_1; \theta_1)$ surface on the _exact_ diagonal is due to the presence of the nodal plane; for the reasons given earlier, both the HF and correlated description of the system predict a small probability when $p_{12}=p_1$, so that the difference between these two values is _very_ small.

As θ_1 is increased, our ability to distinguish between the two lobes of the 2p orbital decreases markedly, with the result that the $\Delta g(p_{12}, p_1; \theta_1)$ surface eventually displays only a negative region along the diagonal, flanked on each side by the previously noted positive features. It is interesting to note that when $\theta_1 = 90°$ the disappearance of the 'parallel' feature from the $\Delta g(p_{12}, p_1; \theta_1)$ surface allows us to trace the 'diagonal' feature back to smaller values of p_{12} and p_1 than was previously possible. Furthermore, for this value of θ_1, the principal maximum in the surface occurs when $p_{12} < p_1$, which again reflects the form of the angular shift $\Delta P(\gamma)$ for this state.

Let us now consider the θ_1-dependent surfaces for 2^3P. As before, we shall begin by examining the $\theta_1 = 0^\circ$ surface. The 'parallel' feature in this surface is seen to be broadly similar to that for 2^1P and can be explained in the same manner. Inspection of the alternative view of the surfaces given in Figure (II.2.17) reveals that for 2^3P, the 'diagonal' feature consists of a positive region on the $(p_{12} > p_1)$ side of the $(p_{12} = p_1)$ axis, a negative region on the $(p_{12} < p_1)$ side and, just beyond that, a further, minor positive feature. This basic structure of a negative region flanked by two positive features is similar to that observed in 2^1P, and reflects the shift to higher momentum of the '2p' electron. It is interesting to note that, as for the singlet state, the influence of the nodal plane again results in minimal change along the exact leading diagonal; for 2^3P, this line corresponds to the boundary between the major positive and negative features which flank the $(p_{12} = p_1)$ axis. However, in contrast to 2^1P, the enhancement of probability on the $(p_{12} < p_1)$ side of the diagonal in the 2^3P surface is now <u>smaller</u> than that on the $(p_{12} > p_1)$ side. This is obviously a reflection of the difference between the angular shifts for the two states; in 2^3P, correlation causes a <u>reduction</u> in probability of small values of γ, whereas in 2^1P it causes an <u>increase</u>. In further contrast to the singlet state, the surface for 2^3P displays a much greater degree of a symmetry about the diagonal than is seen in the 2^1P surface. This dissimilarity between the two 2P states may arise from the fact that when comparing Figures II.2.6 and II.2.7 we noted that for 2^1P, $\Delta P(\gamma)$ possesses a

zero in the region of the corresponding value of γ^{MAX}, while the angular shift for 2^3P displays a maximum close to its associated γ^{MAX}.

As θ_1 is increased, the behaviour of the 'parallel' feature in the 2^3P surface follows that seen in the singlet state, gradually reducing in magnitude until it disappears completely when $\theta_1 = 90°$. At the same time, the locations and magnitudes of the positive and negative features in the region of the diagonal also change; the major positive feature is reduced in height, while the smaller positive feature approaches the $(p_{12}=p_1)$ axis. When $\theta_1 = 90°$, the triplet surface, like that for 2^1P, displays a negative region along the diagonal, with positive features flanking it on both sides. However, in contrast to the surface for 2^1P, the principal maximum in the $\Delta g(p_{12},p_1;\theta_1=90°)$ surface for 2^3P occurs when $p_{12} > p_1$. This difference is, of course, consistent with the dissimilarity which exists between the $\Delta P(\gamma)$ curves for the two states.

Finally for the P states, we consider the overall effects of correlation on the interparticle distributions by examining the Coulomb shifts, presented in Figure (II.2.9). It is seen that the $\Delta f(p_{12})$ curves for 2^1P display an enhancement of probability at small p_{12}, and a reduction at large values; as p_{12} is increased further, the Coulomb shift for the larger Tweed wavefunction shows a slight positive feature. We have already seen that the major radial effect of correlation in this state is an increase in the momentum of the L-shell electron. In the absence of any other

correlation effects, such a change would be expected to produce an overall _increase_ in p_{12}. However, we have also seen that in addition to this radial change, correlation produces an overall reduction in the angle γ between the momentum vectors. In the absence of other effects, _this_ change would produce a general _decrease_ in p_{12}. From the shape of the Coulomb shifts for 2^1P, we must conclude that in the singlet state the angular effect of correlation is dominant, and therefore governs the change in the $f(p_{12})$ distribution. Interestingly, there is a significant difference in magnitude between the Coulomb shifts produced by the two Tweed wavefunctions for this state. The difference, which may be quantified by inspection of the Y values presented in Table (II.2.4), suggests that the balance between the radial and angular effects produced by these two wavefunctions in momentum space is somewhat different to that in position space, where the variation between the $\Delta f(r_{12})$ curves was less pronounced.

In direct contrast to the behaviour of the 2^1P curves, the Coulomb shifts for 2^3P show a decrease in probability at small p_{12}, with an increase at large values; as p_{12} is increased further still, both $\Delta f(p_{12})$ curves for this state become slightly negative once more. For 2^3P, the principal radial effect of correlation is again an increase in the momentum of the L-shell electron, but the major angular change is now a shift to _larger_ values of γ. Both of these effects lead to increased interparticle separations in momentum space, with the result that the $\Delta f(p_{12})$ curve for 2^3P displays a shift from small to larger p_{12}. From the Y

values in Table (II.2.4), the difference between the Coulomb

shifts evaluated from the two Tweed wavefunctions is seen to

be somewhat smaller in this state. The 'flatness' of these

Coulomb shifts near to the origin is, as for the 2^3S state,

due to the Fermi effect, which causes both $f^{corr}(p_{12})$ and

$f^{HF}(p_{12})$ to be vanishingly small as p_{12} tends to zero.

The different shapes of the Coulomb shifts for both P

states is reflected quite clearly in the $\langle p_{12}^n \rangle$ expectation

values, presented in Table (II.2.4). For 2^1P, $\langle p_{12}^{-1} \rangle$ is

increased by correlation, and $\langle p_{12} \rangle$ and $\langle p_{12}^2 \rangle$ are both

decreased, whereas each of these changes is reversed in 2^3P.

In the singlet state, correlation causes $\sigma(p_{12})$ to increase

slightly, indicating a slight spreading out of the inter-

particle distribution, while for the triplet state, this

quantity is reduced, indicating a 'sharpening up' of $f(p_{12})$.

CHAPTER (II.2.4)

SUMMARY

Electron correlation effects in momentum space for the 2^3S, 2^1P and 2^3P states of He have been analysed in terms of various radial, angular and interparticle momentum density distribution functions and expectation values. In view of the relatively unfamiliar nature of momentum space, the corresponding Hartree-Fock quantities were also analysed in some detail.

Examination of the one- and two-particle radial shifts, $\Delta D_1(p_1)$ and $\Delta D_{12}(p_1,p_2)$, revealed that the principal radial effect of correlation in each of the three states is an increase in the momentum of the L-shell electron; such an effect is in keeping with the inward movement of probability seen in position space.

In contrast to the similarity of the radial effects within the three states, it was found that there is a significant difference between the angular effect of correlation in 2^3P and that in the other two states. For 2^3S and 2^1P, angular correlation produces a shift of probability towards smaller values of γ, the angle between the momentum vectors of the two electrons. For 2^3P, on the other hand, the introduction of correlation increases γ; this change in the angular behaviour can be traced to the triplet nature of the spin multiplicity, combined with the specific P-symmetry of this $(1s,nl)$ state.

Not surprisingly, the fundamental difference in the behaviour of the angular component of correlation resulted in the Coulomb shift, $\Delta f(p_{12})$, for 2^3P being <u>markedly</u> different from those for the other two states. For 2^3S and 2^1P, angular and radial correlations clearly have <u>opposing</u> effects on the p_{12}-distribution function; as in the ground state, radial correlation tends to increase the value of p_{12}, whereas angular correlation produces a shift in probability towards smaller p_{12}. For the triplet P state, on the other hand, both radial <u>and</u> angular correlation emphasize larger p_{12} values, and hence the two components of correlation work in unison, as in position space.

The partial Coulomb shifts, $\Delta g(p_{12}, p_1)$, for these excited states were exceedingly complex by comparison with that for the ground state. This complexity could, however, be rationalised by considering the combined radial and angular effects of correlation, together with a detailed analysis of the corresponding $g^{HF}(p_{12}, p_1)$ functions, the form of which tended to dictate the shape of the $\Delta g(p_{12}, p_1)$ surfaces. In particular it was of interest to examine the characteristics of both the $g^{HF}(p_{12}, p_1)$ and $\Delta g(p_{12}, p_1)$ surfaces when the test electron, with momentum p_1, was located firstly in the L shell, and then in the K shell. Finally, for the P states, the distributions $g^{HF}(p_{12}, p_1; \theta_1)$ and $\Delta g(p_{12}, p_1; \theta_1)$ illustrated the influence of Fermi and Coulomb correlation on the lobes of the 2p orbitals in momentum space.

FIGURES AND TABLES - SECTION (II.2)
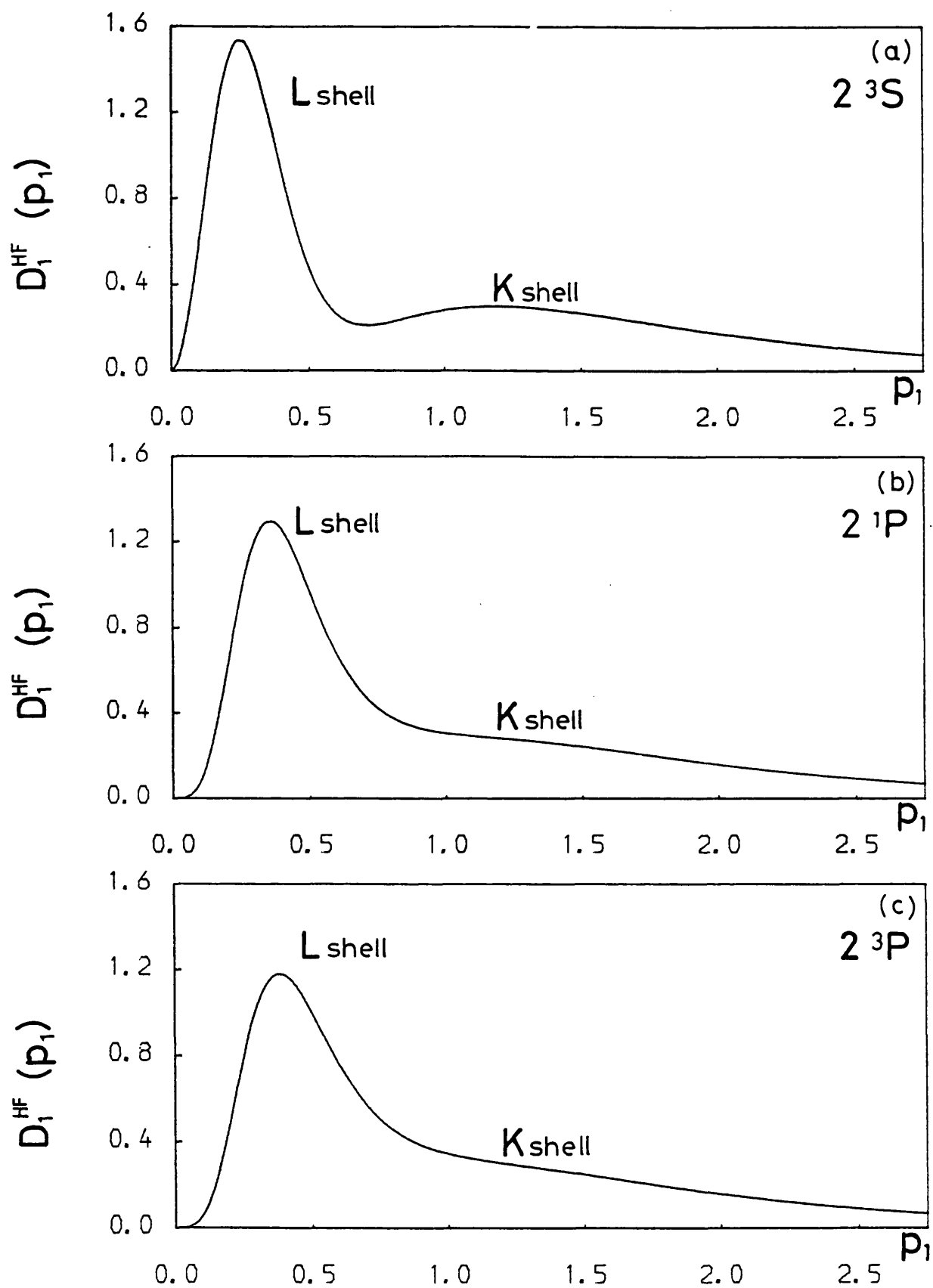
Figure (II.2.1)

The $D_1^{HF}(p_1)$ distributions for the (a) 2^3S, (b) 2^1P and (c) 2^3P states of He.
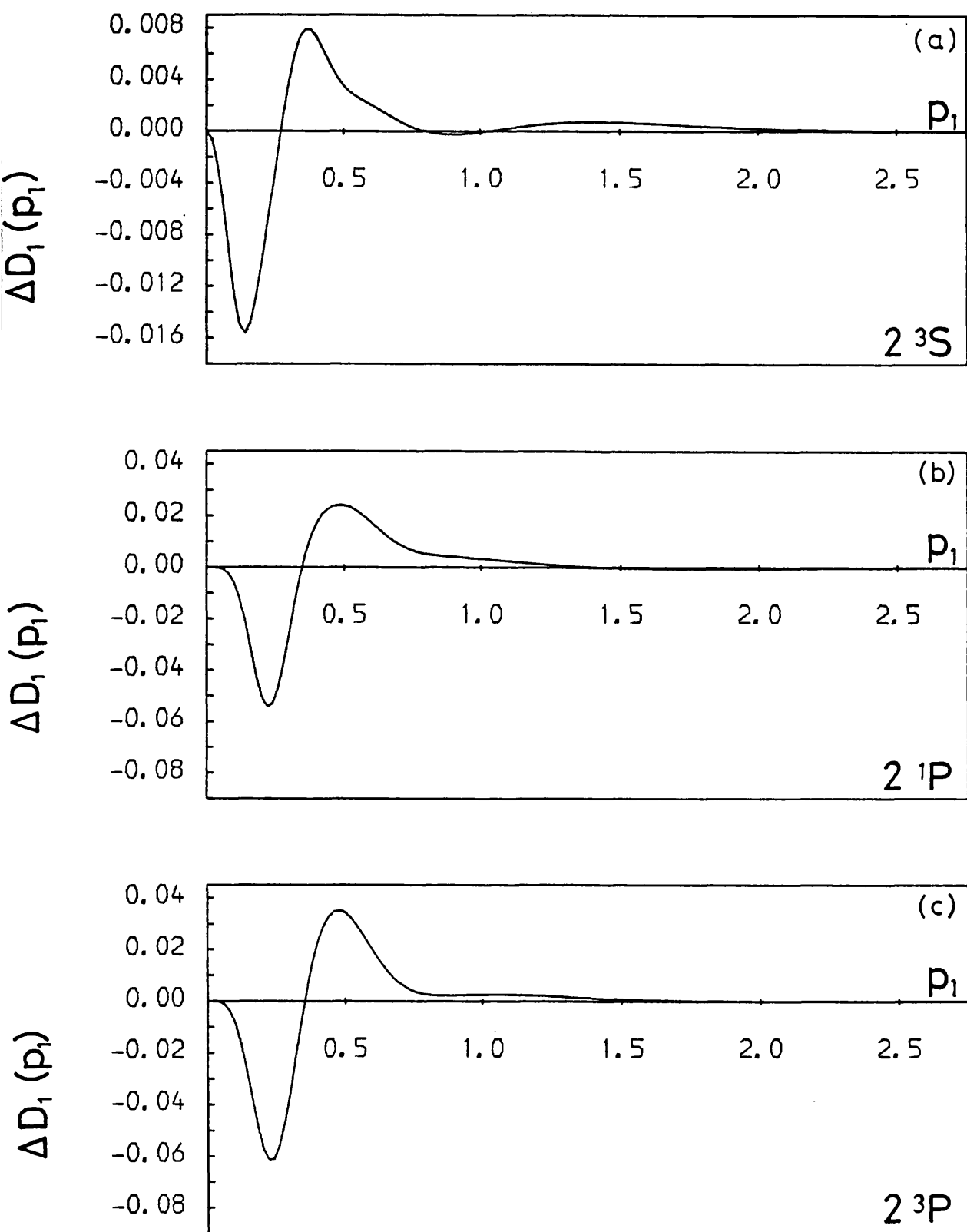
<u>Figure (II.2.2)</u>

The one-particle radial shifts $\Delta D_1(p_1)$ for the

(a) $2\,^3S$, (b) $2\,^1P$ and (c) $2\,^3P$ states of He.
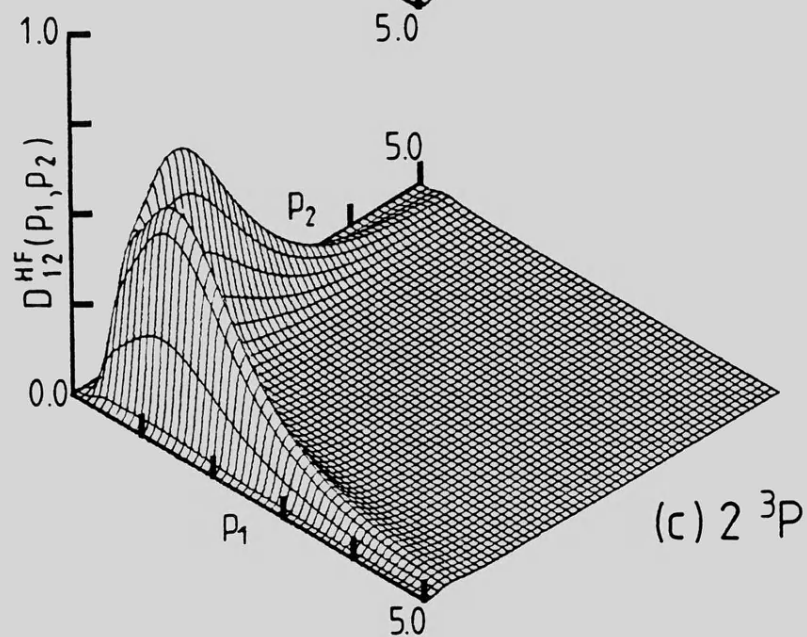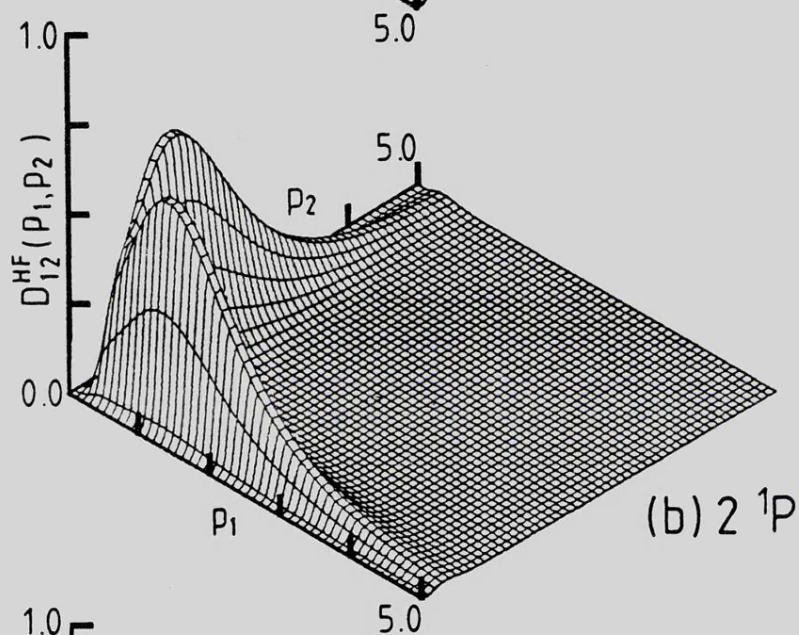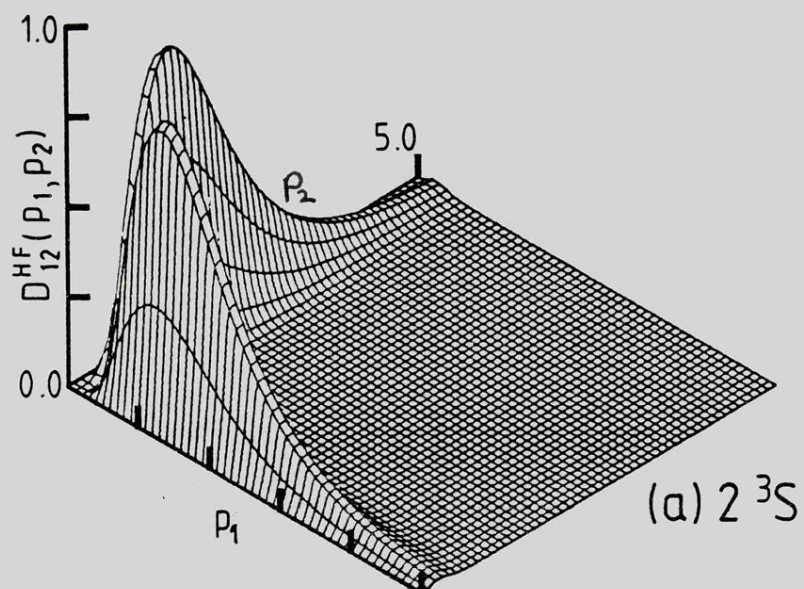
Figure (II.2.3)

The $D_{12}^{HF}(p_1, p_2)$ distributions for the
(a) 2^3S, (b) 2^1P and (c) 2^3P states of He.

139
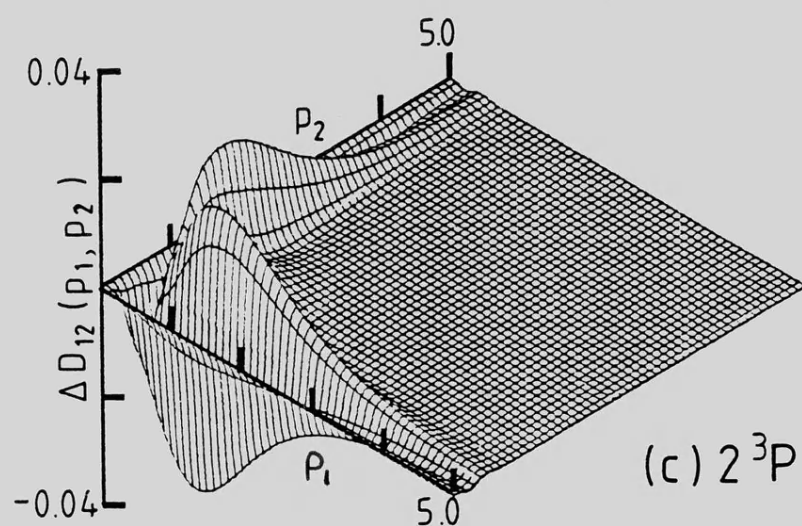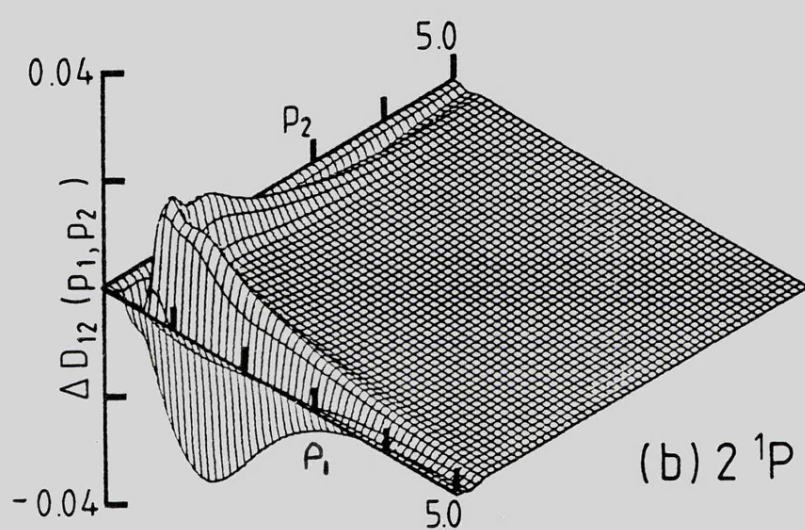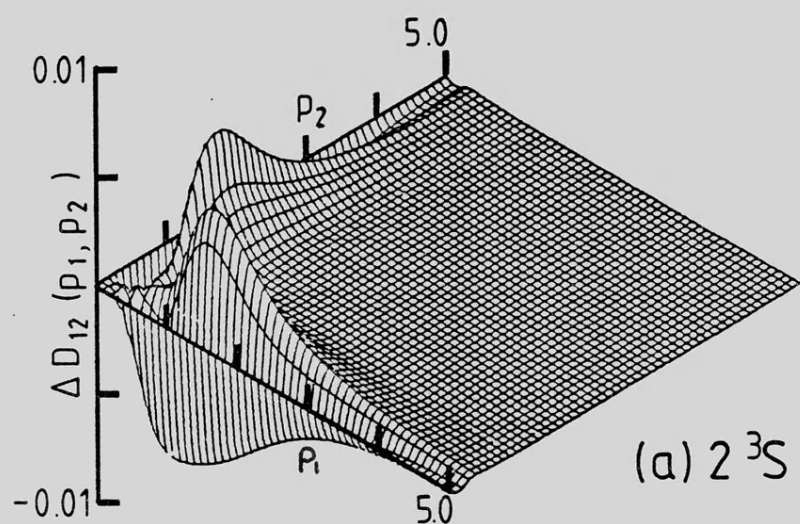
Figure (II.2.4)

The two-particle radial shifts $\Delta D_{12}(p_1, p_2)$ for the

(a) $2\,^3S$, (b) $2\,^1P$ and (c) $2\,^3P$ states of He.

140
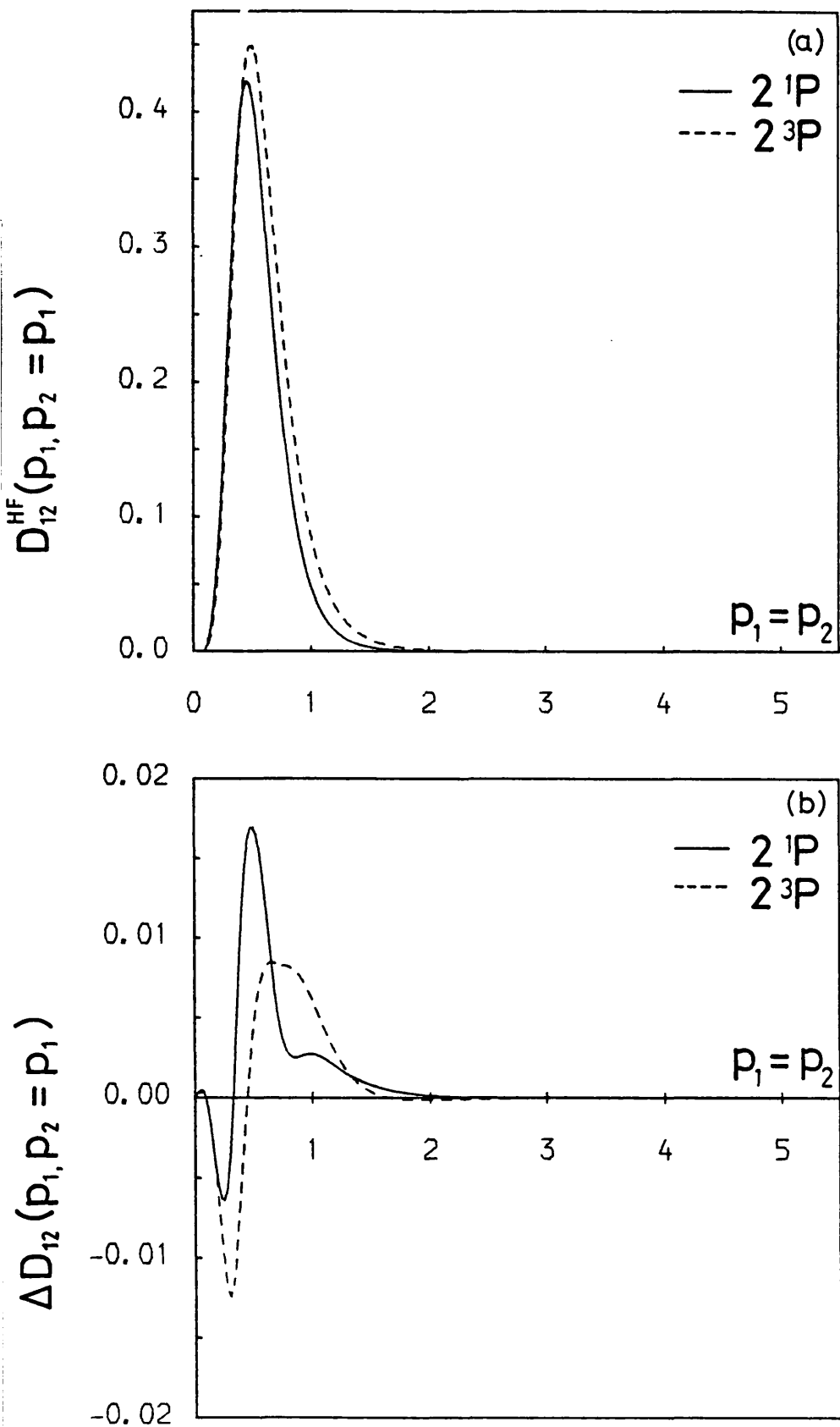
Figure (II.2.5)

A comparison of the (a) $D_{12}^{HF}(p_1, p_2 = p_1)$ and
(b) $\Delta D_{12}(p_1, p_2 = p_1)$ cross-sections for the 2^1P and
2^3P states of He.
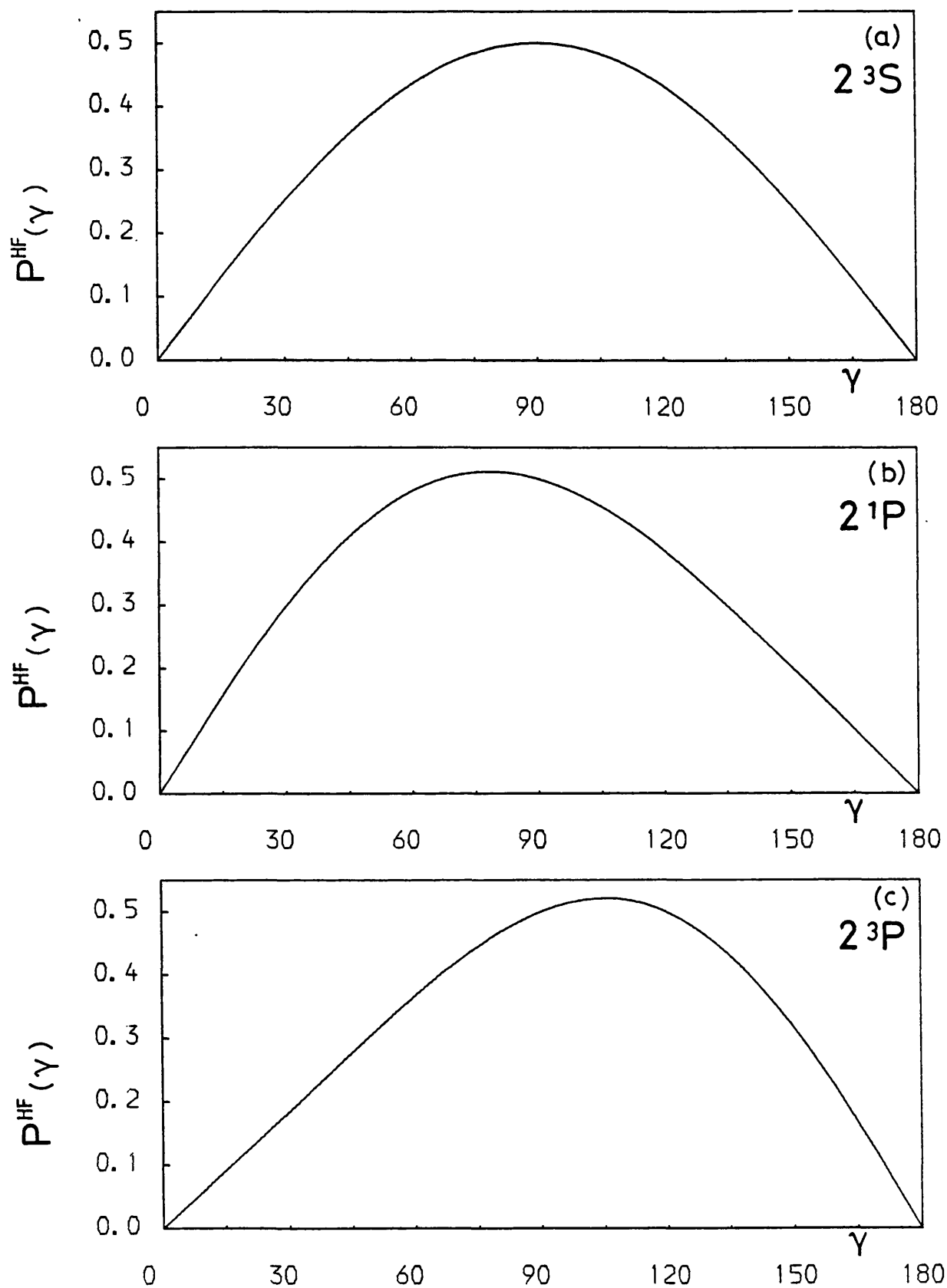
Figure (II.2.6)

The $P^{HF}(\gamma)$ distributions for the (a) 2^3S, (b) 2^1P and (c) 2^3P states of He.
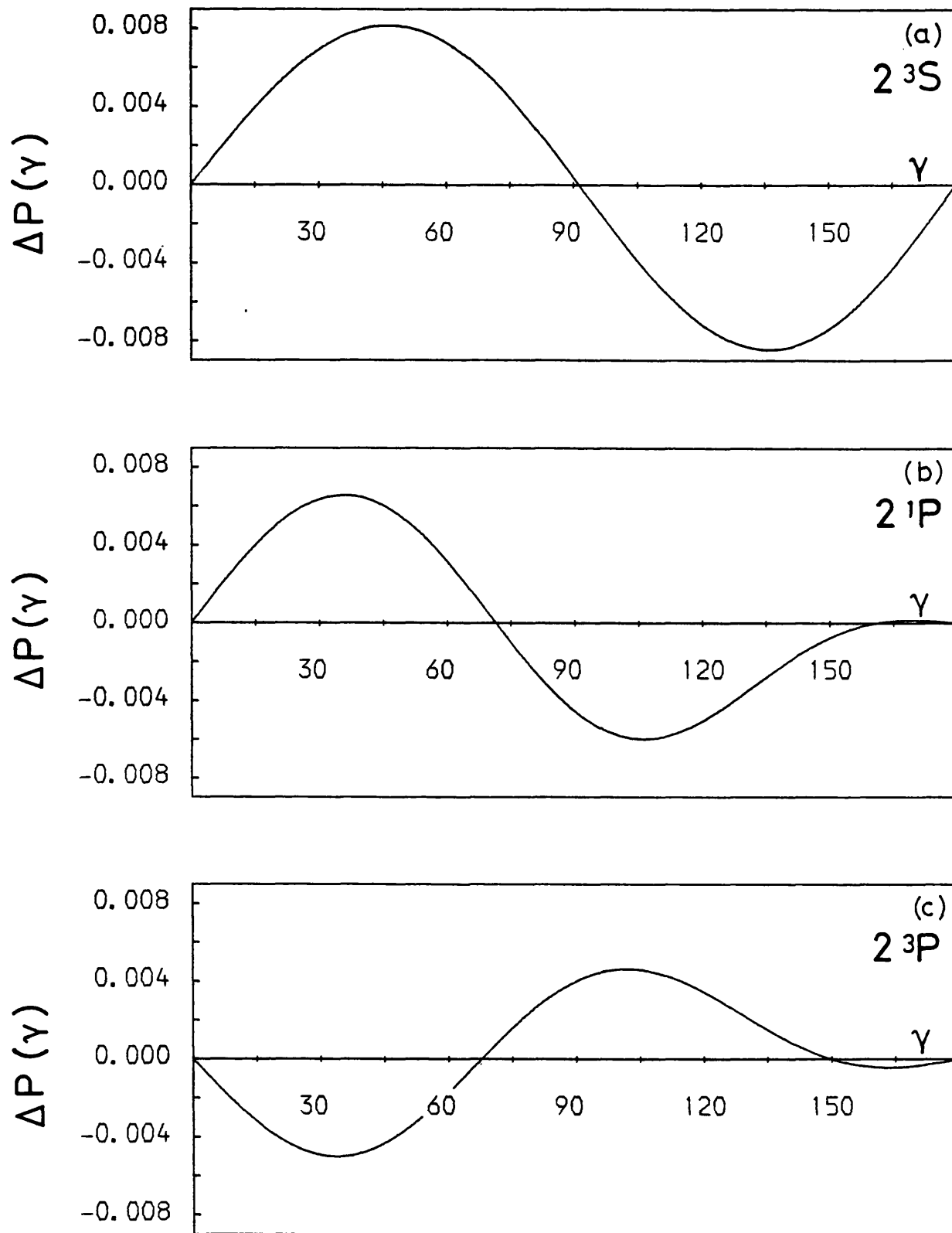
Figure (II.2.7)

The angular shifts $\Delta P(\gamma)$ for the (a) 2^3S, (b) 2^1P and (c) 2^3P states of He.
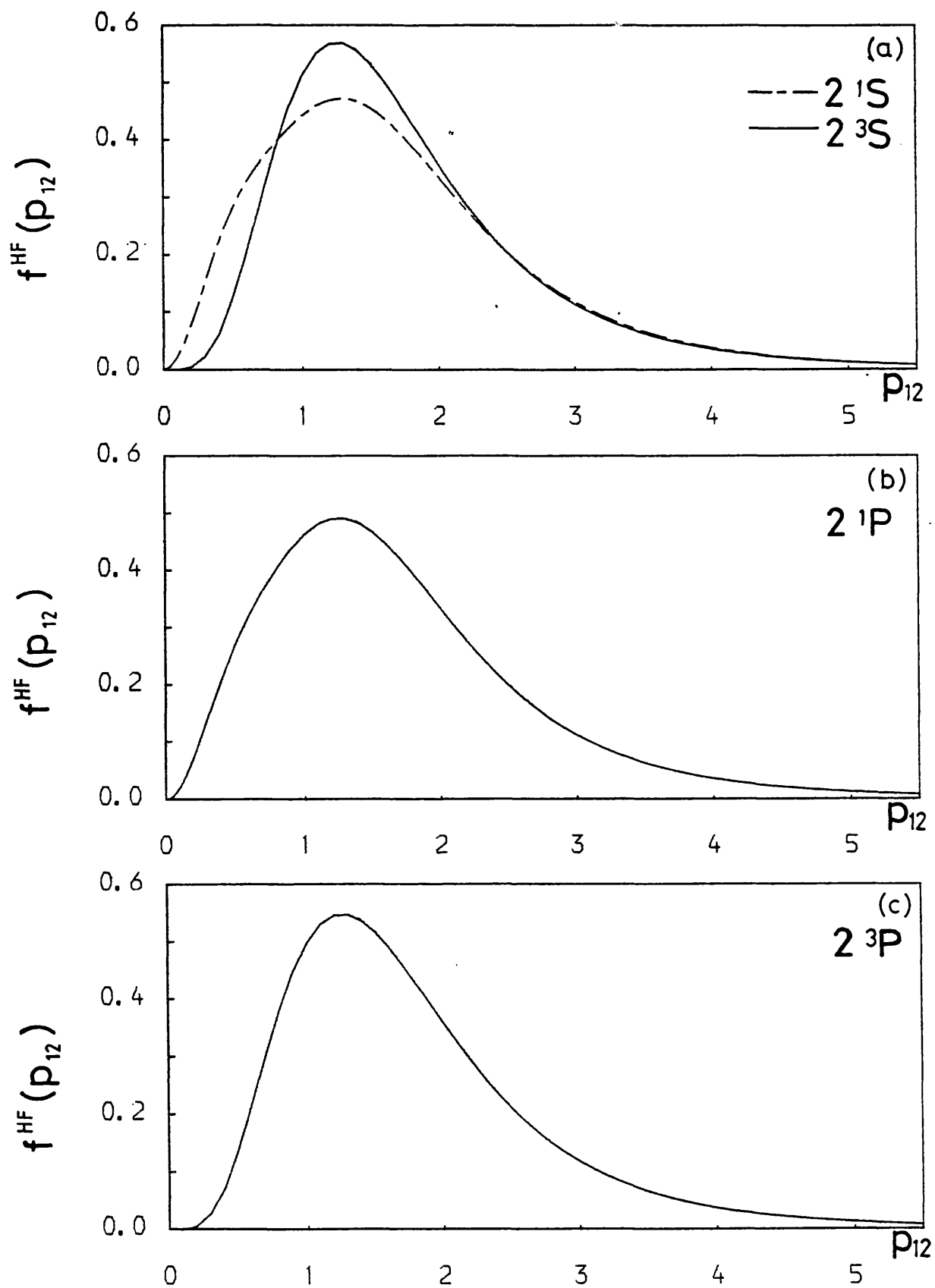
Figure (II.2.8)

The $f^{HF}(p_{12})$ distributions for the (a) 2^1S and 2^3S, (b) 2^1P and (c) 2^3P states of He.
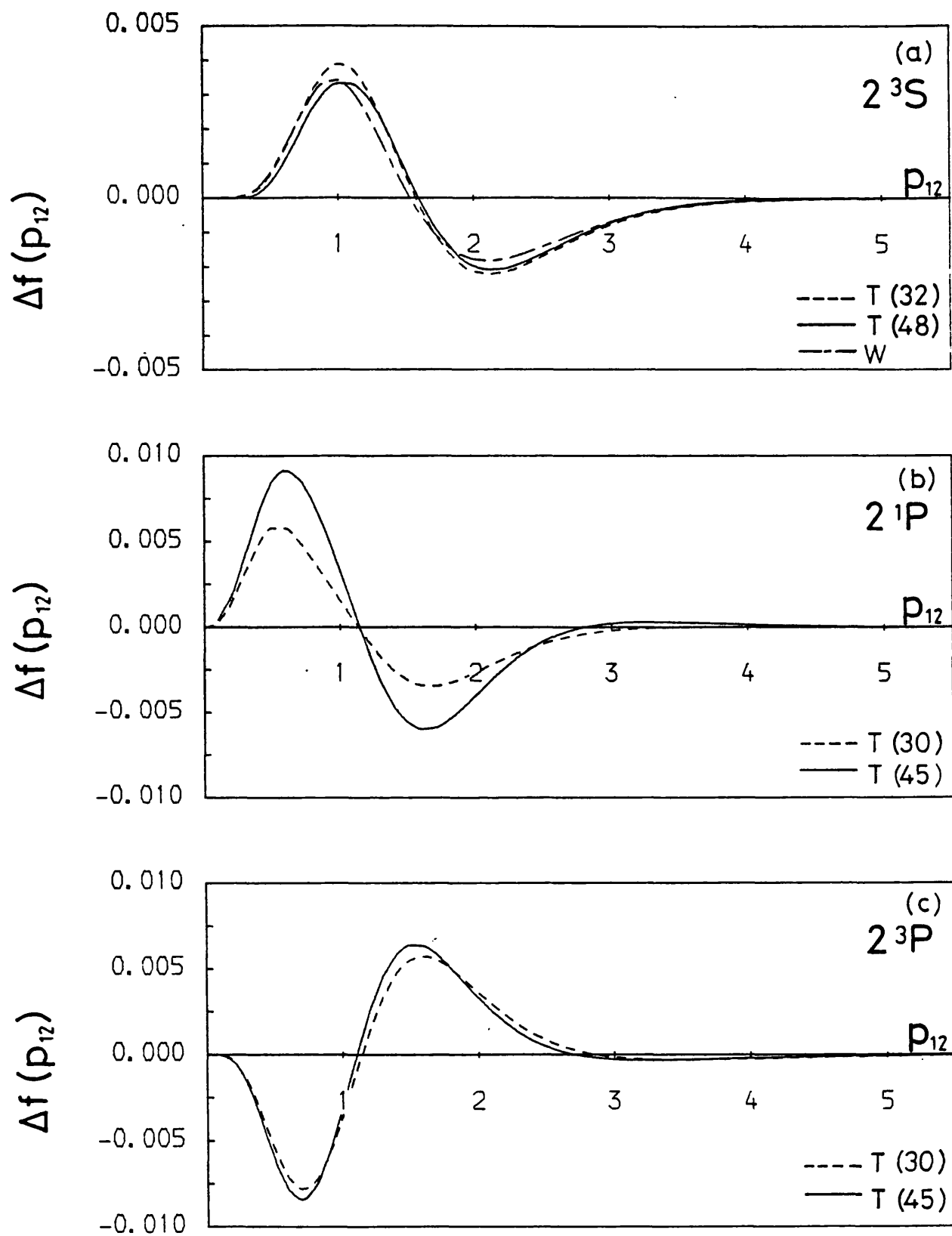
<u>Figure (II.2.9)</u>

The Coulomb shifts $\Delta f(p_{12})$ for the (a) $2\,^3S$, (b) $2\,^1P$ and (c) $2\,^3P$ states of He.
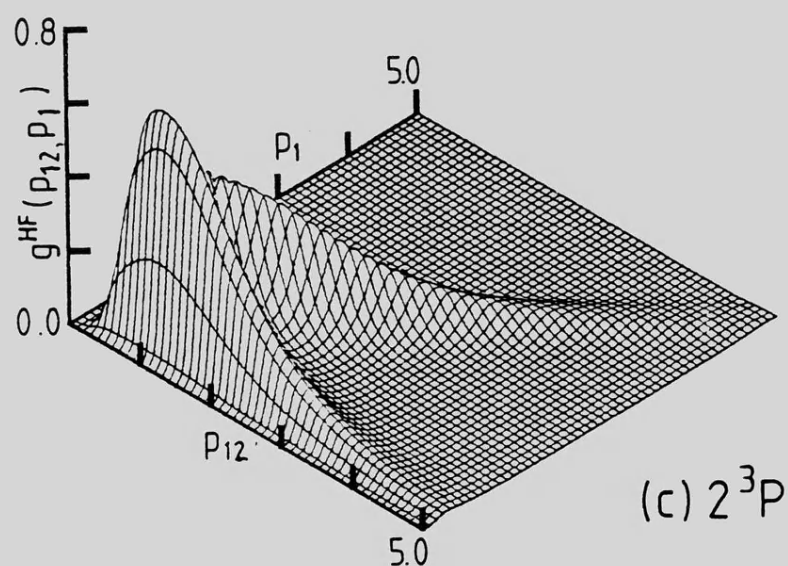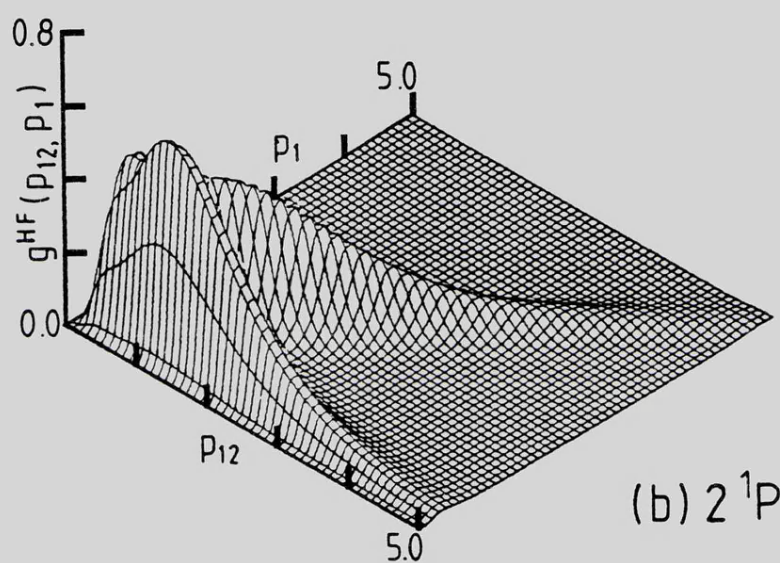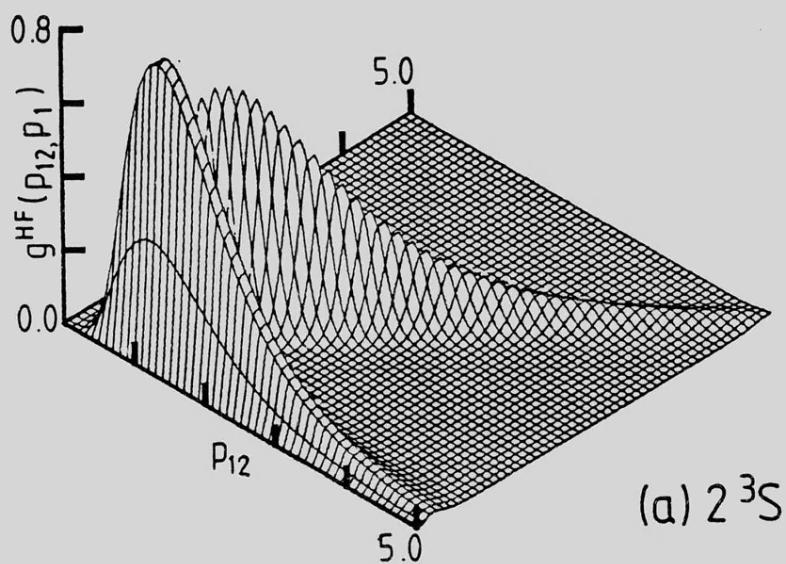
Figure (II.2.10)

The $g^{HF}(p_{12}, p_1)$ distributions for the

(a) 2^3S, (b) 2^1P and (c) 2^3P states of He.

146

$g^{HF}(p_{12},p_1)$ — 0.8

p_{12}

5.0

p_1

5.0

(a) $2\,^3S$

$g^{HF}(p_{12},p_1)$ — 0.8

p_{12}

5.0

p_1

5.0

(b) $2\,^1P$

$g^{HF}(p_{12},p_1)$ — 0.8

p_{12}

5.0

p_1

5.0
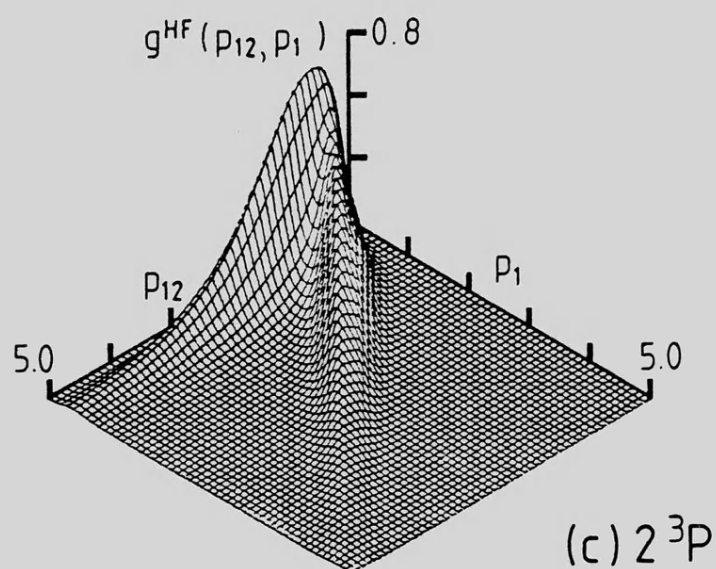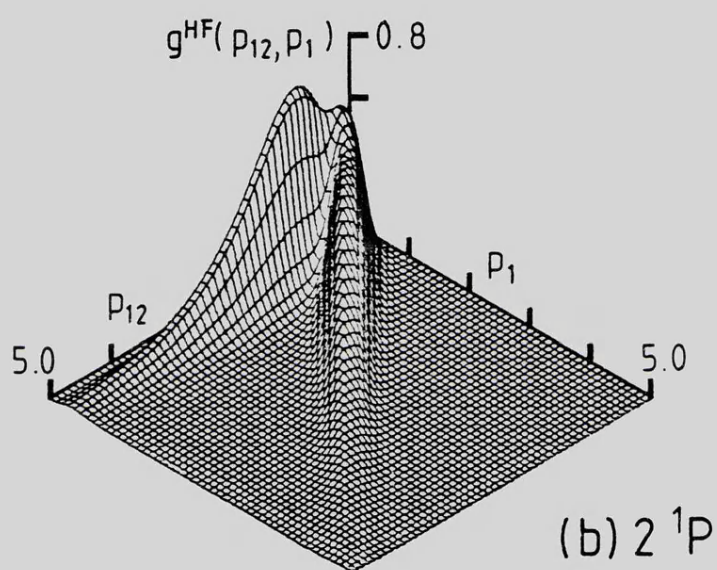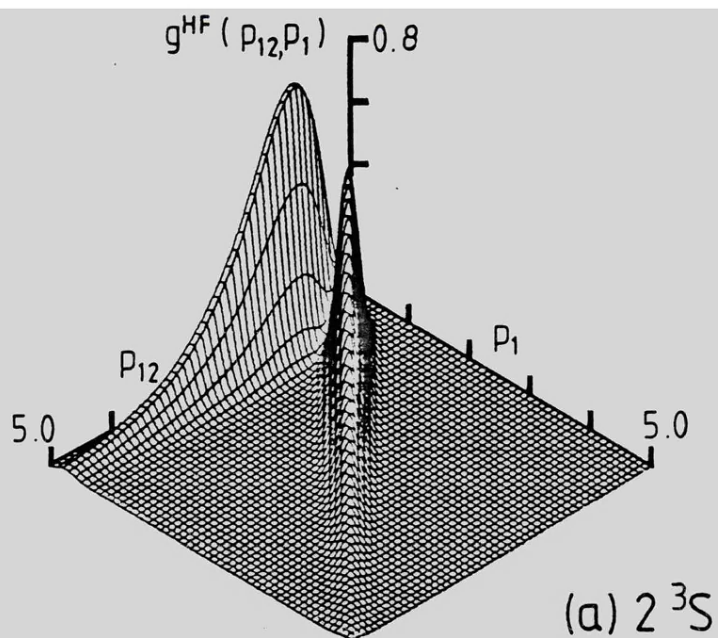
(c) $2\,^3P$

<u>Figure (II.2.11)</u>

An alternative view of the $g^{HF}(p_{12},p_1)$ surfaces
presented in Figure (II.2.10).
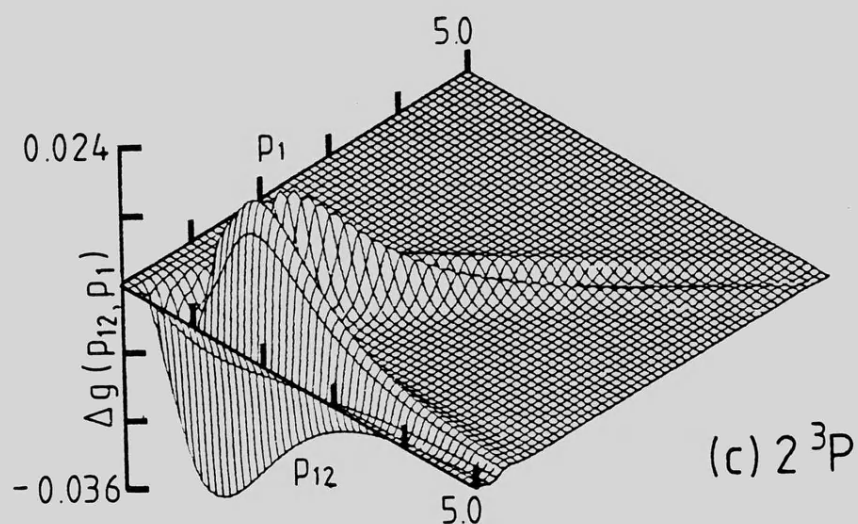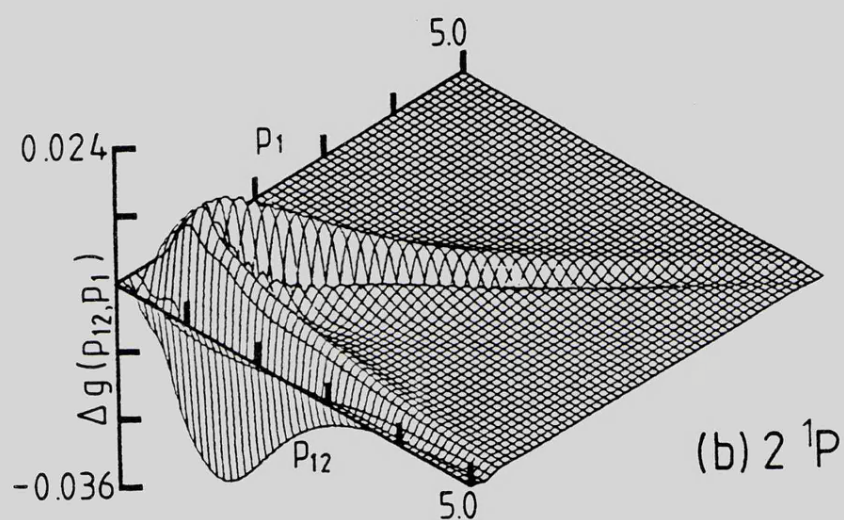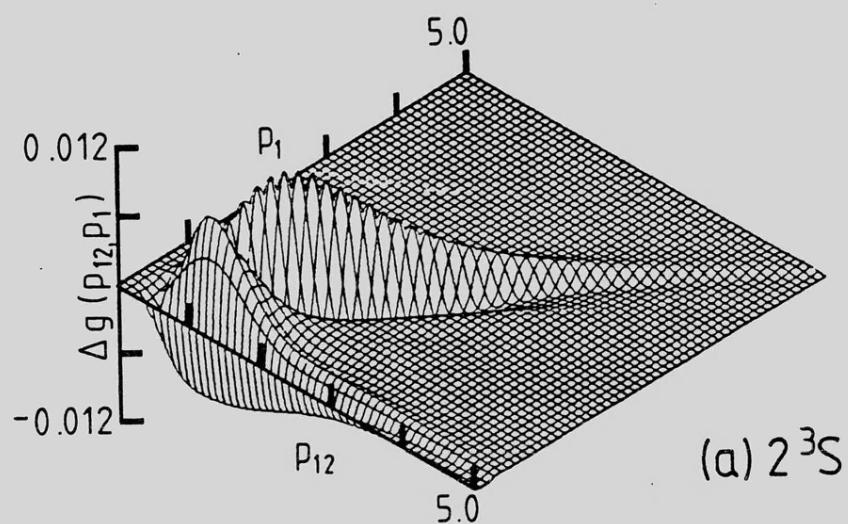
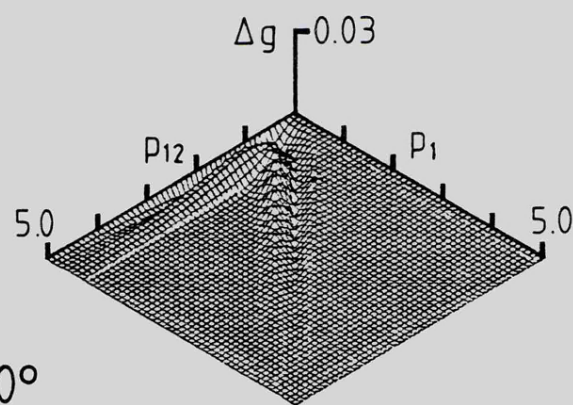<u>Figure (II.2.12)</u>

The partial Coulomb shifts $\Delta g(p_{12}, p_1)$ for the

(a) 2^3S, (b) 2^1P and (c) 2^3P states of He.

148

$\Delta g (p_{12}, p_1)$ ⌐0.006

p_{12}

5.0

p_1

5.0

(a) $2\,^3S$

$\Delta g (p_{12}, p_1)$ ⌐0.012

p_{12}

5.0

p_1

5.0

(b) $2\,^1P$

$\Delta g (p_{12}, p_1)$ ⌐0.012

p_{12}

5.0

p_1

5.0

(c) $2\,^3P$
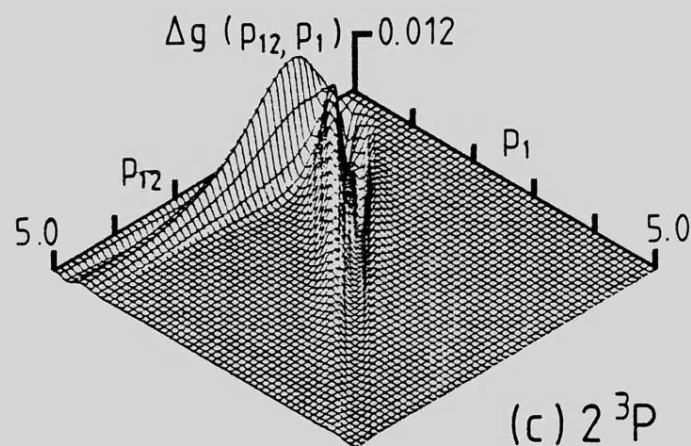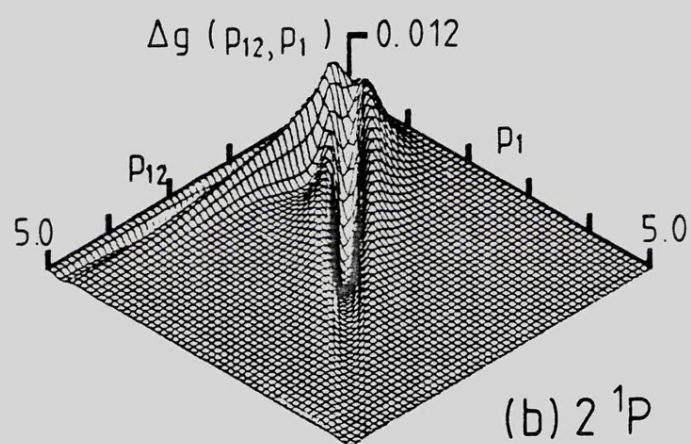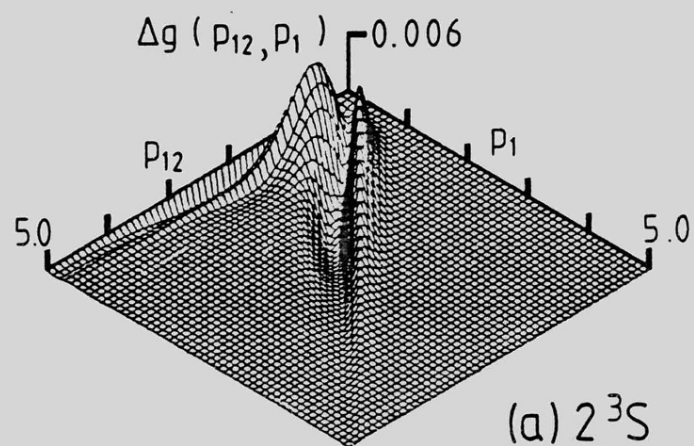
Figure (II.2.13)

An alternative view of the $\Delta g(p_{12}, p_1)$ surfaces

presented in Figure (II.2.12).

149

Figure (II.2.14)

(see over)

Figure (II.2.14)

The $g^{HF}(p_{12}, p_1; \theta_1)$ distributions for the (a)2^1P and (b)2^3P states of He.
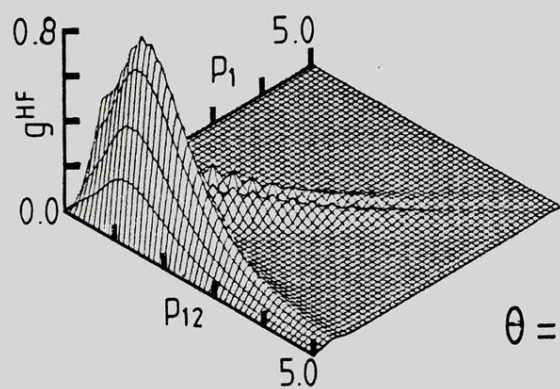
$\theta = 0°$
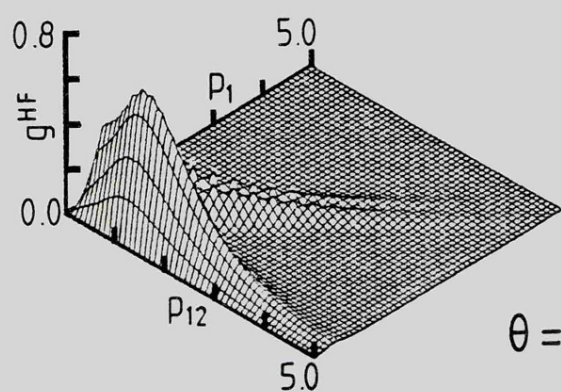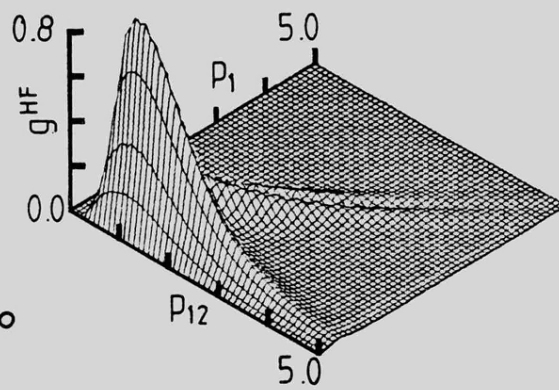
$\theta = 30°$
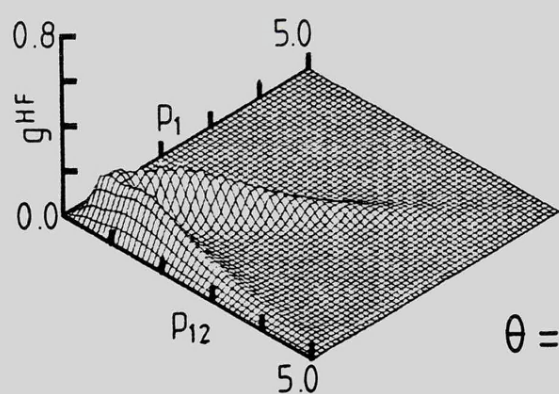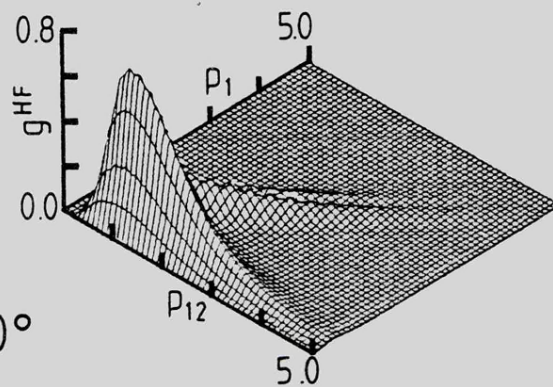
$\theta = 60°$

$\theta = 90°$
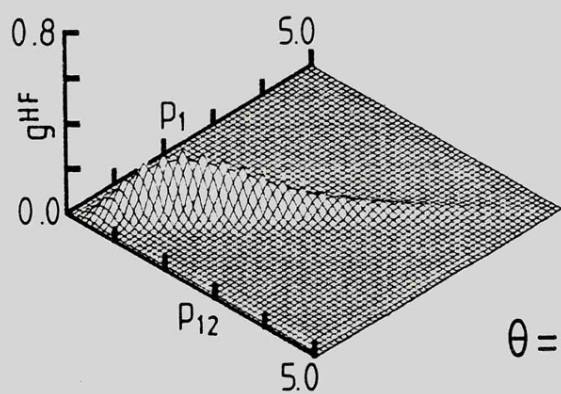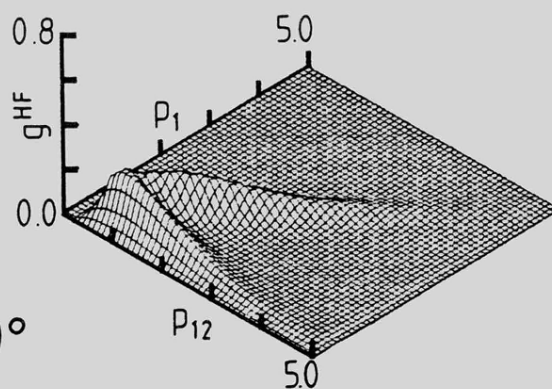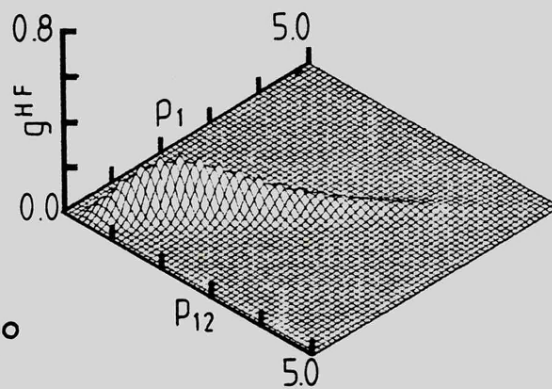
(a) $2\,^1P$ (b) $2\,^3P$

Figure (II.2.15)

(see over)

Figure (II.2.15)

An alternative view of the $g^{HF}(p_{12}, p_1; \theta_1)$ surfaces presented in Figure (II.2.14).

$\theta_1 = 0°$

$\theta_1 = 30°$

$\theta_1 = 60°$

$\theta_1 = 90°$
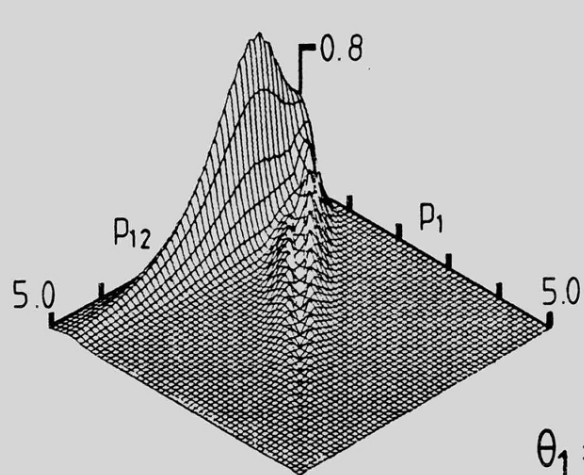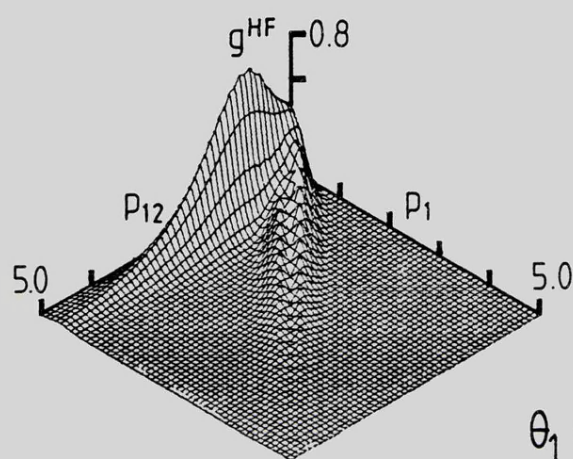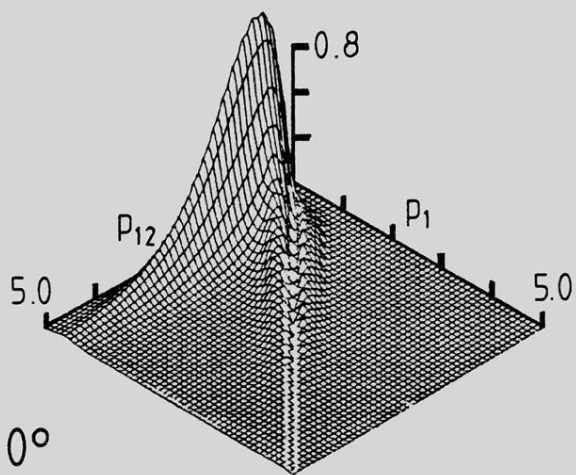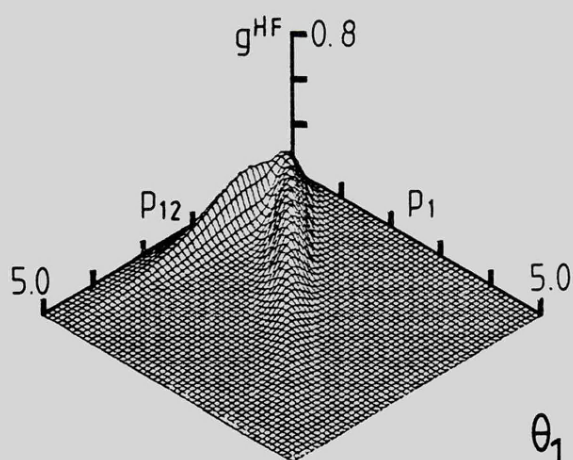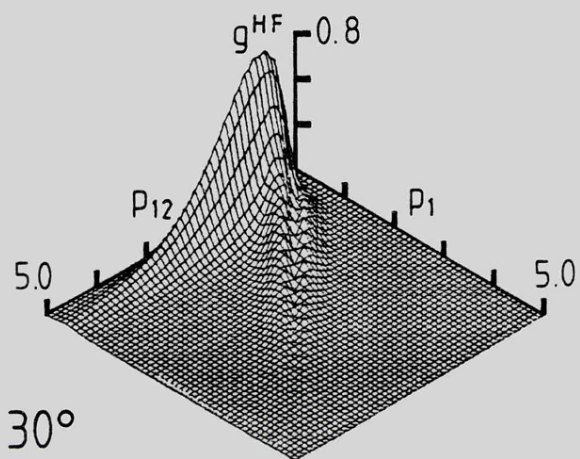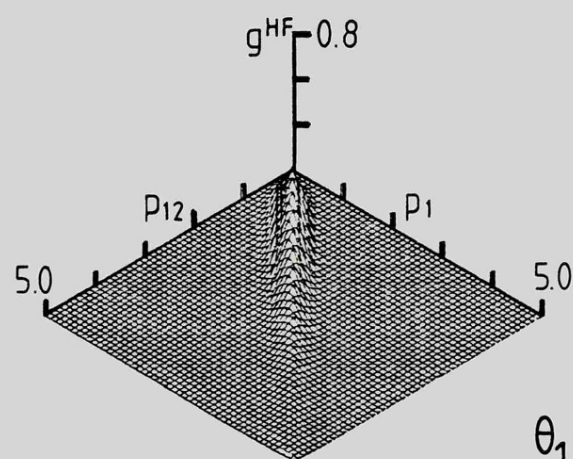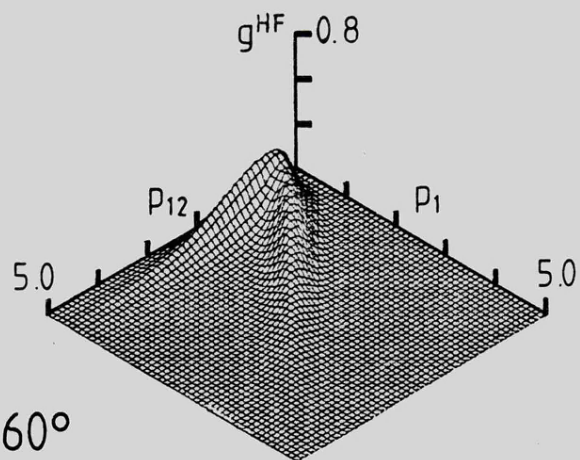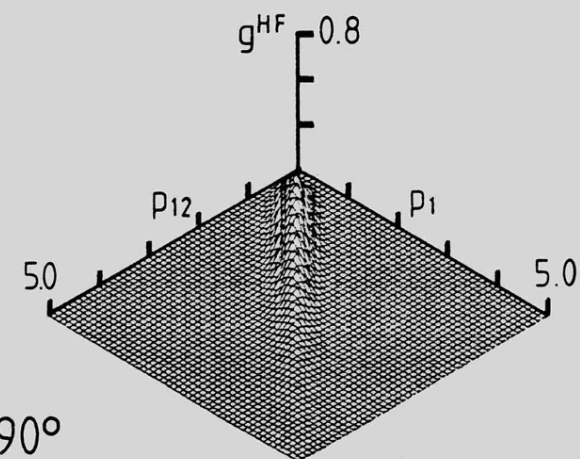
(a) $2\,^1P$ (b) $2\,^3P$

Figure (II.2.16)

(see over)

<u>**Figure (II.2.16)**</u>

The partial Coulomb shifts $\Delta g(P_{12}, P_1; \theta_1)$ for the

(a) $2^1 P$ and (b) $2^3 P$ states of He.

$\theta_1 = 0°$

$\theta_1 = 30°$

$\theta_1 = 60°$

$\theta_1 = 90°$
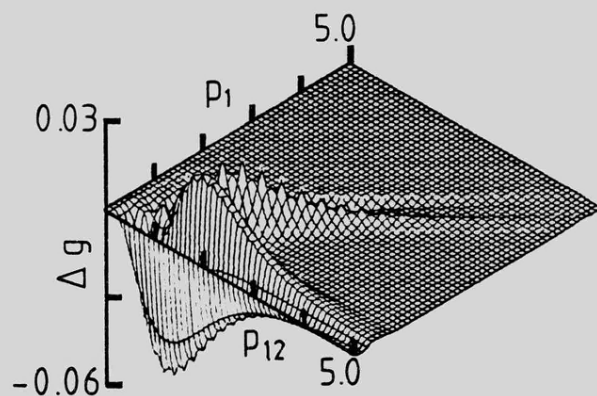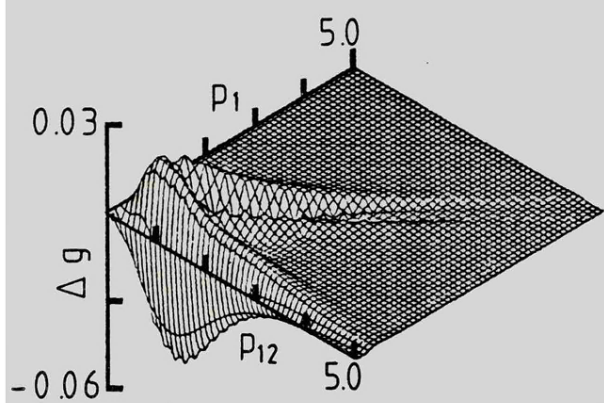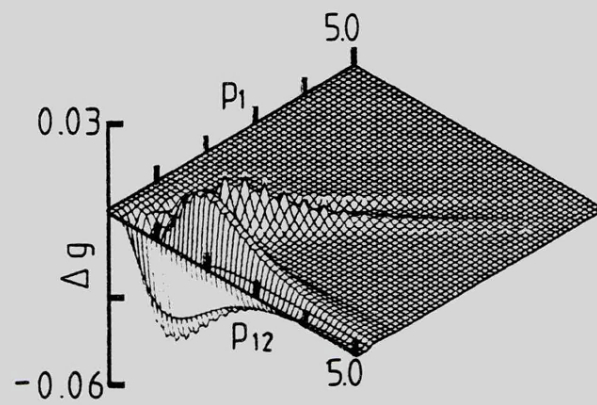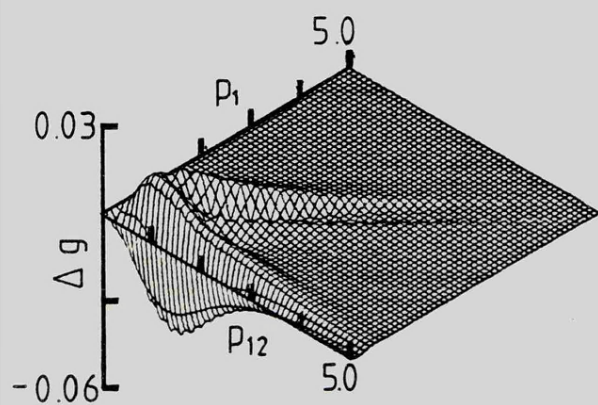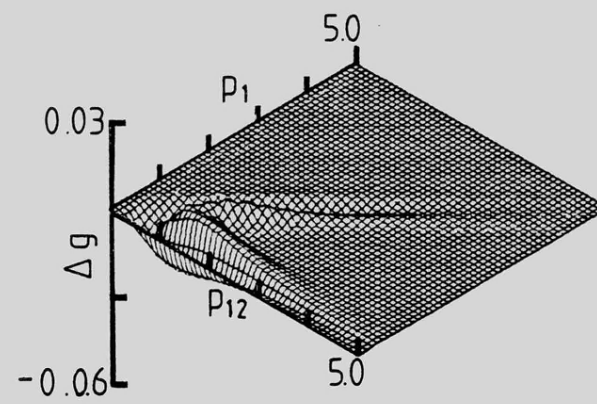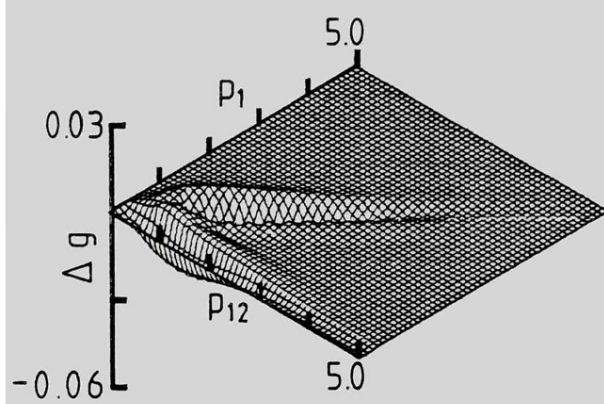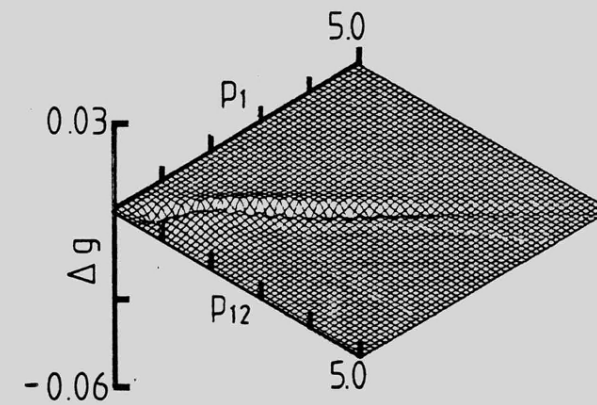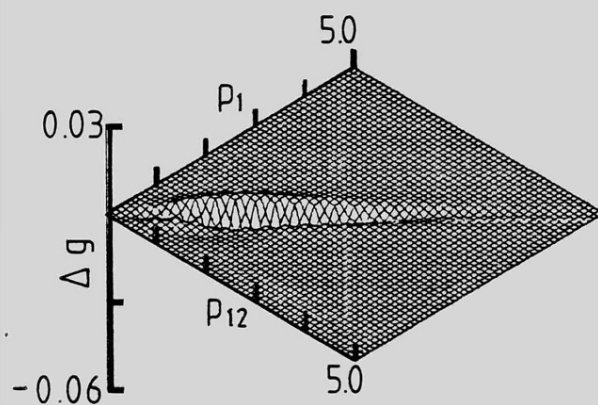
(a) $2\,^1P$

(b) $2\,^3P$

Figure (II.2.17)

(see over)

Figure (II.2.17)

An alternative view of the $\Delta g(p_{12}, p_1; \theta_1)$

surfaces presented in Figure (II.2.16).

$\theta_1 = 0°$
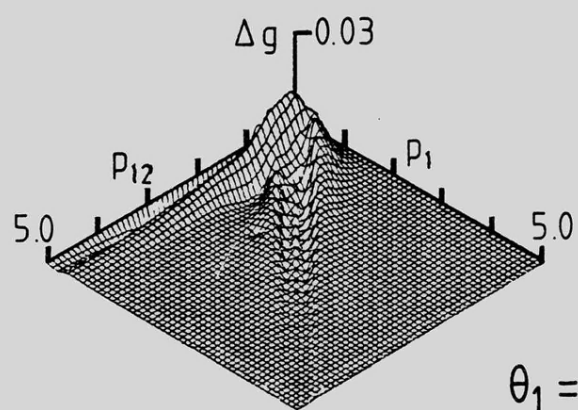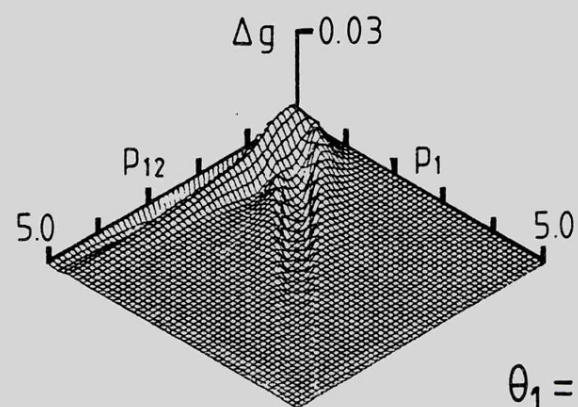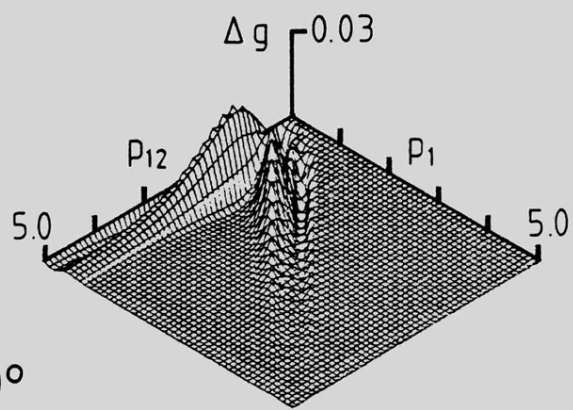
$\theta_1 = 30°$

$\theta_1 = 60°$

$\theta_1 = 90°$
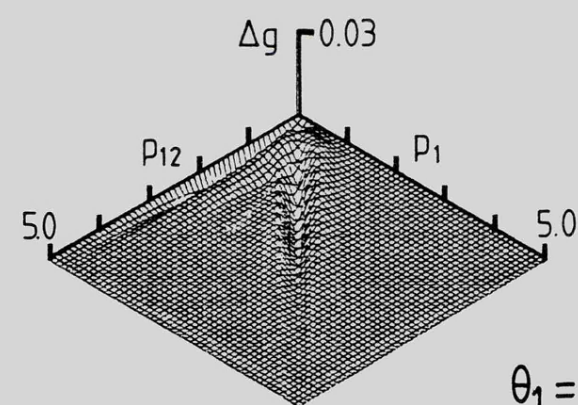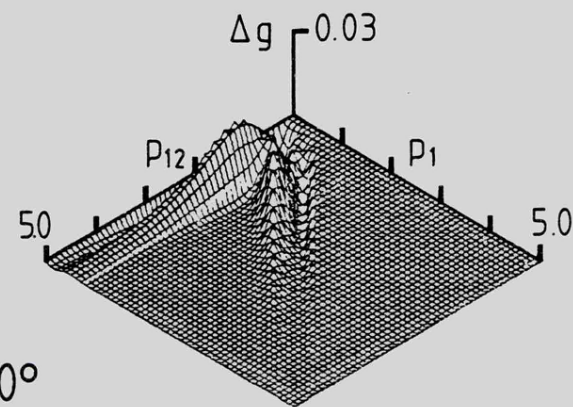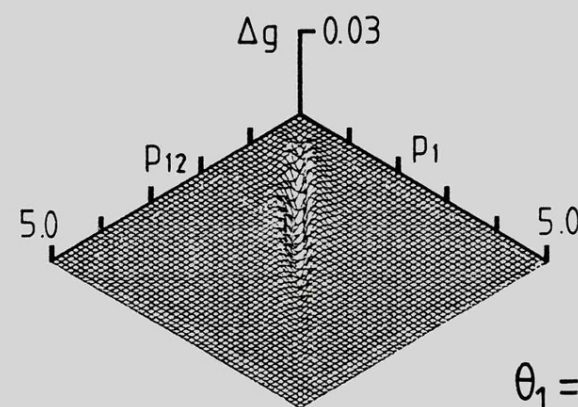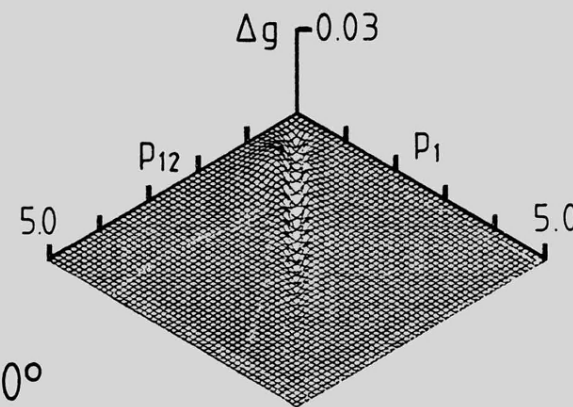
(a) $2\,^1P$ (b) $2\,^3P$
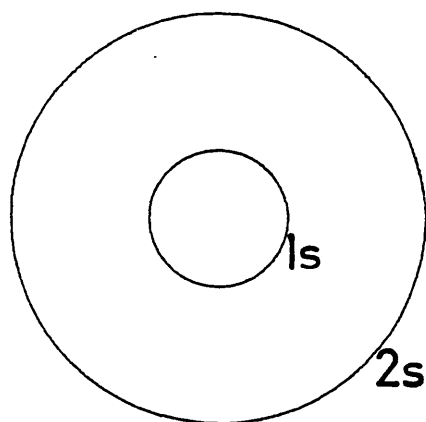
(a) Is 2s: Position Space
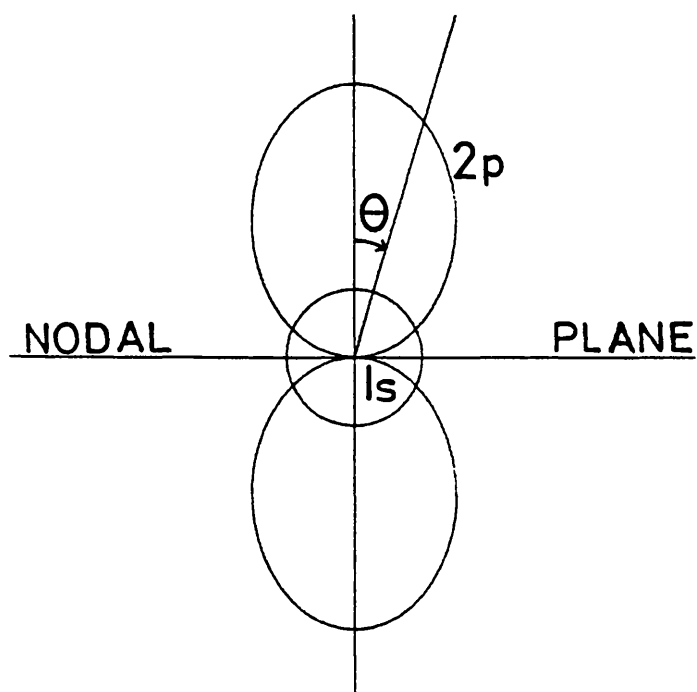
(b) Is 2p: Position Space
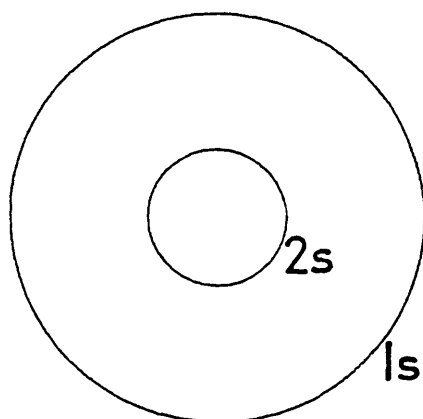
(c) Is 2s: Momentum Space
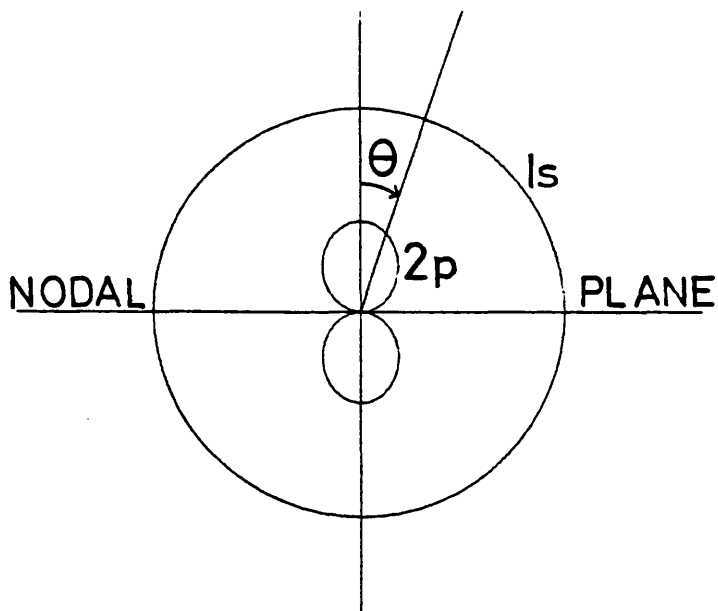
(d) Is 2p: Momentum Space

Figure (II.2.18)

A schematic, 2-D representation of the electron distributions in 1s2s and 1s2p states of He in position and momentum space (not to relative scale).

154

State	Ψ	$\langle p_1^{-2} \rangle$	$\langle p_1^{-1} \rangle$	$\langle p_1 \rangle$	$\langle p_1^2 \rangle$	$\sigma(p_1)$
2^3S	T(32)	0.15723^2	0.25469^1	0.10419^1	0.21752^1	0.10438^1
	T(48)	0.15715^2	0.25463^1	0.10423^1	0.21752^1	0.10435^1
	W	0.15853^2	0.25536^1	0.10419^1	0.21753^1	0.10439^1
	D(HF)	0.15931^2	0.25605^1	0.10410^1	0.21743^1	0.10444^1
2^1P	T(30)	0.53092^1	0.17908^1	0.10727^1	0.21235^1	0.98628^0
	T(45)	0.53001^1	0.17895^1	0.10729^1	0.21236^1	0.98613^0
	D(HF)	0.54871^1	0.18143^1	0.10701^1	0.21224^1	0.98865^0
2^3P	T(30)	0.45459^1	0.16722^1	0.10919^1	0.21327^1	0.96984^0
	T(45)	0.45430^1	0.16718^1	0.10919^1	0.21328^1	0.96979^0
	D(HF)	0.47721^1	0.17017^1	0.10883^1	0.21314^1	0.97310^0

Table (II.2.1)

The one-particle radial expectation values $\langle p_1^n \rangle$ when n = -2, -1, +1 and +2, and the standard deviation $\sigma(p_1)$, for the 2^3S, 2^1P and 2^3P states of He. The superscripts denote the power of ten by which each entry is to be multiplied.

155

State	Ψ	$\langle p_1^{-2} p_2^{-2} \rangle$	$\langle p_1^{-1} p_2^{-1} \rangle$	$\langle p_1 p_2 \rangle$	$\langle p_1^2 p_2^2 \rangle$
2^3S	T(32)	0.22597^2	0.32160^1	0.53895^0	0.48748^0
	T(48)	0.22570^2	0.32143^1	0.53924^0	0.48817^0
	W	0.22812^2	0.32263^1	0.53836^0	0.48723^0
	D(HF)	0.22962^2	0.32380^1	0.53569^0	0.48025^0
2^1P	T(30)	0.11560^2	0.23156^1	0.75788^0	0.96567^0
	T(45)	0.11580^2	0.23135^1	0.75869^0	0.96817^0
	D(HF)	0.12037^2	0.23529^1	0.74686^0	0.93493^0
2^3P	T(30)	0.99539^1	0.21281^1	0.83593^0	0.11992^1
	T(45)	0.99476^1	0.21274^1	0.83622^0	0.12002^1
	D(HF)	0.10631^1	0.21856^1	0.82782^0	0.12005^1

Table (II.2.2)

The two-particle radial expectation values $\langle p_1^n p_2^n \rangle$ when $n = -2, -1, +1$ and $+2$, for the 2^3S, 2^1P and 2^3P states of He. The superscripts denote the power of ten by which each entry is to be multiplied.

State Ψ		$\langle \underline{p}_1 \cdot \underline{p}_2 / p_1^2 p_2^2 \rangle$	$\langle \cos \gamma \rangle$	$\langle \underline{p}_1 \cdot \underline{p}_2 \rangle$	$\langle \gamma \rangle (°)$
2^3S	T(32)	0.21469^{-1}	0.11156^{-1}	0.76469^{-2}	89.361
	T(48)	0.21298^{-1}	0.11040^{-1}	0.74917^{-2}	89.368
	W	0.19637^{-1}	0.10319^{-1}	0.71470^{-2}	89.409
	D(HF)	0.0	0.0	0.0	90.000
2^1P	T(30)	0.28967^{0}	0.78390^{-1}	0.43625^{-1}	85.504
	T(45)	0.28996^{0}	0.78554^{-1}	0.43622^{-1}	85.495
	D(HF)	0.28711^{0}	0.72819^{-1}	0.35147^{-1}	85.824
2^3P	T(30)	-0.32853^{0}	-0.10568^{0}	-0.65054^{-1}	96.067
	T(45)	-0.32871^{0}	-0.10586^{0}	-0.65306^{-1}	96.077
	D(HF)	-0.32512^{0}	-0.10201^{0}	-0.66098^{-1}	95.855

<u>Table (II.2.3)</u>

Values of $\langle \underline{p}_1 \cdot \underline{p}_2 / p_1^n p_2^n \rangle$ when n = 2, 1 and 0, and $\langle \gamma \rangle$, the average angle between the momentum vectors, for the 2^3S, 2^1P and 2^3P states of He. The superscripts denote the power of ten by which each entry is to be multiplied.

State	Ψ	$\langle p_{12}^{-1} \rangle$	$\langle p_{12} \rangle$	$\langle p_{12}^{2} \rangle$	$\sigma(p_{12})$	$Y(\%)$
2^3S	T(32)	0.72527^0	0.18054^1	0.43351^1	0.10372^1	0.265^0
	T(48)	0.72498^0	0.18060^1	0.43355^1	0.10362^1	0.231^0
	W	0.72512^0	0.18059^1	0.43362^1	0.10368^1	0.228^0
	D(HF)	0.72356^0	0.18092^1	0.43486^1	0.10369^1	$-$
2^1P	T(30)	0.87041^0	0.17279^1	0.41597^1	0.10835^1	0.344^0
	T(45)	0.86828^0	0.17215^1	0.41599^1	0.10938^1	0.513^0
	D(HF)	0.86525^0	0.17326^1	0.41746^1	0.10828^1	$-$
2^3P	T(30)	0.72249^0	0.18215^1	0.43956^1	0.10382^1	0.490^0
	T(45)	0.72253^0	0.18220^1	0.43962^1	0.10375^1	0.509^0
	D(HF)	0.72674^0	0.18182^1	0.43950^1	0.10436^1	$-$

Table (II.2.4)

Values of $\langle p_{12}^{n} \rangle$ when n = -1, +1 and +2, the standard deviation, $\sigma(p_{12})$, and Y, the percentage of $f(p_{12})$ shifted by correlation, for the 2^3S, 2^1P and 2^3P states of He. The superscripts denote the power of ten by which each entry is to be multiplied.

REFERENCES - SECTION (II)

REFERENCES - SECTION (II)

1) A. Brickstock and J.A. Pople, Phil. Mag. 43 1090 (1952)

2) Sir J. Lennard-Jones and J.A. Pople, Phil. Mag. 43 581 (1952)

3) P.-O. Löwdin, Adv. Chem. Phys. 2 207 (1959)

4) R.J. Boyd and C.A. Coulson, J. Phys. B: Atom. Molec. Phys. 6 782 (1973)

5) R.J. Boyd and J. Katriel, Int. J. Quant. Chem. 8 255 (1974)

6) N. Moiseyev, J. Katriel and R.J. Boyd, Theoret. Chim. Acta (Berlin) 45 61 (1977)

7) D.J. Ellis, Ph.D. Thesis, 'Angular Correlation in Atoms and the Calculation of Molecular Wavefunctions', University of Leicester (1974)

8) K.E. Banyard and D.J. Ellis, Mol. Phys. 24 1291 (1972)

9) N. Moiseyev and J. Katriel, Chem. Phys. 10 67 (1975)

10) M.P. Barnett, F.W. Birss and C.A. Coulson, Mol. Phys. 1 44 (1958)

11) C.A. Coulson and A.H. Neilson, Proc. Phys. Soc. (London) 78 831 (1961)

12) W.A. Lester,Jr. and M. Krauss, J. Chem. Phys. 41 1407 (1964)

13) R.F. Curl,Jr. and C.A. Coulson, Proc. Phys. Soc. (London) 85 647 (1965)

14) F.L. Pilar, 'Elementary Quantum Chemistry', McGraw-Hill Book Company : New York (1968)

15) R.J. Tweed, J. Phys. B: Atom. Molec. Phys. 6 770 (1973)

16) M.E. Rose, 'Elementary Theory of Angular Momentum', J. Wiley and Sons, Inc. : New York (1957)

17) A.W. Weiss, Phys. Rev. 122 1826 (1961)

18) J.F. Perkins, J. Chem. Phys. 39 687 (1963)

19) E.R. Davidson, J. Chem. Phys. 42 4199 (1965)

20) See, for example, R.McWeeny and B.T. Sutcliffe, 'Methods of Molecular Quantum Mechanics', Academic Press : London (1976)

21) R. Benesch, Int. J. Quant. Chem. 6 181 (1972)

22) J.-L. Calais and P.-O. Löwdin, J. Mol. Spect. $\underline{8}$ 203 (1962)

23) C.E. Reed, Ph.D. Thesis, ´Properties of Electron Momentum Distributions: A Study of Correlation Effects in Some Two-Electron Systems and an Examination of Directional Compton Profiles for the Lithium Halides´, University of Leicester (1980)

24) For documentation relating to the most recent implementation of this library, see "NAG Fortran Library Manual, Mark 10´ (1983)

25) T.N.L. Patterson, Math. Comp. $\underline{53}$ 592 (1975)

26) See, for example, H. Cramér, ´The Elements of Probability Theory´, Wiley : New York (1955)

27) J. Gruninger, Y. Öhrn and P.-O. Löwdin, J. Chem. Phys. $\underline{52}$ 5551 (1970)

28) See, for example, D.W. Cruickshank, Acta. Cryst. $\underline{2}$ 65 (1949) and references therein.

29) ´The Ghost Graphical Output System´ User Manual, UKAEA Culham Laboratory (1977)

30) Private communication : $g^{corr}(r_{12}, r_1)$ values supplied for the explicitly correlated wavefunction of Perkins (see Reference (18))

31) See, for example, S. Fraga and G. Malli, ´Many Electron Systems : Properties and Interactions´, W.B. Saunders : Philadelphia (1968)

32) See, for example, B.I. Bleaney and B. Bleaney, ´Electricity and Magnetism´, Oxford University Press : Oxford (1968)

33) See, for example, J.H. Van Vleck, ´The Theory of Electric and Magnetic Susceptibities´, Oxford University Press : Oxford (1932)

34) See, for example, A. Dalgarno, Advanc. Phys. $\underline{11}$ 281 (1962)

35) K.E. Banyard and C.E. Reed, J. Phys. B: Atom. Molec. Phys. $\underline{11}$ 2957 (1978)

36) K.E. Banyard and R.J. Mobbs, J. Chem. Phys. $\underline{75}$ 3433 (1981)

37) K.E. Banyard and G.J. Seddon, J. Chem. Phys. $\underline{58}$ 1132 (1973)

38) K.E. Banyard and C.E. Reed, J. Phys. B: Atom. Molec. Phys. $\underline{14}$ 411 (1981) and private communication

39) C.C. Baker, Ph.D. Thesis, 'Correlation Effects and Electron Densities in Some Two-Electron Systems', University of Leicester (1974)

40) Y. Accad, C.L. Pekeris and B. Schiff, Phys. Rev. 4A 516 (1971)

41) Private communication

42) A.J. Thakkar and V.H.Smith Jr., Phys.Rev. 23A 473 (1981)

43) B.G. Williams, 'Compton Scattering-The Investigation of Electron Momentum Distributions', Ed. B.G. Williams, McGraw-Hill Book Co. : London (1977)

44) A.S. Eve, Phil. Mag. 8 669 (1904)

45) W.H. Bragg, Phil. Mag. 14 429 (1907)

46) D.C.H. Florance, Phil. Mag. 20 921 (1910)

47) J.A. Gray, Phil. Mag. 26 611 (1913)

48) J.A. Gray, J. Franklin Inst. 190 633 (1920)

49) A.H. Compton, Bull. Natl. Res. Counc. 4 (1922)

50) A.H. Compton, Phys. Rev. 21 483 (1923)

51) A.H. Compton, Phys. Rev. 22 409 (1923)

52) a) G.E.M. Jauncey, Phys. Rev. 24 204 (1924)

    b) G.E.M. Jauncey, Phys. Rev. 25 314 (1925)

    c) G.E.M. Jauncey, Phys. Rev. 25 723 (1925).

53) J.W.M. DuMond, Phys. Rev. 33 643 (1929)

54) E.A. Hylleraas, Z. Physik 74 216 (1932)

55) V. Fock, Z. Physik 98 145 (1935)

56) N. Svartholm, Ph.D. Thesis, 'The Binding Energies of the Lightest Atomic Nuclei', University of Lund (1945)

57) a) R. McWeeny and C.A. Coulson, Proc. Phys. Soc. (London) 62A 509 (1949); see also :-

    b) J. Navaza and G. Tsoucaris, Phys. Rev. 24A 683 (1981)

58) R. McWeeny, Proc. Phys. Soc. (London) 62A 519 (1949)

59) M. Levy, Proc. Roy. Soc. (London) A204 145 (1950)

60) E.E. Salpeter, Phys. Rev. 84 1226 (1951)

61) E.E. Salpeter and J.S. Goldstein, Phys. Rev. 90 983 (1953)

62) P.A.M. Dirac, 'The Principles of Quantum Mechanics', Oxford University Press : Oxford, 4'th edition (1958)

63) J.L. Powell and B. Crasemann, 'Quantum Mechanics', Addison-Wesley Publishing Company Inc. : Reading, Massachusetts, U.S.A. (1961)

64) P. Kaijser and V.H. Smith, Adv. Quant. Chem. $\underline{10}$ 37 (1977)

65) a) B. Podolsky and L. Pauling, Phys. Rev. $\underline{34}$ 109 (1929)

   For interesting comments on this paper, see also

   b) J.R. Lombardi, Phys. Rev. $\underline{22A}$ 797 (1980)

66) B. Hicks, Phys. Rev. $\underline{52}$ 436 (1937)

67) J.W.M. DuMond and H.A. Kirkpatrick, Phys. Rev. $\underline{52}$ 419 (1937)

68) H.A. Kirkpatrick and J.W.M. DuMond, Phys. Rev. $\underline{54}$ 802 (1938)

69) a) C.A. Coulson, Proc. Camb. Phil. Soc. $\underline{37}$ 55 (1941)

   b) C.A. Coulson and W.E. Duncanson, Proc. Camb. Phil. Soc. $\underline{37}$ 67 (1941)

   c) C.A. Coulson, Proc. Camb. Phil. Soc. $\underline{37}$ 74 (1941)

   d) W.E. Duncanson, Proc. Camb. Phil. Soc. $\underline{37}$ 397 (1941)

   e) W.E. Duncanson and C.A. Coulson, Proc. Camb. Phil. Soc. $\underline{37}$ 406 (1941)

   f) C.A. Coulson and W.E. Duncanson, Proc. Camb. Phil. Soc. $\underline{38}$ 100 (1942)

70) R.J.Weiss, Acta. Cryst. $\underline{25a}$ 248 (1969)

71) O. Inkinen, V. Halonen and S. Manninen, Chem. Phys. Lett. $\underline{9}$ 639 (1971)

72) a) V.H. Smith Jr. and R. Benesch, in 'Proceedings of the International Symposium on the Physics of One- and Two-Electron Atoms', Munich (1968) (unpublished)

   b) R. Bensech, Phys. Rev. $\underline{A6}$ 573 (1972) (There is an error in this work--see (c))

   c) R. Bensech, J.Phys. B: Atom. Molec. Phys. $\underline{9}$ 2587 (1976)

73) R. Benesch and V.H. Smith Jr., Int. J. Quant. Chem. $\underline{4S}$ 131 (1971)

74) R. Benesch and V.H. Smith Jr., Chem. Phys. Lett. $\underline{5}$ 601 (1970)

75) R. Benesch and V.H. Smith Jr., Phys. Rev. $\underline{A5}$ 114 (1972)

76) R.E. Brown and V.H. Smith Jr., Phys. Rev. $\underline{A5}$ 140 (1972)

77) V.H. Smith Jr. and R.E. Brown, Chem. Phys. Lett. $\underline{20}$ 424 (1973)

78) R. Ahlberg and P. Lindner, J. Phys. B: Atom. Molec. Phys. $\underline{9}$ 2963 (1976)

79) K.E. Banyard and J.C. Moore, J. Phys. B: Atom. Molec. Phys. $\underline{10}$ 2781 (1977)

80) W. Kutzelnigg, A. Del Re and A. Berthier, Phys. Rev. $\underline{172}$ 49 (1968)

81) K.E. Banyard and C.C. Baker, J. Chem. Phys. $\underline{51}$ 2680 (1969)

82) J.C. Moore, Ph.D. Thesis, 'Electron Capture From Hydrogen Negative Ions and a Study of Electron Correlation in Momentum Space', University of Leicester (1978)

83) G. Doggett, Mol. Phys. $\underline{38}$ 853 (1979)

84) G. Doggett, Mol. Phys. $\underline{34}$ 1739 (1977)

85) R.J. Mobbs and K.E. Banyard, J. Chem. Phys. $\underline{78}$ 6106 (1983)

86) O. Sinanoglu and K.A. Brueckner, 'Three Approaches to Electron Correlation in Atoms', Yale University : New Haven (1970)

87) R.J. Boyd : Private communication

88) R. Benesch and S. Thomas, Phys. Rev. $\underline{A19}$ 931 (1979)

89) R. Benesch and V.H. Smith Jr., in 'Wave Mechanics - The First Fifty Years', Eds. W.C. Price, S.S. Chissick and T. Ravensdale, Butterworths : London (1973)

90) I.R. Epstein, 'International Review of Science, Physical Chemistry, Series 2: Volume I, Theoretical Chemistry, Eds. A.D. Buckingham and C.A. Coulson, Butterworths : London (1975)

91) I.R. Epstein, Phys. Rev. $\underline{8A}$ 160 (1973)

92) S. Gadre and P. Narasimhan, Mol. Phys. $\underline{31}$ 1613 (1976)

93) H.A. Bethe and E.E. Salpeter, 'Quantum Mechanics of One- and Two-Electron Atoms', Springer-Verlag : Berlin (1957)

94) S.R. Gadre, S. Chakravorty and R.K. Pathak, J. Chem. Phys. $\underline{78}$ 4581 (1983)

95) W.E. Duncanson and C.A. Coulson, Proc. Phys. Soc. $\underline{60}$ 175 (1948)

SECTION (III)

MOMENTUM-SPACE CORRELATION EFFECTS IN THE

2^2S AND 2^2P STATES OF LITHIUM

INTRODUCTION

The effects of correlation in open-shell excited states of helium are quite different to those which occur in the ground state of the atom. This suggests that in a many-electron system, the interaction between two electrons in the same shell will be quite distinct from that which occurs between electrons in different shells. Of course, it might be argued that the relatively long range of Coulombic potentials means that, in reality, the motion of any one electron will be inextricably linked with that of all the others, so that attempts to differentiate between correlation effects in this way are meaningless. However, comparisons between experimental electron densities and those calculated from Hartree-Fock wavefunctions indicate that the exact electron density of an atom possesses a shell structure very similar to that predicted by the uncorrelated description[1]. As a consequence, electron-electron interactions in a many-electron atom can indeed be classified broadly as intrashell or intershell effects. If we are to be able to extend our analysis of electron correlation from two-electron atoms to more complicated systems, we must consider how these different effects may be isolated and quantified.

For an N-electron atom described by a normalised position-space wavefunction $\phi(\underline{x}_1, \underline{x}_2, \ldots, \underline{x}_N)$, the distribution function of the distance r_{mn} between electrons m and n is defined by

$$f(r_{mn}) = \int \Pi(\underline{x}_m, \underline{x}_n) \, d\underline{x}_m . d\underline{x}_n / dr_{mn} \quad . \qquad \text{(III.1.1)}$$

The spin-dependent two-particle density, $\Pi(\underline{x}_m, \underline{x}_n)$, is defined in turn by

$$\Pi(\underline{x}_m, \underline{x}_n) = \binom{N}{2} \times$$

$$\int \phi^*(\underline{x}_1, \underline{x}_2, \ldots, \underline{x}_m, \ldots, \underline{x}_n, \ldots, \underline{x}_N) \phi(\underline{x}_1, \underline{x}_2, \ldots, \underline{x}_m, \ldots, \underline{x}_n, \ldots, \underline{x}_N)$$

$$\times \, d\underline{x}_1 d\underline{x}_2 \ldots d\underline{x}_{m-1} d\underline{x}_{m+1} \ldots d\underline{x}_{n-1} d\underline{x}_{n+1} \ldots d\underline{x}_N . \qquad \text{(III.1.2)}$$

The binomial factor $\binom{N}{2}$ ensures that the two-particle density is normalised to the number of electron pairs in the system. In Chapter (II.1.2) we saw that, by analogy with the work of Coulson and Neilson[2], the <u>total</u> Coulomb hole for the electron pair (m,n) can be defined by

$$\Delta f(r_{mn}) = f^{corr}(r_{mn}) - f^{HF}(r_{mn}) \quad , \qquad \text{(III.1.3)}$$

where $f(r_{mn})$ is evaluated at the correlated and Hartree-Fock levels respectively. Now, in a helium atom, there is only one pair of electrons, and the Coulomb hole therefore measures the average extent to which those two electrons avoid each other. For larger atoms, however, the indistinguishability of the electrons and the averaging process which is implicit in Equation (III.1.2) together imply that $\Delta f(r_{mn})$ will only measure the average extent to which <u>any</u> two electrons avoid each other. As a consequence,

Equation (III.1.3) gives no indication of how the various intrashell and intershell effects in the system differ in magnitude or characteristics; similar problems occur when we consider any other correlation property derived from the two-particle density. Clearly, if we are to obtain a complete understanding of correlation effects in a many-electron atom we must first find a way to divide the system into _identifiable_ electron pairs, each of which can be studied in relative isolation from the remainder.

A number of attempts have been made to describe atomic systems in terms of separated groups of electrons.[3] One of the earliest was that of Hurley, Lennard-Jones and Pople[3a] in 1953. In their approach, which has become known as the Separated Pair Approximation, the wavefunction for an N(=2n) electron atom is written in the form

$$\Phi(\underline{x}_1,\underline{x}_2,\ldots,\underline{x}_N) = A[\Lambda_1(\underline{x}_1,\underline{x}_2)\,\Lambda_2(\underline{x}_3,\underline{x}_4)\ldots\Lambda_n(\underline{x}_{N-1},\underline{x}_N)]\,,$$

$$(III.1.4)$$

where the antisymmetrising operator A includes an appropriate normalising constant, and the two-electron functions Λ_i (now usually referred to as geminals[4]) describe localised electron pairs. One of the disadvantages of the method is that the equations determining the optimum geminals are coupled, and rapidly become difficult to solve as the number of electrons increases. Furthermore, in order to obtain tractable formulae for the determination of the geminals, it is necessary to introduce the arbitrary condition that

$$\int \Lambda_p(\underline{x}_i,\underline{x}_j) \, \Lambda_q(\underline{x}_i,\underline{x}_k) \, d\underline{x}_i \equiv 0 \quad . \qquad \text{(III.1.5)}$$

$$p \neq q$$

As Arai[5] and Löwdin[6] have pointed out, the strong orthogonality condition expressed by Equation (III.1.5) implies a complete separation of the Hilbert space into n distinct and orthogonal sub-spaces. Each geminal has an expansion within one of these subspaces only, with the result that no intershell correlation effects are taken into account. Several attempts[7] have been made to extend the method by considering more than two electrons at a time, but most of the methods suffer from the restrictions of arbitrary orthogonality conditions of some form.

Following the success of Brueckner and Gammel[8] in calculating the energy and density of nuclear matter, it was suggested that Brueckner's[9] many-body theory of nuclear structure might be equally applicable to atomic and molecular problems. In contrast to the familiar Hartree-Fock approach, in which one considers a particle moving in the potential due to an undisturbed charge distribution, the Brueckner theory allows nucleons to correlate in pairs while moving in a medium which they are constantly polarising. Unfortunately, although the method is useful for dealing with idealised problems involving infinite 'seas' of matter, complications arise when the theory is applied to systems of finite size, such as atoms or molecules. For example, the potential due to the polarised medium is strongly dependent on the orbital upon which it acts; as a consequence, the

orthogonal ground state orbitals cannot be obtained easily[10].

Other attempts to describe many-electron systems have made use of the theory of the 'infinite electron gas'[11]. In this approach, which is concerned principally with metals, one replaces the periodic lattice of nuclei by a smeared out, positive charge distribution. However, for such a system it is found that the Hartree-Fock 'orbitals' are, in fact, plane waves, and the resultant delocalisation of the electrons prevents any meaningful partitioning of the system into identifiable particle groups.

In an effort to avoid the problems associated with the introduction of _ad hoc_ constraints or simplifications such as those which occur in the methods discussed above, Sinanoglu[12] and his coworkers have developed a method of describing an N-electron atom by considering the electrons in groups of 1,2,3,...,N at a time. The method takes as its starting point an orbital description of the system, which can be (but is not necessarily) the Hartree-Fock wavefunction. This particular choice is appropriate for our present purposes, since it allows correlation effects between progressively larger numbers of electrons to be introduced in a systematic way.

A complete discussion of Sinanoglu's formulation, which has become known as 'Many-Electron Theory' (MET), lies beyond the scope of the present work[13]. However, in order to appreciate the application of MET to the analysis of

correlation effects, it is necessary to have both an understanding of the basic principles involved and some familiarity with the nomenclature used.

According to Sinanoglu, the exact wavefunction $\phi(\underline{x}_1, \underline{x}_2, \ldots, \underline{x}_N)$ for an N-electron atom can be written as

$$\phi(\underline{x}_1, \underline{x}_2, \ldots, \underline{x}_N) = A[(\varphi_1(\underline{x}_1)\varphi_2(\underline{x}_2)\ldots\varphi_N(\underline{x}_N)) \times$$

$$(1 +$$

$$(\sum_i f_i(\underline{x}_i)/\varphi_i(\underline{x}_i)) +$$

$$(2!)^{-1/2} (\sum_{i<j} U_{ij}(\underline{x}_i, \underline{x}_j)/\varphi_i(\underline{x}_i)\varphi_j(\underline{x}_j)) +$$

$$+\ldots+$$

$$(N!)^{-1/2} (U_{12\ldots N}(\underline{x}_1, \underline{x}_2, \ldots, \underline{x}_N)/\varphi_1(\underline{x}_1)\varphi_2(\underline{x}_2)\ldots\varphi_N(\underline{x}_N)))].$$

$$(III.1.6)$$

In Equation (III.1.6), $\underline{x}_i$ denotes the space and spin coordinates of the ´i´th electron, A is the antisymmetrising operator (which also contains the normalisation factor $(N!)^{-1/2}$), $\varphi_i(\underline{x}_i)$ is a normalised orbital, $f_i(\underline{x}_i)$ is the orbital correction term corresponding to $\varphi_i(\underline{x}_i)$, and $U_{ij}(\underline{x}_i, \underline{x}_j)$ is the pair correction function associated with $\varphi_i(\underline{x}_i)$ and $\varphi_j(\underline{x}_j)$; the higher order U terms represent correction functions corresponding to larger aggregates of electrons. The f and U functions satisfy orthogonality conditions of the form

$$\langle\varphi_1|f_i\rangle = 0$$

$$\langle\varphi_1|U_{ij}\rangle = 0$$

$$\langle\varphi_1|U_{ijk}\rangle = 0 \quad \underline{etc}, \quad\quad (III.1.7)$$

where, for example,

$$\langle \varphi_1 | U_{ij} \rangle = \int \varphi_1^*(\underline{x}_i) \, U_{ij}(\underline{x}_i, \underline{x}_j) \, d\underline{x}_i .$$

It is important to note that these orthogonality conditions are <u>rigorous</u> and are not, therefore, arbitrary simplifications such as Equation (III.1.5) was.

If we select the $\varphi_i(x_i)$ terms in Equation (III.1.6) to be Hartree-Fock orbitals, we can rewrite $\phi(\underline{x}_1, \underline{x}_2, \ldots, x_N)$ in the form

$$\phi(\underline{x}_1, \underline{x}_2, \ldots, \underline{x}_N) = \phi^{HF}(\underline{x}_1, \underline{x}_2, \ldots, \underline{x}_N) + X(\underline{x}_1, \underline{x}_2, \ldots, \underline{x}_N) ,$$
(III.1.8)

where $\phi^{HF}(\underline{x}_1, \underline{x}_2, \ldots, \underline{x}_N)$ is the Hartree-Fock wavefunction (normalised to unity), defined by

$$\phi^{HF}(\underline{x}_1, \underline{x}_2, \ldots, \underline{x}_N) = A[\varphi_1(\underline{x}_1)\varphi_2(\underline{x}_2)\ldots\varphi_N(\underline{x}_N)],$$
(III.1.9)

and $X(\underline{x}_1, \underline{x}_2, \ldots, \underline{x}_N)$ is the correlation correction to it, defined by

$$X(\underline{x}_1, \underline{x}_2, \ldots, \underline{x}_N) = A[(\varphi_1(\underline{x}_1)\varphi_2(\underline{x}_2)\ldots\varphi_N(\underline{x}_N)) \times$$

$$\left(\left(\sum_i f_i(\underline{x}_i)/\varphi_i(\underline{x}_i) \right) + \right.$$

$$(2!)^{-1/2} \left(\sum_{i<j} U_{ij}(\underline{x}_i, \underline{x}_j)/\varphi_i(\underline{x}_i)\varphi_j(\underline{x}_j) \right)$$

$$+ \ldots +$$

$$(N!)^{-1/2} \left. \left(U_{12\ldots N}(\underline{x}_1, \underline{x}_2, \ldots, \underline{x}_N)/\varphi_1(\underline{x}_1)\varphi_2(\underline{x}_2)\ldots\varphi_N(\underline{x}_N) \right) \right)].$$
(III.1.10)

It is important to note that it is not <u>necessary</u> for the $\varphi_i(\underline{x}_i)$ terms in Equation (III.1.6) to be Hartree-Fock orbitals; the first term on the RHS of Equation (III.1.8) <u>could</u> be constructed from any other suitable set of spin orbitals, but would not then be the Hartree-Fock wavefunction. Similarly, in such circumstances, the <u>second</u> term in Equation (III.1.8), although still a correction function, would not be solely a <u>correlation</u> correction function. Thus, for the purposes of the present analysis, the choice of $\varphi_i(\underline{x}_i)$ as Hartree-Fock orbitals will be seen to be the most <u>convenient</u>. From the orthogonality conditions (Equations (III.1.7)), we have

$$\langle \phi^{HF} | X \rangle = 0, \qquad (III.1.11)$$

where $\langle | \rangle$ denotes integration over all appropriate space and spin variables. As a result, ϕ and ϕ^{HF} obey the so called intermediate normalisation condition

$$\langle \phi^{HF} | \phi \rangle = 1, \qquad (III.1.12)$$

so that the normalisation of ϕ is arbitrarily expressed as

$$\langle \phi | \phi \rangle = 1 + \langle X | X \rangle. \qquad (III.1.13)$$

The technique by which Sinanoglu obtained Equation (III.1.6) has become known as the Method of Successive Partial Orthogonalisations[14] (MSPO). The same procedure may be used to obtain expressions for the correction functions f_i, U_{ij} etc. For convenience, we

define the product of all occupied Hartree-Fock orbitals by

$$\Pi = (\varphi_1(\underline{x}_1)\varphi_2(\underline{x}_2)\ldots\varphi_N(\underline{x}_N)) \quad . \qquad \text{(III.1.14a)}$$

In a similar manner, we define

$$\Pi_i = (\varphi_1(\underline{x}_1)\varphi_2(\underline{x}_2)\ldots\varphi_{i-1}(\underline{x}_{i-1})\varphi_{i+1}(\underline{x}_{i+1})\ldots\varphi_N(\underline{x}_N))$$

$$\text{(III.1.14b)}$$

and

$$\Pi_{ij} = (\varphi_1(\underline{x}_1)\varphi_2(\underline{x}_2)\ldots\varphi_{i-1}(\underline{x}_{i-1})\varphi_{i+1}(\underline{x}_{i+1})\ldots$$

$$\varphi_{j-1}(\underline{x}_{j-1})\varphi_{j+1}(\underline{x}_{j+1})\ldots\varphi_N(\underline{x}_N)) \quad . \qquad \text{(III.1.14c)}$$

Furthermore, to simplify our notation we shall, unless stated otherwise, adopt an ´implied labelling´ convention. That is, prior to the action of any antisymmetriser, the functions f_i and φ_i are functions of $\underline{x}_i$, U_{ij} is a function of $\underline{x}_i$ and $\underline{x}_j$, and so on. Multiplication of Equation (III.1.6) by Π_i^*, followed by integration over the space-spin variables $\underline{x}_1, \underline{x}_2, \ldots, \underline{x}_{i-1}, \underline{x}_{i+1}, \ldots, \underline{x}_N$ results in the following expression

$$\langle \Pi_i | \phi \rangle = M(\varphi_i + f_i) \quad , \qquad \text{(III.1.15)}$$

where the integration denoted by $\langle | \rangle$ is understood to be over all variables which are common to both the bra and ket. The constant M in Equation (III.1.15) arises from the normalising constant implicit in the antisymmetriser A.

Multiplying Equation (III.1.15) throughout by $\varphi_i^*(\underline{x}_i)$ and

integrating over $\underline{x}_i$, we find

$$\langle \pi | \phi \rangle = M, \qquad \text{(III.1.16)}$$

whereupon we have

$$f_i(\underline{x}_i) = \langle \pi_i | \phi \rangle / \langle \pi | \phi \rangle - \varphi_i \; . \qquad \text{(III.1.17)}$$

By means of a similar process we may obtain an explicit expression for the pair functions U_{ij}. Thus, multiplication of Equation (III.1.6) by π_{ij}^* and integration over the space-spin coordinates $\underline{x}_1, \underline{x}_2, \ldots, \underline{x}_{i-1}, \underline{x}_{i+1}, \ldots, \underline{x}_{j-1} \underline{x}_{j+1}, \ldots \underline{x}_N$ yields

$$\langle \pi_{ij} | \phi \rangle = M[(\varphi_i(\underline{x}_i)\varphi_j(\underline{x}_j) - \varphi_i(\underline{x}_j)\varphi_j(\underline{x}_i)) +$$

$$(\varphi_i(\underline{x}_i)f_j(\underline{x}_j) - \varphi_i(\underline{x}_j)f_j(\underline{x}_i)) +$$

$$(f_i(\underline{x}_i)\varphi_j(\underline{x}_j) - f_i(\underline{x}_j)\varphi_j(\underline{x}_i)) +$$

$$(2)^{1/2} U_{ij}(\underline{x}_i, \underline{x}_j)] \; . \qquad \text{(III.1.18)}$$

Substitution for M from Equation (III.1.16) and some rearrangement then yields

$$U_{ij}(\underline{x}_i, \underline{x}_j) = (2)^{-1/2} [(\langle \pi_{ij} | \phi \rangle / \langle \pi | \phi \rangle) - (\varphi_i \varphi_j - \varphi_j \varphi_i) -$$

$$(\varphi_i f_j - f_j \varphi_i) - (f_i \varphi_j - \varphi_j f_i)] \; . \qquad \text{(III.1.19)}$$

173

In Equation (III.1.19) we have introduced the additional convention that the explicit dependence on electron coordinates is indicated by the ordering of the product functions; thus, for example,

$$\varphi_i \varphi_j - \varphi_j \varphi_i \equiv \varphi_i(\underline{x}_i)\varphi_j(\underline{x}_j) - \varphi_j(\underline{x}_i)\varphi_i(\underline{x}_j)) \ .$$

Clearly, the method of Successive Partial Orthogonalisations may be used to obtain explicit expressions for any of the other correlation functions in Equation (III.1.6). Furthermore, although the analysis given here has been for the exact wavefunction, it is obvious that, given an appropriate set of Hartree-Fock orbitals $\varphi_i(\underline{x}_i)$ we may apply this procedure to __any__ approximate wavefunction and thereby obtain expressions for the various correlation effects which are implicitly contained in that function. At this point it is appropriate to consider the physical significance of the various terms in Equation (III.1.6).

The effects of electron correlation in an atom or molecule are due to the difference between the instantaneous Coulomb potential experienced by each electron and the average potential predicted by the Hartree-Fock wavefunction; Sinanoglu has referred to this difference as the 'fluctuation potential'[15]. The major features of this potential are that it has a shorter range than the full Coulomb potential, and that it possesses attractive as well as repulsive characteristics. When two electrons approach each other to within the range of their mutual fluctuation potential, the event is described as a 'collision' between

174

the electrons. In Equation (III.1.8), ϕ^{HF} may be thought of as a medium in which the N electrons are moving, each seeing a static potential. The function f_i in Equation (III.1.10) then adjusts orbital φ_i to the field of the other electrons to an extent beyond the HF potential, and the U terms correct for collisions among progressively larger groups of electrons at a time. (References to 'time' are permissible since the theory could have been based equally well on a time-dependent formalism such as the one used by Goldstone[16].) Clearly, an 'n-electron' correlation term will be large only when the probability of finding n electrons within the range of each others fluctuation potential becomes appreciable. By analogy with the theory of imperfect gases[17], we may refer to the successive correlation terms in Equation (III.1.10) as one-, two-, three-, etc electron 'clusters'. The further classification of these clusters into 'linked' or 'unlinked' types has been discussed by Sinanoglu[18].

In terms of CI nomenclature, the f_i functions depend on the presence of configurations in the wavefunction which arise from single excitations within a basis set of HF orbitals. A consideration of Brillouin's theorem[19] indicates that the f_i functions will appear in the wavefunction to second order only, and will therefore contribute to the total energy only in the fourth order. In 1963, Sinanoglu and Tuan[20] gave a number of reasons for expecting these orbital correction functions to be small. Since then, however, a number of workers have suggested that the f_i functions could be significant when determining

properties other than the energy; in particular, Stanton[21] has claimed that orbital correction functions may be important when evaluating electron densities. In an effort to gain further insight into the importance of the f_i terms, Taylor and Banyard[22] studied the orbital correction functions derived from CI wavefunctions for a number of two-, three-, and four-electron atomic ions. They evaluated the changes produced by the f_i functions in the one-particle radial densities, and attempted to rationalise those changes in terms of the corresponding fluctuation potentials. Of particular interest was their discovery that for the Be-like ions, where the 2s and 2p orbitals are nearly degenerate, the orbital correction function produces a relatively <u>large</u> change in the 2s orbital density - an effect apparently not anticipated by Sinanoglu and Tuan[20].

Banyard and Taylor[23] then extended their analysis to an examination of the pair correlation functions for the same set of ions. From a correlation point of view, these U_{ij} terms, which result from doubly-excited configurations in the CI expansion, play the most important role in the correlation function X because they represent a direct change in the wavefunction due to the instantaneous electron-electron correlation interactions. Since U_{ij} is a function of six space variables, any pictorial representation of it can be accomplished only by specifying explicit values for some of those variables, and then varying the others. Using a series of contour diagrams obtained in this manner, Banyard and Taylor were able to highlight several differences between K- and L-shell pair

correlation effects in the four-electron ions. Furthermore, when compared with the results obtained by other workers, their analysis was also particularly fruitful in revealing certain deficiencies in the Be intershell description afforded by the wavefunction of Weiss[24].

To overcome the difficulties encountered in the graphical description of the U_{ij} functions, Banyard and Mashat[25] then proposed a more compact method of analysing correlation effects between specific electron pairs, based on a partitioned form of the Coulomb hole. Using Many-Electron Theory, they were able to show that, with certain approximations, Equation (III.1.3) can be written in partitioned form as

$$\Delta f(r_{mn}) \approx \sum_{i<j} \Delta f_{ij}(r_{mn}) \quad , \qquad \text{(III.1.20)}$$

where $\quad \Delta f_{ij}(r_{mn}) = f_{ij}^{corr}(r_{mn}) - f_{ij}^{HF}(r_{mn}) \qquad \text{(III.1.21)}$

$$\Rightarrow \quad \Delta f_{ij}(r_{mn}) = \int \pi_{ij}^{corr}(\underline{x}_m,\underline{x}_n) \, d\underline{x}_m.d\underline{x}_n/dr_{mn}$$

$$- \int \pi_{ij}^{HF}(\underline{x}_m,\underline{x}_n) \, d\underline{x}_m.d\underline{x}_n/dr_{mn}. \qquad \text{(III.1.22)}$$

In each case, the ordered pairs (i<j) refer to occupied HF orbitals. The Hartree-Fock and correlated densities π_{ij}^{corr} and π_{ij}^{HF} are obtained by substituting Equations (III.1.9) and (III.1.6) respectively into Equation (III.1.2) and then partitioning the resulting total densities into their pairwise components. For a single-determinant Restricted Hartree-Fock (RHF) wavefunction, this procedure is exact,

whereas the resolution of $\Pi^{corr}(\underline{x}_m,\underline{x}_n)$ into intrashell and intershell terms alone can be achieved only approximately. (Inspection of Equation (III.1.10) reveals that the relatively insignificant higher order correlation correction terms involving three or more electrons cannot be partitioned unambiguously, and must be omitted from the expansion of ϕ before its substitution into Equation (III.1.2)).

For a series of Be-like ions, Banyard and Mashat[25] used Equation (III.1.22) to obtain the Coulomb hole corresponding to each pair of Hartree-Fock orbitals. For the correlated description of each system they used the CI wavefunctions of Weiss[24], which are constructed from a non-orthogonal basis set; to make the resulting analysis more tractable, terms of second order in the correlation correction to ϕ^{HF} were omitted from the final expressions for $\Pi_{ij}^{corr}(\underline{x}_m,\underline{x}_n)$. Although the single $\Delta f(r_{mn})$ curve obtained for each electron pair contained less detail than the contour diagrams used by Banyard and Taylor[23], it possessed the particular advantage of providing an immediate visual comparison, not only between systems, but also between different effects in the same system.

Banyard and Mashat found that the $\Delta f(r_{mn})$ curves for the K shell were very similar to those obtained for the corresponding two-electron ions. The Coulomb holes for the ($1s\alpha\ 2s\alpha$) and ($1s\alpha\ 2s\beta$) pairs were particularly interesting; the ($1s\alpha\ 2s\alpha$) curves were <u>inverted</u> by comparison with the 'holes' obtained by Boyd and Katriel[26] for the 2^3S state

178

of the He-like ions. To investigate the possibility that such findings were the result of restrictions imposed by Weiss when constructing his wavefunctions, Banyard and Mobbs[27] then applied a similar analysis to a variety of other accurate wavefunctions, each describing the ground state of Be. For the comparison of these relatively sophisticated wavefunctions, the partitioning technique used to obtain $\pi_{ij}^{corr}(\underline{x}_m,\underline{x}_n)$ was extended to a higher level of approximation by the retention of all the 'second-order' product terms omitted by Banyard and Mashat[25].

Banyard and Mobbs[27] found that for the K- and L-shell Coulomb holes, the differences among the various wave-functions were relatively small. For both shells, all the wavefunctions produced curves of the same general shape and magnitude as the corresponding Coulomb holes obtained by Banyard and Mashat using the Weiss wavefunction. In contrast to this, although all the Coulomb holes corresponding to a given intershell electron pair possessed the same general characteristics, the variation among the curves calculated from the different wavefunctions was quite marked; these differences were sufficiently large to produce significant changes in the total Coulomb holes.

To examine the sensitivity of their results with respect to the approximations made in the partitioning of the correlated two-particle density, Banyard and Mobbs also calculated the Coulomb holes for the energetically best wavefunction using the simplified analysis of Banyard and Mashat. The K-shell curve was found to be essentially

unchanged to within graphical accuracy, and the changes in the intershell 'holes' were also small. The greatest effect occurred for the 2s-2p near-degeneracy effect which exists in Be. It was calculated that for systems in which such effects do not occur, the partitioning technique of Banyard and Mashat should prove to be adequate for the analysis of correlation effects.

Following the observation that momentum space provides an interesting alternative view of the effects of electron correlation, Mobbs and Banyard[28] then extended their analysis by performing a momentum-space study of Be. Interestingly, they found that, whereas in position space the correlation effects in the K and L shells are of comparable magnitude, in momentum space the effects in the L-shell are significantly greater than those in the K-shell -- so much so that the total Coulomb shift is almost completely dominated by the L-shell component. This is in direct contrast to the results in position space, where it is found that the total Coulomb hole for Be exhibits distinct intershell effects.

Recently, Al-Bayati[29] has extended the earlier work of Taylor and Banyard[22] by using Many-Electron Theory to examine the Coulomb holes and a variety of other position-space correlation effects in the 2^2S and 2^2P states of a series of Li-like ions. To complement his analysis, we present here a study of the same two states of the neutral Li atom in momentum space. For both states, we have treated the atom as three identifiable electron pairs, and have

assessed the effects of correlation on each component pair by examining several different aspects of the corresponding two-electron distribution. In keeping with our earlier study of excited states of helium, we have attempted to construct, for each electron pair, a self-consistent model of electron correlation which encompasses all of the observed effects. Where appropriate, comparisons are made with the corresponding position-space results of Al-Bayati, as well as with the results of earlier momentum-space studies of other two- and four-electron systems.

In Chapter (III.1.2), we consider how the necessary partitioning of the description of the Li atom may be achieved at both the Hartree-Fock and correlated levels.

CHAPTER (III.1.2)

PARTITIONING OF THE TWO-PARTICLE MOMENTUM DENSITY

Our investigation of electron correlation effects in Li is based on properties derived from the spin-dependent two-particle momentum density, $\Gamma(\underline{x}_m, \underline{x}_n)$. For an N-electron **momentum-space** wavefunction, $\Psi(\underline{x}_1, \underline{x}_2, \underline{x}_3)$, normalised to unity, $\Gamma(\underline{x}_m, \underline{x}_n)$ is defined by

$$\Gamma(\underline{x}_m, \underline{x}_n) = \binom{N}{2} \int \Psi^*(\underline{x}_1, \underline{x}_2 \ldots \underline{x}_N) \; \Psi(\underline{x}_1, \underline{x}_2 \ldots \underline{x}_N) \quad \times$$

$$d\underline{x}_1 \, d\underline{x}_2 \ldots d\underline{x}_{m-1} \, d\underline{x}_{m+1} \ldots d\underline{x}_{n-1} \, d\underline{x}_{n+1} \ldots d\underline{x}_N \, ,$$

$$(\text{III}.1.23)$$

where $\underline{x}_i$ denotes the momentum space and spin coordinates of the i'th electron, and $\Gamma(\underline{x}_m, \underline{x}_n)$ normalises to the number of distinct electron pairs in the system. Due to the indistinguishability of the electrons, the choice of m and n in Equation (III.1.23) is quite arbitrary, and for convenience we set $m = 1$ and $n = 2$. For the Li atom, Equation (III.1.23) then becomes

$$\Gamma(\underline{x}_1, \underline{x}_2) = 3 \int \Psi^*(\underline{x}_1, \underline{x}_2, \underline{x}_3) \; \Psi(\underline{x}_1, \underline{x}_2, \underline{x}_3) \, d\underline{x}_3 . \quad (\text{III}.1.24)$$

At the Hartree-Fock level, the partitioning of Equation (III.1.24) into pairwise components is relatively straightforward. We assume that the Restricted Hartree-Fock wavefunction, $\Psi^{HF}(\underline{x}_1, \underline{x}_2, \underline{x}_3)$ is a single determinant, constructed from orthonormal orbitals φ_i. (If the φ_i are **not** orthonormal, they can be made so by application of the

Schmidt[30] procedure, prior to the analysis presented here.) We have then

$$\Psi^{HF}(\underline{x}_1,\underline{x}_2,\underline{x}_3) = A\ (\varphi_1(\underline{x}_1)\varphi_2(\underline{x}_2)\varphi_3(\underline{x}_3)), \qquad (III.1.25)$$

where A is an antisymmetriser, which also contains the normalisation factor $(3!)^{-1/2}$. The usual interpretation of the operator A is that it permutes the electron coordinates within the expression that it acts upon, while maintaining the ordering of the orbital labels, so that

$$A\ (\varphi_1(\underline{x}_1)\varphi_2(\underline{x}_2)\varphi_3(\underline{x}_3)) = (3!)^{-1/2}\ [\ \varphi_1(\underline{x}_1)\varphi_2(\underline{x}_2)\varphi_3(\underline{x}_3)$$
$$-\varphi_1(\underline{x}_1)\varphi_2(\underline{x}_3)\varphi_3(\underline{x}_2)$$
$$+\varphi_1(\underline{x}_3)\varphi_2(\underline{x}_1)\varphi_3(\underline{x}_2)$$
$$\underline{etc} \qquad\qquad]\ .$$

It is, of course, equally correct to maintain the ordering of the coordinates in the expression, while permuting the orbital labels. Thus we can write

$$A\ (\varphi_1(\underline{x}_1)\varphi_2(\underline{x}_2)\varphi_3(\underline{x}_3)) = (3!)^{-1/2}\ [\ \varphi_1(\underline{x}_1)\varphi_2(\underline{x}_2)\varphi_3(\underline{x}_3)$$
$$-\varphi_1(\underline{x}_1)\varphi_3(\underline{x}_2)\varphi_2(\underline{x}_3)$$
$$+\varphi_3(\underline{x}_1)\varphi_1(\underline{x}_2)\varphi_2(\underline{x}_3)$$
$$\underline{etc} \qquad\qquad]\ .$$

Although the difference between these two approaches appears to be trivial, the latter grouping of terms is significantly more convenient for the analysis that follows, since it provides a means of factorising out all references to electron coordinates $\underline{x}_1$ and $\underline{x}_2$, thereby facilitating the

183

integration over $\underline{x}_3$ required by Equation (III.1.24). Accordingly, Equation (III.1.25) can be rewritten as

$$\psi^{HF}(\underline{x}_1, \underline{x}_2, \underline{x}_3) =$$

$$(3!)^{-1/2} \; \Sigma \; (\varphi_i(\underline{x}_1)\varphi_j(\underline{x}_2) - \varphi_j(\underline{x}_1)\varphi_i(\underline{x}_2)) \; \varphi_k(\underline{x}_3) \; (-1)^p ,$$

$$(III.1.26)$$

where p represents the permutation from the product $(\varphi_1(\underline{x}_1)\varphi_2(\underline{x}_2)\varphi_3(\underline{x}_3))$. To simplify our notation, we shall hereafter assume that each occurrence of the symbol "Σ" implies a summation over all allowed values of the summation index (or indices) on the terms that follow it. Thus, for example, in Equation (III.1.26) the summation is taken over the ordered pairs (i<j). Further simplification is achieved by again adopting an `implied-labelling` convention, so that Equation (III.1.26) becomes

$$\psi^{HF}(\underline{x}_1, \underline{x}_2, \underline{x}_3) = (3!)^{-1/2} \; \Sigma \; (\varphi_i\varphi_j - \varphi_j\varphi_i) \; \varphi_k \; (-1)^p . \quad (III.1.27)$$

Substitution of Equation (III.1.27) into Equation (III.1.24) then yields

$$\Gamma^{HF}(\underline{x}_1, \underline{x}_2) =$$

$$(2)^{-1} \; \Sigma \; \Sigma \; (\varphi_I^*\varphi_J^* - \varphi_J^*\varphi_I^*) \; (\varphi_i\varphi_j - \varphi_j\varphi_i) \; (-1)^{P+p} \; \int \varphi_K^*\varphi_k \, d\underline{x}_3 .$$

$$(III.1.28)$$

Now, since the HF orbitals are orthonormal, we have

$$\int \varphi_K^* \varphi_k \, d\underline{x}_3 = \delta_{Kk} \quad , \tag{III.1.29}$$

and when $K = k$, the ordered pairs $(I < J)$ and $(i < j)$ must be the same. As a result, the permutations P and p must also be identical, so that Equation (III.1.28) becomes

$$\Gamma^{HF}(\underline{x}_1, \underline{x}_2) = (2)^{-1} \Sigma (\varphi_i^* \varphi_j^* - \varphi_j^* \varphi_i^*)(\varphi_i \varphi_j - \varphi_j \varphi_i) \quad , \tag{III.1.30}$$

or $\quad \Gamma^{HF}(\underline{x}_1, \underline{x}_2) = \Sigma \Gamma_{ij}^{HF}(\underline{x}_1, \underline{x}_2) \quad ,$ (III.1.31)

where

$$\Gamma_{ij}^{HF}(\underline{x}_1, \underline{x}_2) = (2)^{-1} (\varphi_i^* \varphi_j^* - \varphi_j^* \varphi_i^*)(\varphi_i \varphi_j - \varphi_j \varphi_i) \quad , \tag{III.1.31a}$$

which is the (exact) partitioned form of the Hartree-Fock two-particle momentum density. Thus, the uncorrelated spin-dependent two-particle momentum density has been partitioned into a number of component densities, $\Gamma_{ij}^{HF}(\underline{x}_1, \underline{x}_2)$, each of which is associated with an identifiable pair of occupied spin orbitals φ_i and φ_j in the Restricted Hartree-Fock representation of the system. The analogous spin-<u>less</u> component two-particle momentum densities, $\varrho_{ij}^{HF}(\underline{p}_1, \underline{p}_2)$, may then be defined in the usual way by

$$\varrho_{ij}^{HF}(\underline{p}_1, \underline{p}_2) = \int \Gamma_{ij}^{HF}(\underline{x}_1, \underline{x}_2) \, d\underline{s}_1 d\underline{s}_2 \quad , \tag{III.1.32}$$

where $\underline{s}_i$ is the spin coordinate of the i'th electron.

As we saw in the previous Chapter, the partitioning of

185

the correlated two-particle momentum density requires the use of Many-Electron Theory. Although MET was developed by Sinanoglu[13] for application to position-space problems, the principles of the theory are equally valid in momentum space. Furthermore, as a result of the isomorphism of the Dirac[31] transform which connects the position and momentum representations, the cluster expansion of a correlated N-electron wavefunction Ψ^{corr} in momentum space has exactly the same form as its position-space counterpart, ϕ^{corr}. Thus Ψ^{corr} can be expressed in the form

$$\Psi^{corr}(\underline{x}_1,\underline{x}_2,\ldots\underline{x}_n) = A\{ \quad\quad \pi$$

$$+ \quad\quad \Sigma\ \pi_i\ \ f_i(\underline{x}_i)$$

$$+(2!)^{-1/2}\ \Sigma\ \pi_{ij}\ \ U_{ij}(\underline{x}_i,\underline{x}_j)$$

$$+\ldots$$

$$+\ldots$$

$$+(N!)^{-1/2} \quad\quad U_{12\ldots N}(\underline{x}_1,\underline{x}_2\ldots\underline{x}_N)\},$$

(III.1.33)

where we have retained the symbols φ_i, f_i, U_{ij} etc to denote respectively HF orbitals and correction functions in momentum-space, and the HF orbital products, π, π_i etc are defined by analogy with the corresponding position-space terms (see Equation (III.1.14)). The orthogonality relations expressed in Equation (III.1.7) also apply in momentum-space.

Clearly, for the three-electron systems studied here, the complete expansion of Ψ^{corr} would terminate with the U_{ijk} terms in Equation (III.1.33). However, in order to decompose the wavefunction, and hence the momentum density, into contributions from identifiable electron pairs, it is necessary to truncate the expansion of Ψ^{corr} after the U_{ij} terms, whereupon for the Li atom, we have

$$\Psi^{corr}(\underline{x}_1, \underline{x}_2, \underline{x}_3) \approx$$

$$c \, A \, \{ \, \pi + \Sigma \, \pi_i \, f_i(\underline{x}_i) + (2!)^{-1/2} \, \Sigma \, \pi_{ij} \, U_{ij}(\underline{x}_i, \underline{x}_j) \, \} \, ,$$

$$(III.1.34)$$

or

$$\Psi^{corr}(\underline{x}_1, \underline{x}_2, \underline{x}_3) \approx c \, [\, \Psi^{HF}(\underline{x}_1, \underline{x}_2, \underline{x}_3) + \psi(\underline{x}_1, \underline{x}_2, \underline{x}_3) \,] \, .$$

$$(III.1.35)$$

In Equation (III.1.35), Ψ^{HF} is the Hartree-Fock wavefunction of the system, ψ is the truncated correlation correction function defined by

$$\psi(\underline{x}_1, \underline{x}_2, \underline{x}_3) =$$

$$A \, \{ \, \Sigma \, \pi_i f_i(\underline{x}_i) + (2!)^{-1/2} \, \Sigma \, \pi_{ij} \, U_{ij}(\underline{x}_i, \underline{x}_j) \, \} ,$$

$$(III.1.36)$$

and the introduction of the constant c ensures that Ψ^{corr} now normalises to <u>unity</u> (compare Equation (III.1.13)).

If we now substitute Equation (III.1.35) into

Equation (III.1.23) we obtain

$$\Gamma^{corr}(\underline{x}_1,\underline{x}_2) \approx$$

$$3 c^2 \int (\Psi^{HF}(\underline{x}_1,\underline{x}_2,\underline{x}_3) + \psi(\underline{x}_1,\underline{x}_2,\underline{x}_3))^* \times$$

$$(\Psi^{HF}(\underline{x}_1,\underline{x}_2,\underline{x}_3) + \psi(\underline{x}_1,\underline{x}_2,\underline{x}_3))\, d\underline{x}_3 \, , \qquad \text{(III.1.37)}$$

or

$$\Gamma^{corr}(\underline{x}_1,\underline{x}_2) \approx$$

$$3 c^2 \{ \langle \Psi^{HF}|\Psi^{HF}\rangle_3 + \langle \Psi^{HF}|\psi\rangle_3 + \langle \psi|\Psi^{HF}\rangle_3 + \langle \psi|\psi\rangle_3 \} \, ,$$

$$\text{(III.1.38)}$$

where $\langle | \rangle_3$ denotes integration over $\underline{x}_3$ only. Now, following Banyard and Mashat[25], we discard the last term in Equation (III.1.38) and renormalise, so that

$$\Gamma^{corr}(\underline{x}_1,\underline{x}_2) \approx$$

$$3 \{ \langle \Psi^{HF}|\Psi^{HF}\rangle_3 + \langle \Psi^{HF}|\psi\rangle_3 + \langle \Psi^{HF}|\psi\rangle_3 \} . \qquad \text{(III.1.39)}$$

(The new normalisation constant is unity). From symmetry considerations, it can be shown that

$$\langle \Psi^{HF}|\psi\rangle_3 = \langle \psi|\Psi^{HF}\rangle_3 \, , \qquad \text{(III.1.40)}$$

whereupon

$$\Gamma^{corr}(\underline{x}_1,\underline{x}_2) \approx 3 \{ \langle \Psi^{HF}|\Psi^{HF}\rangle_3 + 2\langle \Psi^{HF}|\psi\rangle_3 \} . \qquad \text{(III.1.41)}$$

The first term in Equation (III.1.41) is, of course, the

Hartree-Fock two-particle momentum density, which we have already expressed in partitioned form (see Equation (III.1.30)). We have then

$$\Gamma^{corr}(\underline{x}_1, \underline{x}_2) \approx [(2)^{-1} \Sigma (\varphi_i^* \varphi_j^* - \varphi_j^* \varphi_i^*)(\varphi_i \varphi_j - \varphi_j \varphi_i)]$$

$$+ [6 \langle \Psi^{HF} | \psi \rangle_3]. \qquad (III.1.42)$$

We consider now the evaluation of $\langle \Psi^{HF} | \psi \rangle_3$, and begin by partitioning the correlation correction function, ψ.

From Equation (III.1.36) we can write

$$\psi(\underline{x}_1, \underline{x}_2, \underline{x}_3) = \psi_1(\underline{x}_1, \underline{x}_2, \underline{x}_3) + \psi_2(\underline{x}_1, \underline{x}_2, \underline{x}_3) , \qquad (III.1.43)$$

where

$$\psi_1(\underline{x}_1, \underline{x}_2, \underline{x}_3) = \boldsymbol{A} [\Sigma \Pi_i f_i(\underline{x}_i)] \qquad (III.1.44)$$

and

$$\psi_2(\underline{x}_1, \underline{x}_2, \underline{x}_3) = (2!)^{-1/2} \boldsymbol{A} [\Sigma \Pi_{ij} U_{ij}(\underline{x}_i, \underline{x}_j)]. \qquad (III.1.45)$$

Now from Equation (III.1.44)

$$\psi_1(\underline{x}_1, \underline{x}_2, \underline{x}_3) = \boldsymbol{A} [\quad f_1(\underline{x}_1) \varphi_2(\underline{x}_2) \varphi_3(\underline{x}_3)$$

$$+ \varphi_1(\underline{x}_1) f_2(\underline{x}_2) \varphi_3(\underline{x}_3)$$

$$+ \varphi_1(\underline{x}_1) \varphi_2(\underline{x}_2) f_3(\underline{x}_3)] , \qquad (III.1.46)$$

and to partition this, we note that the action of the

antisymmetriser produces a total of 18 terms, which fall into three distinct categories:

1) Those where the f term is a function of $\underline{x}_1$,

2) Those where the f term is a function of $\underline{x}_2$

and 3) Those where the f term is a function of $\underline{x}_3$.

By analogy with Equation (III.1.26) for the HF wavefunction, the partitioned form of ψ_1 may then be written as

$$\psi_1(\underline{x}_1,\underline{x}_2) = (3!)^{-1/2} \Sigma [((f_i\varphi_j - \varphi_j f_i) \varphi_k$$

$$+ (\varphi_i f_j - f_j\varphi_i) \varphi_k$$

$$+ (\varphi_i\varphi_j - \varphi_j\varphi_i) f_k) (-1)^p] ,$$

(III.1.47)

where p represents the permutation from the reference term.

We now attempt to partition ψ_2 in a similar manner. Following the action of the antisymmetriser, Equation (III.1.45) also produces 18 terms, which now fall into two categories:

1) Those where the pair function U_{ij} contains a reference to $\underline{x}_1$ and $\underline{x}_2$,

and 2) Those where the pair function U_{ij} contains a reference to $\underline{x}_1$ or $\underline{x}_2$ but not both.

Now, it can be shown that

$$U_{ij}(\underline{x}_m,\underline{x}_n) = -U_{ij}(\underline{x}_n,\underline{x}_m) \quad , \qquad \text{(III.1.48)}$$

and therefore we can write the partitioned form of the 6 terms in the first category as

$$(2!)^{-1/2} \ (3!)^{-1/2} \ \Sigma \ 2 \ U_{ij} \ \varphi_k \ (-1)^P \ .$$

Clearly, by their very nature, the terms in the second category cannot be partitioned so that references to electrons (1) and (2) can be factorised out simultaneously. Fortunately, this difficulty can be resolved quite easily, as we shall demonstrate in due course. For convenience, we introduce a new antisymmetriser, $\tilde{A}$, which, like A, includes a factor of $(3!)^{-1/2}$, but which now produces all permutations _except_ those where the pair function contains a reference to $\underline{x}_1$ and $\underline{x}_2$. Thus, $\tilde{A} \ (U_{ij}\varphi_k)$ does not yield any of the terms already accounted for. Furthermore, it is important to note that _all_ the terms produced by the action of $\tilde{A}$ involve the pair function being a function of $\underline{x}_3$.

Making use of $\tilde{A}$, we can then write

$$\psi_2(\underline{x}_1,\underline{x}_2,\underline{x}_3) = (2!)^{-1/2} \ \Sigma \ [\ (\ 2(3!)^{-1/2} \ U_{ij}\varphi_k \ (-1)^P \ )$$

$$+(\qquad \tilde{A} \ (U_{ij}\varphi_k) \qquad) \ ] \ ,$$

$$\text{(III.1.49)}$$

and substituting Equations (III.1.47) and (III.1.49) into

191

Equation (III.1.43), we obtain

$$\Psi(\underline{x}_1,\underline{x}_2,\underline{x}_3) = \{ (3!)^{-1/2} \Sigma [((f_i\varphi_j - \varphi_j f_i) \varphi_k$$

$$+ (\varphi_i f_j - f_j \varphi_i) \varphi_k$$

$$+ (\varphi_i \varphi_j - \varphi_j \varphi_i) f_k \quad) (-1)^P] \}$$

$$+ \{ 2(2!)^{-1/2} (3!)^{-1/2} \Sigma [(\qquad\qquad U_{ij}\varphi_k \ (-1)^P)$$

$$+ (((3!)^{1/2}/2) \tilde{A}(U_{ij}\varphi_k))] \}.$$

$$(III.1.50)$$

Now, by analogy with Equation (III.1.19), the momentum-space pair function is defined by

$$U_{ij}(\underline{x}_i,\underline{x}_j) = (2)^{-1/2} [I_{ij} - (\varphi_i \varphi_j - \varphi_j \varphi_i)$$

$$- (f_i \varphi_j - \varphi_j f_i)$$

$$- (\varphi_i f_j - f_j \varphi_i)], \qquad (III.1.51)$$

where

$$I_{ij} = (\langle \pi_{ij} | \Psi^{corr} \rangle / \langle \pi | \Psi^{corr} \rangle) \qquad ,$$

and, it will be recalled, $\langle | \rangle$ denotes integration over all variables common to the bra and ket. Using Equation (III.1.51) to substitute for the first occurrence of U_{ij} in Equation (III.1.50), we find

192

$$\psi(\underline{x}_1, \underline{x}_2, \underline{x}_3) = (3!)^{-1/2} \, \Sigma \, [\, (\, (f_i \varphi_j - \varphi_j f_i) \, \varphi_k$$

$$+ \, (\varphi_i f_j - f_j \varphi_i) \, \varphi_k$$

$$+ \, (\varphi_i \varphi_j - \varphi_j \varphi_i) \, f_k \,) \, (-1)^p \,]$$

$$+ \, 2(2!)^{-1/2} \, (3!)^{-1/2} \, \Sigma \, [\, (\, (2)^{-1/2} \, (\quad I_{ij}$$

$$- \, (\varphi_i \varphi_j - \varphi_j \varphi_i)$$

$$- \, (f_i \varphi_j - \varphi_j f_i)$$

$$- \, (\varphi_i f_j - f_j \varphi_i) \,) \, \varphi_k (-1)^p)$$

$$+ \, (((3!)^{1/2}/2) \tilde{A}(U_{ij} \varphi_k))].$$

$$(\text{III}.1.52)$$

Clearly, p and P represent the same permutation, so after some cancelling we obtain

$$\psi(\underline{x}_1, \underline{x}_2, \underline{x}_3) = (3!)^{-1/2} \, \Sigma \, [\, (\qquad (\varphi_i \varphi_j - \varphi_j \varphi_i) \, f_k \, (-1)^p \,)$$

$$+ \, (\qquad I_{ij} \qquad \varphi_k \, (-1)^p \,)$$

$$- \, (\qquad (\varphi_i \varphi_j - \varphi_j \varphi_i) \, \varphi_k \, (-1)^p \,)$$

$$+ \, (((3!)^{1/2}/(2!)^{-1/2}) \, \tilde{A} \, (U_{ij} \varphi_k))].$$

$$(\text{III}.1.53)$$

Then from Equations (III.1.26) and (III.1.53) we find

$\langle \Psi^{HF} | \psi \rangle_3 =$

$(3!)^{-1} \{ \Sigma \Sigma$

$[((\varphi_I^* \varphi_J^* - \varphi_J^* \varphi_I^*) (\varphi_i \varphi_j - \varphi_j \varphi_i) (-1)^{P+p} \int \varphi_K^* f_k \, d\underline{x}_3)$

$+ ((\varphi_I^* \varphi_J^* - \varphi_J^* \varphi_I^*) \quad I_{ij} \quad (-1)^{P+p} \int \varphi_K^* \varphi_k \, d\underline{x}_3)$

$- ((\varphi_I^* \varphi_J^* - \varphi_J^* \varphi_I^*) (\varphi_i \varphi_j - \varphi_j \varphi_i) (-1)^{P+p} \int \varphi_K^* \varphi_k \, d\underline{x}_3)$

$+ ((\varphi_I^* \varphi_J^* - \varphi_J^* \varphi_I^*) \int \varphi_k^* (((3!)^{1/2}/2(2!)^{-1/2}) \tilde{A} (U_{ij} \varphi_k)) \, d\underline{x}_3)]\},$

$$(III.1.54)$$

where the sub- and super-scripts in upper case now refer to the conjugated Ψ^{HF} term, while those in lower case refer to the ψ term.

Now, from the orthogonality relations expressed in Equation (III.1.7), the first term in Equation (III.1.54) is identically zero. Furthermore, the operator $\tilde{A}$ was defined in such a way that $\tilde{A} (U_{ij} \varphi_k)$ produces $\underline{only}$ terms where U_{ij} is a function of $\underline{x}_3$. Thus, the orthogonality conditions also imply that

$$\int \varphi_k^* (\tilde{A} (U_{ij} \varphi_k)) \, d\underline{x}_3 = 0 , \qquad (III.1.55)$$

and hence the last term in Equation (III.1.54) is also zero. Using Equation (III.1.29) to substitute for the overlap integrals we find

$$\langle \Psi^{HF} | \psi \rangle_3 =$$

$$(3!)^{-1} \{ \Sigma \Sigma [((\varphi_I^* \varphi_J^* - \varphi_J^* \varphi_I^*) \quad I_{ij} \quad (-1)^{P+p} \delta_{Kk})$$

$$- ((\varphi_I^* \varphi_J^* - \varphi_J^* \varphi_I^*) (\varphi_i \varphi_j - \varphi_j \varphi_i) (-1)^{P+p} \delta_{Kk})] \} .$$

$$(III.1.56)$$

When $K = k$, the ordered pairs $(I < J)$ and $(i < j)$ must be the same. The permutations P and p are then identical, and Equation (III.1.56) becomes

$$\langle \Psi^{HF} | \psi \rangle_3 =$$

$$(3!)^{-1} \{ \Sigma [((\varphi_i^* \varphi_j^* - \varphi_j^* \varphi_i^*) \quad I_{ij})$$

$$- ((\varphi_i^* \varphi_j^* - \varphi_j^* \varphi_i^*) (\varphi_i \varphi_j - \varphi_j \varphi_i))] \} . \quad (III.1.57)$$

We can now substitute Equation (III.1.57) into Equation (III.1.42), and after some cancelling we obtain

$$\Gamma^{corr}(\underline{x}_1, \underline{x}_2) \approx$$

$$\Sigma [(\quad (\varphi_i^* \varphi_j^* - \varphi_j^* \varphi_i^*) \quad I_{ij} \quad)$$

$$- ((2)^{-1} (\varphi_i^* \varphi_j^* - \varphi_j^* \varphi_i^*) (\varphi_i \varphi_j - \varphi_j \varphi_i))] .$$

$$(III.1.58)$$

Thus,

$$\Gamma^{corr}(\underline{x}_1, \underline{x}_2) \approx \Sigma \Gamma_{ij}^{corr}(\underline{x}_1, \underline{x}_2) , \qquad (III.1.59a)$$

where

$$\Gamma^{corr}_{ij}(\underline{x}_1,\underline{x}_2) = [\quad (\quad (\varphi^*_i \varphi^*_j - \varphi^*_j \varphi^*_i) \quad I_{ij} \quad)$$

$$- ((2)^{-1} (\varphi^*_i \varphi^*_j - \varphi^*_j \varphi^*_i) (\varphi_i \varphi_j - \varphi_j \varphi_i))] ,$$

$$(III.1.59b)$$

which is the (approximate) partitioned form of the correlated spin-dependent two-particle momentum density. The corresponding correlated spin-less component densities are then defined by

$$\varrho^{corr}_{ij}(\underline{p}_1,\underline{p}_2) = \int \Gamma^{corr}_{ij}(\underline{x}_1,\underline{x}_2) \, d\underline{s}_1 d\underline{s}_2 , \qquad (III.1.60)$$

where once again $\underline{s}_i$ denotes the spin coordinate of the i'th electron.

To proceed further with this analysis requires the assumption of a particular form for the function Ψ^{corr}, and hence results in a loss of generality; accordingly, we terminate our development at this point. In Chapter (III.1.3) we discuss the wavefunctions which have been used for the evaluation of $\varrho^{corr}_{ij}(\underline{p}_1,\underline{p}_2)$ and $\varrho^{HF}_{ij}(\underline{p}_1,\underline{p}_2)$. In addition, we also consider the various aspects of the momentum density which have been used to analyse correlation effects in the 2^2S and 2^2P states of lithium.

CHAPTER(III.1.3)

WAVEFUNCTIONS AND

EVALUATION OF CORRELATION PROPERTIES

For consistency with the position-space analysis of Al-Bayati[29], we have performed our analysis of momentum-space correlation effects in lithium using the same wavefunctions. Thus, for the correlated description of the ground state we used the configuration interaction (CI) wavefunction of Weiss[24]. In _position_ space, this wavefunction has the form

$$\Phi(\underline{x}_1,\underline{x}_2,\underline{x}_3) = \Sigma \; c_i \; \phi_i(\underline{x}_1,\underline{x}_2,\underline{x}_3) \quad , \qquad (III.1.61)$$

where $\underline{x}_j$ denotes the collection of space and spin coordinates for the j'th electron. The coefficients c_i are those which minimise the total energy of the system, and each configuration ϕ_i is an antisymmetrised product of one-electron spin orbitals. Two general types of linearly independent configuration were constructed by Weiss. The first type corresponds to the situation in which two electrons couple together to produce ^1S symmetry, and the resulting pair is then coupled with the orbital description of the third electron to produce the overall ^2S symmetry of the state. In the second type of configuration, the two electrons are coupled to produce ^3S symmetry, and the resulting pair is again coupled with the third electron to produce a ^2S state. The two types of configuration have the forms

$$\varphi_{pqk,\lambda} = (X_p \, X_q)^1 S \, X_k$$

$$= (6D_\lambda)^{-1/2} \, \Sigma \, [\,|\tilde{X}^\mu_{p\lambda}\alpha(1) \; X^\mu_{q\lambda}\beta(2) \; X_k\alpha(3)|$$

$$+ \quad |\tilde{X}^\mu_{q\lambda}\beta(1) \; X^\mu_{p\lambda}\alpha(2) \; X_k\alpha(3)|\,] \qquad\qquad (III.1.62)$$

and

$$\varphi_{pqk,\lambda} = (X_p \, X_q)^3 S \, X_k$$

$$= (1/3)\,(2D_\lambda)^{-1/2} \, \Sigma \, [2|\tilde{X}^\mu_{p\lambda}\alpha(1) \; X^\mu_{q\lambda}\alpha(2) \; X_k\beta(3)|$$

$$-|\tilde{X}^\mu_{p\lambda}\alpha(1) \; X^\mu_{q\lambda}\beta(2) \; X_k\alpha(3)|$$

$$-|X_k\alpha(1) \; \tilde{X}^\mu_{p\lambda}\beta(2) \; X^\mu_{q\lambda}\alpha(3)|\,] $$

$$(III.1.63)$$

respectively, where $D_\lambda = (2\lambda+1)$ and, for example,

$$|\tilde{X}^\mu_{p\lambda}\alpha(1) \; X^\mu_{q\lambda}\beta(2) \; X_k\alpha(3)|$$

represents the determinant

$$\begin{vmatrix} \tilde{X}^\mu_{p\lambda}\alpha(1) & X^\mu_{q\lambda}\beta(1) & X_k\alpha(1) \\[2mm] \tilde{X}^\mu_{p\lambda}\alpha(2) & X^\mu_{q\lambda}\beta(2) & X_k\alpha(2) \\[2mm] \tilde{X}^\mu_{p\lambda}\alpha(3) & X^\mu_{q\lambda}\beta(3) & X_k\alpha(3) \end{vmatrix}$$

The basis set {X} consists of non-orthogonal Slater-type orbitals (STO´s), which have the form

$$X_{nlm}(r,\theta,\phi;\epsilon) = [(2\epsilon)^{2n+1}/(2n!)]^{1/2}\, r^{n-1}\, e^{-\epsilon r}\, Y_{l,m}(\theta,\phi)$$

$$\text{(III.1.64)}$$

where each function X_{nlm} is normalised to unity. In Equations (III.1.62) and (III.1.63) the α and β functions represent spin functions, and the summations are over the azimuthal quantum number μ, which takes on values from $-\lambda$ to $+\lambda$. This ensures that the electron pair forms either ^{1}S or ^{3}S symmetry, respectively. The orbital angular momentum quantum number λ specifies the symmetry of the space orbital X, and D_{λ} denotes its degeneracy. Finally, the occurrence of a ($\tilde{\ }$) over some of the orbitals denotes the complex conjugate of the angular part of the given orbital.

The wavefunction contains 45 configurations, formed from 20 basis orbitals; these 20 orbitals are subdivided into seven of "s" symmetry (1s, 1s´, 1s´´, 2s, 2s´, 2s´´, 3s´), six of "p" (2p, 2p´, 2p´´, 3p, 3p´, 3p´´), four of "d" (3d, 3d´, 4d, 5d), two of "f" (4f,5f) and one of "g" symmetry (5g). The primes associated with orbitals of the same quantum number (1) indicate a different orbital exponent (ϵ). The STO exponents for the K-shell basis functions were identical to those obtained by Weiss from a 35-term CI study of the $1^{1}S$ state of helium[24]. For lithium, Weiss then optimised the exponents of the basis functions for the outer shell and all the CI coefficients by means of the energy variation method.

For the uncorrelated description of the ground state we used the restricted Hartree-Fock (RHF) function also

constructed by Weiss[32]. In _position_ space, this wavefunction is written as a single determinant of one-electron functions, namely

$$\phi^{HF}(\underline{x}_1, \underline{x}_2, \underline{x}_3) = (3!)^{-1/2} \; |\varphi_{1s}\alpha(1) \; \varphi_{1s}\beta(2) \; \varphi_{2s}\alpha(3)|$$

$$(III.1.65)$$

The function $\varphi_{nlm}(r, \theta, \phi; \varepsilon)$ is the spatial part of the one-electron spin-orbital, and is constructed from a basis set of s-type orbitals,

$$\varphi_{nl} = \sum c_n^i \; X_{nl}^i \; , \qquad (III.1.66)$$

where the summation over i contains six terms. The basis functions X were again taken as standard normalised STO's, as defined in Equation (III.1.64), and to obtain his wavefunction, Weiss minimised the energy of the system with respect to all parameters, including the orbital exponents.

For the analysis of correlation effects in the ^{2}P state of lithium, we again used wavefunctions by Weiss[32]. These functions are constructed in much the same way as those for the ground state, and consequently we shall present only brief details here. The correlated description of the ^{2}P state was provided by a 45-term CI wavefunction formed from a basis set {X} of 38 STO's extending as far as the "5g" orbitals. In the basis set used by Weiss, the functions 1s, 1s', 2s, 2s', 2p, 2p', 3s', 3p, 3p', 3d, 4d, 4f, 5d, 5f and 5g were obtained from the energy minimisation calculations for the 1^1S ground state of He. Weiss then introduced

additional basis functions to describe the outer electron in the ^{2}P state of lithium. As for the ground state, all the configuration coefficients for the excited state wavefunction were optimised, along with the orbital exponents, by the energy variation method.

The uncorrelated description of the system was provided by the ^{2}P restricted Hartree-Fock wavefunction, again by Weiss[32]. The wavefunction, which is constructed from a basis set of four s-type and 5 p-type orbitals, is written in <u>position</u> space as

$$\phi^{HF}(\underline{x}_1,\underline{x}_2,\underline{x}_3) = (3!)^{-1/2} |\varphi_{1s}\alpha(1) \ \varphi_{1s}\beta(2) \ \varphi_{2p}\alpha(3)|,$$

$$(III.1.67)$$

where

$$\varphi_{nl} = \Sigma \ c_n^i \ X_{nl}^i \ , \qquad (III.1.68)$$

and the summation over i contains either 4 or 5 terms, depending on whether nl = 1s or 2p. Once again, the functions X are standard normalised STO´s, as defined in Equation (III.1.64), and Weiss minimised the total energy of the system with respect to all parameters, including the exponents ε.

Since our interests in the present investigation are the effects of correlation on the <u>momentum</u> distributions in the 2^2S and 2^2P states of lithium, it was necessary to obtain the momentum-space counterpart of each of the position-space wavefunctions discussed above. In Chapter (II.2.1), we saw that the conversion of a position-space wavefunction, ϕ, to

its momentum-space equivalent, Ψ, is achieved by the application of a Dirac transformation to ϕ. We also saw that the isomorphic nature of this process means that it is actually only necessary to transform the component spin-orbitals from which ϕ is constructed, since the analytical _form_ of the wavefunction is the same in both spaces. Thus, to obtain the momentum-space description of the ^{2}S and ^{2}P states of lithium, we constructed the Weiss functions using the momentum-_space_ form of the Slater-type orbitals. The method by which each position-space STO was transformed to momentum space has been described in some detail by Reed[33].

In the previous chapter we saw that the spin-free two-particle momentum density of lithium may be partitioned into a number of component densities, $\varrho_{ij}(\underline{p}_i, \underline{p}_j)$, each of which is associated with an identifiable pair of occupied spin-orbitals φ_i and φ_j in the RHF description of the system. For each orbital pair (i,j) we analysed the effects of correlation on the momentum distribution of the electrons by studying a number of one- and two-particle distribution functions and expectation values derived from the component densities $\varrho_{ij}(\underline{p}_i, \underline{p}_j)$. For any such component, the definitions of the various radial, angular and interparticle momentum distribution functions, as well as those of the associated expectation values, are exactly the same as those given in Chapter (II.2.2) for the excited states of helium; clearly there is no need to repeat those definitions here.

In addition to studying properties associated with

individual electron pairs, we also examined the corresponding quantities for the `total´ atom. Thus, for example, in addition to studying the $D_1^{HF}(p_1)$ distribution for each of the electron pairs (1,2), (1,3) and (2,3), we also evaluated the (renormalised) sum of these quantities, defined by

$$D_1^{HF(TOTAL)}(p_1) =$$
$$[D_1^{HF(1,2)}(p_1) + D_1^{HF(1,3)}(p_1) + D_1^{HF(2,3)}(p_1)] / 3.$$

In this way, we were able to compare, in an approximate manner, each component of the uncorrelated one-particle radial momentum distribution with the corresponding quantity for the whole atom. Finally, we note here that for the 2^2S state, the (i,j) pairs (1,2), (1,3) and (2,3) were taken to represent the electron pairs (1sα 1sβ), (1sα 2sα) and (1sβ 2sα) respectively, while for the 2^2P state, the same (i,j) pairs correspond to the electron pairs (1sα 1sβ), (1sα 2pα) and (1sβ 2pα).

Presentation of Results

In Figures (III.1.1) and (III.1.2) we present the uncorrelated one-particle radial distribution functions $D_1^{HF}(p_1)$ for the ^2S and ^2P states respectively. The effects of correlation on these distributions are seen in the $\Delta D_1(p_1)$ curves shown in Figures (III.1.3) and (III.1.4). The uncorrelated two-particle radial distributions, $D_{12}^{HF}(p_1,p_2)$, are presented as surfaces in Figures (III.1.5) and (III.1.7); in order to maximise the information provided by these surfaces, we present alternative views of the

distributions in Figures (III.1.6) and (III.1.8), respectively. The $\Delta D_{12}(p_1, p_2)$ surfaces are shown in Figures (III.1.9) and (III.1.11), with alternative views being presented in Figures (III.1.10) and (III.1.12). In Table (III.1.1) we present the one-particle radial expectation values $\langle p_1^n \rangle$, as well as the standard deviation, $\sigma(p_1)$. The corresponding two-particle expectation values, $\langle p_1^n p_2^n \rangle$ are given in Table (III.1.2) The uncorrelated angular distribution functions $P^{HF}(\gamma)$ for the ^2P state are shown in Figure (III.1.13). (The distributions for the ground state are identical to that for the 1s2s ^3S state of helium, presented in Section (II.2); see Chapter (III.1.4) for further comments.) The effects of correlation on the angular distribution of the electron momenta is shown in the $\Delta P(\gamma)$ curves presented in Figures (III.1.14) and (III.1.15). The angular expectation values $\langle \underline{p}_1 \cdot \underline{p}_2 / p_1^n p_2^n \rangle$ and $\langle \gamma \rangle$ are presented in Table (III.1.3); as before, γ is the angle between the momentum vectors of electrons 1 and 2.

In Figures (III.1.16) and (III.1.17) we show the uncorrelated interparticle momentum distributions $f^{HF}(p_{12})$ for the ^2S and ^2P states, respectively. The Coulomb shifts, $\Delta f(p_{12})$, corresponding to these distributions are presented in Figures (III.1.18) and (III.1.19). The $g^{HF}(p_{12}, p_1)$ surfaces for ^2S and ^2P are shown in Figures (III.1.20) and (III.1.22); alternative views of these surfaces are presented in Figures (III.1.21) and (III.1.23), respectively. The corresponding partial Coulomb shifts, $\Delta g(p_{12}, p_1)$, are presented in Figures (III.1.24) and (III.1.26), with alternative views again being presented in

Figures (III.1.25) and (III.1.27). In Figure (III.1.28) we present the $g^{HF}(p_{12},p_1;\theta_1)$ surfaces for $\theta_1 = 0°$, $30°$, $60°$ and $90°$ for the intershell electron pairs of the ^2P state; as before, θ_1 is the angle between the momentum vector $\underline{p}_1$ and the symmetry axis of the 2p orbital in momentum space. An alternative view of these surfaces is shown in Figure (III.1.29). The effects of correlation on these distributions are shown in the $\Delta g(p_{12},p_1;\theta_1)$ surfaces presented in Figures (III.1.30) and (III.1.31). Finally, in Table (III.1.4) we present the various interparticle expectation values $\langle p_{12}^n \rangle$. Also given in this table are the standard deviations, $\sigma(p_{12})$, of the various $f(p_{12})$ distributions, and the fraction, Y, of probability density which is redistributed as the result of introducing correlation into the description of each electron pair.

CHAPTER (III.1.4)

DISCUSSION

We shall begin our discussion of momentum-space correlation effects in lithium by examining the $(1s)^2 2s\ ^2S$ (ground) state. As we have seen, this system can be partitioned in such a way as to allow us to examine three distinct electron pairs, and we shall refer to these as $(1s\alpha\ 1s\beta)$, $(1s\alpha\ 2s\alpha)$ and $(1s\beta\ 2s\alpha)$. In our discussion of the excited states of helium, we saw that a knowledge of the Hartree-Fock properties of a system is often central to the understanding of the corresponding correlation effects. Accordingly, we shall include here a description of each of the electron pairs in lithium at the uncorrelated level. For convenience, we shall consider first the $(1s\alpha\ 1s\beta)$ intrashell electron pair, and then move on to compare and contrast the two intershell pairs.

We begin by examining the $D_1^{HF}(p_1)$ curve for $(1s\alpha\ 1s\beta)$, presented in Figure (III.1.1a). With both electrons in the same shell, the one-particle radial momentum density displays a single maximum. We shall denote the value of p_1 at which this maximum occurs by p_K. Recalling the nature of the Fourier transform which connects the momentum- and position-space descriptions of a system, we note that the $D_1^{HF}(p_1)$ curve is considerably more diffuse than the $D_1^{HF}(r_1)$ curve obtained by Al-Bayati[29]; the ratio of $\sigma(p_1)$ to $\sigma(r_1)$ is found to be $(1.48:0.34)$. Not surprisingly, the two-particle radial momentum density, $D_{12}^{HF}(p_1,p_2)$, presented in Figure (III.1.5b), also displays a single peak,

distributed symmetrically about the $(p_1=p_2)$ diagonal, with the maximum occurring when $p_1=p_2=p_K$.

Since (1sα 1sβ) is spherically symmetric at the uncorrelated level, the angular distribution function $P^{HF}(\gamma)$ for this electron pair is exactly the same as that for the 1s2s ^{3}S state of helium, presented in Figure (II.2.6a); consequently, we have not presented the intrashell curve here. As a result of the spherical symmetry exhibited by (1sα 1sβ), $\langle\gamma\rangle^{HF}=90°$ for this electron pair. Therefore, at the HF level, we may consider the 1sα and 1sβ electrons as having the same momentum, while moving in directions which are orthogonal.

In keeping with this model, the $g^{HF}(p_{12},p_1)$ distribution function, shown in Figure (III.1.20b), displays a single peak, the coordinates of which are found to be $(p_{12}=\sqrt{(2p_K^2)}, \ p_1=p_K)$. At this point, it is interesting to make the following observation. For the excited states of helium, where the two electrons are in different shells, it was found that $g^{HF}(p_{12},p_1)$ displays two principal features: one parallel to the p_{12}-axis and one lying along the $(p_{12}=p_1)$ diagonal. These two features were explained by considering a test electron at small and large values of p_1, respectively. It was also seen that the extent to which these two features are merged together is directly related to the degree of radial overlap which exists between the two shells in the system -- the greater the radial overlap, the less distinction there is between the features in $g^{HF}(p_{12},p_1)$. If we now return to an examination of the

$g^{HF}(p_{12}, p_1)$ surface for the (1sα 1sβ) electron pair in lithium, it is relatively easy to imagine this surface as the limiting case of a split-shell distribution. Thus, when there is _total_ radial overlap between the descriptions of the two electrons, such as there is for (1sα 1sβ), there is _no_ distinction at all between the `parallel´ and `diagonal´ features in $g^{HF}(p_{12}, p_1)$. As a result, we see only a single feature, largely confined to the $(p_{12} > p_1)$ region.

The $f^{HF}(p_{12})$ curve, obtained by integrating $g^{HF}(p_{12}, p_1)$ over all p_1, is presented in Figure (III.1.16a). Like the radial momentum distribution, the _interparticle_ momentum distribution is more diffuse than its position-space counterpart, as may be seen if one compares the $\sigma(p_{12})$ value in Table (III.1.4) with the corresponding $\sigma(r_{12})$ result obtained by Al-Bayati[29].

Having established the nature of the electron distribution for (1sα 1sβ) at the Hartree-Fock level, we consider now the effects of introducing correlation into the description. In _position_ space, Boyd _et al_[34] have shown that for the ground state of the helium isoelectronic series, the principal radial effect of correlation is to produce some `splitting´ of the one-particle radial distribution. This is characterised by a _reduction_ in probability when $r_1 \approx r_K$, and _increases_ in probability when r_1 is smaller _or_ greater than this. Recently, Al-Bayati[29] has shown that the $\Delta D_1(r_1)$ curve for the (1sα 1sβ) electron pair in the ground state of lithium _also_ displays this sort of structure. Recalling the similarity between the

description of an S state in the position and momentum representations, we might anticipate that this effect _should_ manifest itself in the $\Delta D_1(p_1)$ curve as a reduction in probability when $p_1 \approx p_K$, with increases in probability at lower and higher values of p_1. However, comparison of the $\Delta D_1(p_1)$ curve in Figure (III.1.3a) with the corresponding $D_1^{HF}(p_1)$ distribution in Figure (III.1.1a) appears to indicate that correlation actually causes the greatest _increase_ in probability when $p_1 \approx p_K$, with the greatest reduction occurring on the `large-p_1´ side of this increase. In view of this somewhat unexpected finding, we turn to the $\Delta D_{12}(p_1, p_2)$ surface for ($1s\alpha$ $1s\beta$), presented in Figure (III.1.9b), in the hope that it will provide further insight into the problem; an alternative view of this difference function is provided in Figure (III.1.10b). The principal minimum in this surface occurs on the ($p_1 = p_2$) axis, and closer inspection reveals that, except at very small values of momentum, $\Delta D_{12}(p_1, p_2 = p_1)$ is always negative. In contrast to this, the two principal maxima in the surface occur in the off-diagonal regions. A comparison of the coordinates of these maxima with the coordinates of the single peak in the corresponding $D_{12}^{HF}(p_1, p_2)$ surface reveals that correlation causes a significant _increase_ in the momentum of one electron and a marginal _reduction_ in that of the other. Thus, correlation does indeed cause a `splitting´ of the radial momentum distribution. The conflicting picture created by inspection of the $\Delta D_1(p_1)$ curve is apparently an unfortunate consequence of the `cancelling´ of various regions of the $\Delta D_{12}(p_1, p_2)$ surface which occurs as a result of integrating over the momentum of

electron 2. It is interesting to note that the $\Delta D_{12}(p_1, p_2)$ surface for ($1s\alpha$ $1s\beta$) in the ground state of lithium is very similar to the corresponding surface for the Li^+ ion, obtained by Reed[33].

The one-particle radial momentum expectation values, presented in Table (III.1.1), are seen to be in accord with the shape of $\Delta D_1(p_1)$; for n<0, $\langle p_1^n \rangle$ is seen to be slightly reduced by correlation, whereas for n>0, this expectation value is increased. Furthermore, correlation also increases $\sigma(p_1)$, thereby indicating that the one-particle radial momentum distribution is indeed made more diffuse by the introduction of correlation. Similar results have been found by Moore[35] for the Li^+ ion. For the two-particle radial momentum expectation values, it is found that correlation reduces $\langle p_1^n p_2^n \rangle$ for all n -- a result which is obviously in keeping with the reduction in $D_{12}(p_1, p_2)$ for all ($p_1 = p_2$).

We consider next the effects of correlation on the angular distribution of the electrons. Inspection of the $\Delta P(\gamma)$ curve in Figure (III.1.14a) reveals that the major angular effect of correlation is to reduce the probability of large values of γ and to increase the probability of small values; the cross-over in the angular shift occurs at $\gamma \approx 94°$. Not surprisingly, this reduction in the angular separation of the electron momentum vectors is also reflected in the $\langle p_1 \cdot p_2 / p_1^n p_2^n \rangle$ expectation values, presented in Table (III.1.3). It is seen that correlation increases each quantity from its Hartree-Fock value of zero. In

contrast to this, Al-Bayati found that the values of $\langle \underline{r}_1 \cdot \underline{r}_2 / r_1^n r_2^n \rangle$ were all <u>decreased</u>, indicating that correlation causes an <u>increase</u> in the angular separation of the electron <u>position</u> vectors. It will be recalled that a similar difference between the angular effects of correlation in the position and momentum representations was also observed in the 1s2s ^{3}S state of helium. As in that instance, the two effects can again be rationalised by considering the electrons as oscillating about the nucleus along paths which are orthogonal, with a phase difference of $\pi/2$ between their motions. (For a more complete discussion of this point, see Chapter (II.2.3)). Interestingly, comparison of the $\Delta P(\gamma)$ curve for (1sα 1sβ) in Figure (III.1.14a) with that for the 1s2s ^{3}S state of helium in Figure (II.2.7a) reveals that the angular effects of correlation are much greater for the lithium intrashell electron pair. This is particularly evident when one notes that for (1sα 1sβ), correlation reduces $\langle \gamma \rangle$ by 2.16%, while for the excited state of helium, the reduction in $\langle \gamma \rangle$ is only 0.64%. In contrast to this, a comparison of the corresponding ΔD_1 (p_1) curves reveals that the radial shift for (1sα 1sβ) is much smaller than that for helium.

Thus far, we have seen that in momentum space, the radial and angular effects of correlation in (1sα 1sβ) act in <u>opposition</u>. The radial effect decreases the momentum of one electron and increases that of the other, thereby tending to <u>increase</u> the interelectronic momentum variable. The angular effect, on the other hand, produces a reduction in the angular separation of the momentum vectors, which

leads to a _decrease_ in p_{12}. Clearly, it is now of interest to study the manner in which these two effects combine to change the interparticle momentum distributions. In particular, it will be interesting to compare the partial Coulomb shift with the corresponding partial Coulomb _hole_. The $\Delta g(r_{12}, r_1)$ surface obtained by Al-Bayati[29] revealed that in $(1s\alpha\ 1s\beta)$, r_{12} is _always_ increased by correlation, whatever the radial location of the test electron. This is due to the fact that in _position_ space, the radial and angular effects of correlation _reinforce_ each other. Inspection of the $\Delta g(p_{12}, p_1)$ surface presented in Figures (III.1.24b) and (III.1.25b) reveals that it is very similar, in both shape and magnitude, to the corresponding surface for the Li^+ ion, obtained by Reed[33]. For a test electron with a small value of p_1, correlation causes an increase in p_{12}. However, as we increase the momentum of the test electron, the shape of the $\Delta g(p_{12}, p_1)$ surface changes, and it is seen that for a test electron with a _large_ value of p_1, correlation causes a reduction in p_{12}. The value of p_1 at which the boundary between these two effects occurs is found to be very close to p_K. Thus, for a test electron with a momentum $p_1 < p_K$, the radial effects of correlation are seen to be dominant, while for a test electron with $p_1 > p_K$, the angular effect dominates. Clearly, this ability to distinguish between the radial and angular effects of electron correlation is one of the major advantages that a momentum-space study has over the more traditional position-space approach.

We conclude our analysis of correlation effects in

(1sα 1sβ) by considering the Coulomb shift, which is presented in Figure (III.1.18a). At large and intermediate values of p_{12}, the $\Delta f(p_{12})$ curve bears a strong resemblance to the Coulomb shift obtained by Reed[33] for the Li^+ ion. In particular, the principal maxima in the two shifts occur at approximately the same values of p_{12} in the two states, and are of roughly equal magnitudes; a similar observation holds for the two principal minima. In contrast to this, the local minimum seen at very small p_{12} in Figure (III.1.18a) is barely discernible by comparison with the corresponding feature in the Li^+ curve obtained by Reed. For the positively charged Li-like ions, Al-Bayati[29] has demonstrated that the Coulomb shift for the (1sα 1sβ) electron pair displays no local minimum at small p_{12}. Since each Coulomb shift is obtained by integration (with respect to p_1) of the associated $\Delta g(p_{12}, p_1)$ surface, it is clear that such differences among the $\Delta f(p_{12})$ curves should also be evident in the partial Coulomb shifts. The $\Delta g(p_{12}, p_1)$ surfaces obtained by Al-Bayati for the (1sα 1sβ) electron pair in the positive Li-like ions all possess a distinct positive feature in the region very close to the origin; careful inspection of the partial Coulomb shift for the neutral atom, shown in Figure (III.1.24b), reveals that this surface also has a very slight positive feature in this region. On the other hand, the $\Delta g(p_{12}, p_1)$ surface for the Li^+ ion is found to possess no such feature. From this, it is clear that the differences between the $\Delta f(p_{12})$ curves as p_{12} approaches zero are due principally to the differences in the partial Coulomb shifts when p_{12} and p_1 are both very small. To gain further insight into this, it is useful to

discuss the _position_-space representation of the K-shell electrons in Li. If p_{12} _and_ p_1 are small, it follows that in position space, both electrons must be located in the far outer regions of the K shell, where they are in close proximity to the L shell. For the ground state of the Li-like systems, this shell is occupied by an orbiting 2s electron. Although the properties of this electron are effectively `integrated out´ during the partitioning process, its presence will still be felt, in an _averaged_ way, by any electron which approaches the L shell closely. We have already noted that in position space, the principal radial effect of correlation for the intrashell electron pair is to cause one electron to approach the nucleus, and the other to move away from it. For the Li-like systems, if the 1sα and 1sβ electrons are both located close to the L shell, the outward movement of either electron will be suppressed by the presence of the 2s electron; as a consequence, the radial effect of correlation is reduced, while the angular effect is enhanced. In _momentum_ space, this dominance of angular over radial effects leads to an _increase_ in the probability of very small p_{12} values for a given p_1. In contrast to this, in the Li$^+$ ion, the radial effect of correlation is obviously not affected by the presence of a third electron, and is therefore dominant. In _momentum_ space this leads to a _reduction_ in the probability of very small p_{12} values for a given p_1. From the foregoing, we may conclude that the differences among the various Coulomb shifts near to the origin are due principally to the presence of the L-shell electron in the Li-like systems. With this in mind, it is interesting to

note that for Be, the Coulomb shift for the K-shell electron pair obtained by Mobbs and Banyard[28] reveals $\underline{no}$ local minimum at small p_{12}. This suggests that the presence of the $\underline{two}$ orbiting 2s electrons in the system causes an even greater suppression of radial correlation effects in the K shell. Finally, we note that the overall shape of $\Delta f(p_{12})$ for $(1s\alpha\ 1s\beta)$ in Li suggests that, on average, the angular effect of correlation is dominant, leading to a general reduction in p_{12}. In keeping with this observation, inspection of Table (III.1.4) reveals that when $n<0$, $\langle p_{12}^n \rangle$ is increased by correlation, but when $n>0$, this expectation value is increased; the reduction in $\sigma(p_{12})$ indicates that correlation also produces a `sharpening up' of the interelectronic distribution in momentum space.

Let us now consider the two electron pairs $(1s\alpha\ 2s\alpha)$ and $(1s\beta\ 2s\alpha)$; as for the intrashell pair, we begin by examining the Hartree-Fock properties. In Figure (III.1.1b) we present the $D_1^{HF}(p_1)$ distributions for the two intershell electron pairs. Inspection of the corresponding analysis reveals that these two functions are, in fact, identical, and consequently only one curve is displayed here. It is seen that this $D_1^{HF}(p_1)$ curve is very similar to that for the 1s2s ^{3}S state of He. The larger, localised peak at small p_1 is associated with the L-shell electron, while the more diffuse peak at larger p_1 corresponds to the K-shell electron. For convenience, we denote the values of p_1 at which these peaks occur by p_L and p_K, respectively.

The $\underline{two}$-particle radial distributions for $(1s\alpha\ 2s\alpha)$ and $(1s\beta\ 2s\alpha)$ are presented in Figure (III.1.5). Unlike the

corresponding one-particle functions, there are differences between the $D_{12}^{HF}(p_1,p_2)$ distributions for the two intershell pairs. Inspection of the alternative view of these surfaces, presented in Figure (III.1.6), confirms that this is indeed so. For ($1s\alpha$ $2s\alpha$) the Fermi effect prevents the two electrons from having the same momentum, and consequently for this electron pair, $D_{12}^{HF}(p_1,p_2)$ is identically zero for all ($p_1=p_2$). In contrast to this, the surface for ($1s\beta$ $2s\alpha$) possesses a local positive feature on the ($p_1=p_2$) diagonal; this corresponds to the situation in which one electron is in the high-momentum region of the L shell, while the other is in the low-momentum region of the K shell, which results in both electrons having the same momentum. In position space, Al-Bayati[29] has noted the existence of a small local maximum, near to the origin of the $D_{12}^{HF}(r_1,r_2)$ surface for ($1s\beta$ $2s\alpha$), which corresponds to both electrons being in the K-shell region. (Recall that in Chapter (II.1.4) we saw that the $g^{HF}(r_{12},r_1)$ surface for the 2^1S state of helium also reveals a small positive region at small (r_{12},r_1), again due to the double occupancy of the K shell). In contrast to the results for ($1s\beta$ $2s\alpha$), Al-Bayati found that the $D_{12}^{HF}(r_1,r_2)$ surface for ($1s\alpha$ $2s\alpha$) possesses no such local maximum near to the origin due, of course, to the presence of Fermi correlation. In the light of these observations, we might anticipate that somewhere on the $D_{12}^{HF}(p_1,p_2)$ surface for ($1s\beta$ $2s\alpha$) there should exist a feature, corresponding to the $D_{12}^{HF}(r_1,r_2)$ local maximum seen by Al-Bayati, which is absent from the $D_{12}^{HF}(p_1,p_2)$ surface for ($1s\alpha$ $2s\alpha$). The view of the two-particle radial distribution function presented in Figure (III.1.5d) shows

no evidence of any such structure. However, the alternative view of this surface shown in Figure (III.1.6d) reveals that as we move out from the origin along the ($p_1 = p_2$) diagonal, we encounter first the local maximum discussed earlier, and then a second, barely discernible, positive feature. The coordinates of this second feature, which is absent from the ($1s\alpha$ $2s\alpha$) surface, are found to be the same as those of the principal maximum in the ($1s\alpha$ $1s\beta$) surface. Clearly, this supports the view that this feature does indeed correspond to a double occupancy of the K shell.

Like that of the intrashell electron pair, the momentum distributions of both ($1s\alpha$ $2s\alpha$) and ($1s\beta$ $2s\alpha$) are spherically symmetric at the uncorrelated level. As a result, the $P^{HF}(\gamma)$ distributions for these intershell electron pairs are exactly the same as that for the $1s2s$ ^3S state of He, presented in Figure (II.2.6a). In view of the identity between the angular distributions, and bearing in mind the similarity of the radial descriptions, noted earlier, it is not surprising that the $g^{HF}(p_{12}, p_1)$ surfaces for both intershell electron pairs are also very similar to that for the excited state of He. Both of the Li intershell surfaces presented in Figure (III.1.20) possess the `parallel` and `diagonal` features which we have come to associate with test electrons possessing small and large momenta, respectively. It is seen that the surface for ($1s\alpha$ $2s\alpha$) is `flatter` at very small values of p_{12} than that for ($1s\beta$ $2s\alpha$). We have already established that such `flatness` in a $g^{HF}(p_{12}, p_1)$ surface is due to the effects of Fermi correlation. The alternative view of the two $g^{HF}(p_{12}, p_1)$ surfaces, presented in Figure (III.1.21),

reveals the slightly smaller degree of merging between the 'diagonal' and 'parallel' features in the (1sα 2sα) surface. This is also due to the presence in this electron pair of the Fermi effect, which produces a greater radial separation of the two electrons in momentum space. This contrast between the $g^{HF}(p_{12},p_1)$ surfaces for the two intershell electron pairs is consistent with the differences seen on the $(p_1=p_2)$ diagonal of the corresponding $D_{12}^{HF}(p_1,p_2)$ surfaces, discussed above.

Earlier, we noted the existence of a small local maximum on the $(p_1=p_2)$ diagonal axis of the $D_{12}^{HF}(p_1,p_2)$ surface for (1sβ 2sα), which we attributed to the double occupancy of the K shell. Such an effect should, presumably, also manifest itself in the corresponding $g^{HF}(p_{12},p_1)$ surface. However, comparison between the intershell surfaces presented in Figure (III.1.20) reveals no obvious local maximum in the (1sβ 2sα) surface which could be ascribed to such an effect. To gain further insight into this somewhat unexpected observation we evaluated and plotted the Hartree-Fock density difference function defined by

$$\Delta g^{HF}(p_{12},p_1) = g_{\beta\alpha}^{HF}(p_{12},p_1) - g_{\alpha\alpha}^{HF}(p_{12},p_1).$$

This function is simply the difference between the uncorrelated $g(p_{12},p_1)$ distribution functions for the (1sβ 2sα) and (1sα 2sα) electron pairs. Although not shown here, the resulting surface displayed a distinct local maximum at values of p_{12} and p_1 which correspond quite closely to a double occupancy of the K shell. That this effect is not observable in a straightforward comparison of

the $g^{HF}(p_{12}, p_1)$ surfaces for the intershell electron pairs seems to be due to the location (between the two principal maxima) and diffuse nature of the region of increased probability in the $(1s\beta\ 2s\alpha)$ surface.

The $f^{HF}(p_{12})$ curves derived from the $g^{HF}(p_{12}, p_1)$ distributions are presented in Figure (III.1.16b). The value of p_{12} at which $f^{HF}(p_{12})$ peaks can be related to the corresponding values of p_K and p_L by Pythagoras's Theorem. Not surprisingly, the Fermi effect causes the curve for $(1s\alpha\ 2s\alpha)$ to be somewhat `flat' at very small values of p_{12}. This feature results in the $f^{HF}(p_{12})$ distribution for $(1s\alpha\ 2s\alpha)$ being slightly less diffuse than that for $(1s\beta\ 2s\alpha)$ -- compare, for example, the uncorrelated $\sigma(p_{12})$ values presented in Table (III.1.4).

Having discussed the Hartree-Fock momentum distributions for the intershell pairs, we now consider the effects of introducing correlation into the descriptions. In Figure (III.1.3b) we present the $\Delta D_1(p_1)$ curves for the $(1s\alpha\ 2s\alpha)$ and $(1s\beta\ 2s\alpha)$ electron pairs. For $0 < p_1 < 0.75$, it is seen that the two curves are nearly coincident, with both showing an initial reduction in probability and then, as p_1 is increased, an enhancement, with the cross-over occurring at a value of p_1 very close to p_L. This shift to higher momentum in the L-shell region is consistent with the results of Al-Bayati[29], who found that in <u>position</u> space, correlation causes the outer electron to approach the nucleus. Returning to Figure (III.1.3b), we see that the correlation effects in the K-shell region are significantly

smaller than in the L shell. The oscillatory form of the $\Delta D_1(p_1)$ curve for (1sα 2sα) appears. to suggest that correlation also causes a shift to higher momentum for the K-shell electron. For (1sα 2sα), on the other hand, the situation is rather less clear cut; although this curve also displays a local minimum at $p_1 \approx 1.3$, it does not pass below the p_1-axis. Similar differences between the radial effects of correlation in the K-shell region have also been noted in position space by Al-Bayati[29] and are, no doubt, due to the effects of Fermi correlation. The overall form of the $\Delta D_1(p_1)$ curves is reflected in the one-particle radial expectation values, presented in Table (III.1.1). It is seen that for both intershell electron pairs, correlation reduces $\langle p_1^n \rangle$ for n<0, and increases it for n>0. However, the $\sigma(p_1)$ values, also presented in Table (III.1.1), reveal that for (1sα 2sα), correlation increases slightly the spread of $D_1(p_1)$, but for (1sβ 2sα), it produces a marginal `tightening up´ of the one-particle radial distribution.

We consider next the $\Delta D_{12}(p_1,p_2)$ surfaces presented in Figures (III.1.9c&d). The surface for (1sα 2sα) shows clearly the increase in the momentum of the L-shell electron. Furthermore, inspection of a contour diagram of this density difference function (not included here) confirms that the K-shell electron does indeed also experience an increase in momentum; the coordinates of the principal maxima in $\Delta D_{12}(p_1,p_2)$ for this electron pair are greater, in both directions, than those of the corresponding maxima in the $D_{12}^{HF}(p_1,p_2)$ distribution. A similar analysis of $\Delta D_{12}(p_1,p_2)$ for (1sβ 2sα) reveals that while the momentum

increase of the L-shell electron is quite clear, the K-shell electron appears not to undergo any such change. Interestingly, the coordinates of the principal minima in $\Delta D_{12}(p_1, p_2)$ are identical to those of the maxima in the associated uncorrelated distributions. Inspection of the alternative view of the $\Delta D_{12}(p_1, p_2)$ surfaces presented in Figure (III.1.10) reveals that the principal differences between (1sα 2sα) and (1sβ 2sα) occur in the region of the $(p_1 = p_2)$ diagonal. We have already noted that the Fermi effect causes $D_{12}^{HF}(p_1, p_2 = p_1)$ to be identically zero, and this is naturally true for the correlated distribution also, with the result that $\Delta D_{12}(p_1, p_2)$ for (1sα 2sα) is zero on the $(p_1 = p_2)$ diagonal. For (1sβ 2sα), however, we see that for some values of p_1, correlation causes a significant increase in the probability that the two electrons have the same momenta. As we increase p_1, we encounter a local minimum on the $(p_1 = p_2)$ diagonal of the (1sβ 2sα) surface. The position of this minimum coincides exactly with that of the local maximum seen in the $D_{12}^{HF}(p_1, p_2)$ surface for this electron pair. Thus, it would appear that this feature results from the more loosely bound L-shell electron drifting into the K-shell region; the effects of correlation are similar to those already observed for the (1sα 1sβ) electron pair, where there was a reduction in probability when $p_1 = p_2$, and an enhancement in the off-diagonal regions. Naturally, for (1sα 2sα), the Fermi effect prevents the double occupancy of the K shell. A similar contrast between the effects of correlation in the K-shell regions of the intershell two-particle radial distributions has also been noted in position space by Al-Bayati[29].

The two-particle radial expectation values presented in Table (III.1.2) are in keeping with the above observations. Thus, for both intershell electron pairs $\langle p_1^n p_2^n \rangle$ is increased by correlation when n<0. The quantity $\langle p_1 p_2 \rangle$ is increased by correlation in both (1sα 2sα) and (1sβ 2sα). However, correlation increases $\langle p_1^2 p_2^2 \rangle$ in the (1sα 2sα) pair, but reduces it in (1sβ 2sα) -- a difference which is almost certainly due to the local minimum in the (1sβ 2sα) $\Delta D_{12}(p_1, p_2)$ surface, discussed above.

We now turn our attention to the effects of correlation on the angular distribution of the electrons in the intershell electron pairs. The $\Delta P(\gamma)$ curves, presented in Figure (III.1.14b), show that for both (1sα 2sα) and (1sβ 2sα), correlation causes an enhancement in the probability of small values of γ and a reduction in that of large values. Despite this overall similarity, there are differences between the curves. For (1sα 2sα), $\Delta P(\gamma)$ crosses the γ-axis very close to $\gamma = 90°$, which was the location of the maximum in $P^{HF}(\gamma)$. On the other hand, the crossover for the (1sβ 2sα) curve occurs at a slightly smaller value of γ. Furthermore, it is interesting to note that the angular shift for (1sα 2sα) is larger than that for (1sβ 2sα). The shift to smaller values of γ displayed by both curves is similar to that observed for (1sα 1sβ), but the intershell angular shifts are both seen to be considerably smaller than that for the intrashell electron pair. Similarly, a comparison of Figure (III.1.14b) with the $\Delta P(\gamma)$ curve for the 1s2s ^{3}S state of He reveals that,

although the characteristics of the curves are quite similar, the angular shift in the excited state of He is somewhat larger than those for the lithium intershell electron pairs.

The angular expectation values presented in Table (III.1.3) are seen to be in accord with our observations regarding $\Delta P(\gamma)$. Interestingly, the $\langle \underline{r}_1 \cdot \underline{r}_2 / r_1^n r_2^n \rangle$ expectation values calculated by Al-Bayati[29] reveal that in <u>position</u> space, correlation produces an <u>increase</u> in the interparticle angular separation θ_{12}. Thus, the intershell electron pairs in lithium are two more examples of `systems' in which the angular effects of correlation are different in the position and momentum representations.

Thus far, we have established that the principal radial effect of correlation in the two intershell electron pairs is a shift to higher momentum of the L-shell electron, there being a minimal change in the momentum of the K-shell electron in each instance. Taken in isolation, this radial effect would lead to an increase in the interparticle momentum difference p_{12}. On the other hand, the major angular effect of correlation is to reduce the angular separation of the two electron momentum vectors, and this feature leads to <u>reduced</u> values of p_{12}. As a consequence, we might anticipate that when we study the $\Delta g(p_{12}, p_1)$ and $\Delta f(p_{12})$ functions, we should see a combination of these two opposing effects. We begin by examining the partial Coulomb shifts, presented in Figures (III.1.24c&d). Broadly

speaking, both $\Delta g(p_{12}, p_1)$ surfaces are similar to that for the 1s2s ^{3}S state of He, with each displaying its principal characteristics in the region parallel to the p_{12}-axis at small p_1, and in the region of the $(p_{12}=p_1)$ diagonal. For both electron pairs, the parallel feature, which results from a test electron with a small momentum, reveals the shift to higher momentum of the L-shell electron. If we then consider a test electron with a <u>large</u> value of p_1, it is seen that both surfaces show an increase in probability when $p_{12}<p_1$, a reduction when $p_{12}=p_1$ and a further increase when $p_{12}>p_1$. These characteristics may be understood by considering the following. At the uncorrelated level, there is a positive feature along the $(p_{12}=p_1)$ diagonal of the $g^{HF}(p_{12}, p_1)$ surface for both electron pairs; this feature is due to the `appearance` of the tightly bound, spherically symmetric L-shell momentum distribution, as viewed from a test electron in the K shell. Following the introduction of correlation, the radial momentum distribution of the L-shell electron undergoes an expansion. Naturally, this radial expansion leads to a reduction in probability along the $(p_{12}=p_1)$ diagonal and commensurate increases in probability when $p_{12}<p_1$ and $p_{12}>p_1$. We have already noted that, in addition to the radial effect, there is an angular relocation of the electrons following the introduction of correlation; this change causes an additional shift of probability to the $(p_{12}<p_1)$ side of the $(p_{12}=p_1)$ axis. Clearly, the combination of radial <u>and</u> angular effects should lead to a greater probability enhancement on the $(p_{12}<p_1)$ side of the diagonal than that on the $(p_{12}>p_1)$ side, and inspection of Figures (III.1.25c&d) reveals that

this is indeed the case. Interestingly, as the momentum of the test electron is reduced from this large value, the positive feature on the $(p_{12} > p_1)$ side of the diagonal is seen to disappear from the $(1s\alpha\ 2s\alpha)$ surface; this effect is presumably related to the presence of the Fermi effect in this intershell electron pair. Finally for the partial Coulomb shifts, we note that the $(1s\alpha\ 2s\alpha)$ surface possesses a small `flat' region near to the origin, which is the result of Fermi correlation causing both $g^{HF}(p_{12}, p_1)$ and $g^{corr}(p_{12}, p_1)$ to be vanishingly small when p_{12} and p_1 both tend to zero.

We conclude our discussion of correlation effects for the intershell electron pairs by considering the Coulomb shifts, which are presented in Figure (III.1.18b). As expected, the $\Delta f(p_{12})$ curves for both electron pairs display an overall shift to smaller p_{12}. However, although the <u>shapes</u> of the two Coulomb shifts are quite similar, the spread between the values of $\Delta f(p_{12})$ at the principal maximum and minimum is much greater for $(1s\beta\ 2s\alpha)$ than for $(1s\alpha\ 2s\alpha)$. Inspection of the Y values given in Table (III.1.4), reveals that the Coulomb shift for $(1s\beta\ 2s\alpha)$ is approximately 1.7 times greater than that for $(1s\alpha\ 2s\alpha)$. This result is, no doubt, a reflection of the fact that the <u>angular</u> shift for $(1s\alpha\ 2s\alpha)$ was somewhat larger than that for $(1s\beta\ 2s\alpha)$; since the angular effect of correlation acts in opposition to the radial effects in these two electron pairs, the <u>total</u> effect of correlation should be smaller in $(1s\beta\ 2s\alpha)$. Surprisingly, despite the basic similarities in shape between the $\Delta f(p_{12})$ curves, the

changes due to correlation in the $\langle p_{12}^n \rangle$ expectation values,
presented in Table (III.1.4), are found to be quite
different. Thus, for the (1sα 2sα) electron pair $\langle p_{12}^{-1} \rangle$ is
reduced by correlation, while $\langle p_{12} \rangle$ and $\langle p_{12}^2 \rangle$ are both
increased; for (1sβ 2sα), on the other hand, these changes
are reversed. Similar differences are to be found in the
$\langle r_{12}^n \rangle$ expectation values calculated by Al-Bayati[29].

Having discussed the effects of correlation in each of
the three individual electron pairs, we shall complete our
discussion of the ^2S state of lithium by making a few very
brief comments regarding the 'total' correlation effects in
the system. As we might anticipate, the total $D_1^{HF}(p_1)$ curve
in Figure (III.1.1c) displays two clear peaks, which
correspond to the K and L shells. When compared with this
uncorrelated distribution, the $\Delta D_1(p_1)$ curve shown in
Figure (III.1.3c) reveals a clear shift to higher momentum
in the L shell, and a shift to lower momentum in the K-shell
region. The $D_{12}^{HF}(p_1,p_2)$ surface, presented in
Figures (III.1.5a) and (III.1.6a) shows quite clearly the
different contributions from the individual electron pairs.
On the other hand, the $\Delta D_{12}(p_1,p_2)$ surface in
Figures (III.1.9a) and (III.1.10a) is quite complicated,
due to various cancellations and enhancements of
probability. It is interesting to note that, in spite of
this, both $\Delta D_1(p_1)$ and $\Delta D_{12}(p_1,p_2)$ reveal quite clearly the
extent to which the total radial correlation effects are
dominated by contributions from the intershell electron
pairs. In direct contrast to this, the total $\Delta P(\gamma)$ curve in
Figure (III.1.14c) shows that it is the <u>intrashell</u> electron

pair which dominates the angular effect of correlation. Finally, the Coulomb shift (Figure (III.1.18c)) and partial Coulomb shift (Figures (III.1.24a) and (III.1.25a)) are seen to be quite complicated. This reinforces our earlier comments concerning the necessity of some form of partitioning technique for the sensible analysis of correlation effects in many-electron atoms, particularly with regard to interparticle properties.

We now turn our attention to the $1s^2 2p$ ^2P (excited) state of lithium. The use of the Sinanoglu partitioning technique described in Chapter (III.1.1) allows us once again to separate the system into three electron pairs, which we shall denote by $(1s\alpha\ 1s\beta)$, $(1s\alpha\ 2p\alpha)$ and $(1s\beta\ 2p\alpha)$. As before, we shall begin by studying the $(1s\alpha\ 1s\beta)$ pair; to distinguish clearly between this pair in the ^2P state and the corresponding pair in the ground state, we shall henceforth refer to the intrashell electron pairs in the ^2S and ^2P states as $(1s\alpha\ 1s\beta)^S$ and $(1s\alpha\ 1s\beta)^P$, respectively.

Inspection of the $(1s\alpha\ 1s\beta)^P$ component of the partitioned uncorrelated two-particle density for the ^2P state reveals that it is identical, in analytical form, to the K-shell description in the ^2S state. This correspondence between the density expressions for the ground and excited states is also found to extend to the one- and two-particle <u>radial</u> momentum distributions for this electron pair. Indeed, the $D_1^{HF}(p_1)$ curve and $D_{12}^{HF}(p_1, p_2)$ surface for the $(1s\alpha\ 1s\beta)^P$ electron pair, shown in Figures (III.1.2a) and (III.1.7b), respectively, are found

to be virtually indistinguishable from their ^{2}S counterparts. Furthermore, the uncorrelated angular distributions, $P^{HF}(\gamma)$, for the two intrashell electron pairs are <u>identical</u>. (All systems possessing S symmetry have the same $P^{HF}(\gamma)$ distribution -- we have already shown this curve in relation to our earlier discussion of the 1s2s ^{3}S state of helium). Not surprisingly, the uncorrelated interparticle distributions for $(1s\alpha \ 1s\beta)^P$ are also found to be very similar to the corresponding quantities in the ^{2}S state. Thus, the $f^{HF}(p_{12})$ curve in Figure (III.1.17a) is seen to be graphically indistinguishable from that in Figure (III.1.16a). A similar observation holds for the $g^{HF}(p_{12},p_1)$ surface for $(1s\alpha \ 1s\beta)^P$, shown in Figures (III.1.22b) and (III.1.23b); this distribution is almost coincident with that for the ^{2}S intrashell pair.

Having established the near identity of the uncorrelated descriptions of $(1s\alpha \ 1s\beta)^P$ and $(1s\alpha \ 1s\beta)^S$, we consider now the effects of correlation in the excited state intrashell pair, and begin with an examination of the radial shift. Comparison of the $\Delta D_1(p_1)$ curve for $(1s\alpha \ 1s\beta)^P$, shown in Figure (III.1.4a), with the corresponding difference function for the ^{2}S state, shown in Figure (III.1.3a), reveals them to be very similar in shape. However, for the ^{2}P curve, the difference between the principal maximum and minimum values of $\Delta D_1(p_1)$ is seen to be smaller than that in ^{2}S. In contrast to this, the reduction in probability at small p_1 is found to be <u>greater</u> in depth, and more extensive in its p_1-spread, in the ^{2}P radial shift than in the corresponding ^{2}S curve. The $\Delta D_{12}(p_1,p_2)$ surface for

$(1s\alpha\ 1s\beta)^P$, shown in Figures (III.1.11b) and (III.1.12b), is also seen to be quite similar to that for $(1s\alpha\ 1s\beta)^S$. Not surprisingly, the changes in the one- and two-particle radial expectation values, presented in Tables (III.1.1) and (III.1.2), reflect the nature of the $\Delta D_1(p_1)$ and $\Delta D_{12}(p_1,p_2)$ functions.

Inspection of the $\Delta P(\gamma)$ curve for $(1s\alpha\ 1s\beta)^P$, presented in Figure (III.1.15a), reveals that it is graphically indistinguishable from that for $(1s\alpha\ 1s\beta)^S$. The near-identity of these two difference functions is emphasized by noting that the value of $\langle\gamma\rangle^{corr}$ for $(1s\alpha\ 1s\beta)^S$ is 87.838°, while that for $(1s\alpha\ 1s\beta)^P$ is 87.885° -- a difference of only 0.047° between the electron pairs.

Having established that both the radial <u>and</u> angular effects of correlation are largely unchanged in passing from $(1s\alpha\ 1s\beta)^S$ to $(1s\alpha\ 1s\beta)^P$, we anticipate that the effects of correlation on the <u>interparticle</u> momentum distributions of these electron pairs will also be quite similar. Comparison of the $\Delta g(p_{12},p_1)$ surface for the ^2P intrashell electron pair, shown in Figure (III.1.26b) and (III.1.27b), with its ^2S counterpart reveals the two surfaces to be almost identical, except at very small values of p_{12} and p_1. It will be recalled that for $(1s\alpha\ 1s\beta)^S$, $\Delta g(p_{12},p_1)$ displays a <u>very</u> slight positive feature close to the origin. The existence of this feature was rationalised by noting that the orbiting 2s electron in the ^2S state will, to some extent, suppress the radial effects and enhance the angular effects of correlation in the K-shell electron pair.

Clearly, in ^2P the angular orthogonality which exists between the 1s and 2p electrons will prevent any such interference in the K-shell correlation effects by the orbiting L-shell electron; as a consequence, it is hardly surprising that the $\Delta g(p_{12}, p_1)$ surfaces for the two intrashell electron pairs are somewhat different in the region close to the origin.

We conclude our discussion of the correlation effects in $(1s\alpha\ 1s\beta)^P$ by studying the Coulomb shift, presented in Figure (III.1.19a). Comparison with the $\Delta f(p_{12})$ curve for $(1s\alpha\ 1s\beta)^S$ in Figure (III.1.18a) reveals that for $p_1 > 4.5$, the two curves are graphically indistinguishable. For $p_{12} < 4.5$, slight differences do exist; most notable of these is the fact that the local minimum at $p_{12} = 1.0$ is significantly deeper than the corresponding feature in the ^2S intrashell curve. This is due principally to the differences between the partial Coulomb shifts when p_{12} and p_1 are both small, discussed above, and demonstrates quite clearly the greater significance of radial correlation effects in $(1s\alpha\ 1s\beta)^P$ when p_{12} is small.

Of course, the difference in the symmetry of the outer orbital in the ^2S and ^2P states should be most noticeable when examining the intershell electron pairs, and we now turn our attention to $(1s\alpha\ 2p\alpha)$ and $(1s\beta\ 2p\alpha)$. Inspection of Figure (III.1.2b) reveals that, as for ^2S, the $D_1^{HF}(p_1)$ curves for both the P-state intershell electron pairs are identically equal. However, by comparison with the intershell $D_1^{HF}(p_1)$ curves for the ^2S state, the one-particle

radial distribution for the (1sα 2pα) and (1sβ 2pα) electron pairs possess very little structure; the obvious intershell minimum seen in the curve for ^{2}S is now absent, and the only evidence for the existence of two shells in the ^{2}P curve is a slight change in slope at $p_1 = 1.5$. Closer inspection reveals that the principal difference between the intershell $D_1^{HF}(p_1)$ curves in ^{2}S and ^{2}P occurs in the location and spread of the peak at small p_1; at larger values of momentum the difference becomes negligible. These findings are most clearly illustrated by examination of the radial expectation values $\langle p_1^n \rangle^{HF}$, presented in Table (III.1.1). Thus, the value of $\langle p_1^{-2} \rangle^{HF}$ for the ^{2}S intershell electron pairs is found to be about 3 times larger than the corresponding quantity for the ^{2}P state, whereas the $\langle p_1^2 \rangle^{HF}$ values are quite similar in the two states.

A similar difference in the degree of structure exhibited by $D_1^{HF}(p_1)$ was observed when comparing the one-particle radial momentum distribution functions of the excited S and P states of helium, studied in Section (II.2). In that instance, the two-shell nature of the electron momentum distribution was revealed by examining the corresponding $D_{12}^{HF}(p_1, p_2)$ surface. Inspection of the uncorrelated two-particle radial momentum distributions for (1sα 2pα) and (1sβ 2pα) presented in Figure (III.1.7) confirms that both the ^{2}P intershell electron pairs also give rise to a two-shell distribution. Interestingly, examination of the associated analysis reveals that $D_{12}^{HF}(p_1, p_2)$ for (1sα 2pα) is identical to that for (1sβ 2pα). This is in contrast to our findings for the ^{2}S intershell

pairs, where the two uncorrelated distributions were seen to be _different_ - principally in the region of the $(p_1=p_2)$ diagonal. For the ground state, this difference arose as a result of the presence of Fermi correlation in the (1sα 2sα) pair, which prevented the two electron momenta from having the same magnitude. In the ^2P state, the _angular_ orthogonality between the 1s and 2p orbitals obviates the need for Fermi correlation to impose any restrictions on the two-particle _radial_ distribution. Earlier, we noted that the $D_{12}^{HF}(p_1,p_2)$ surface for (1sβ 2sα) possesses a slight local maximum on the diagonal which is not seen in the surface for (1sα 2sα). This feature was attributed to the possibility of the L-shell electron drifting into the K-shell region, thereby causing the (1sβ 2sα) electron pair to bear a strong resemblance to the (1sα 1sβ) pair. Clearly, in (1sβ 2pα) the difference in symmetry of the two orbitals precludes the possibility of such an occurrence; in keeping with this, inspection of the alternative view of the $D_{12}^{HF}(p_1,p_2)$ surfaces for the ^2P intershell pairs, presented in Figure (III.1.8), reveals _no_ local maximum on the $(p_1=p_2)$ diagonal of the (1sβ 2pα) surface.

The identity between the uncorrelated two-particle _radial_ distribution for the ^2P intershell electron pairs leads us to anticipate that Fermi correlation will cause the corresponding angular distributions to be different, with (1sα 2pα) favouring orientations such that the angular coordinates of the electron momenta are different; inspection of the $P^{HF}(\gamma)$ curves in Figure (III.1.13b) provides confirmation of this. For (1sβ 2pα), the

uncorrelated angular distribution is found to be the same as that for the S state, whereas for (1sα 2pα), $P^{HF}(\gamma)$ is seen to predict higher probabilities for large values of γ; physically, this corresponds to the two electrons having a greater tendency to be moving in opposite directions. The degree of `skewness´ exhibited by the (1sα 2pα) $P^{HF}(\gamma)$ curve may be quantified by noting that for this electron pair, $\langle\gamma\rangle^{HF} = 93.258°$, whereas for (1sβ 2pα), $\langle\gamma\rangle^{HF} = 90°$.

The $g^{HF}(P_{12},P_1)$ surfaces for (1sα 2pα) and (1sβ 2pα), presented in Figure (III.1.22), appear to be broadly similar to their S-state counterparts. However, inspection of the alternative view of the surfaces for ^2P, presented in Figure (III.1.23), reveals a significantly greater degree of merging between the `parallel´ and `diagonal´ features of the surface than is seen in the ^2S state. This is in keeping with our earlier comments regarding the greater degree of radial overlap exhibited by (1sα 2pα) and (1sβ 2pα).

The $g^{HF}(P_{12},P_1;\theta_1)$ surfaces for the two P-state intershell electron pairs are shown in Figure (III.1.28). It is seen that when θ_1 is small the $g^{HF}(P_{12},P_1;\theta_1)$ surfaces for both (1sα 2pα) and (1sβ 2pα) possess the same general characteristics as their angularly integrated counterparts. However, as θ_1 is increased from 0° to 90°, the feature lying parallel to the P_{12}-axis reduces in height, while the `diagonal´ feature remains fairly constant in magnitude. It will be recalled that the $g^{HF}(P_{12},P_1;\theta_1)$ surfaces for the 2^1P and 2^3P states of He showed a similar behaviour; the

233

reasons for this effect are discussed in Chapter (II.2.3). The alternative view of the ^{2}P intershell $g^{HF}(p_{12},p_1;\theta_1)$ surfaces given in Figure (III.1.29) reveals the effects that the different angular distributions in the two electron pairs have on the shape of the diagonal feature, especially when θ_1 is small.

Finally in our discussion of the uncorrelated momentum distributions for (1sα 2pα) and (1sβ 2pα), we examine the $f^{HF}(p_{12})$ curves, presented in Figure (III.1.17b). It is seen that the curve for (1sα 2pα) is somewhat `flatter' at very small values of p_{12} than that for (1sβ 2pα). As in the S state, this difference between the two intershell $f^{HF}(p_{12})$ distributions is attributable to the presence in (1sα 2pα) of Fermi correlation, which prevents the occurrence of very small interelectronic momenta. Interestingly, it is seen that the difference between the two curves is _smaller_ in ^{2}P than in ^{2}S; this is presumably a reflection of the fact that Fermi correlation is more powerful in the S state.

We consider now the effects of correlation on the momentum distributions of (1sα 2pα) and (1sβ 2pα), and begin by examining the $\Delta D_1(p_1)$ curves, presented in Figure (III.1.4b). It is seen that for $p_1 < 0.8$, the one-particle radial shifts for the ^{2}P intershell electron pairs are very similar to those for the corresponding electron pairs in ^{2}S, discussed earlier. In both (1sα 2pα) and (1sβ 2pα), the L-shell electron undergoes a shift to higher momentum, with the difference between the curves for the two intershell electron pairs being slightly greater in

^{2}P than in ^{2}S. In the ^{2}P state, both $\Delta D_1(p_1)$ curves also show a local minimum in the region of $p_1=1.0$; it is interesting to note that the position of this minimum coincides with the location of the barely detectable change in slope of the corresponding $D_1^{HF}(p_1)$ curve which indicated the intershell nature of the uncorrelated radial momentum distribution. At larger values of momentum, the changes in $D_1(p_1)$ due to correlation are seen to become negligible. Interestingly, despite the similarity between the $\Delta D_1(p_1)$ curves for (1sα 2pα) and (1sβ 2pα), the changes in the one-particle expectation values, presented in Table (III.1.1), are found to be quite different. A similar observation may be made with regard to the momentum-space results for the N^{4+}ion, obtained by Al-Bayati.

As for the ^{2}S state, inspection of the $\Delta D_{12}(p_1,p_2)$ surfaces for the ^{2}P intershell electron pairs, presented in Figure (III.1.11), reveals quite clearly the increase in momentum of the L-shell electron in both instances. However, the alternative view of the $\Delta D_{12}(p_1,p_2)$ surfaces presented in Figure (III.1.12) reveals that there are significant differences between these density difference functions and their ^{2}S counterparts. For (1sα 2sα), we saw that, as expected, the change in $D_{12}(p_1,p_2=p_1)$ is identically zero, due to the presence of Fermi correlation in that electron pair. For (1sα 2pα), however, the angular orthogonality between the 1s and 2p orbitals leads to a non-zero probability for $D_{12}^{HF}(p_1,p_2)$ when $p_1=p_2$, and the introduction of correlation sometimes actually <u>increases</u> the probability that the two electron momenta are the same.

235

Furthermore, the $\Delta D_{12}(p_1, p_2)$ surface for (1sβ 2pα) shows no trace of any structure due to the effects of correlation on a double occupancy of the K-shell, such as was observed on the ($p_1 = p_2$) axis of the corresponding (1sβ 2sα) surface; such an observation is to be expected, of course, since we have already noted in our discussion of the $D_{12}^{HF}(p_1, p_2)$ surfaces that the difference in symmetry between the 1s and 2p orbitals prevents the possibility of the (1sβ 2pα) electron pair resembling a doubly occupied K shell. The two-particle radial expectation values derived from the $D_{12}(p_1, p_2)$ distributions are presented in Table (III.1.2); interestingly, for (1sα 2pα) correlation reduces $\langle p_1^n p_2^n \rangle$ for all n, whereas for (1sβ 2pα), $\langle p_1^n p_2^n \rangle$ is reduced for all n except n=1. This observation, together with our earlier comments concerning the effects of correlation on the $\langle p_1^n \rangle$ values, reinforces the idea that changes in expectation values are a fairly insensitive guide to the detailed effects of correlation.

Having discussed the radial effects of correlation in the ^{2}P intershell electron pairs, we now consider how correlation affects the angular distributions. Inspection of the $\Delta P(\gamma)$ curves for (1sα 2pα) and (1sβ 2pα), presented in Figure (III.1.15b), reveals that they are inverted by comparison with the corresponding curves for the ^{2}S state. For both P-state intershell pairs, it is seen that correlation produces a reduction in probability of small values of γ and an increase in large values, with the greatest change occurring in (1sβ 2pα). Interestingly, both $\Delta P(\gamma)$ curves cross the axis at $\gamma=90°$, despite the fact that

the values of γ at which the uncorrelated angular distributions displayed their maxima were found to be different; in contrast to this, the $P^{HF}(\gamma)$ curves for (1sα 2sα) and (1sβ 2sα) were identically equal but the corresponding $\Delta P(\gamma)$ curves crossed the γ-axis at different values of γ. Comparison of the $\Delta P(\gamma)$ curves for (1sα 2pα) and (1sβ 2pα) with those for the excited P states of helium, studied in Section (II.2), reveals that the angular shifts for both the Li intershell electron pairs have the same general form as that for the 2^3P state of helium (except at very large values of γ). In passing, it is to be recalled that for the excited states of He, the angular shift for 2^1P is inverted with respect to that for 2^3P. For lithium, the shapes of the $\Delta P(\gamma)$ curves for (1sα 2pα) and (1sβ 2pα) are reflected in the angular expectation values, presented in Table (III.1.3). Thus, for example, it is seen that for both (1sα 2pα) and (1sβ 2pα), correlation reduces the value of $\langle \cos\gamma \rangle$.

Finally in our discussion of the P-state intershell electron pairs, we consider the effects of correlation on the interparticle distribution functions, and begin by considering the intershell $\Delta g(p_{12}, p_1)$ surfaces in Figures (III.1.26c&d). These surfaces, like their ^{2}S-state counterparts, both display features parallel to the p_{12} and $(p_{12}=p_1)$ axes. The `parallel' features in both surfaces are seen to possess the same general characteristics of shape as the corresponding surfaces for (1sα 2sα) and (1sβ 2sα), shown in Figure (III.1.24); in each instance, the shift to higher momentum of the L-shell electron is clearly visible.

In distinct contrast to this similarity between the `parallel´ features in all the intershell surfaces, the `diagonal´ features in the (1sα 2pα) and (1sβ 2pα) surfaces are found to be quite different to their counterparts in the (1sα 2sα) and (1sβ 2sα) surfaces. This difference is most clearly illustrated by inspection of the alternative view of the $\Delta g(p_{12}, p_1)$ surfaces, provided in Figures (III.1.25) and (III.1.27). For the ^2S state, we found that the radial effect of correlation produced a shift of probability from the $(p_{12}=p_1)$ axis to the $(p_{12}<p_1)$ and $(p_{12}>p_1)$ regions; at the same time, the angular effect of correlation was to enhance the probability of small values of the interelectronic angular separation, thereby causing the greatest enhancement of probability in the $\Delta g(p_{12}, p_1)$ surface to occur when $p_{12}<p_1$. For the ^2P intershell electron pairs, the radial effect of correlation is effectively the same as in (1sα 2sα) and (1sβ 2sα). However, the principal angular effect is now a shift to larger values of γ, and this causes the greatest enhancement of probability to occur when $p_{12}>p_1$. From the foregoing, it is quite clear that the difference between the intershell $\Delta g(p_{12}, p_1)$ surfaces for the ^2S and ^2P states in the region of the $(p_{12}=p_1)$ diagonal axis is primarily the result of the different angular effects of correlation in the two states.

Further inspection of the alternative views of the $\Delta g(p_{12}, p_1)$ surfaces for all four intershell electron pairs suggests that there are greater differences between the surfaces for (1sα 2sα) and (1sβ 2sα) than there are between those for (1sα 2pα) and (1sβ 2pα). This is consistent with

our earlier comments concerning the relative magnitudes of the effects of _Fermi_ correlation in the S and P states. Since the Fermi effect is quite powerful in $(1s\alpha\ 2s\alpha)$, it is to be expected that there should be distinct differences between the effects of _Coulomb_ correlation in the intershell electron pairs of the S state. In the P state, on the other hand, the effect of Fermi correlation is less pronounced, and consequently produces less significant differences between the effects of Coulomb correlation in the two intershell electron pairs.

The θ_1-dependent partial Coulomb shifts, presented in Figure (III.1.30), show how the effects of correlation change with the angular orientation of the test electron, measured relative to the symmetry axis of the 2p orbital. When $\theta_1=0^\circ$, the surfaces for both $(1s\alpha\ 2p\alpha)$ and $(1s\beta\ 2p\alpha)$ bear a strong resemblance to their angularly integrated counterparts. As θ_1 is increased, the `parallel´ features diminish in magnitude until they disappear completely when $\theta_1=90^\circ$; such behaviour is, of course, a reflection of the behaviour of the corresponding uncorrelated distributions, $g^{HF}(p_{12},p_1;\theta_1)$. From the view of the $\Delta g(p_{12},p_1;\theta_1)$ surfaces presented in Figure (III.1.30), it would appear that for the `diagonal´ features, the principal effect of increasing θ_1 is simply to reduce slightly the height of the maxima which flank the $(p_{12}=p_1)$ diagonal. However, inspection of the alternative view of the density difference surfaces, provided in Figure (III.1.31), reveals that the situation is actually somewhat more complicated. When $\theta_1=0^\circ$, both surfaces display a positive feature lying parallel to the

239

$(p_{12}=p_1)$ axis, on the $(p_{12}>p_1)$ side, and a negative region, also lying parallel to the axis, on the $(p_{12}<p_1)$ side. The zero contour between these two regions is almost coincident with the $(p_{12}=p_1)$ axis. As θ_1 is increased, the positions and magnitudes of the positive and negative features change; when $\theta_1=90°$, we see a negative region <u>along</u> the $(p_{12}=p_1)$ diagonal, with positive features flanking this axis on <u>both</u> sides. For both intershell electron pairs, the positive feature on the $(p_{12}>p_1)$ side of the diagonal is greater in magnitude than that on the $(p_{12}<p_1)$ side. Furthermore, the difference in height between the two positive features is relatively greater in $(1s\alpha\ 2p\alpha)$ than it is in $(1s\beta\ 2p\alpha)$. For the former electron pair, the ratio of the maximum heights of the two features is 1.96:1, while for the latter pair the ratio is only 1.66:1. The shape of the diagonal features in the surfaces for $\theta_1=0°$ and $\theta_1=30°$ seems to indicate quite firmly a dominance of angular correlation effects at small values of θ_1. (If the radial effects of correlation were of any significant magnitude we would expect to see a positive feature on <u>both</u> sides of the diagonal, due to the radial expansion of the L-shell momentum distribution). When $\theta_1=90°$, it appears that the radial effect of correlation has increased, as indicated by the presence of the two positive features flanking the diagonal. The angular effects are, however, still significant, as evidenced by the different magnitudes of these positive regions. Finally, we note that the difference in the relative magnitudes of these two positive features for the two electron pairs is consistent with the difference in magnitude of the angular shifts in $(1s\alpha\ 2p\alpha)$

and ($1s\beta$ $2p\alpha$), discussed earlier.

We conclude our discussion of correlation effects in the ^2P intershell electron pairs by considering the $\Delta f(p_{12})$ curves. Inspection of Figure (III.1.19b) reveals that there are significant differences between the Coulomb shifts for the intershell electron pairs of the ^2P state and those of the ground state. For both ($1s\alpha$ $2s\alpha$) and ($1s\beta$ $2s\alpha$), the principal feature exhibited by $\Delta f(p_{12})$ was a shift to smaller values of p_{12}; for ($1s\alpha$ $2p\alpha$) and ($1s\beta$ $2p\alpha$), on the other hand, there is a major shift to <u>larger</u> values of p_{12}. It will be recalled that the radial shifts for the ^2P intershell electron pairs indicate a barely discernible change in momentum of the K-shell electron, and a shift to higher p_1 for the L-shell electron. Recalling that $\langle \gamma \rangle^{HF} \geqslant 90°$ for these intershell electron pairs, such an effect would, in isolation, clearly lead to larger values of p_{12}. At the same time, the angular shifts for these electron pairs indicated an increase in the probability of large angles between the electron momentum vectors; this change would, by itself, <u>also</u> produce an enhancement in the probability of large values of p_{12}. Clearly, the shapes of the Coulomb shifts for ($1s\alpha$ $2p\alpha$) and ($1s\beta$ $2p\alpha$) reflect the fact that for these electron pairs, the radial and angular effects of correlation reinforce each other. In ^2P, as in ^2S, the intershell pair in which the electron spins are the same undergoes a smaller Coulomb shift than that in which the two spins are opposed; inspection of Table (III.1.4) reveals that the ratio of Y for ($1s\alpha$ $2s\alpha$) to that for ($1s\beta$ $2s\alpha$) is 1.7:1 and the corresponding ratio for the ^2P

intershell pairs is $1.9:1$. At the same time, comparison of the intershell Y values with those for $(1s\alpha\ 1s\beta)^S$ and $(1s\alpha\ 1s\beta)^P$ reveals just how small the <u>inter</u>shell Coulomb shifts are by comparison with the <u>intra</u>shell shifts.

Returning to Figure (III.1.19), we see that when $P_{12} \approx 3.5$, there is a local minimum in the Coulomb shift for $(1s\alpha\ 2p\alpha)$, where $\Delta f(p_{12})$ is negative; a minimum also occurs in the curve for $(1s\beta\ 2p\alpha)$, but in <u>that</u> instance, $\Delta f(p_{12})$ remains positive. A similar distinction may also be observed in the corresponding Coulomb shifts for the ^2P state of the positive ions. Finally, we note that the $\langle p_{12}^n \rangle$ expectation values presented in Table (III.1.4) are in keeping with the shapes of the Coulomb shifts, discussed above. Thus, for both intershell electron pairs, $\langle p_{12}^n \rangle$ is reduced by correlation for $n<0$ and increased by correlation when $n>0$; the increase in $\sigma(p_{12})$ for each pair reflects the increase in the spread of the $f(p_{12})$ distribution in both instances.

We conclude this discussion of the ^2P state of lithium by commenting briefly on some of the more interesting aspects of the <u>total</u> effects of correlation. As for the ^2S state, these effects were obtained by summing the component quantities corresponding to the individual electron pairs and then renormalising.

Of particular interest is the total angular shift for ^2P, shown in Figure (III.1.15c). We have already seen that the angular shift for $(1s\alpha\ 1s\beta)^P$ predicts an increase in the

probability of small values of γ, while the shifts for the two _inter_shell electron pairs show an increase in the probability of _larger_ values of γ. When combined to produce the _total_ angular shift, there is some `cancellation´ between these effects; however, due to the significantly greater magnitude of correlation effects in the intrashell electron pair, the overall effect of correlation in the whole atom is an increase in the probability of small values of γ. A similar total shift was found in ^2S, but in _that_ state, _all_ the component $\Delta P(\gamma)$ curves were seen to predict a shift to small γ. Clearly, without the use of the partitioning technique, it would have been impossible to distinguish between all the various angular effects occurring in the two states.

Finally, comparison of the total Coulomb shift for ^2P, presented in Figure (III.1.19c), with that for ^2S, in Figure (III.1.18c), reveals that the two $\Delta f(p_{12})$ curves have essentially the same characteristics. That is, correlation causes a reduction in the probability of small and large values of p_{12}, and an enhancement in the probability of intermediate values. In ^2S, this enhancement displayed a certain amount of `structure´, due to the overlapping of various features in the three component Coulomb shifts. In contrast to this, the total curve for ^2P is quite smooth, indicating a greater coincidence in the positions of the principal maxima of the three component shifts.

CHAPTER (III.1.5)

SUMMARY

Momentum-space correlation effects have been studied in the $1s^2 2s$ ^2S and $1s^2 2p$ ^2P states of lithium. The analysis was performed by using a partitioning technique to divide each system into a number of identifiable electron pairs; radial, angular and interelectronic momentum distributions and expectation values were then examined for each pair. Where possible, the results obtained were compared with those from studies of other systems -- in particular, the ground and excited states of helium-like systems, and the various electron pairs in beryllium.

The effects of correlation in the intrashell electron pair of both states were found to be very similar to those found in Li^+. Examination of the two-particle radial shift, $\Delta D_{12}(p_1, p_2)$, revealed that in both $(1s\alpha\ 1s\beta)^S$ and $(1s\alpha\ 1s\beta)^P$ the major radial effect of correlation is a 'splitting' of the radial momentum distribution, with the momentum of one electron being significantly increased, and that of the other undergoing a marginal reduction. Taken in isolation, such an effect would lead to an increase in the interelectronic momentum variable p_{12}. In contrast to this, inspection of the angular shifts, $\Delta P(\gamma)$, revealed that the principal angular effect of correlation -- a shift to smaller angles between the momentum vectors -- would lead to a reduction in p_{12}. Thus, in both the intrashell electron pairs, as in Li^+, radial and angular correlation have opposing effects on the interelectronic distribution.

Furthermore, the Coulomb shifts, $\Delta f(p_{12})$, showed that angular correlation is the dominant effect in both instances, again in keeping with the findings for Li^+. The partial Coulomb shifts, $\Delta g(p_{12}, p_1)$, revealed the presence of both radial and angular correlation effects, with radial and then angular correlation dominating the shape of the surface as the momentum, p_1, of the test electron was increased. Certain differences were detected between the partial Coulomb shifts for $(1s\alpha\ 1s\beta)^S$ and $(1s\alpha\ 1s\beta)^P$. These differences, although small, could be accounted for in terms of the change in symmetry of the L-shell electron associated with each of the K-shell electron pairs.

The intershell electron pairs of both states all reveal a shift to higher momentum for the L-shell electron, with the change in the K shell being negligible in each instance. In contrast to this similarity among the radial effects of correlation, the angular effects in $(1s\alpha\ 2s\alpha)$ and $(1s\beta\ 2s\alpha)$ were found to be quite different from those for $(1s\alpha\ 2p\alpha)$ and $(1s\beta\ 2p\alpha)$. For the S state, the angular shifts, $\Delta P(\gamma)$, for the intershell electron pairs revealed that the angle between the momentum vectors of the two electrons is reduced by correlation, whereas in $(1s\alpha\ 2p\alpha)$ and $(1s\beta\ 2p\alpha)$, correlation was found to increase γ.

The differences among the angular characteristics of correlation in the intershell electron pairs resulted in the Coulomb shifts, $\Delta f(p_{12})$, for $(1s\alpha\ 2s\alpha)$ and $(1s\beta\ 2s\alpha)$ being markedly different from those for $(1s\alpha\ 2p\alpha)$ and $(1s\beta\ 2p\alpha)$. In the S state intershell pairs, radial and angular

correlation have _opposing_ effects on the interelectronic momentum distribution; since the shapes of the corresponding Coulomb shifts both indicate an overall movement towards smaller values of p_{12}, it would appear that angular correlation is the dominant effect in both pairs. For the P state, on the other hand, the effect of both radial _and_ angular correlation is to increase the interelectronic momentum, with the result that the Coulomb shifts for both these electron pairs reveal an overall _increase_ in p_{12}.

FIGURES AND TABLES - SECTION (III)
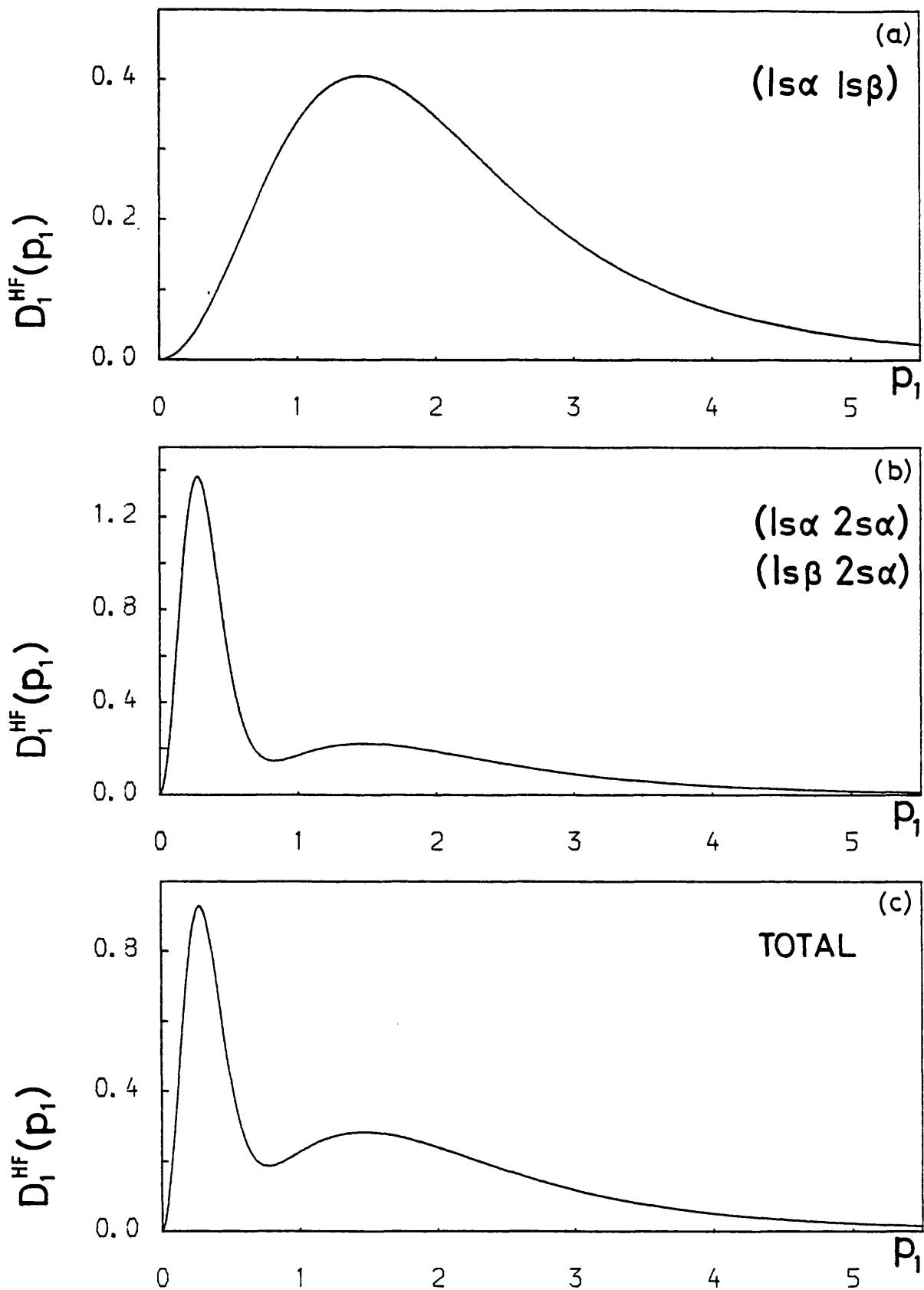
Figure (III.1.1)

The $D_1^{HF}(p_1)$ distributions for the various electron pairs and the ´total´ atom in the 2^2S state of Li.
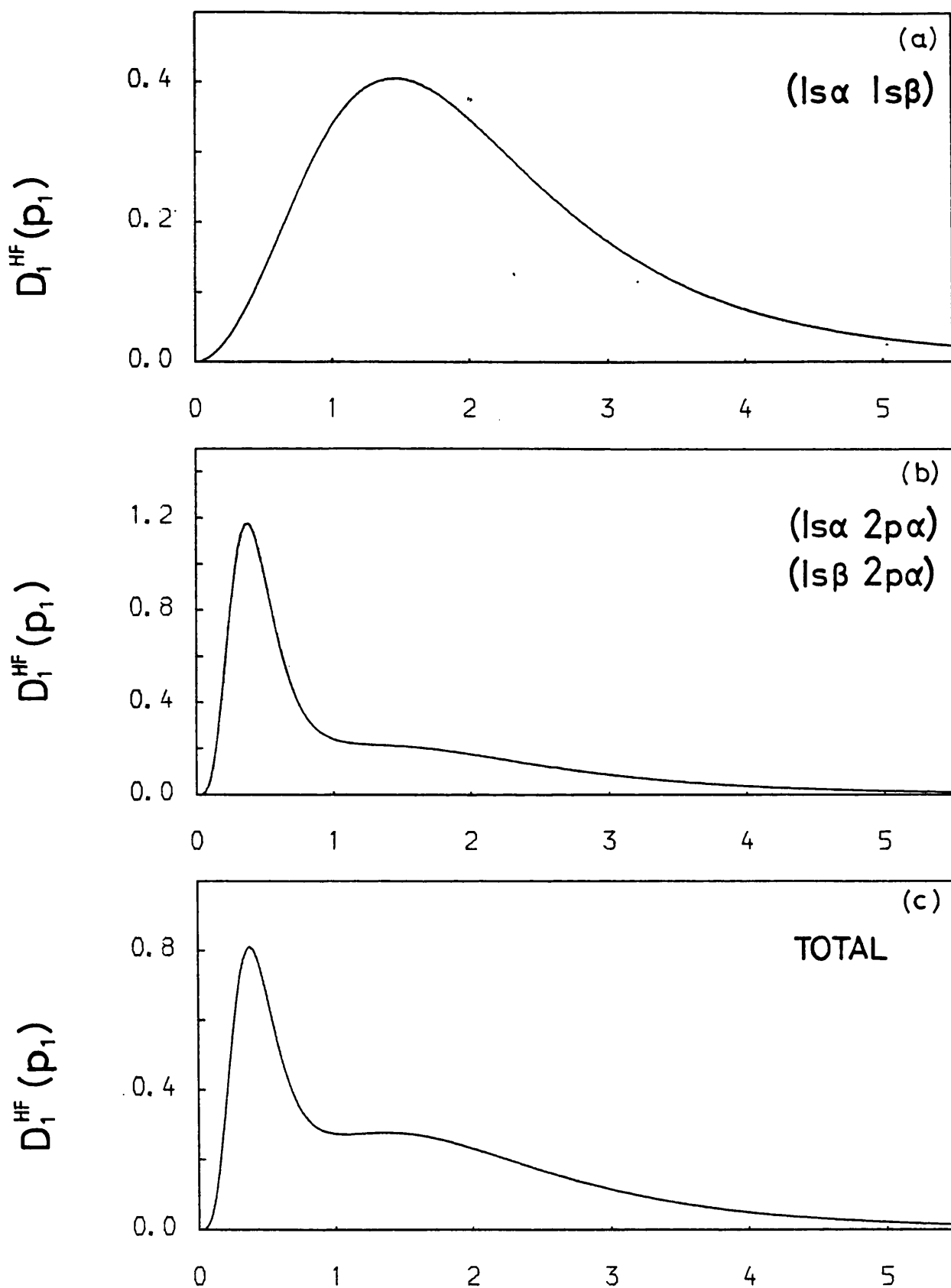
Figure (III.1.2)

The $D_1^{HF}(p_1)$ distributions for the various electron

pairs and the 'total' atom in the 2^2P state of Li.
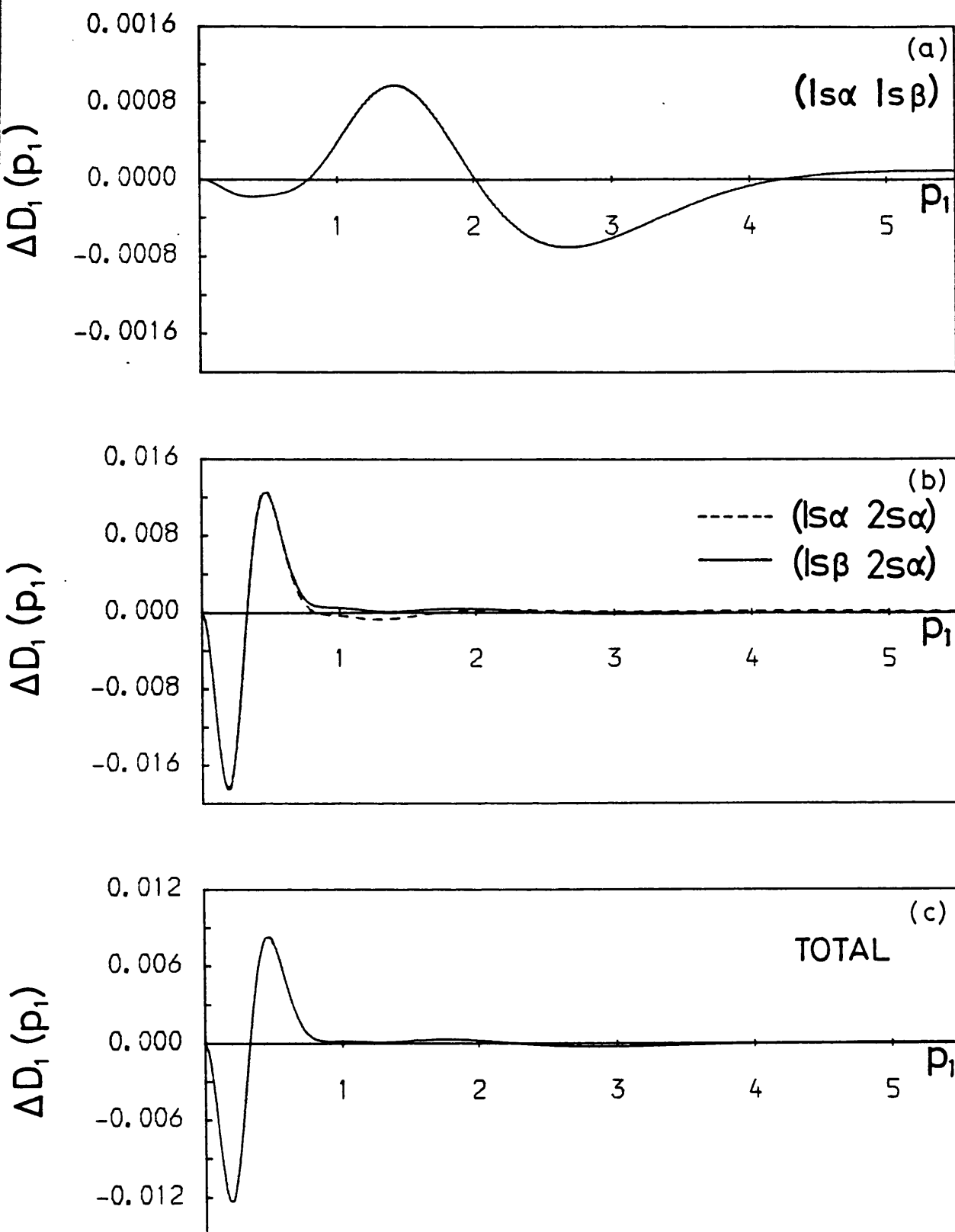
Figure (III.1.3)

The one-particle radial shifts $\Delta D_1 (p_1)$ for the various electron pairs and the 'total' atom in the 2^2S state of Li.
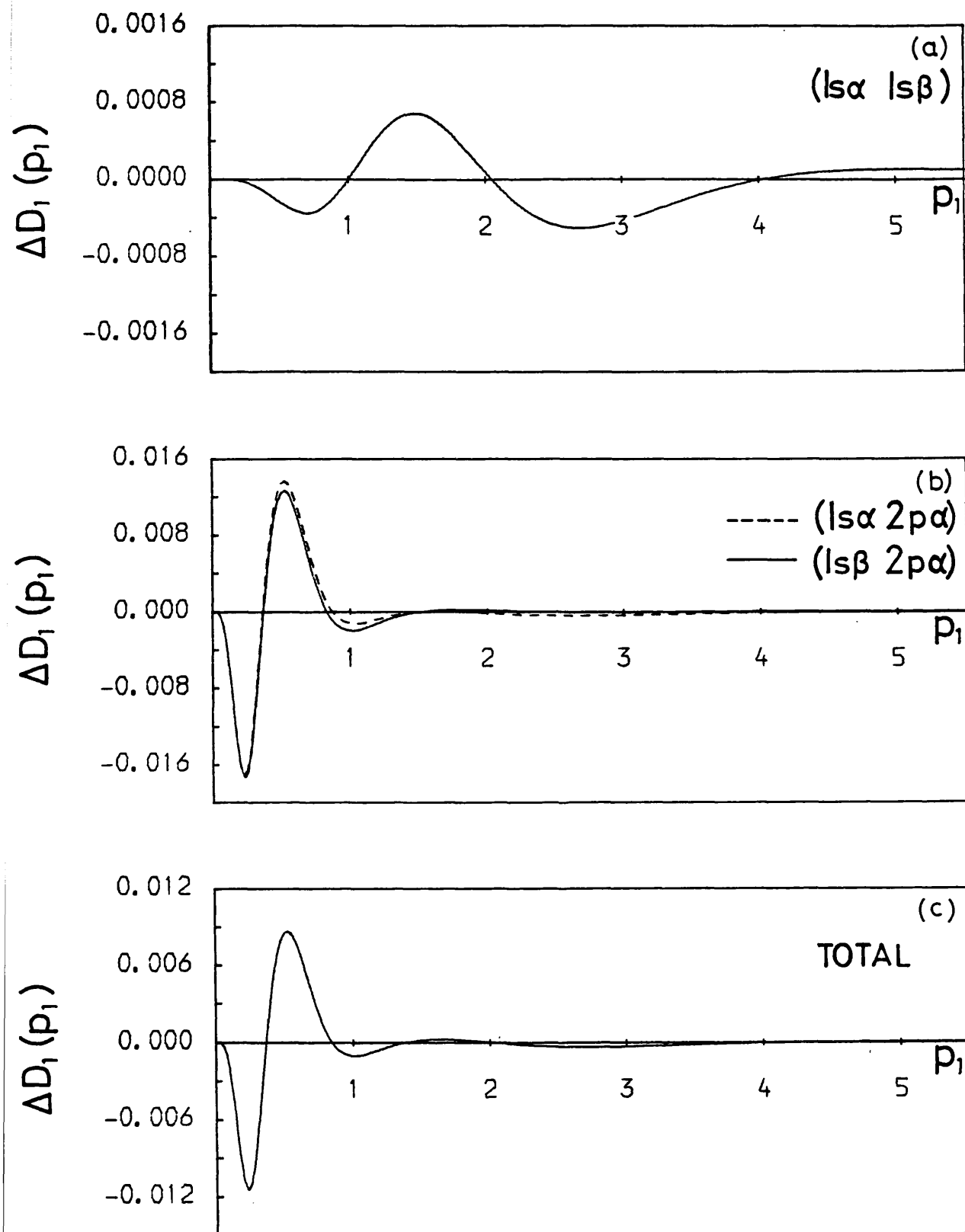
Figure (III.1.4)

The one-particle radial shifts $\Delta D_1(p_1)$ for the various electron pairs and the 'total' atom in the 2^2P state of Li.

<u>Figure (III.1.5)</u>

(see over)

Figure (III.1.5)

The $D_{12}^{HF}(p_1, p_2)$ distributions for the 'total' atom and the various electron pairs in the 2^2S state of Li.

(a) TOTAL

(b) $(1s\alpha\ 1s\beta)^S$

(c) $(1s\alpha\ 2s\alpha)$

(d) $(1s\beta\ 2s\alpha)$

$D_{12}^{HF}(p_1, p_2)$ 0.4

(a) TOTAL

(c) $(1s\alpha\ 2s\alpha)$

$D_{12}^{HF}(p_1, p_2)$ 0.4

(b) $(1s\alpha\ 1s\beta)^S$
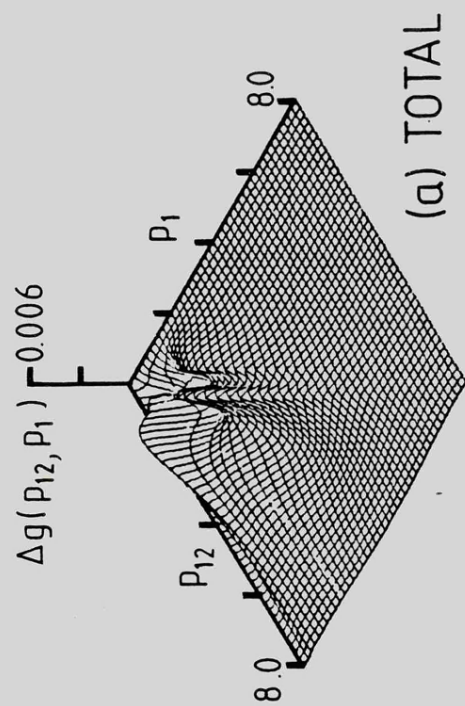
(d) $(1s\beta\ 2s\alpha)$
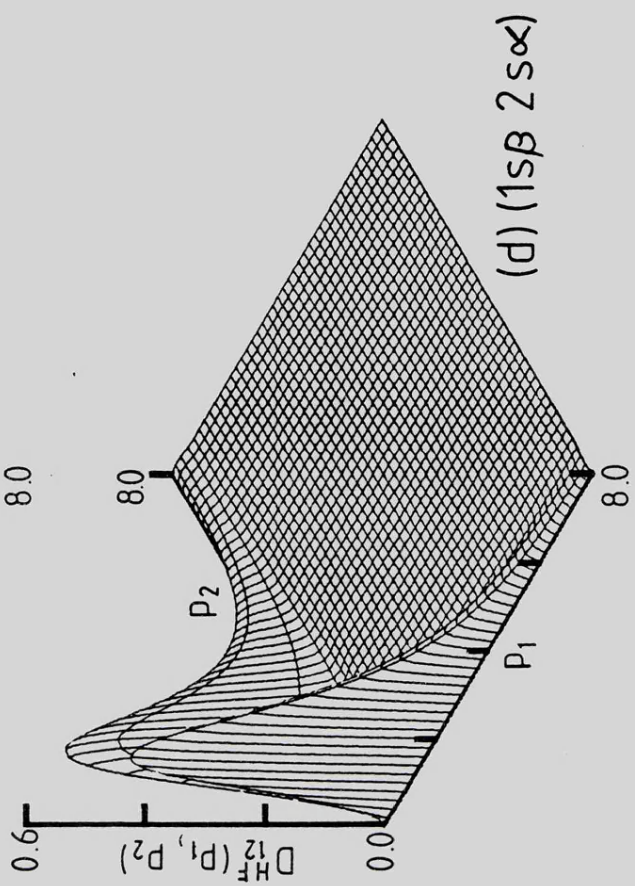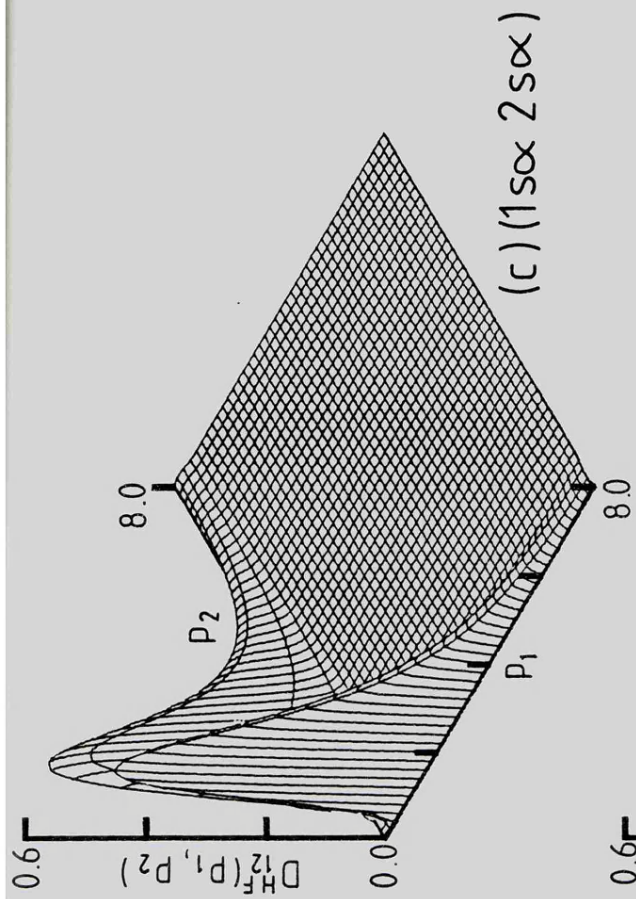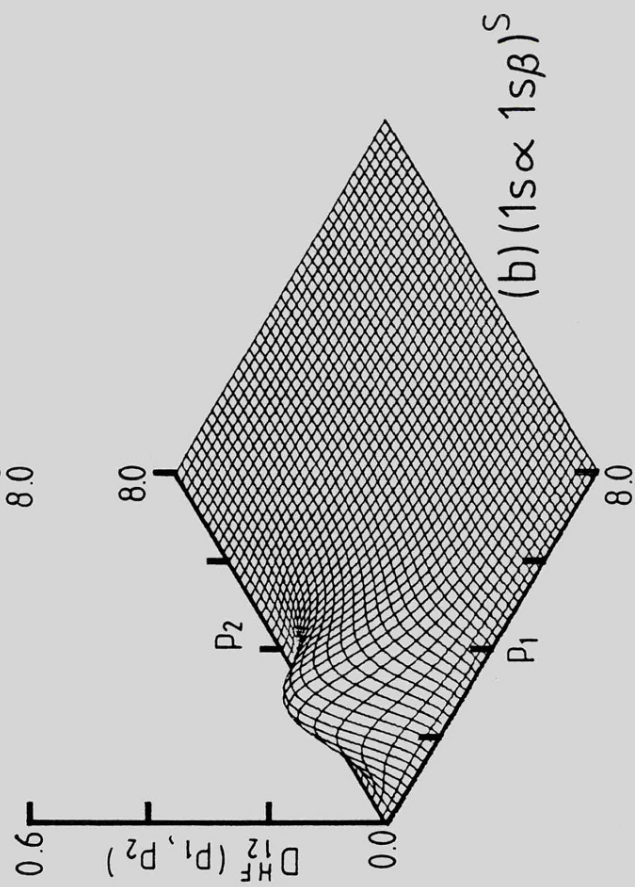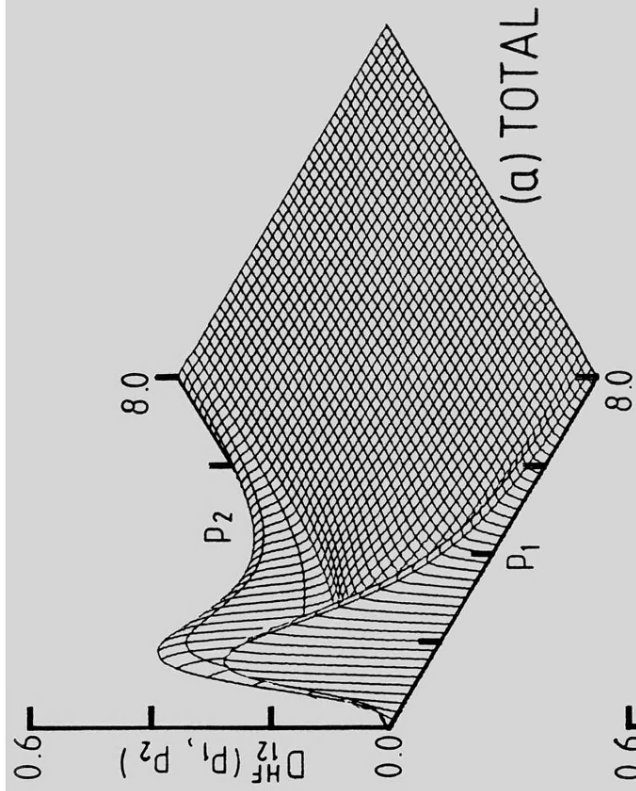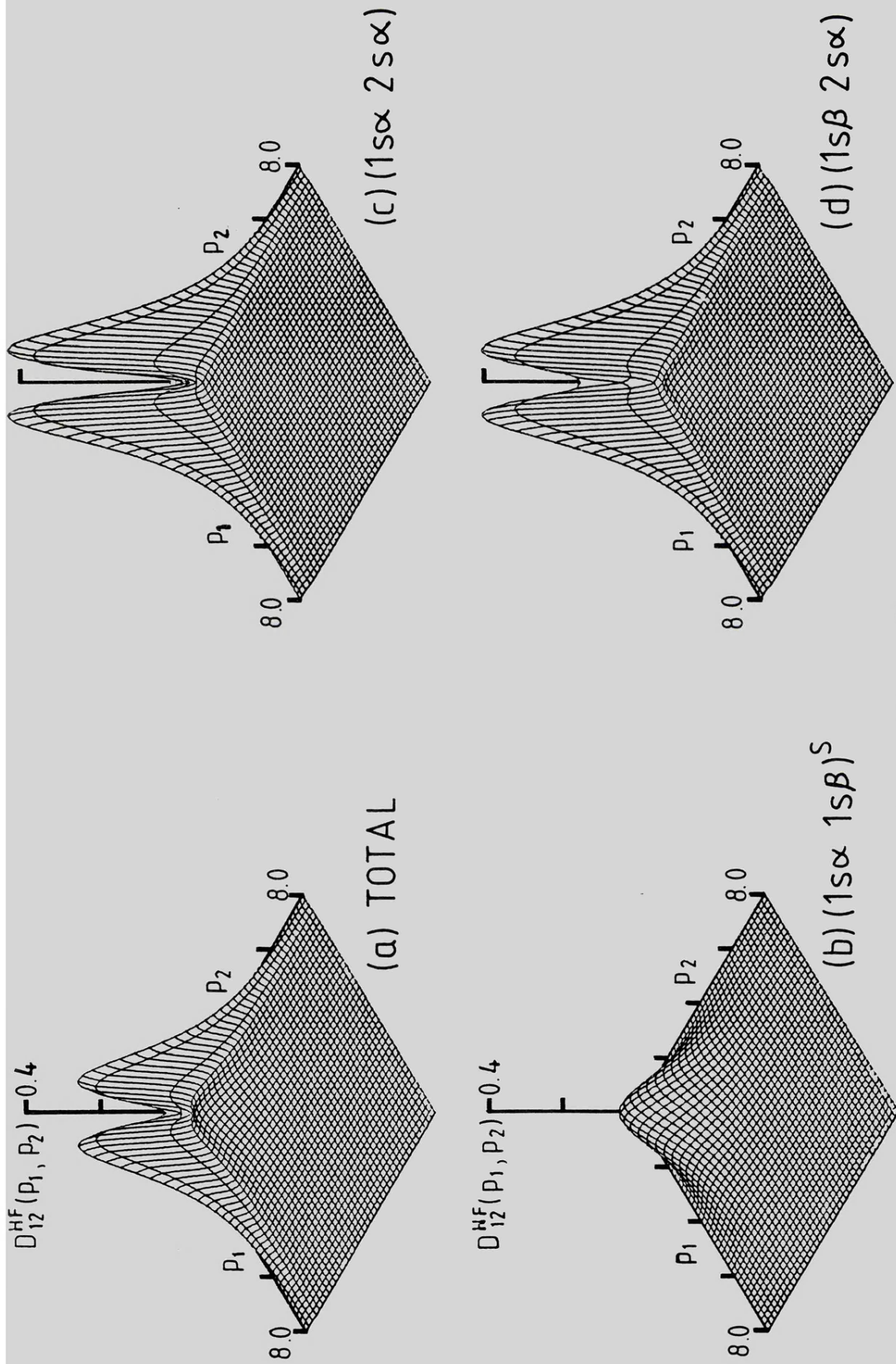
<u>Figure (III.1.6)</u>

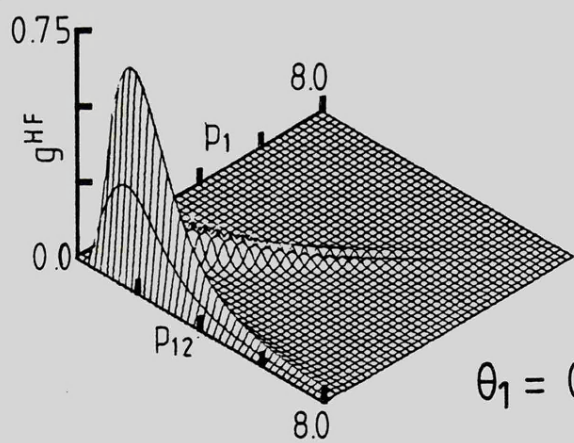An alternative view of the $D_{12}^{HF}(p_1, p_2)$ surfaces presented in Figure (III.1.5).

Figure (III.1.7)

(see over)

Figure (III.1.7)

The $D_{12}^{HF}(p_1, p_2)$ distributions for the 'total' atom and the various electron pairs in the 2^2P state of Li.

(a) TOTAL

(b) $(1s\alpha\ 1s\beta)^P$

(c) $(1s\alpha\ 2p\alpha)$

(d) $(1s\beta\ 2p\alpha)$

(c)(1sα2pα)

(d)(1sβ 2pα)

(a) TOTAL

(b)(1sα1sβ)^P
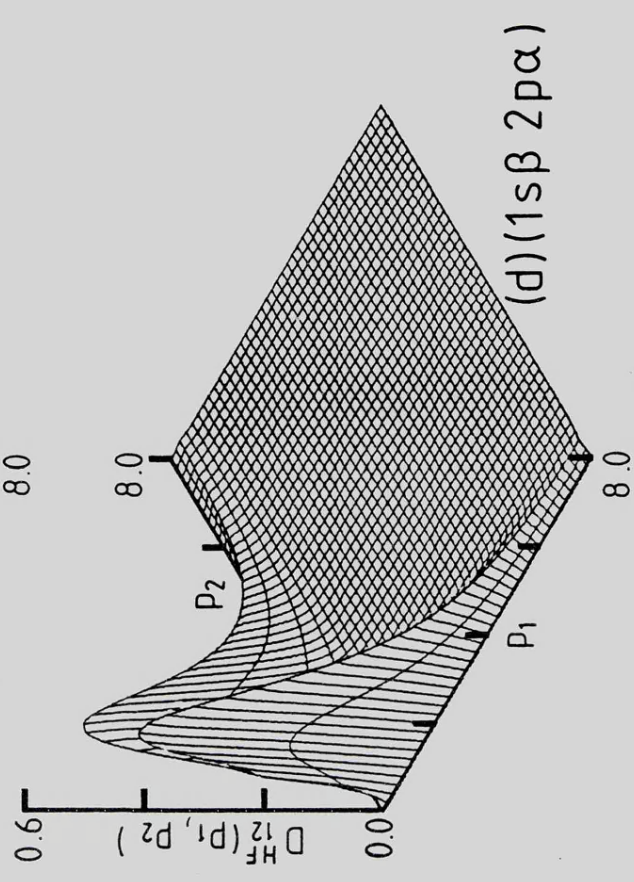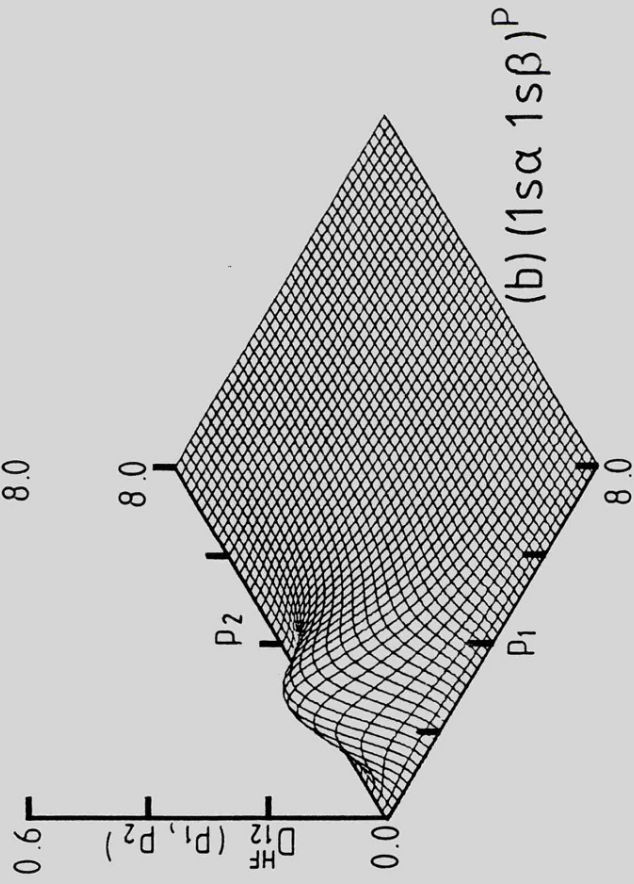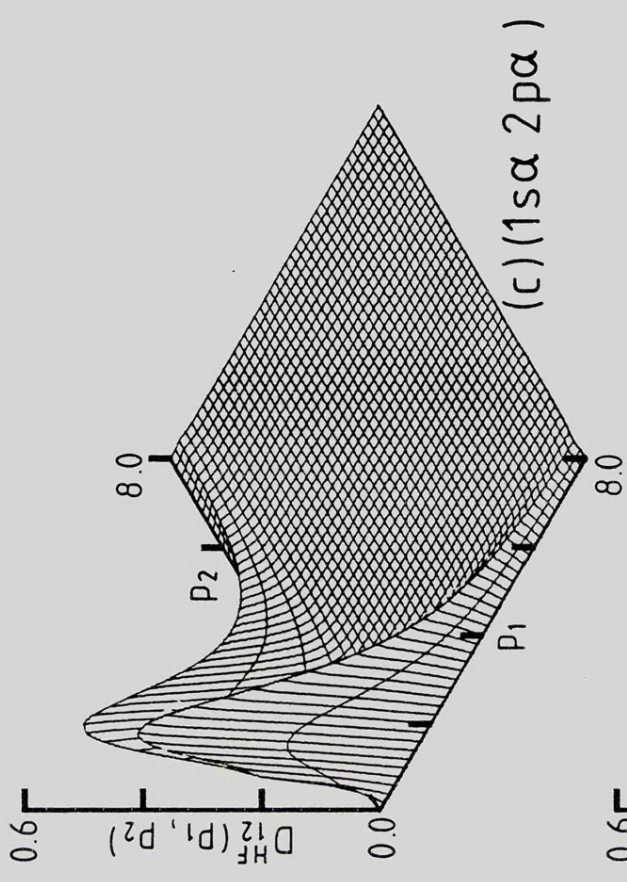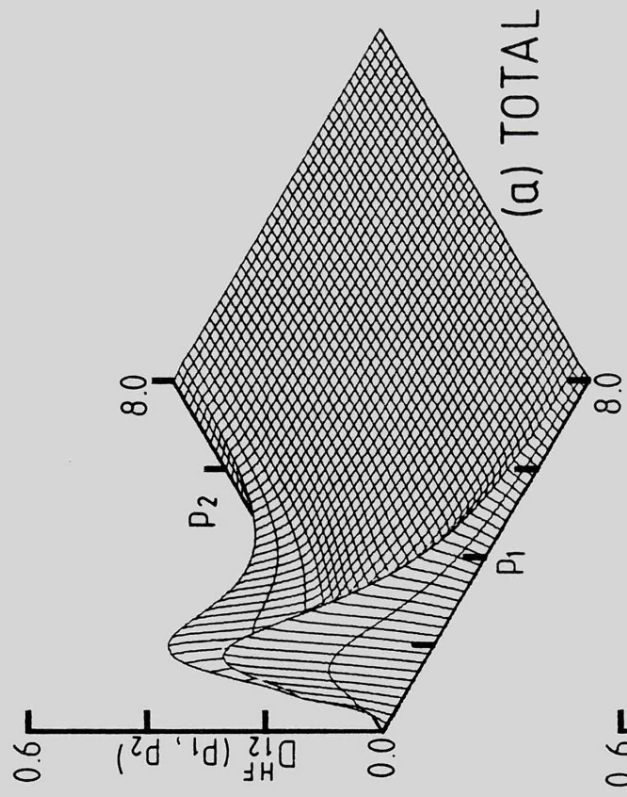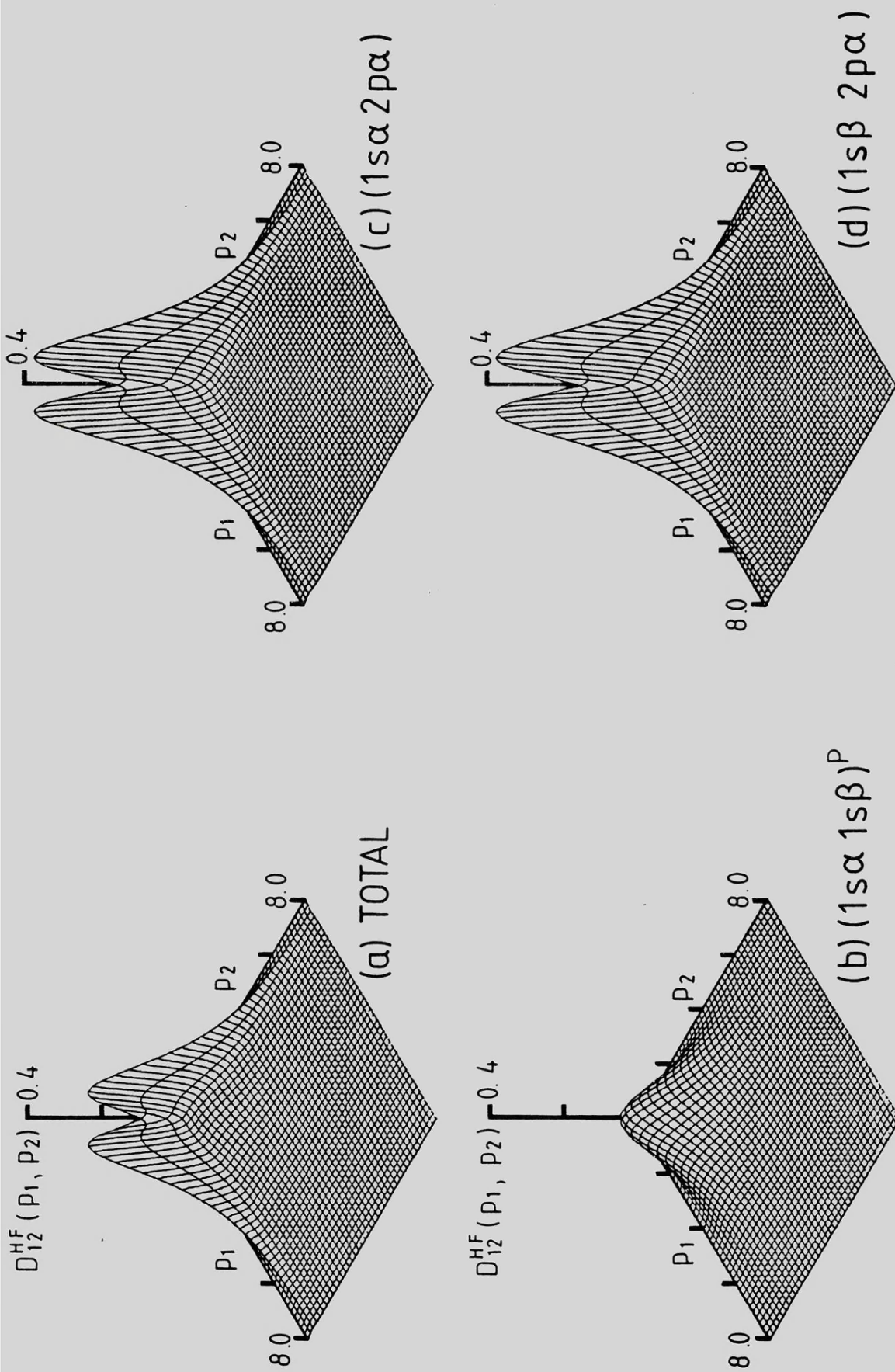
Figure (III.1.8)

An alternative view of the $D_{12}^{HF}(p_1,p_2)$ surfaces presented in Figure (III.1.7).

Figure (III.1.9)

(see over)

<u>Figure (III.1.9)</u>

The two-particle radial shifts $\Delta D_{12}(p_1, p_2)$ for the 'total' atom and the various electron pairs in the 2^2S state of Li.

(a) TOTAL

(b) $(1s\alpha\,1s\beta)^S$

(c) $(1s\alpha\,2s\alpha)$

(d) $(1s\beta\,2s\alpha)$

$\Delta D_{12}(P_1, P_2)$

0.006

-0.012

P_1

P_2

8.0
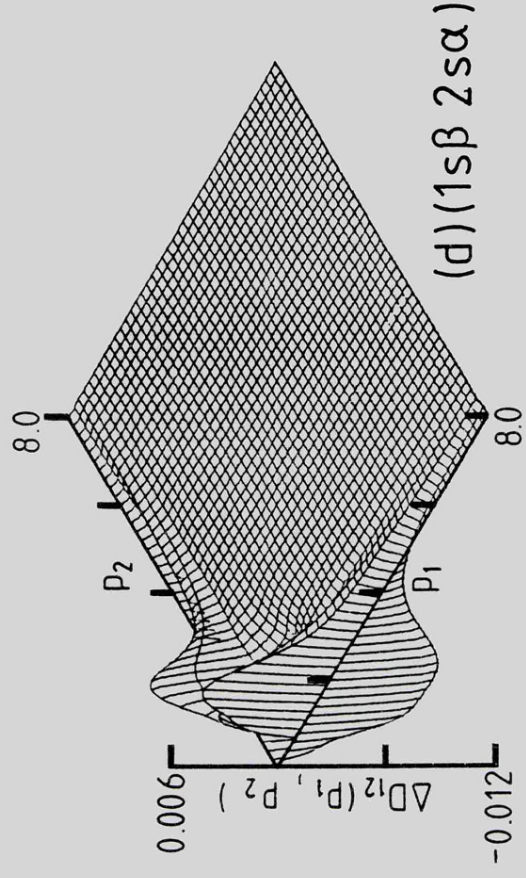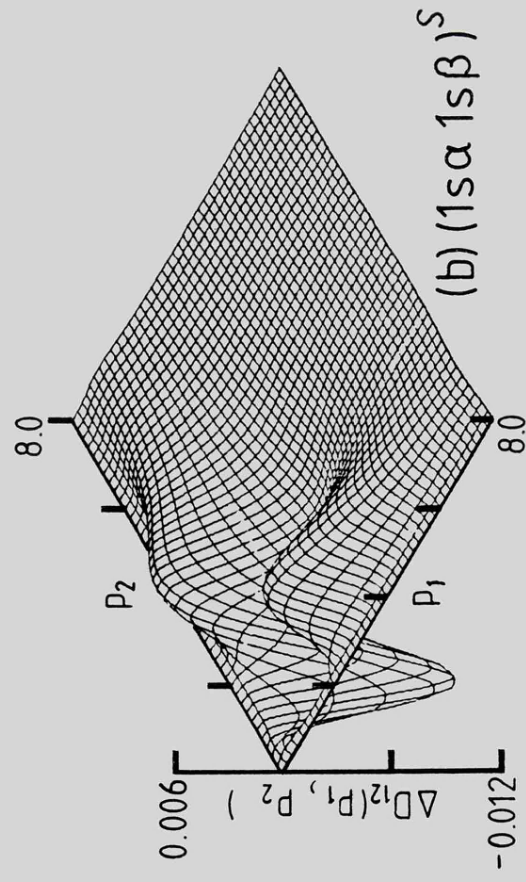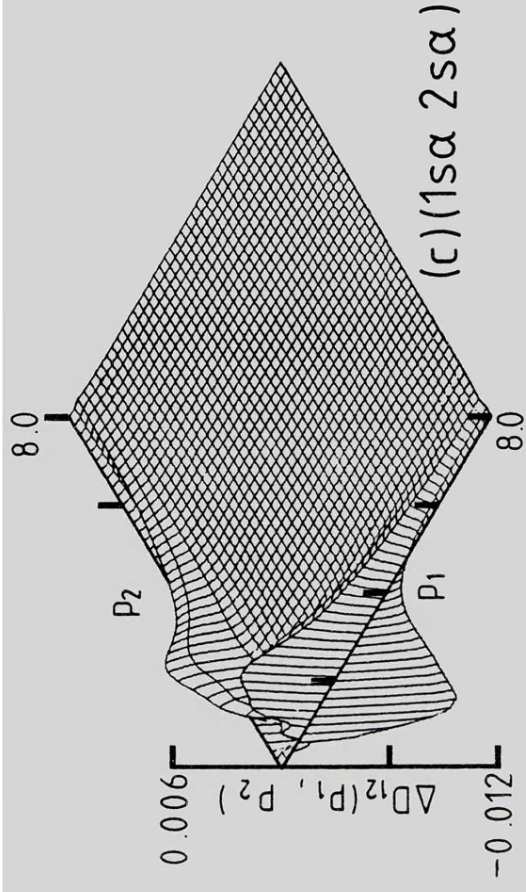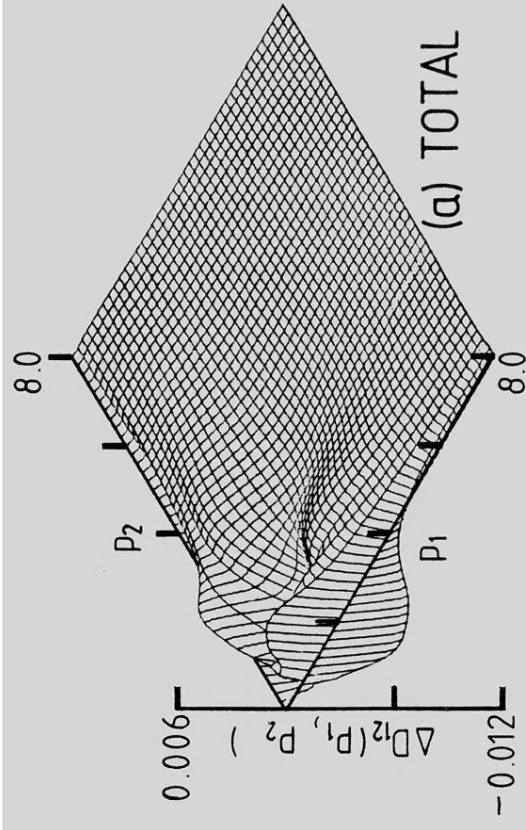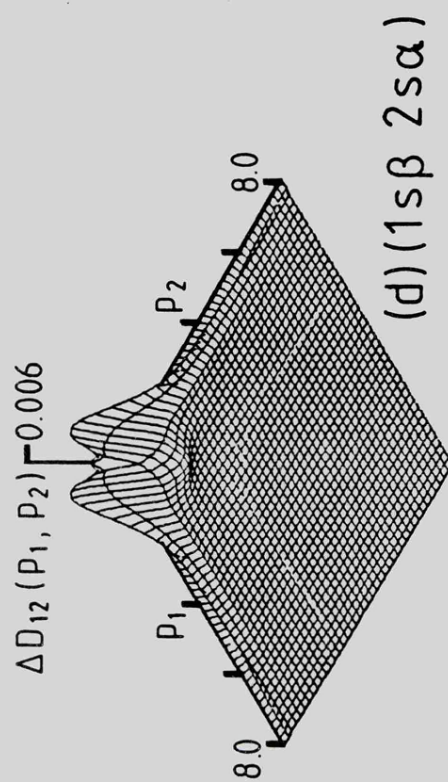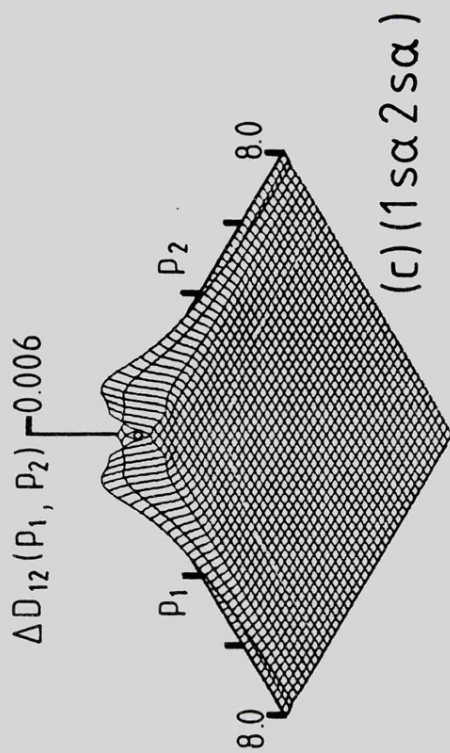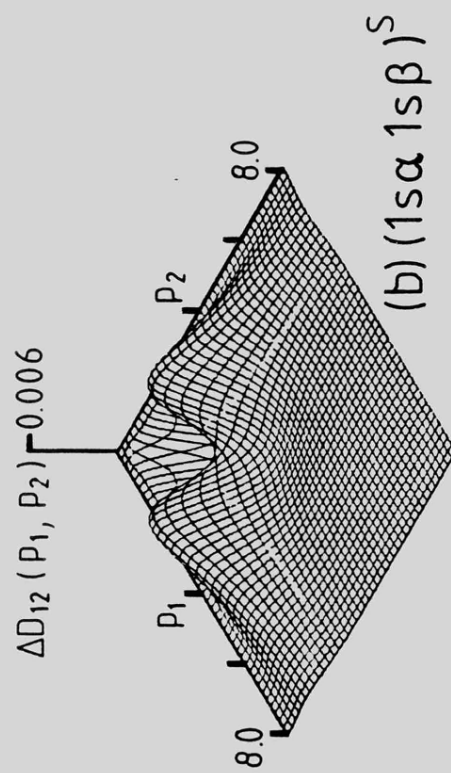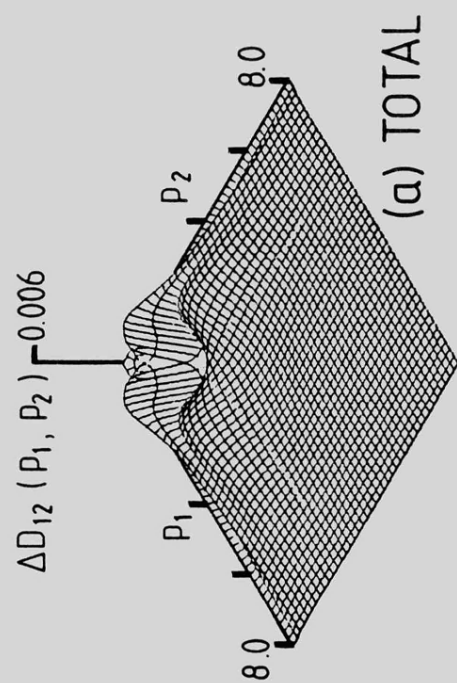
Figure (III.1.10)

An alternative view of the $\Delta D_{12}(P_1, P_2)$ surfaces presented in Figure (III.1.9).

<u>**Figure (III.1.11)**</u>

(see over)

$\Delta D_{12}(P_1, P_2)$ 0.006

(c) $(1s\alpha \ 2p\alpha)$

$\Delta D_{12}(P_1, P_2)$ 0.006

(d) $(1s\beta \ 2p\alpha)$

$\Delta D_{12}(P_1, P_2)$ 0.006

(a) TOTAL

$\Delta D_{12}(P_1, P_2)$ 0.006

(b) $(1s\alpha \ 1s\beta)^P$
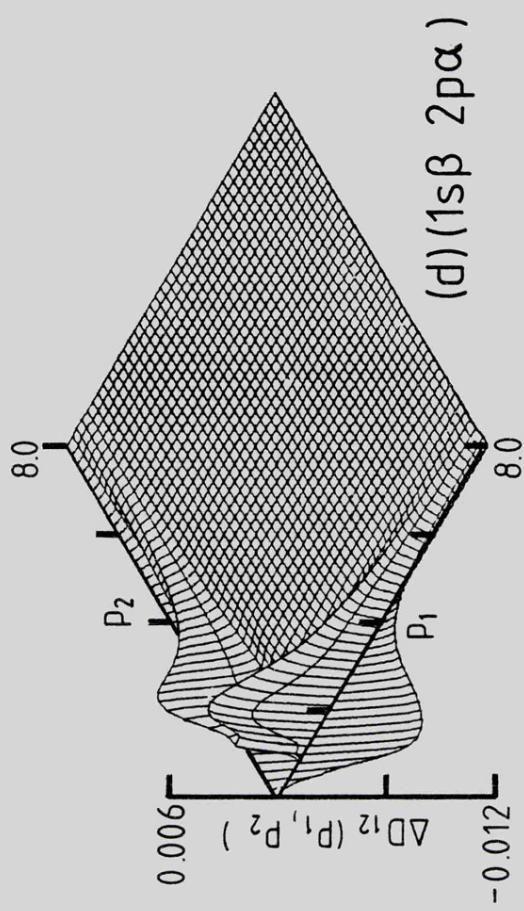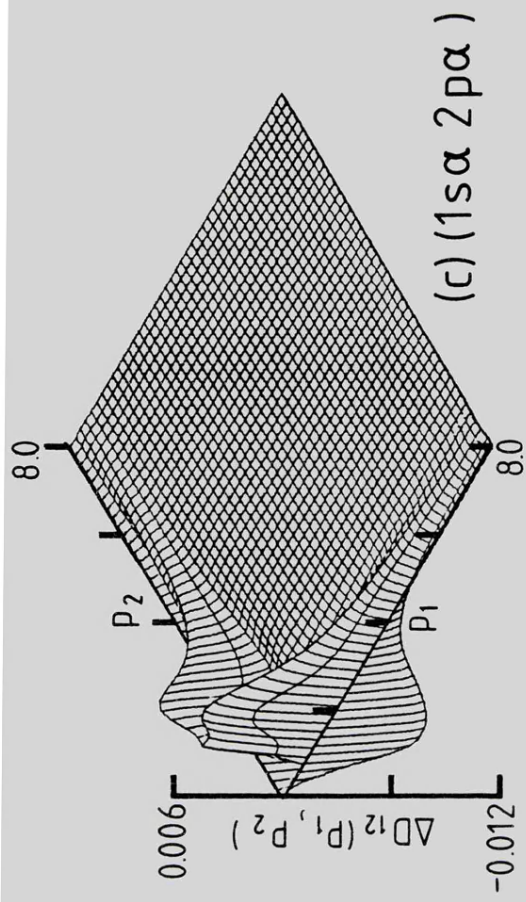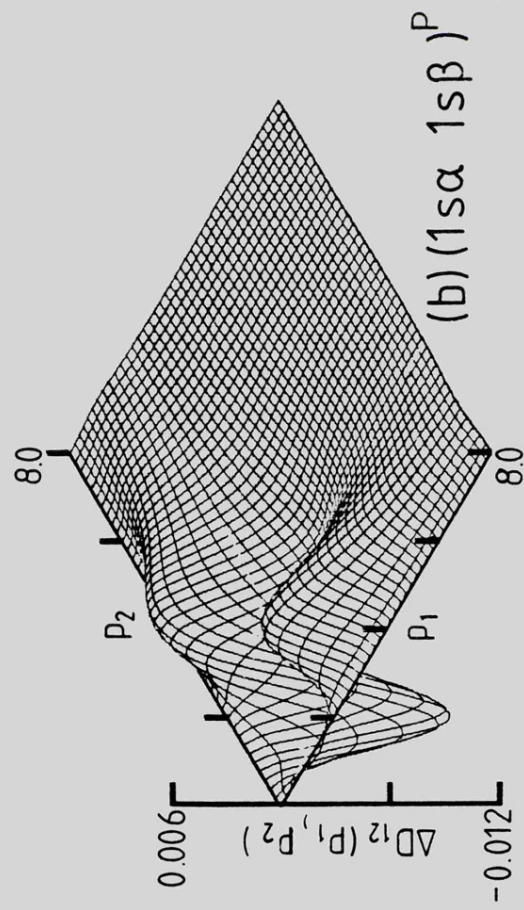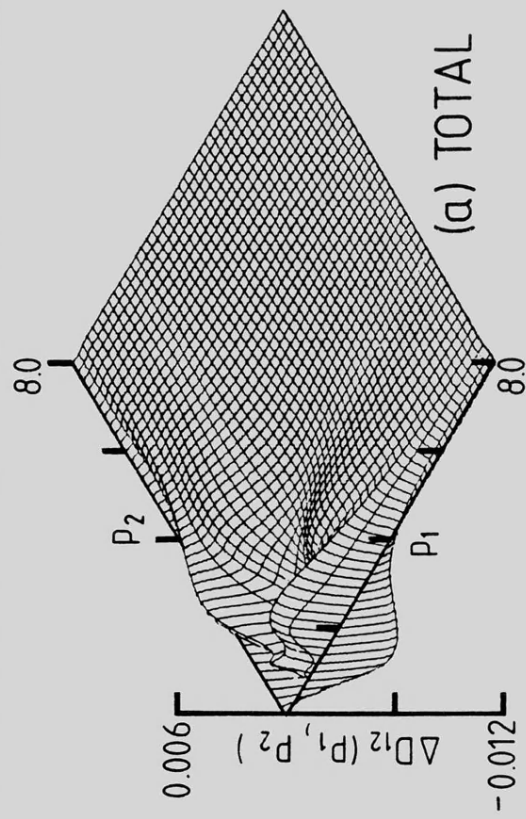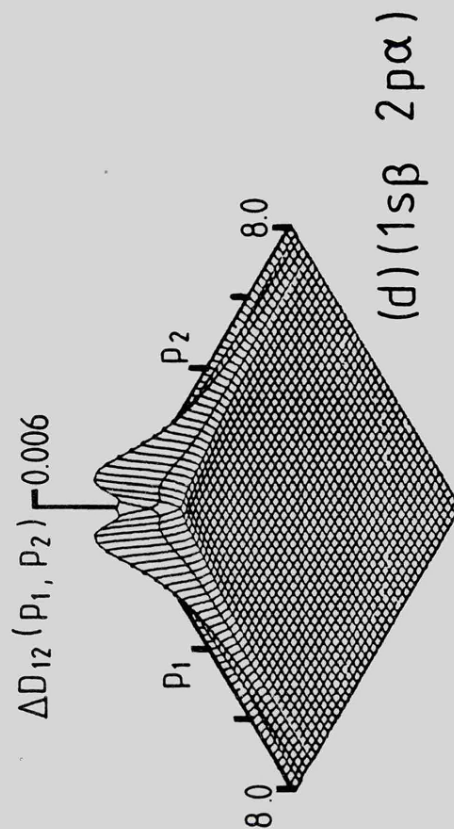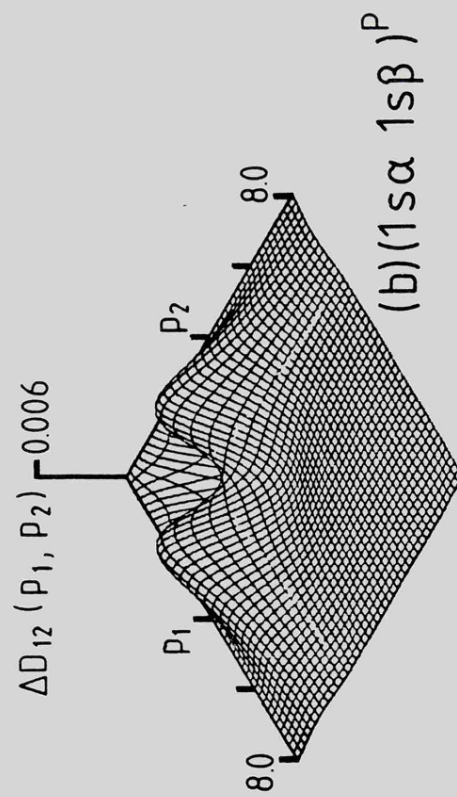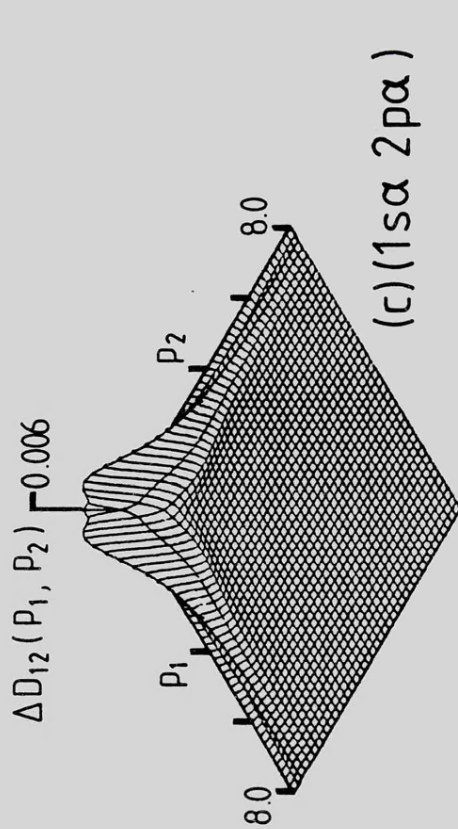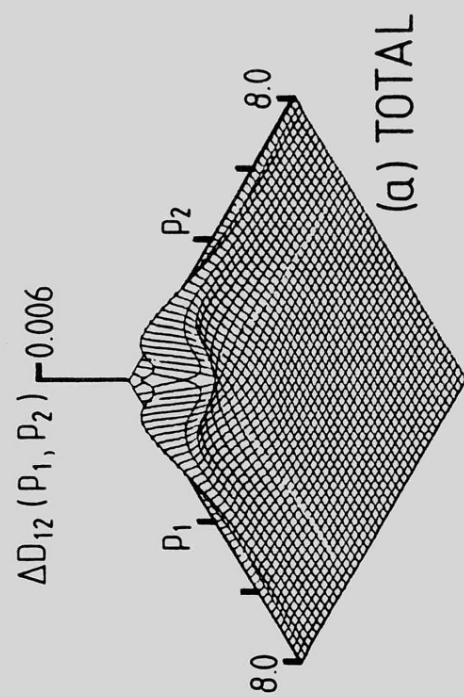
Figure (III.1.12)

An alternative view of the $\Delta D_{12}(P_1, P_2)$ surfaces presented in Figure (III.1.11).
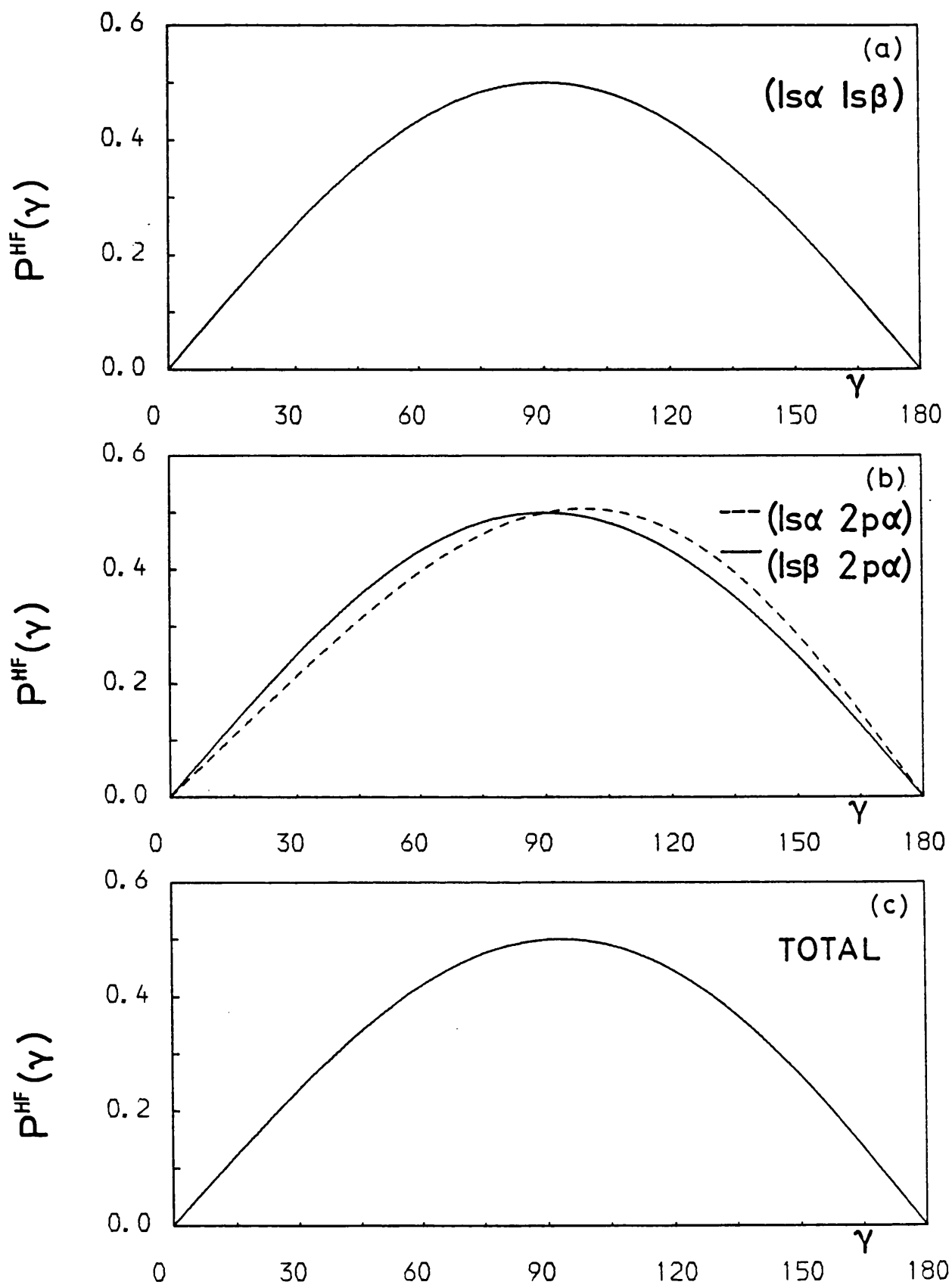
Figure (III.1.13)

The $P^{HF}(\gamma)$ distributions for the various electron pairs and the 'total' atom in the 2^2P state of Li.
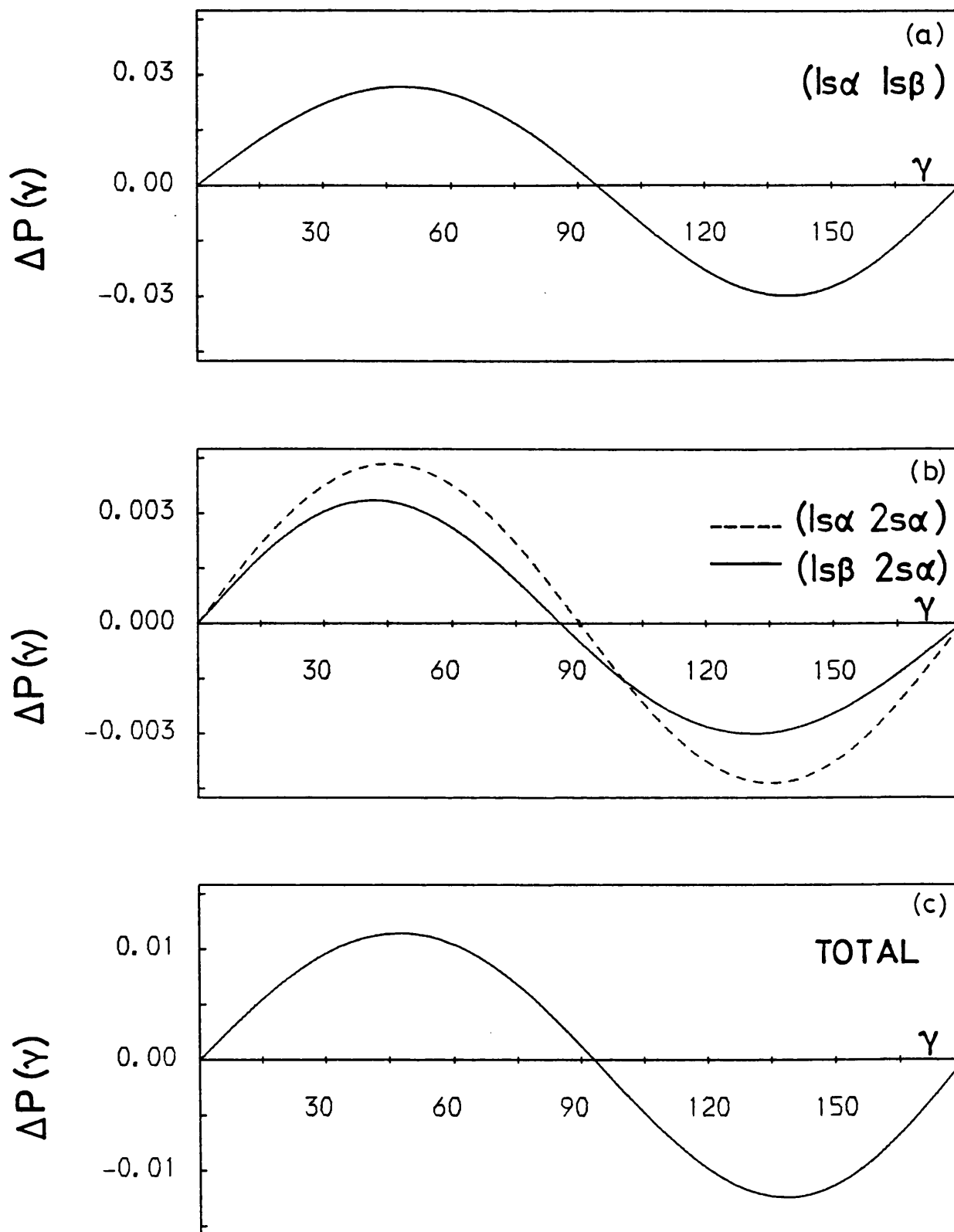
Figure (III.1.14)

The angular shift $\Delta P(\gamma)$ for the various electron pairs and the 'total' atom in the 2^2S state of Li.
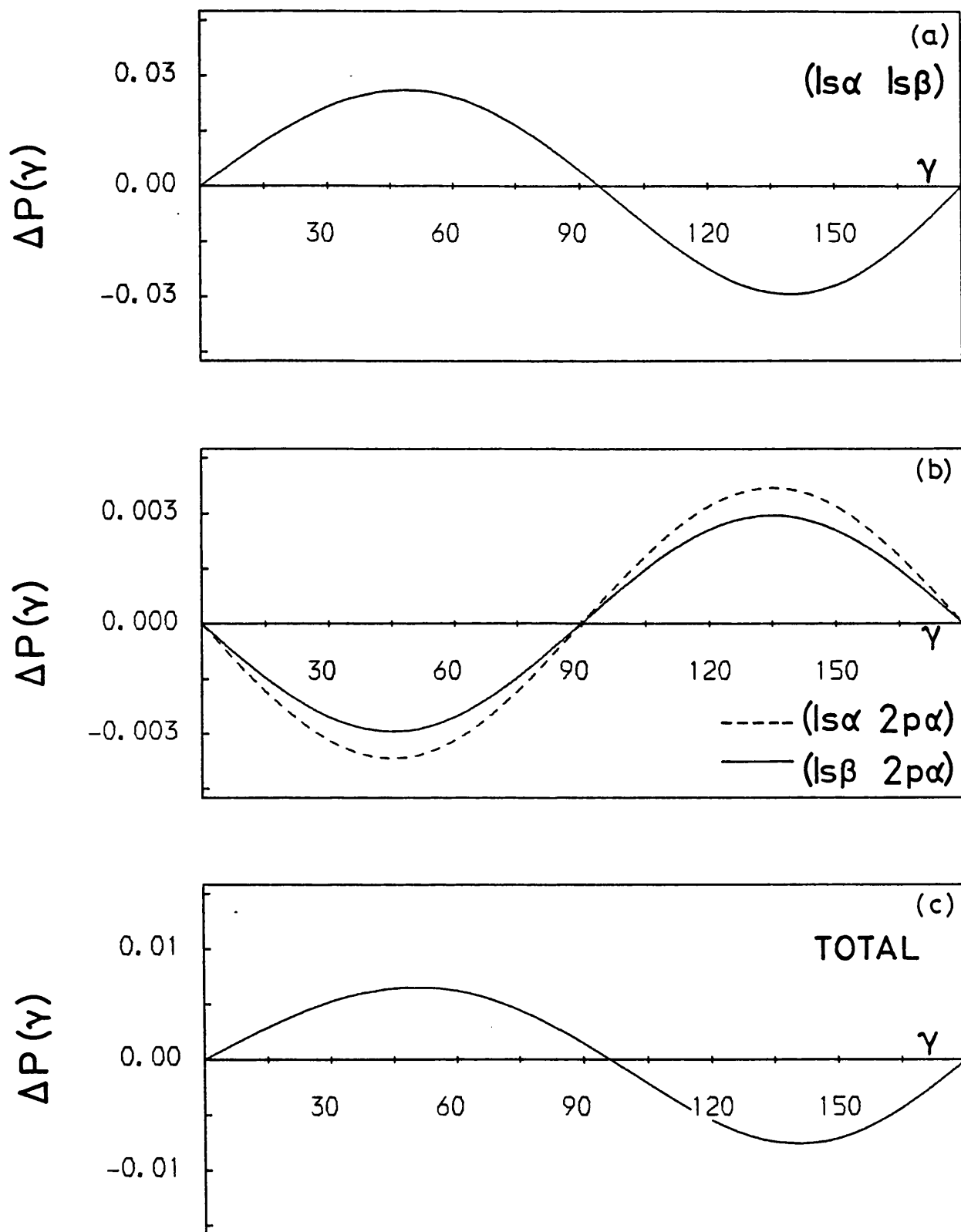
Figure (III.1.15)

The angular shift $\Delta P(\gamma)$ for the various electron
pairs and the 'total' atom in the 2^2P state of Li.

261
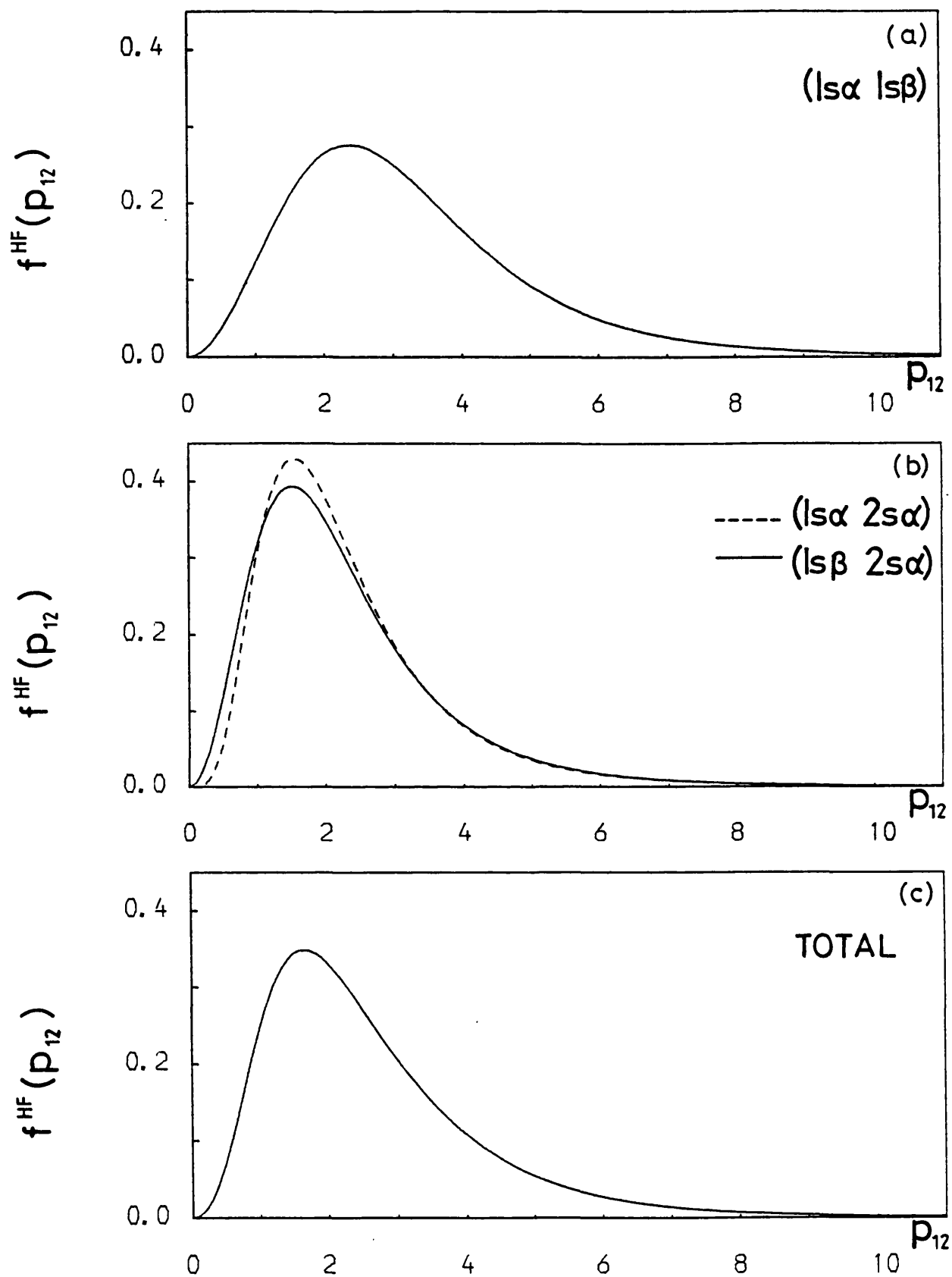
Figure (III.1.16)

The $f^{HF}(p_{12})$ distributions for the various electron pairs and the 'total' atom in the 2^2S state of Li.
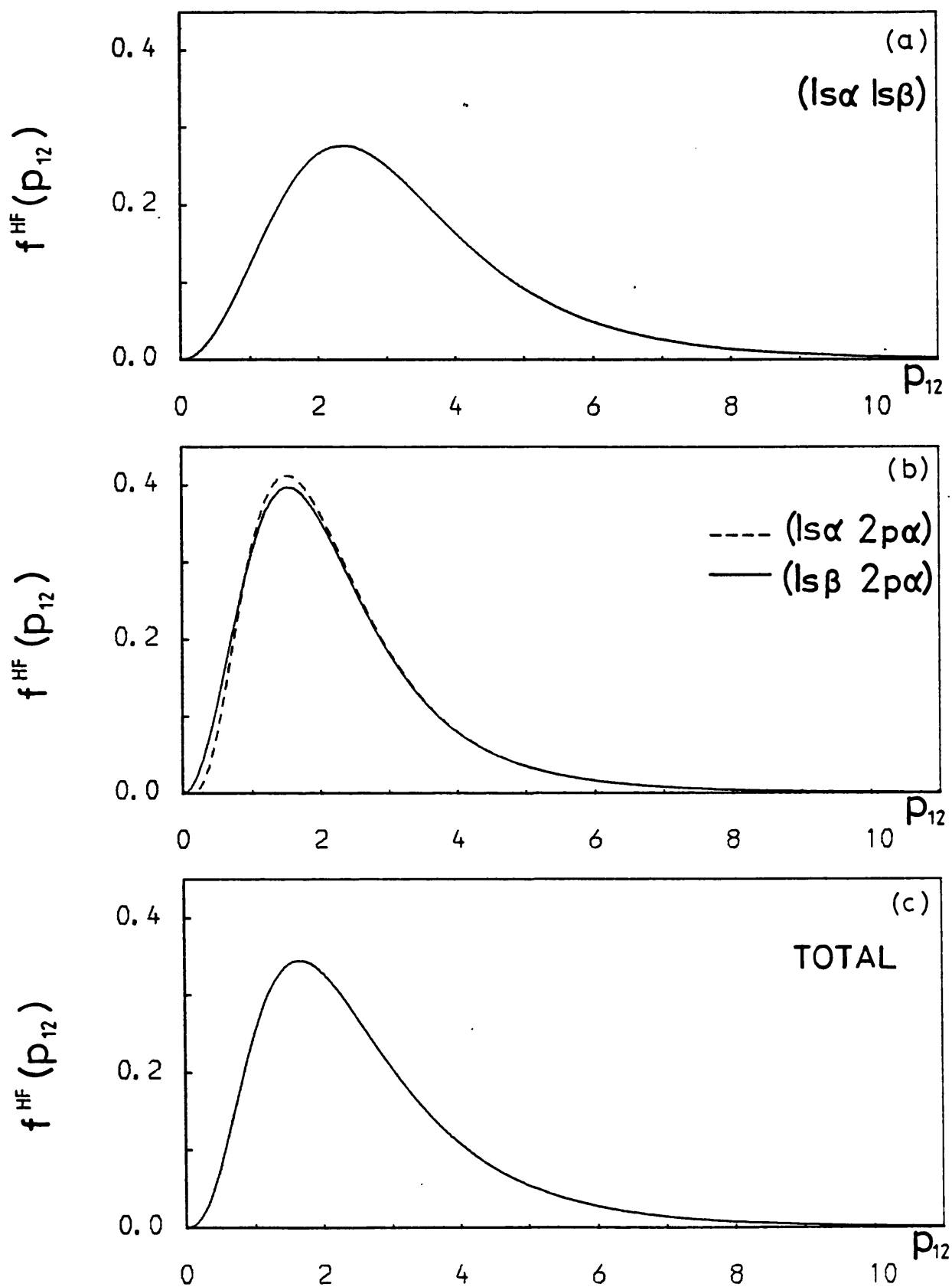
Figure (III.1.17)

The $f^{HF}(p_{12})$ distributions for the various electron pairs and the 'total' atom in the $2\,^2P$ state of Li.

263
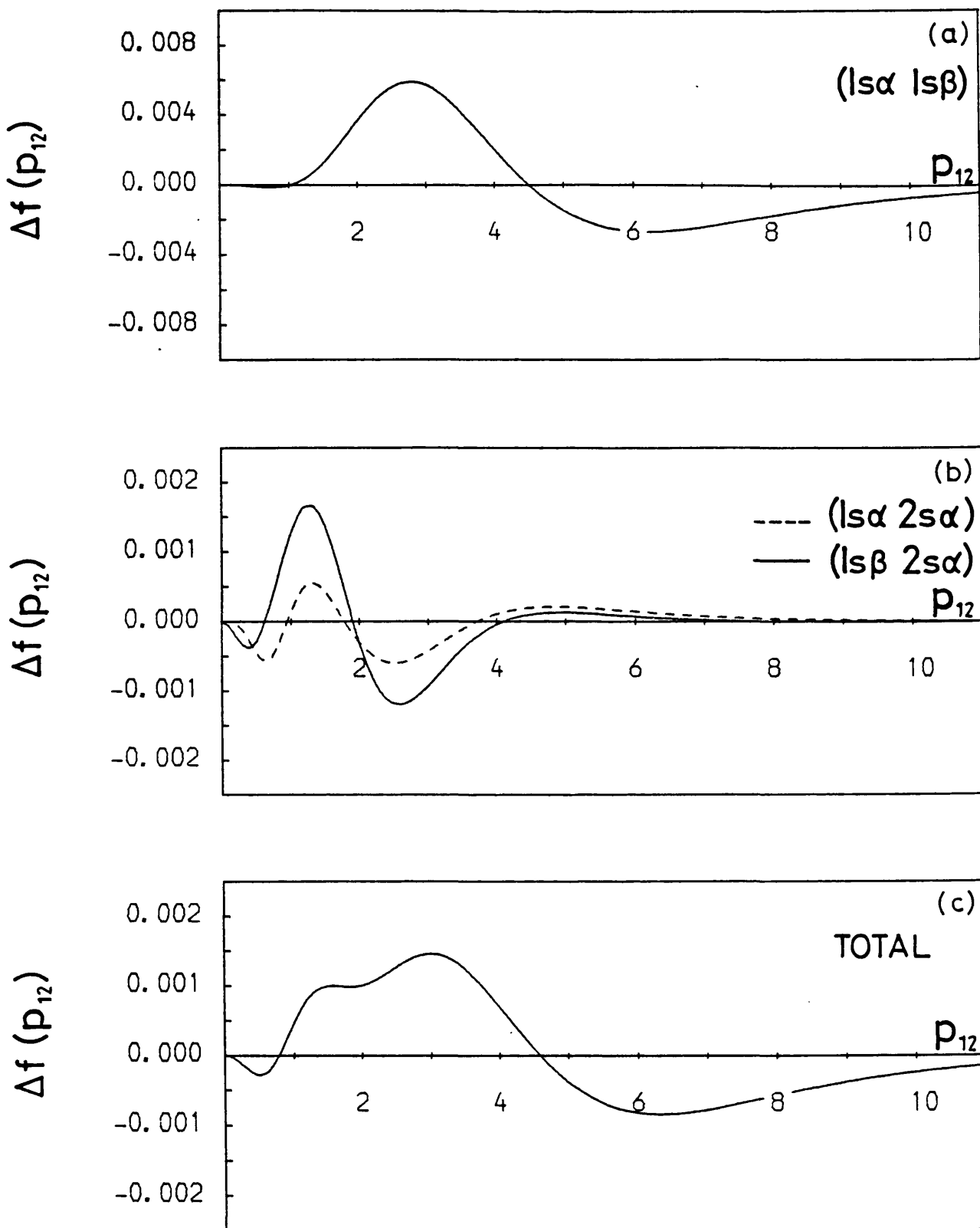
<u>Figure (III.1.18)</u>

The Coulomb shifts $\Delta f(p_{12})$ for the various electron pairs and the 'total' atom in the $2\,^2S$ state of Li.
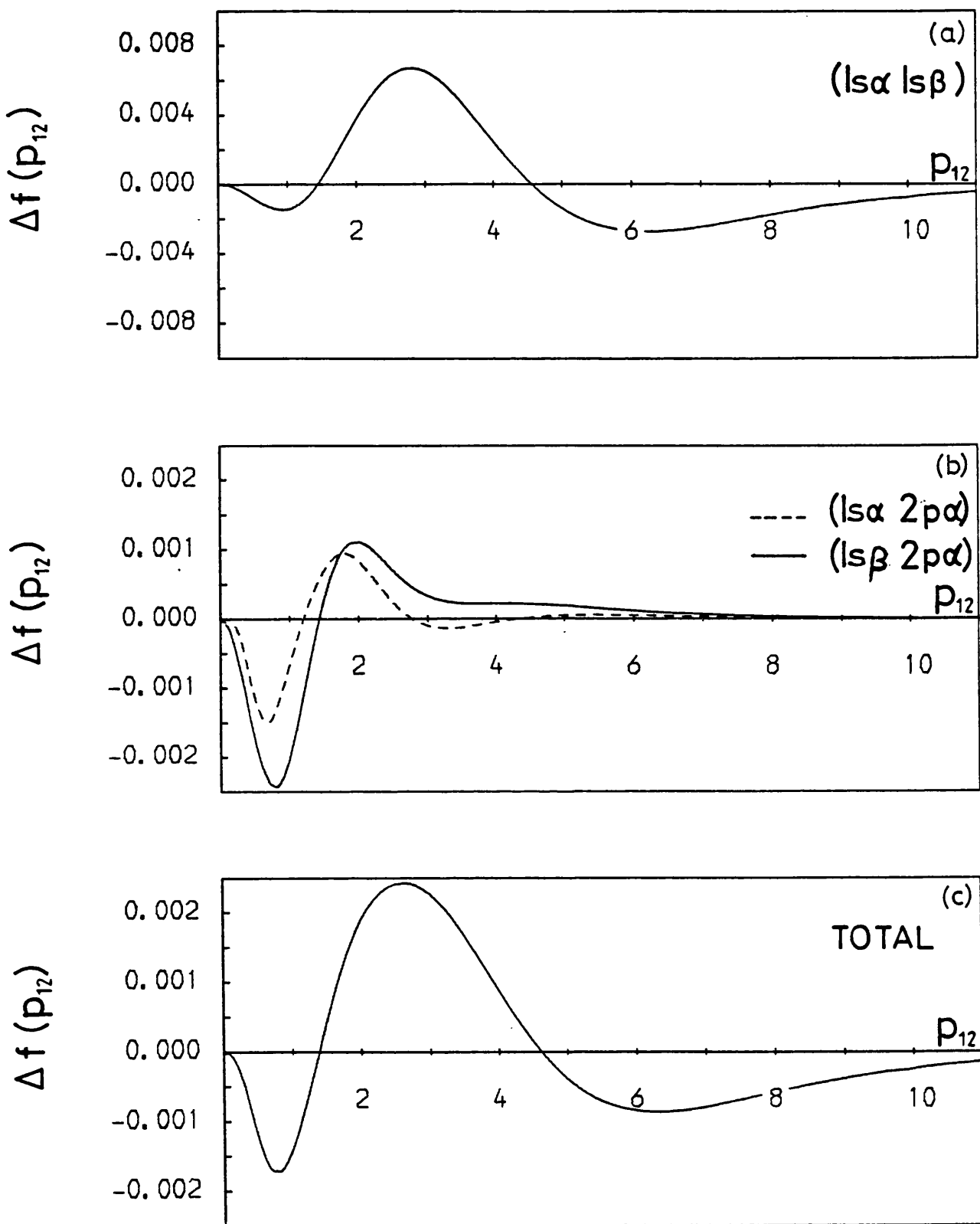
Figure (III.1.19)

The Coulomb shifts $\Delta f(p_{12})$ for the various electron pairs and the 'total' atom in the $2\,{}^2P$ state of Li.

<u>Figure (III.1.20)</u>

(see over)

Figure (III.1.20)

The $g^{HF}(p_{12}, p_1)$ distributions for the 'total' atom and the various electron pairs in the 2^2S state of Li.

(c) $(1s\alpha\ 2s\alpha)$

(d) $(1s\beta\ 2s\alpha)$

(a) TOTAL

(b) $(1s\alpha\ 1s\beta)^S$

$g^{HF}(p_{12}, p_1)$

P_1

P_{12}

8.0

0.6

0.0

$g^{HF}(p_{12}, p_1)$ 0.4

p_1

8.0

p_{12}

8.0

(a) TOTAL

$g^{HF}(p_{12}, p_1)$ 0.4

p_1

8.0

p_{12}

8.0

(b)$(1s\alpha\ 1s\beta)^S$

0.4

p_1

8.0

p_{12}

8.0

(c)$(1s\alpha\ 2s\alpha)$

0.4

p_1

8.0

p_{12}

8.0
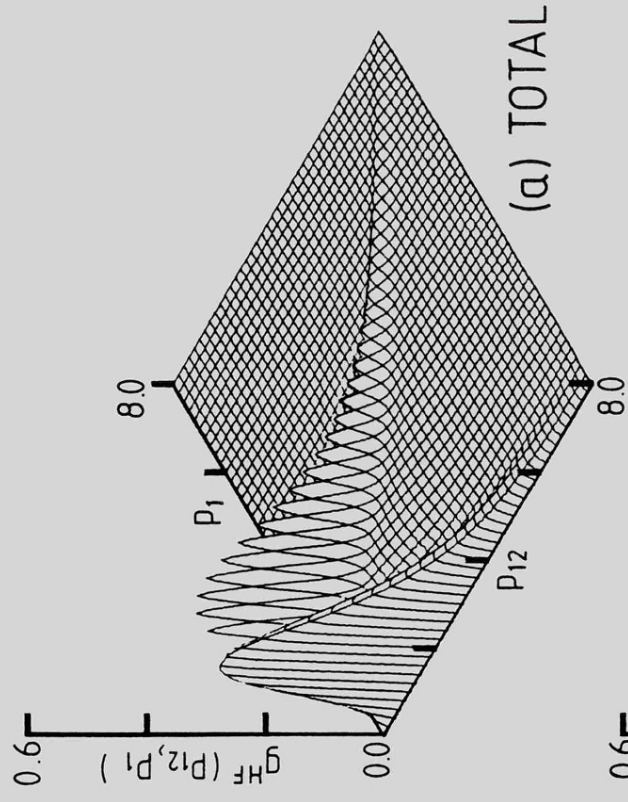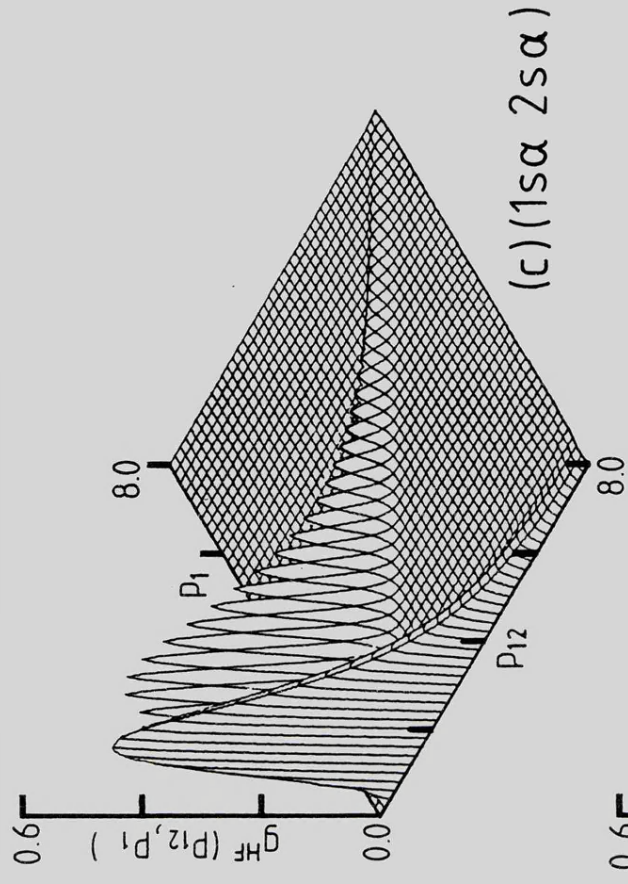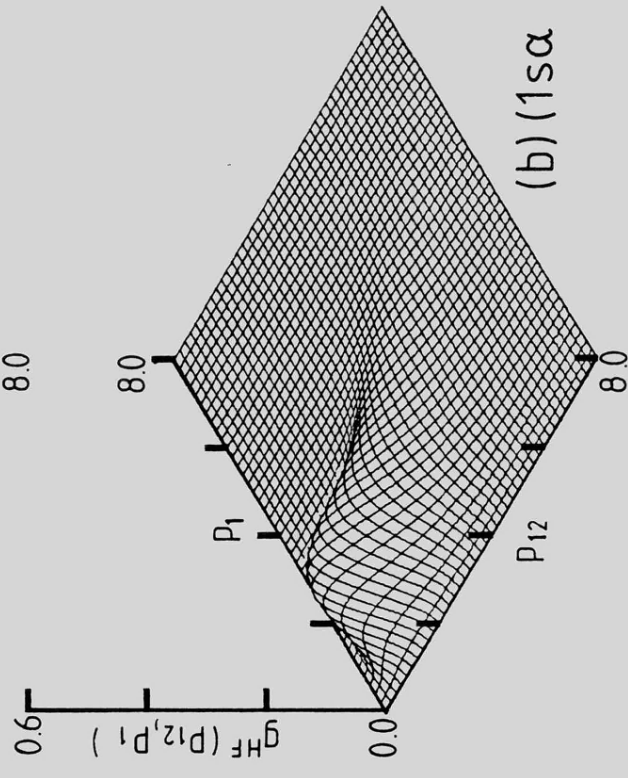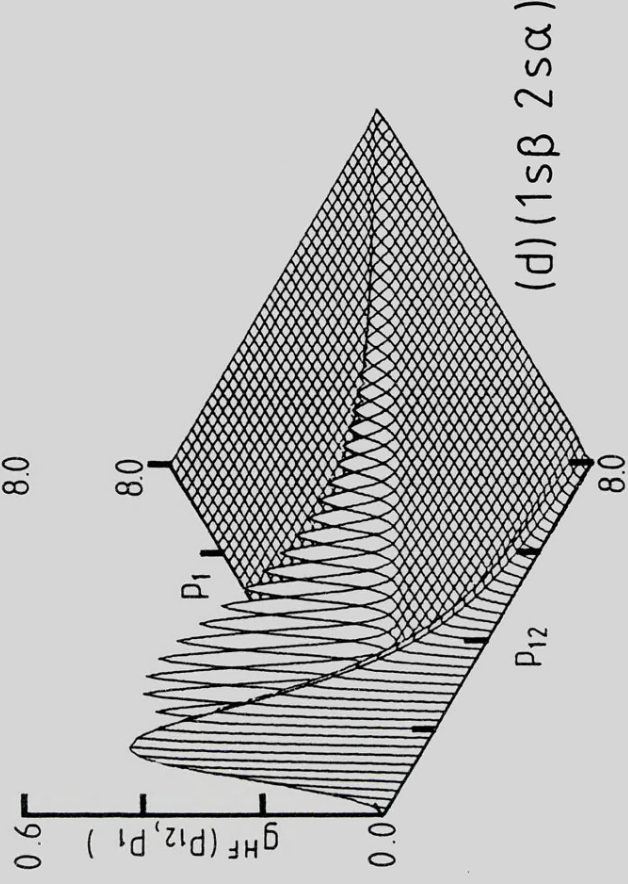
(d)$(1s\beta\ 2s\alpha)$
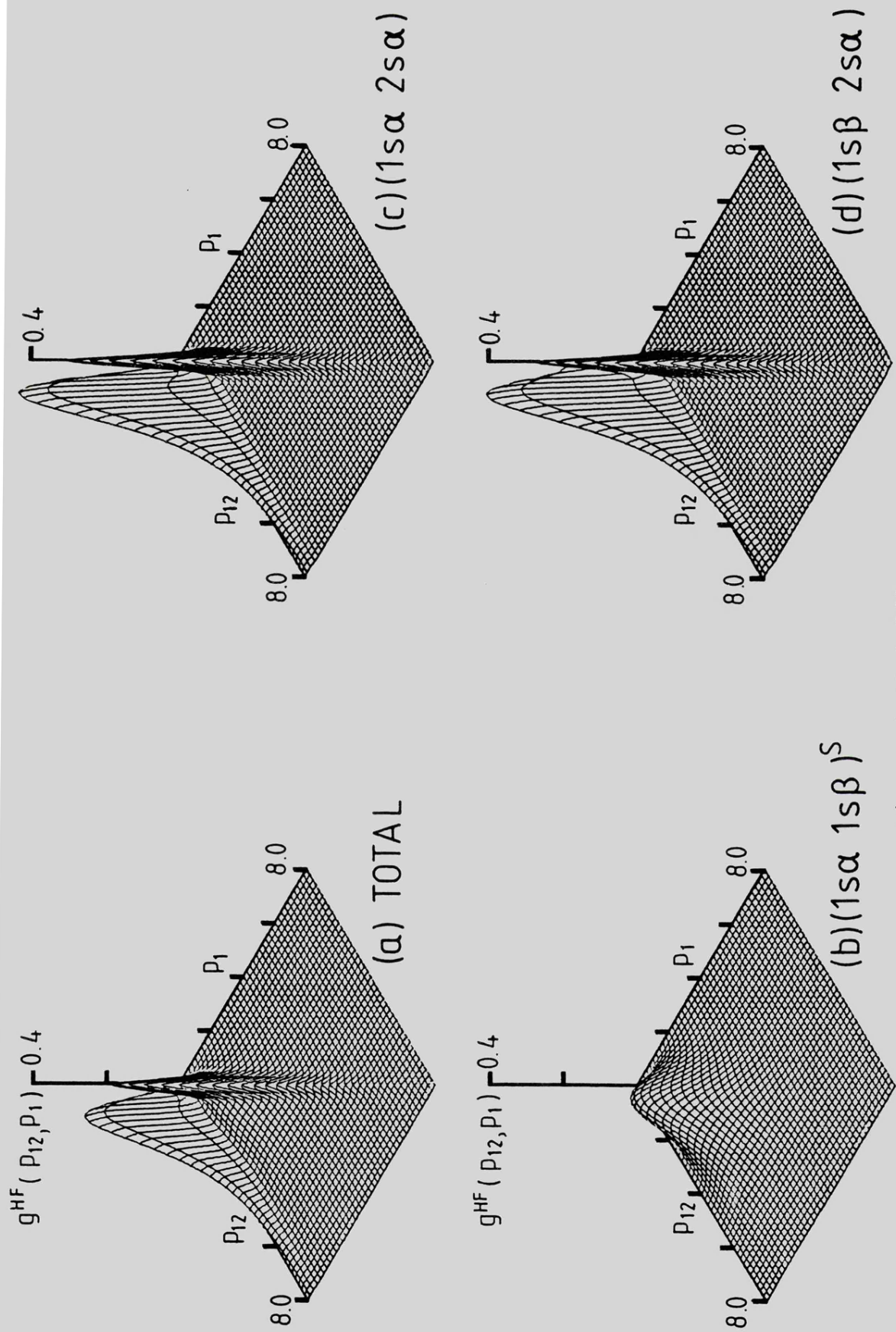
Figure (III.1.21)

An alternative view of the $g^{HF}(p_{12}, p_1)$ surfaces presented in Figure (III.1.20).

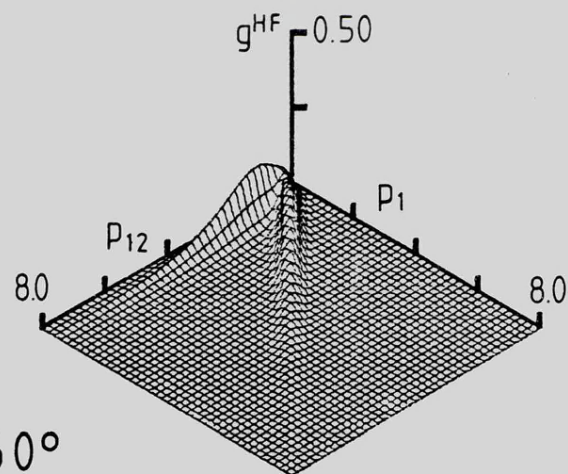Figure (III.1.22)

(see over)

(a) TOTAL

(b) $(1s\alpha \ 1s\beta)^P$

(c) $(1s\alpha \ 2p\alpha)$

(d) $(1s\beta \ 2p\alpha)$

(a) TOTAL

(b) (1sα 1sβ)^P

(c) (1sα 2pα)

(d) (1sβ 2pα)
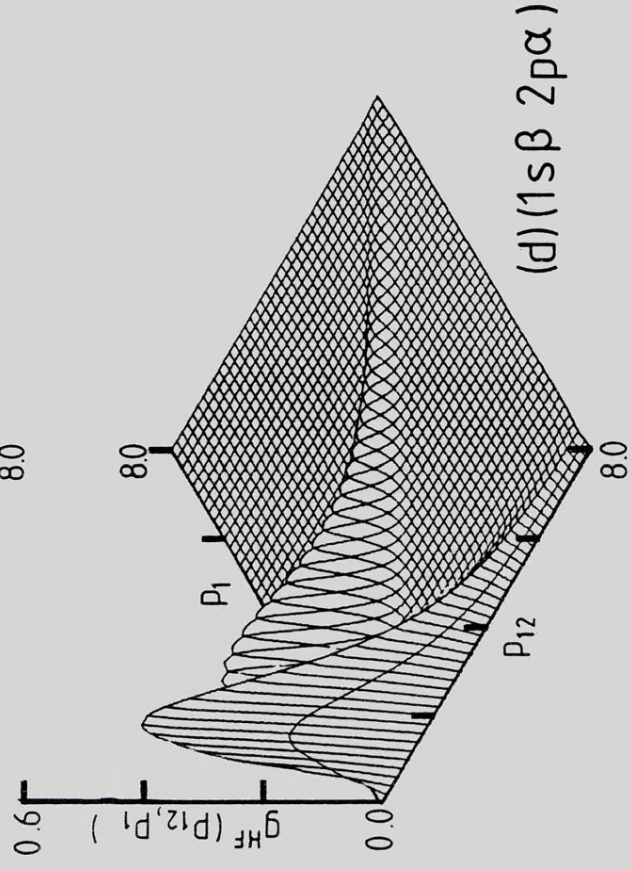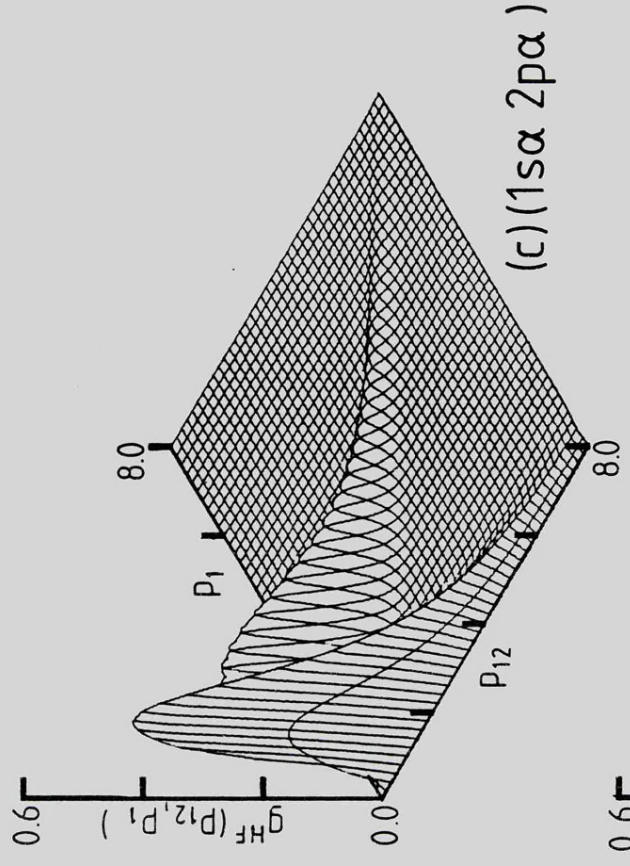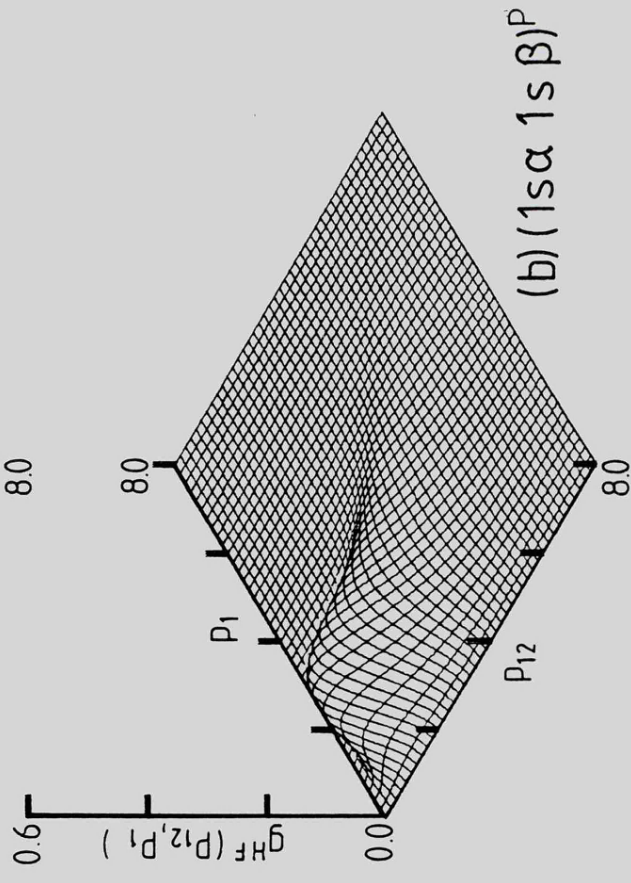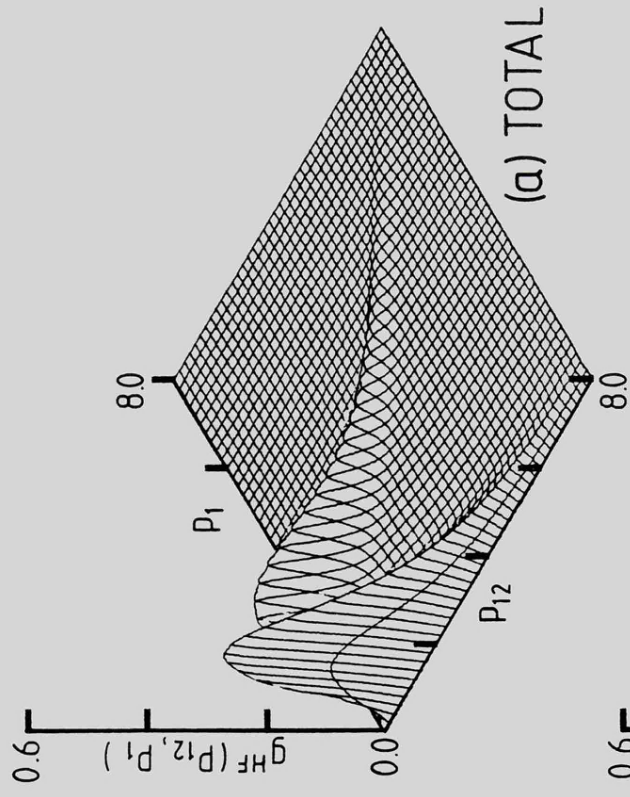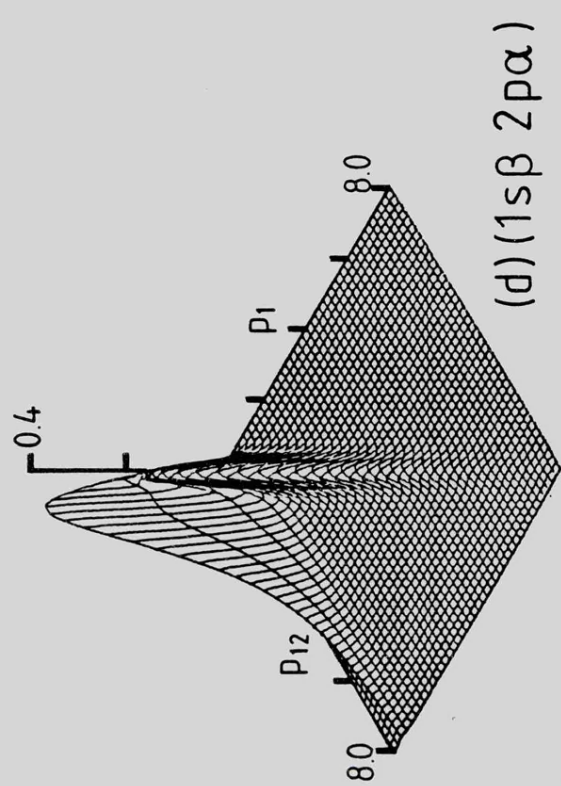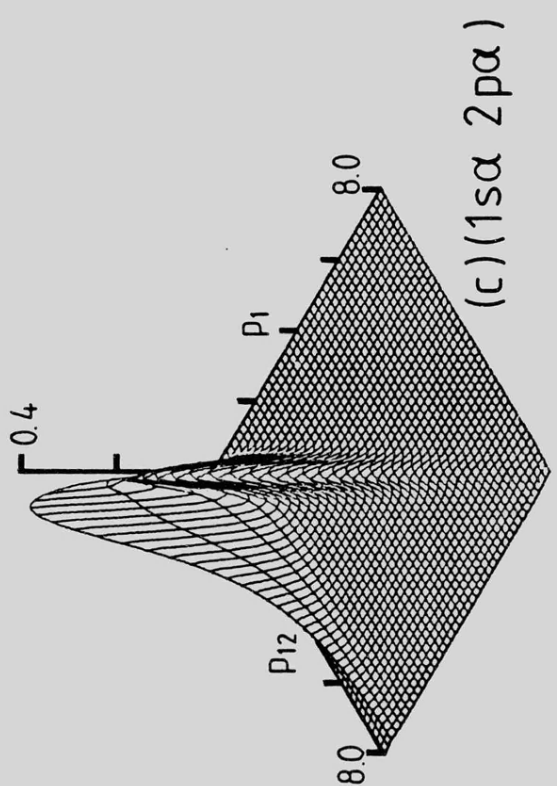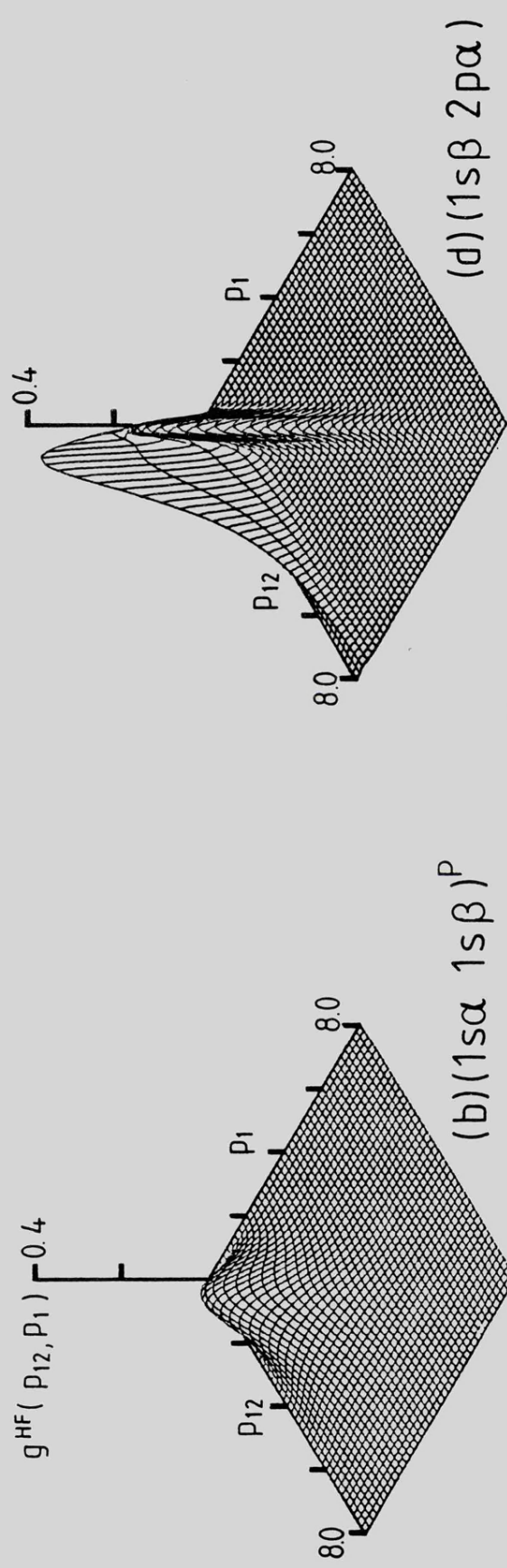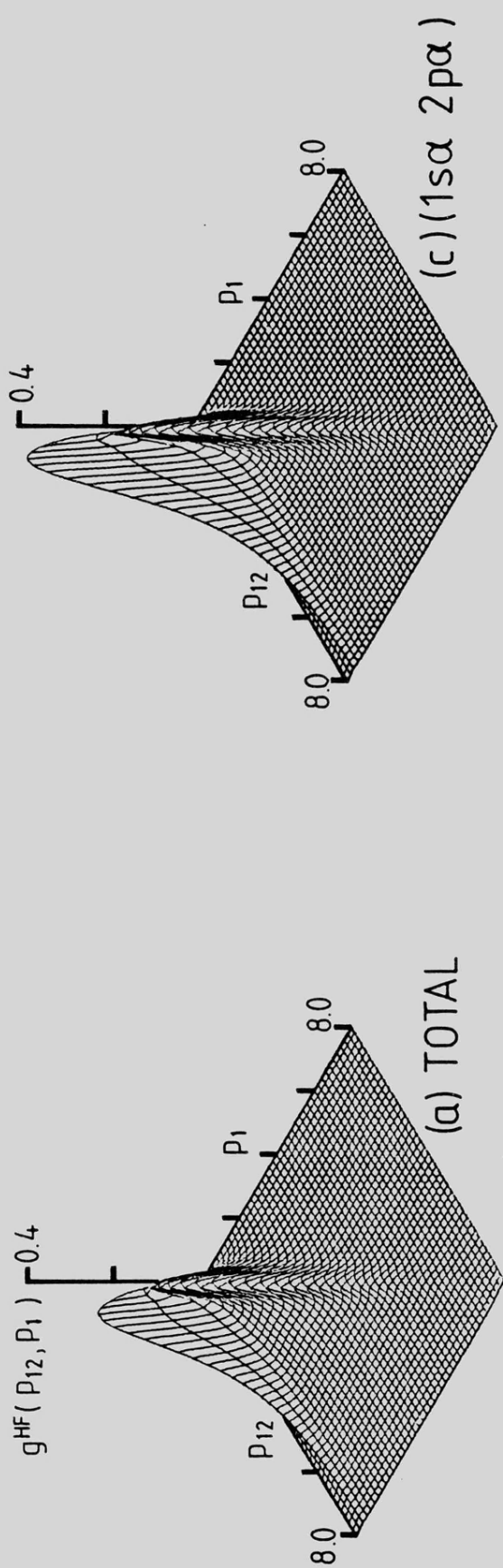
Figure (III.1.23)

An alternative view of the $g^{HF}(p_{12}, p_1)$ surfaces presented in Figure (III.1.22).

269

<u>Figure (III.1.24)</u>

(see over)

The partial Coulomb shifts $\Delta g(p_{12}, p_1)$ for the 'total' atom and the various electron pairs in the 2^2S state of Li.

(c) $(1s\alpha \ 2s\alpha)$

(d) $(1s\beta \ 2s\alpha)$

(a) TOTAL

(b) $(1s\alpha \ 1s\beta)^S$

$\Delta g(p_{12}, p_1)$ — 0.006

(c) $(1s\alpha\ 2s\alpha)$

$\Delta g(p_{12}, p_1)$ — 0.006

(d) $(1s\beta\ 1s\alpha)$

$\Delta g(p_{12}, p_1)$ — 0.006

(a) TOTAL

$\Delta g(p_{12}, p_1)$ — 0.006
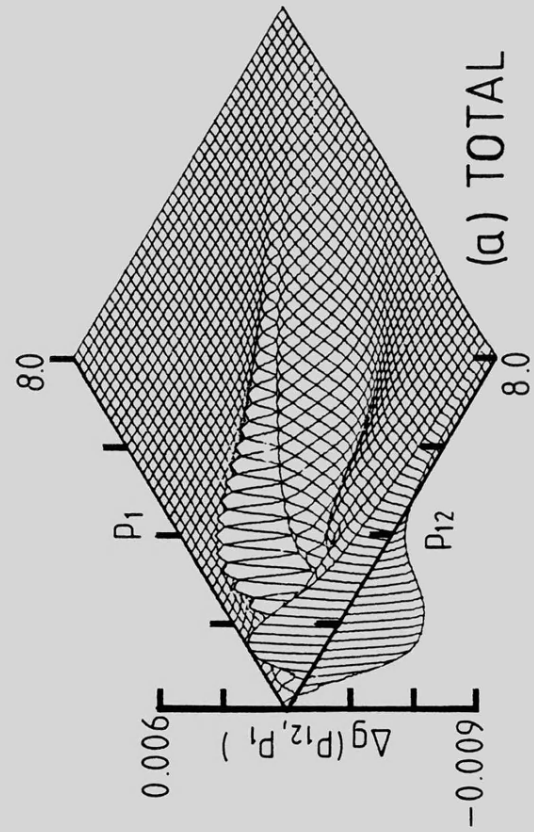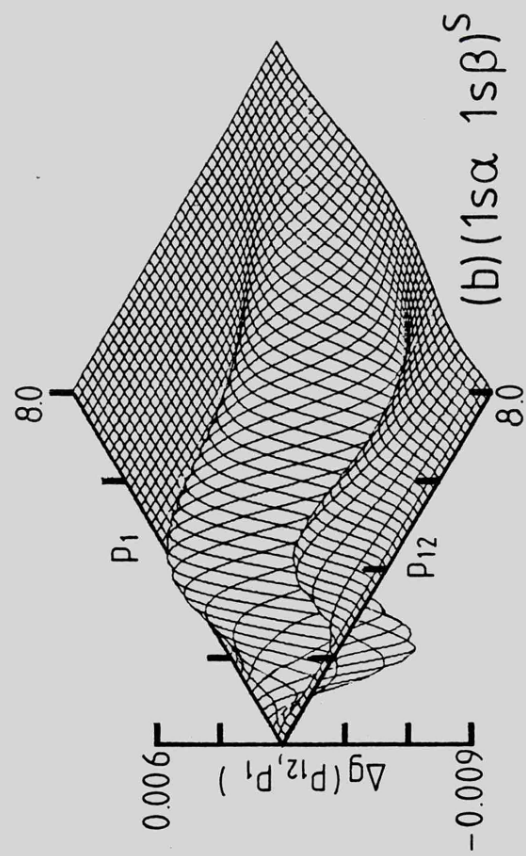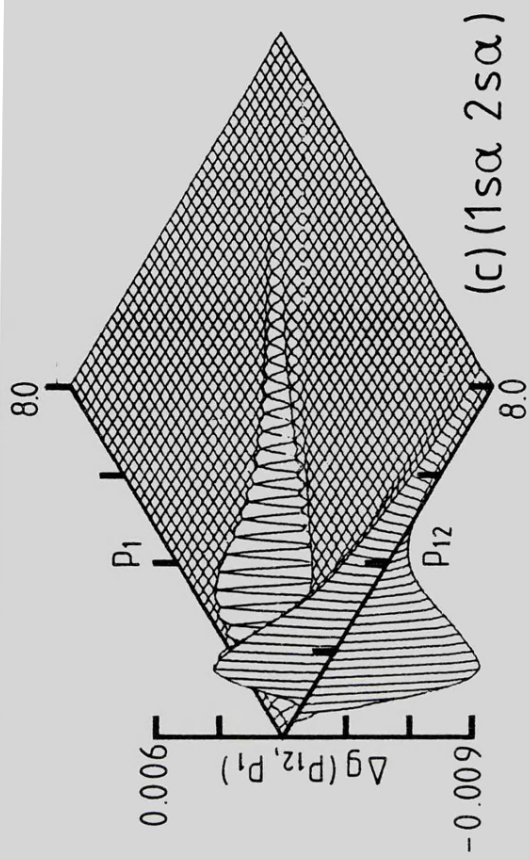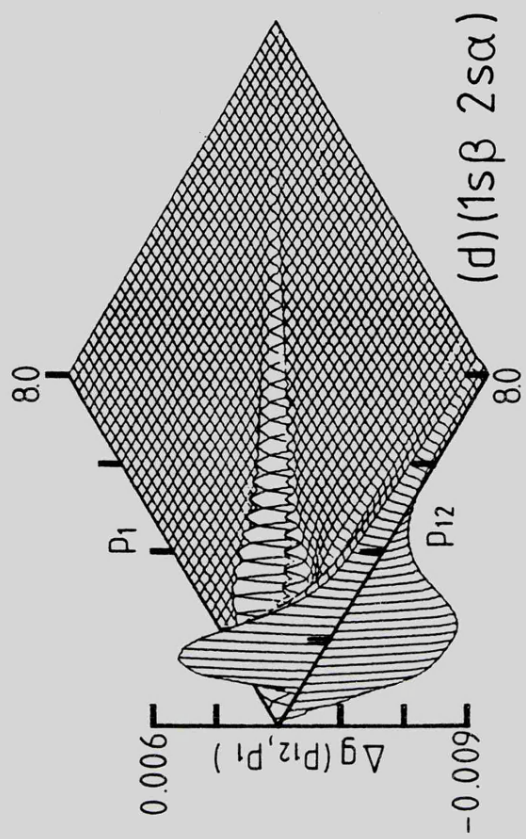
(b) $(1s\alpha\ 1s\beta)^S$
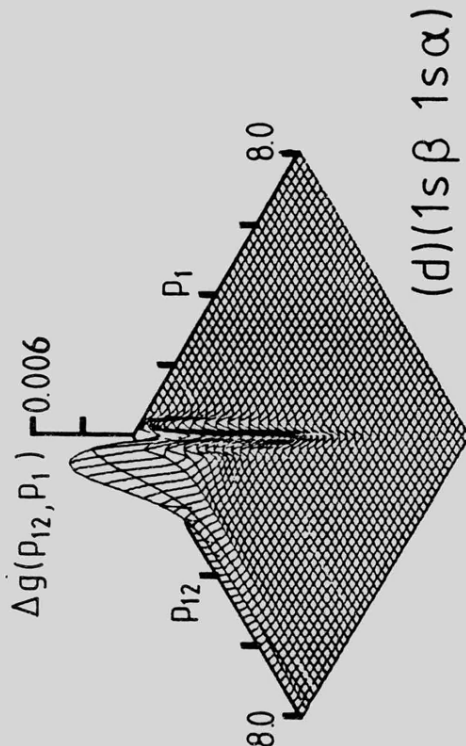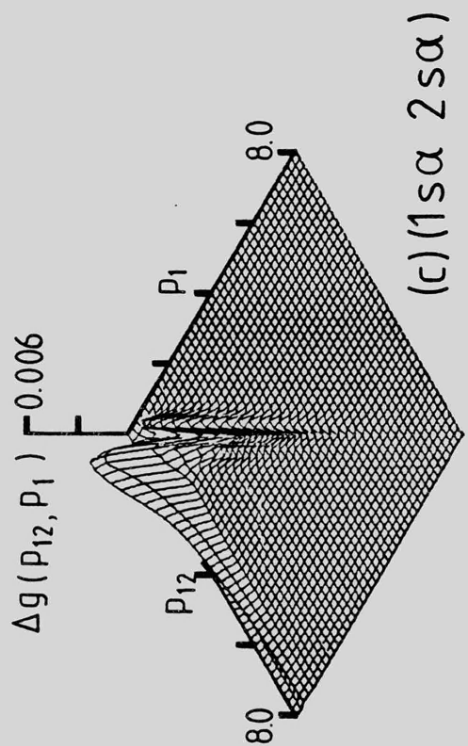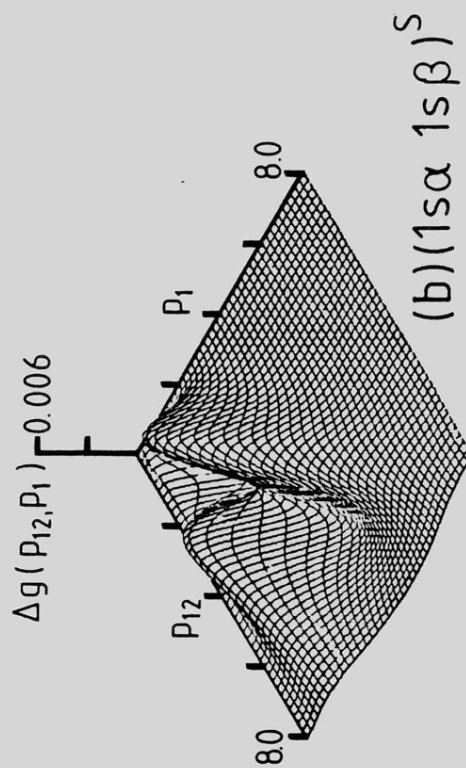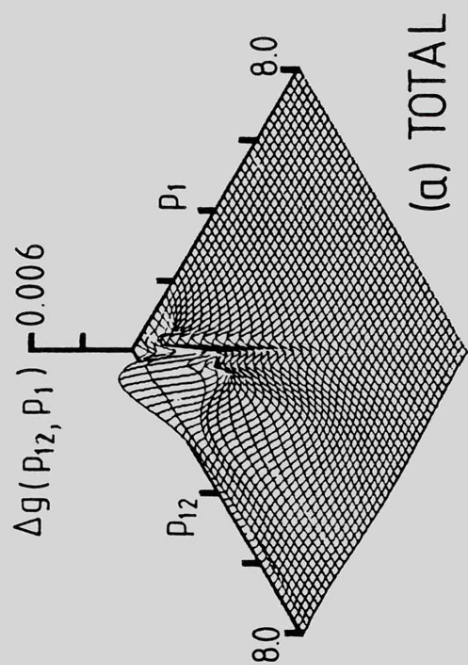
Figure (III.1.25)

An alternative view of the $\Delta g(p_{12}, p_1)$ surfaces presented in Figure (III.1.24).

Figure (III.1.26)

(see over)

(c)(1sα 2pα)

(d)(1sβ 2pα)
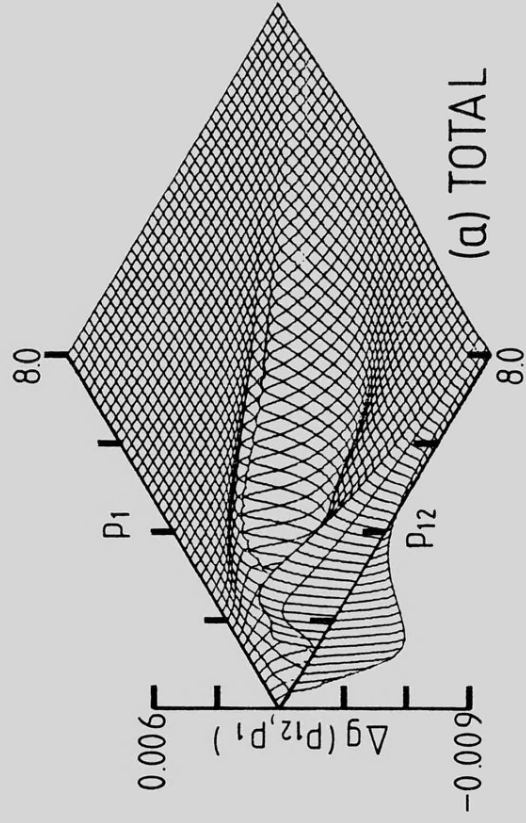
(a) TOTAL
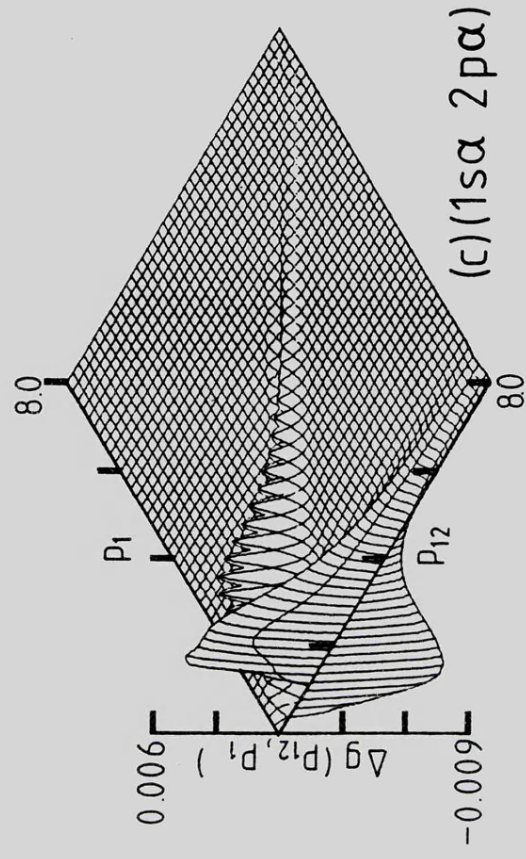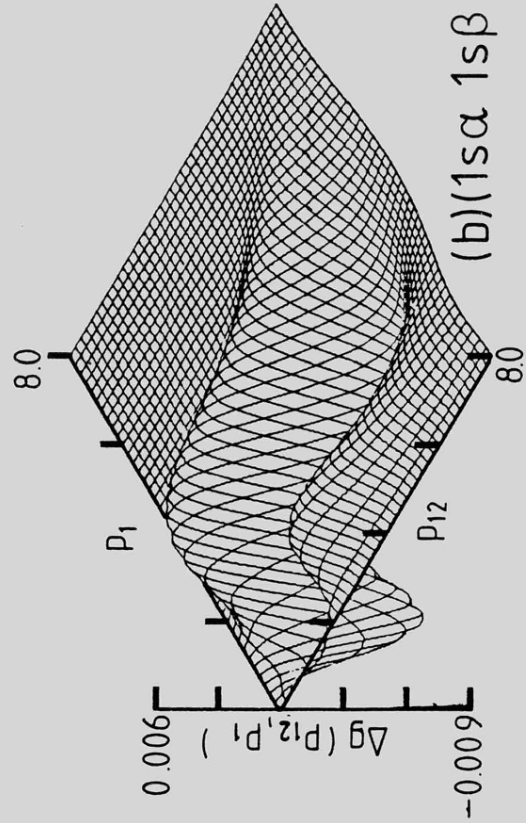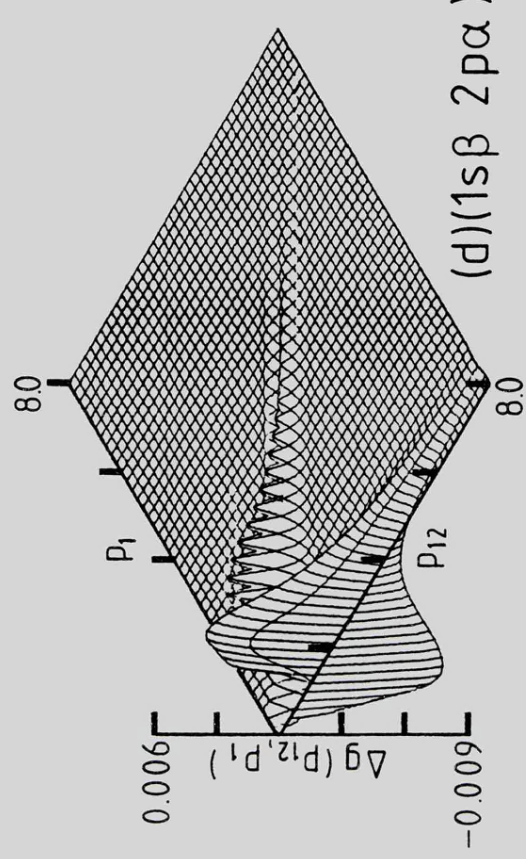
(b)(1sα 1sβ)^P
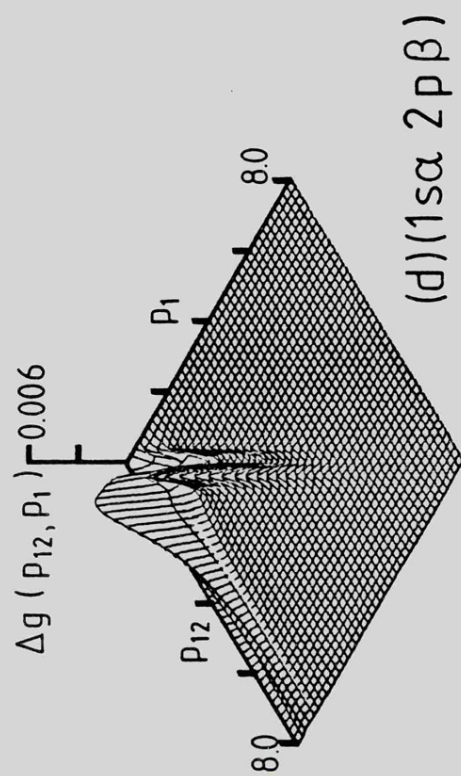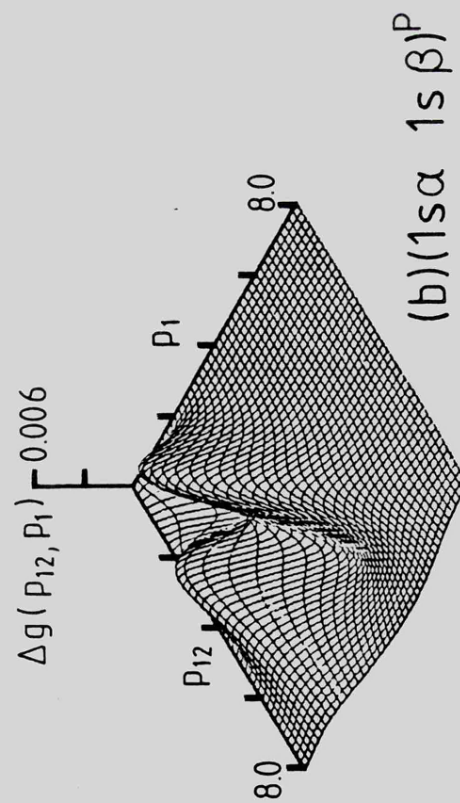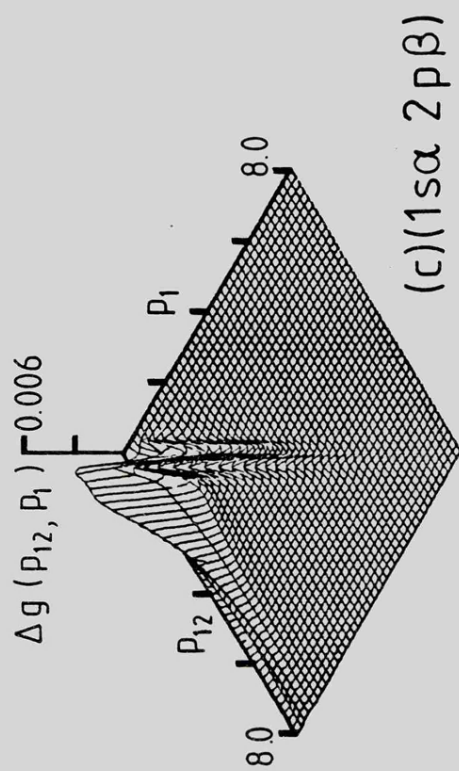
Figure (III.1.27)

An alternative view of the $\Delta g(p_{12}, p_1)$ surfaces presented in Figure (III.1.26).

Figure (III.1.28)

(see over)

<u>Figure (III.1.28)</u>

The $g^{HF}(p_{12}, p_1; \theta_1)$ distributions for the intershell electron pairs in the 2^2P state of Li.

$\theta_1 = 0°$

$\theta_1 = 30°$

$\theta_1 = 60°$

$\theta_1 = 90°$

(a) (1sα 2pα)　　　(b) (1sβ 2pα)
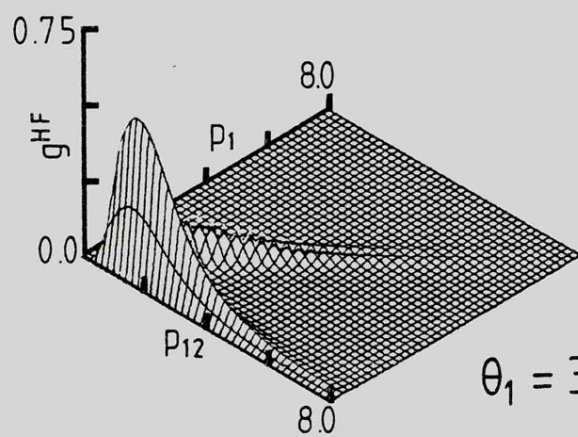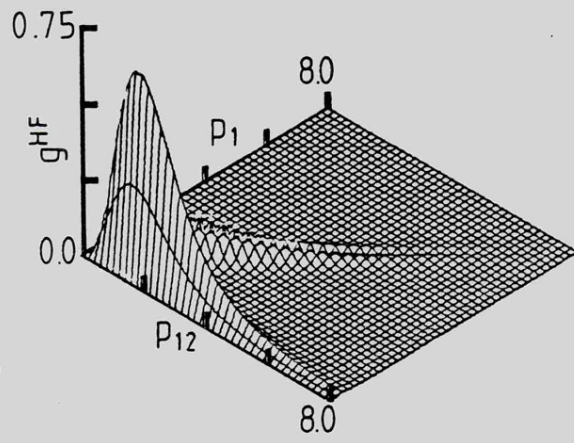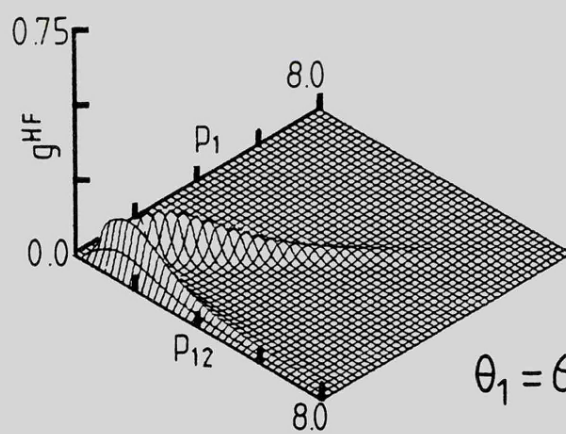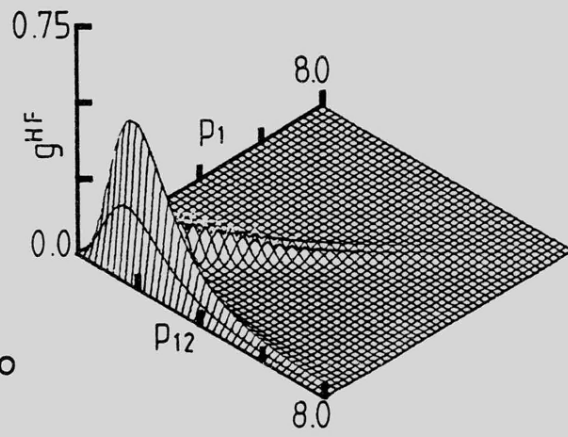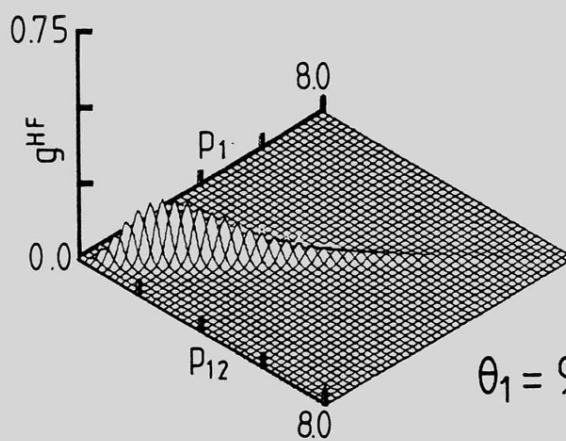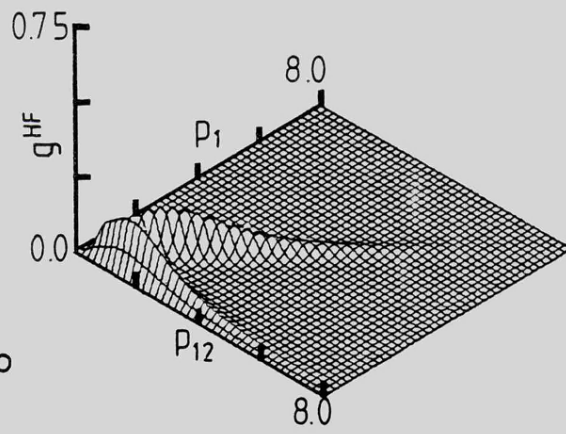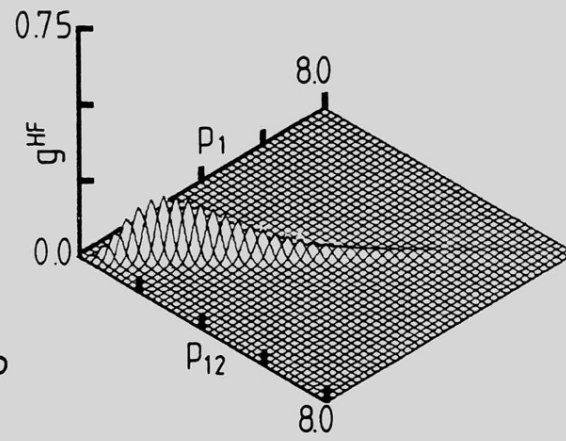
<u>Figure (III.1.29)</u>

(see over)

<u>Figure (III.1.29)</u>

An alternative view of the $g^{HF}(p_{12}, p_1; \theta_1)$ surfaces

presented in Figure (III.1.28).

$\theta_1 = 0°$

$\theta_1 = 30°$

$\theta_1 = 60°$

$\theta_1 = 90°$

(a) (1sα 2pα)　　　　(b) (1sβ 2pα)
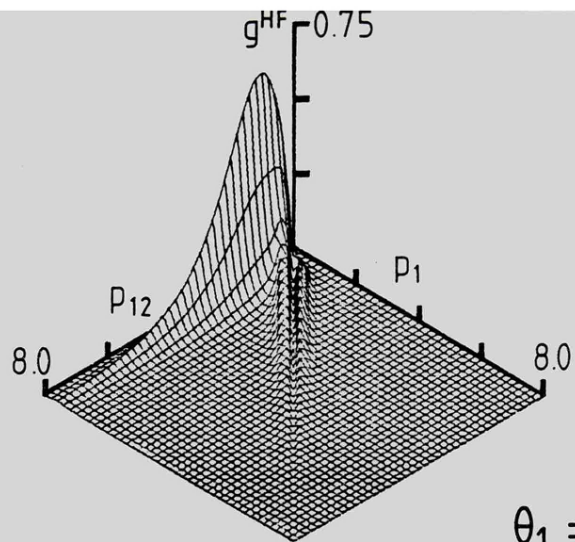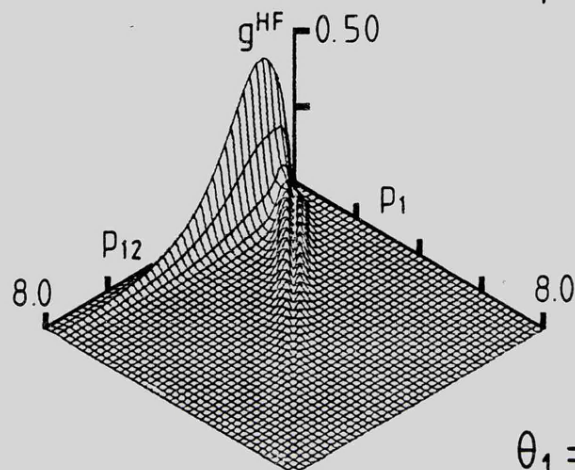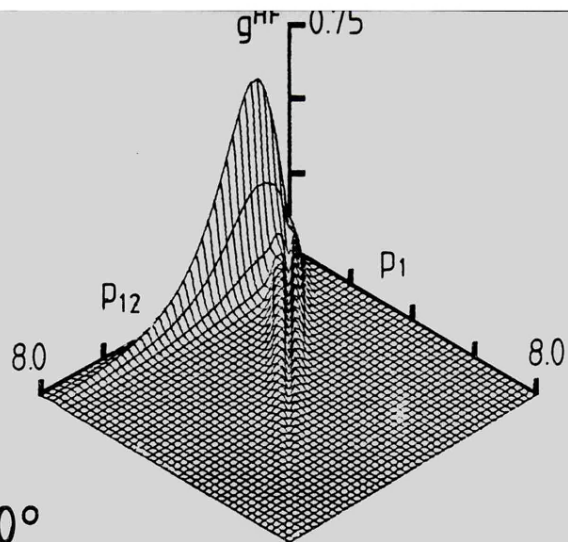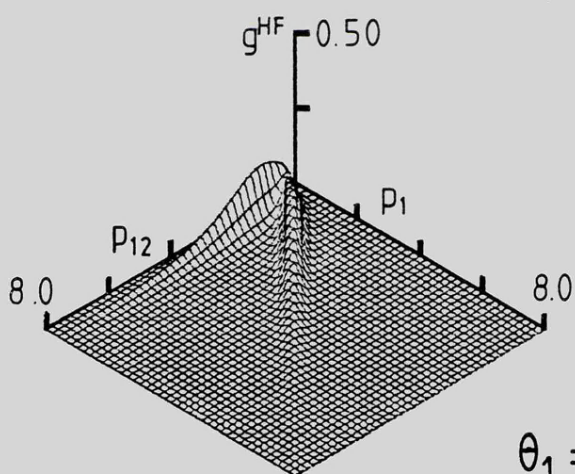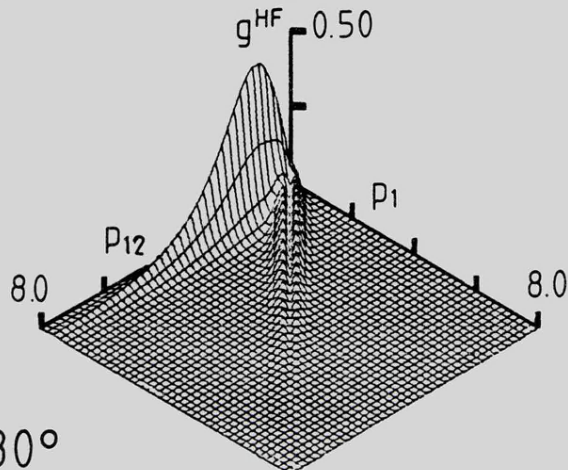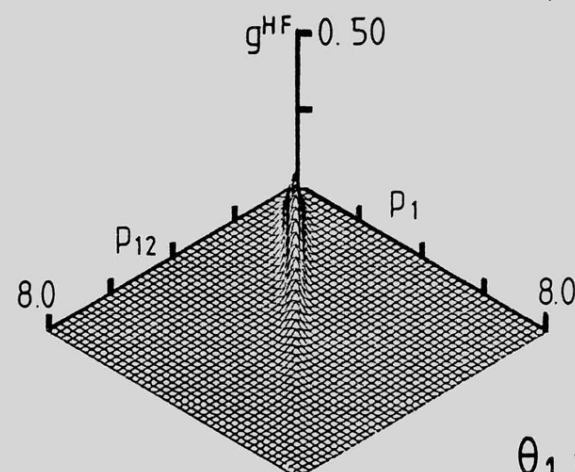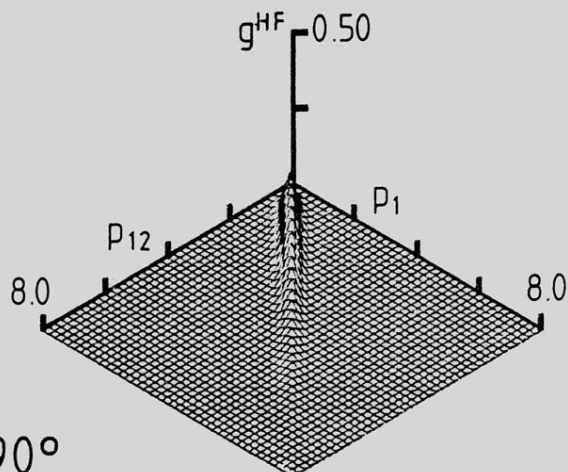
Figure (III.1.30)

(see over)

<u>Figure (III.1.30)</u>

The partial Coulomb shifts $\Delta g(p_{12}, p_1; \theta_1)$ for the intershell electron pairs in the 2^2P state of Li.

$\theta_1 = 0°$

$\theta_1 = 30°$

$\theta_1 = 60°$

$\theta_1 = 90°$

(a) (1sα 2pα)

(b) (1sβ 2pα)
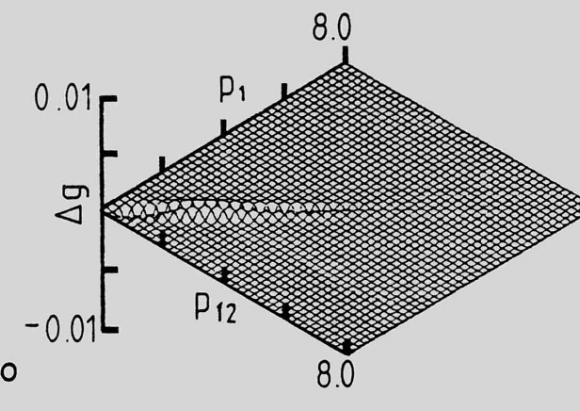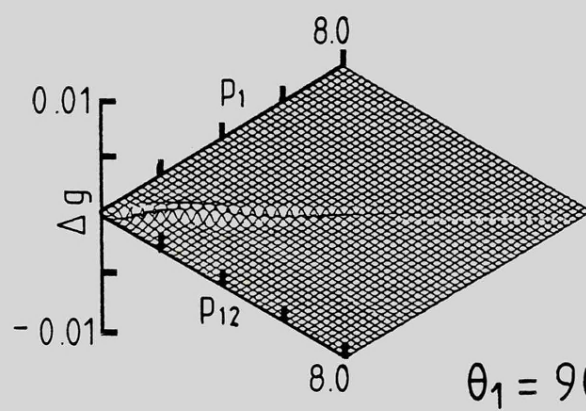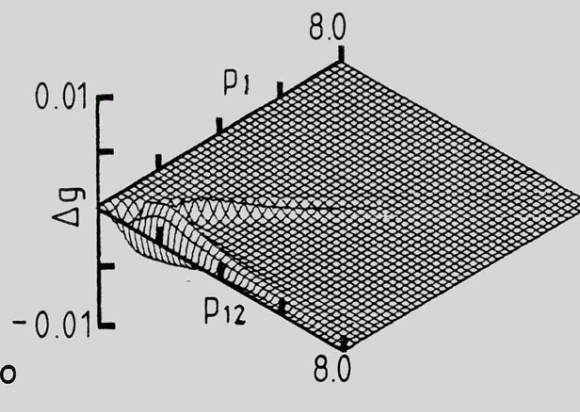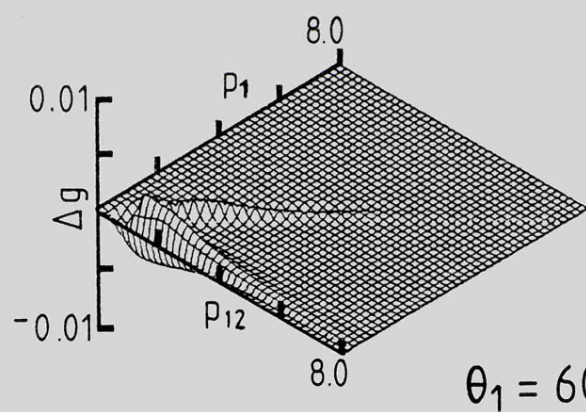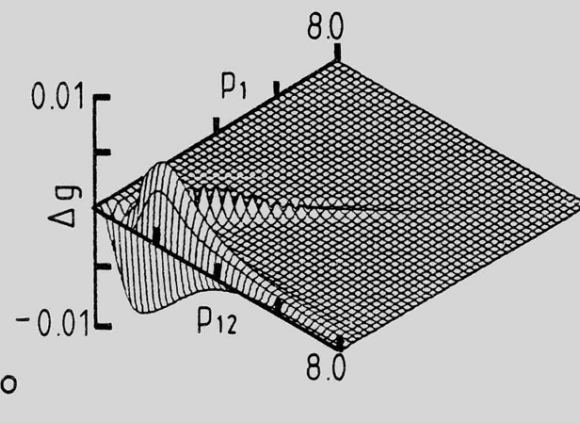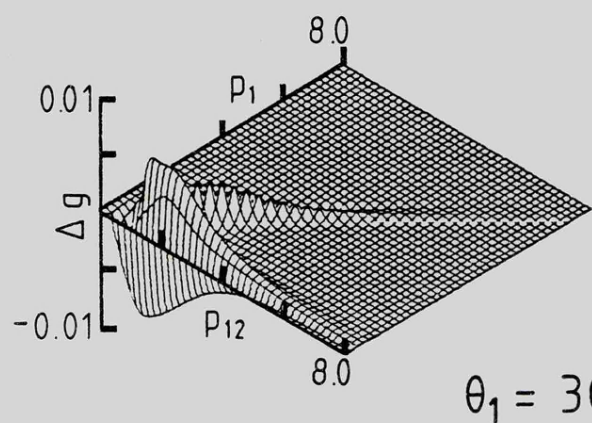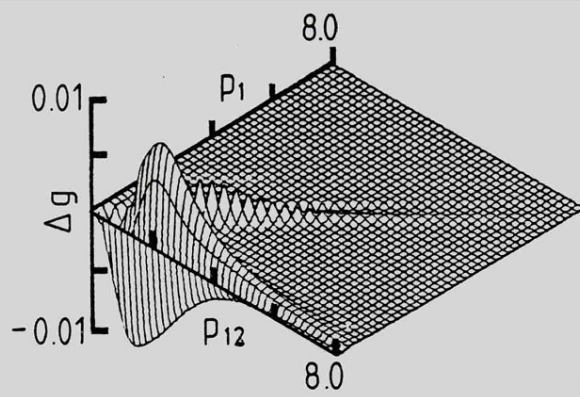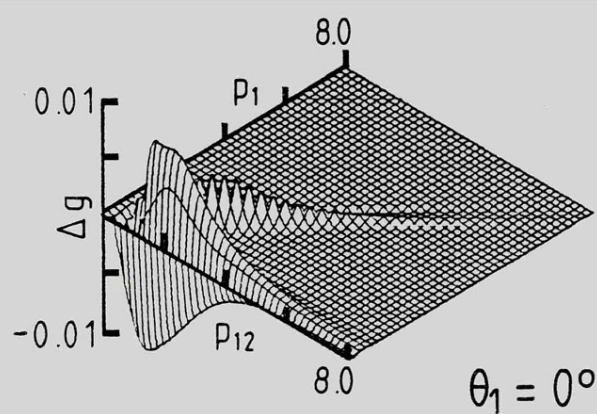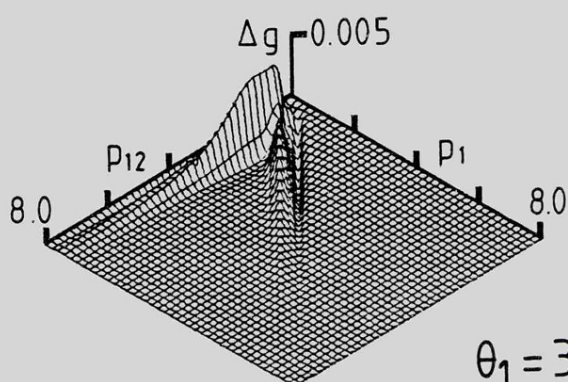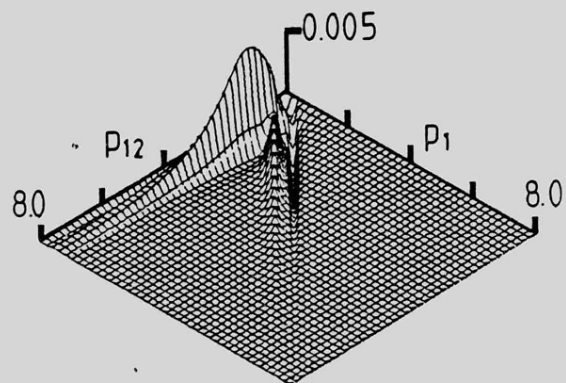
Figure (III.1.31)

(see over)

Figure (III.1.31)

An alternative view of the $\Delta g(p_{12}, p_1; \theta_1)$ surfaces presented in Figure (III.1.30).
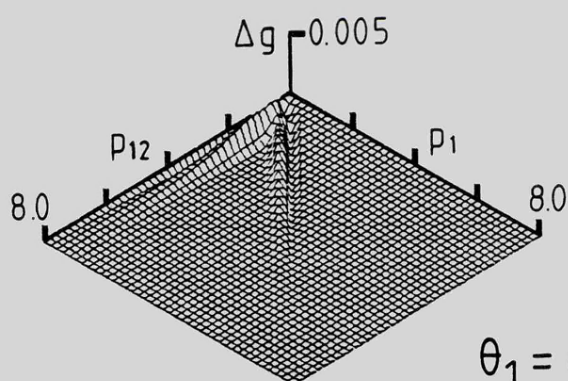
$\theta_1 = 0°$

$\theta_1 = 30°$
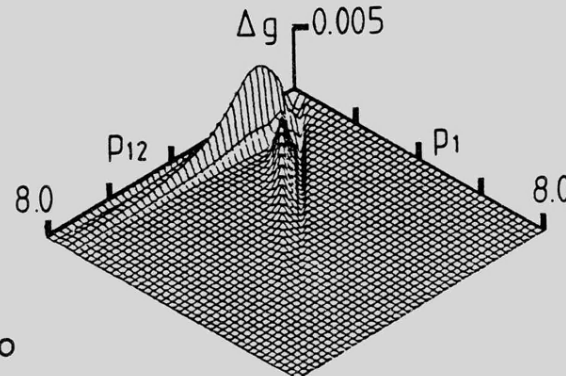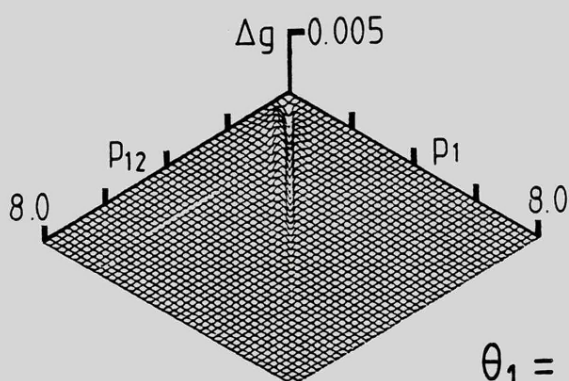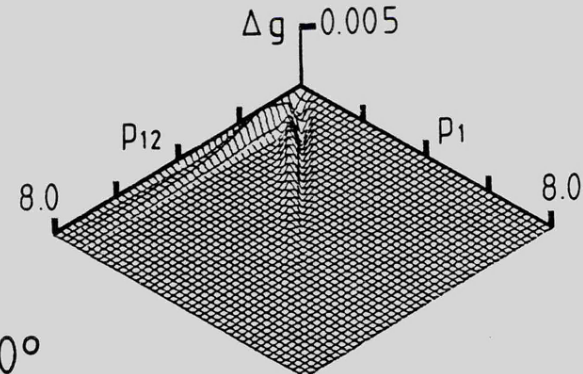
$\theta_1 = 60°$

$\theta_1 = 90°$

(a) (1sα 2pα)

(b) (1sβ 2pα)
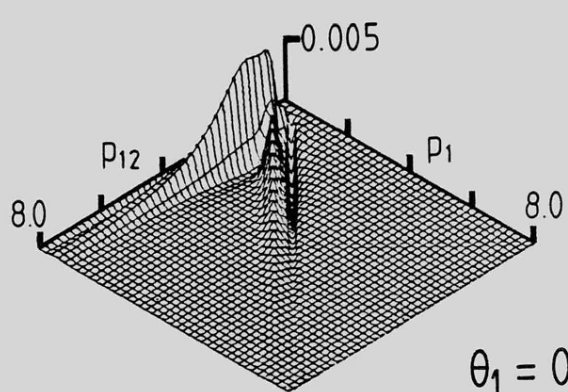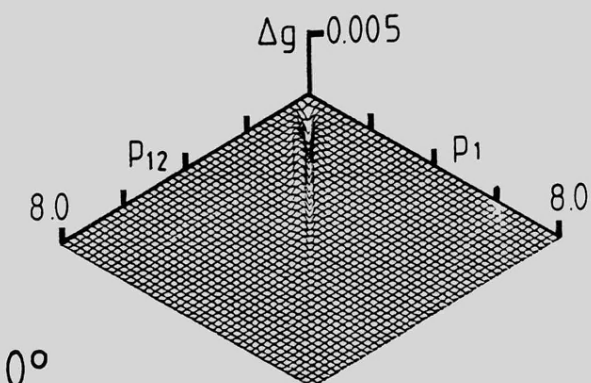
SHELL		Ψ	$\langle p_1^{-2} \rangle$	$\langle p_1^{-1} \rangle$	$\langle p_1 \rangle$	$\langle p_1^2 \rangle$	$\sigma(p_1)$
2^2S	(1sα 1sβ)	CI	0.76336^0	0.65710^0	0.22461^1	0.72288^1	0.14778^1
		HF	0.76439^0	0.65712^0	0.22460^1	0.72238^1	0.14762^1
	(1sα 2sα)	CI	0.12621^2	0.22453^1	0.13332^1	0.38365^1	0.14349^1
		HF	0.12826^2	0.22612^1	0.13298^1	0.38206^1	0.14326^1
	(1sβ 2sα)	CI	0.12620^2	0.22455^1	0.13309^1	0.38215^1	0.14319^1
		HF	0.12826^2	0.22612^1	0.13298^1	0.38206^1	0.14326^1
	TOTAL	CI	0.86681^1	0.17160^1	0.16367^1	0.49623^1	0.14482^1
		HF	0.88055^1	0.17265^1	0.16352^1	0.49550^1	0.14471^1
2^2P	(1sα 1sβ)	CI	0.76384^0	0.65729^0	0.22463^1	0.72323^1	0.14787^1
		HF	0.76422^0	0.65742^0	0.22456^1	0.72237^1	0.14768^1
	(1sα 2pα)	CI	0.46656^1	0.16284^1	0.13603^1	0.37518^1	0.13789^1
		HF	0.47340^1	0.16363^1	0.13605^1	0.37529^1	0.13791^1
	(1sβ 2pα)	CI	0.46617^1	0.16272^1	0.13626^1	0.37629^1	0.13807^1
		HF	0.47340^1	0.16363^1	0.13605^1	0.37529^1	0.13791^1
	TOTAL	CI	0.33637^1	0.13043^1	0.16564^1	0.49157^1	0.14128^1
		HF	0.34107^1	0.13100^1	0.16555^1	0.49098^1	0.14117^1

Table (III.1.1)

The one-particle radial expectation values $\langle p_1^n \rangle$ and the standard deviation, $\sigma(p_1)$, for the 2^2S and 2^2P states of Li. The superscripts denote the power of ten by which each entry is to be multiplied.

Shell		Ψ	$\langle p_1^{-2} p_2^{-2} \rangle$	$\langle p_1^{-1} p_2^{-1} \rangle$	$\langle p_1 p_2 \rangle$	$\langle p_1^2 p_2^2 \rangle$
2^2S	$(1s\alpha\ 1s\beta)$	CI	0.58208^0	0.42599^0	0.49152^1	0.46063^2
		HF	0.58430^0	0.43181^0	0.50447^1	0.52184^2
	$(1s\alpha\ 2s\alpha)$	CI	0.11754^2	0.22827^1	0.78950^0	0.10879^1
		HF	0.12011^2	0.23057^1	0.78041^0	0.10708^1
	$(1s\beta\ 2s\alpha)$	CI	0.18607^2	0.25182^1	0.93345^0	0.29108^1
		HF	0.19024^2	0.25400^1	0.92897^0	0.30163^1
	TOTAL	CI	0.10314^2	0.17423^1	0.22127^1	0.16687^2
		HF	0.10540^2	0.17592^1	0.22514^1	0.18757^2
2^2P	$(1s\alpha\ 1s\beta)$	CI	0.53806^0	0.42260^0	0.49064^1	0.45888^2
		HF	0.58403^0	0.43220^0	0.50429^1	0.52183^2
	$(1s\alpha\ 2p\alpha)$	CI	0.65100^1	0.17069^1	0.10661^1	0.20058^1
		HF	0.66517^1	0.17193^1	0.10675^1	0.20378^1
	$(1s\beta\ 2p\alpha)$	CI	0.64901^1	0.17037^1	0.10706^1	0.20371^1
		HF	0.66517^1	0.17193^1	0.10675^1	0.20378^1
	TOTAL	CI	0.45127^1	0.12777^1	0.23477^1	0.16644^2
		HF	0.46291^1	0.12903^1	0.23926^1	0.18753^2

<u>Table (III.1.2)</u>

The two-particle radial expectation values $\langle p_1^n p_2^n \rangle$ for the 2^2S and 2^2P states of Li. The superscripts denote the power of ten by which each entry is to be multiplied.

Shell	Ψ	$\langle \underline{p}_1 \cdot \underline{p}_2 / p_1^2 p_2^2 \rangle$	$\langle \cos\gamma \rangle$	$\langle \underline{p}_1 \cdot \underline{p}_2 \rangle$	$\langle \gamma \rangle (^\circ)$
2^2S					
(1sα 1sβ)	CI	0.82779^{-2}	0.37721^{-1}	0.31598^{0}	87.838
	HF	0.0	0.0	0.0	90.000
(1sα 2sα)	CI	0.75108^{-2}	0.57920^{-2}	0.59736^{-2}	89.668
	HF	0.0	0.0	0.0	90.000
(1sβ 2sα)	CI	0.82630^{-2}	0.42097^{-2}	0.57793^{-2}	89.759
	HF	0.0	0.0	0.0	90.000
TOTAL	CI	0.80172^{-2}	0.15908^{-1}	0.10924^{0}	89.088
	HF	0.0	0.0	0.0	90.000
2^2P					
(1sα 1sβ)	CI	0.75891^{-2}	0.36897^{-1}	0.31403^{0}	87.885
	HF	0.0	0.0	0.0	90.000
(1sα 2pα)	CI	-0.17687^{0}	-0.61741^{-1}	-0.47157^{-1}	93.540
	HF	-0.17111^{0}	-0.56824^{-1}	-0.41880^{-1}	93.258
(1sβ 2pα)	CI	-0.61787^{-2}	-0.39261^{-2}	-0.38280^{-2}	90.225
	HF	0.0	0.0	0.0	90.000
TOTAL	CI	-0.58487^{-1}	-0.95900^{-2}	0.87682^{-1}	90.550
	HF	-0.57037^{-1}	-0.18941^{-1}	-0.13960^{-1}	91.086

Table (III.1.3)

Values of $\langle \underline{p}_1 \cdot \underline{p}_2 / p_1^n p_2^n \rangle$ for $n = 2$, 1 and 0, and $\langle \gamma \rangle$, the average angle between the momentum vectors for the 2^2S and 2^2P states of Li. The superscripts denote the power of ten by which each entry is to be multiplied.

Shell	Ψ	$\langle p_{12}^{-1}\rangle$	$\langle p_{12}\rangle$	$\langle p_{12}^{2}\rangle$	$\sigma(p_{12})$	$Y(\%)$
2^2S						
(1sα 1sβ)	CI	0.42814^{0}	0.32384^{1}	0.13804^{2}	0.18212^{1}	1.13
	HF	0.42559^{0}	0.32923^{1}	0.14423^{2}	0.18931^{1}	–
(1sα 2sα)	CI	0.57493^{0}	0.23511^{1}	0.75820^{1}	0.14333^{1}	0.91
	HF	0.57528^{0}	0.23490^{1}	0.75632^{1}	0.14302^{1}	–
(1sβ 2sα)	CI	0.63398^{0}	0.23137^{1}	0.75387^{1}	0.14783^{1}	0.16
	HF	0.63378^{0}	0.23156^{1}	0.75553^{1}	0.14810^{1}	–
TOTAL	CI	0.54568^{0}	0.26344^{1}	0.96416^{1}	0.15776^{1}	0.36
	HF	0.54388^{0}	0.26523^{1}	0.98472^{1}	0.16014^{1}	–
2^2P						
(1sα 1sβ)	CI	0.42720^{0}	0.32322^{1}	0.13598^{2}	0.17751^{1}	1.24
	HF	0.42594^{0}	0.32825^{1}	0.14192^{2}	0.18486^{1}	–
(1sα 2pα)	CI	0.59032^{0}	0.23336^{1}	0.75223^{1}	0.14410^{1}	0.10
	HF	0.59130^{0}	0.23318^{1}	0.75102^{1}	0.14398^{1}	–
(1sβ 2pα)	CI	0.62917^{0}	0.23079^{1}	0.74578^{1}	0.14599^{1}	0.19
	HF	0.63149^{0}	0.23028^{1}	0.74267^{1}	0.14573^{1}	–
TOTAL	CI	0.54890^{0}	0.26246^{1}	0.95260^{1}	0.15587^{1}	0.48
	HF	0.54958^{0}	0.26390^{1}	0.97096^{1}	0.15819^{1}	–

Table (III.1.4)

The interparticle expectation values $\langle p_{12}^{n}\rangle$, the standard deviation, $\sigma(p_{12})$, and the fraction, Y, of probability redistributed due to correlation, for the 2^2S and 2^2P states of lithium. The superscripts denote the power of ten by which each entry is to be multiplied.

REFERENCES - SECTION (III)

REFERENCES - SECTION (III)

1) R. Daudel, R. LeFebvre and C. Moser, 'Quantum Chemistry', Interscience Publishers : New York (1959)

2) C.A. Coulson and A.H. Neilson, Proc. Phys. Soc. (London) 78 831 (1961)   *

3) a) A.C. Hurley, J. Lennard-Jones and J.A. Pople, Proc. Roy. Soc. (London) A220 446 (1953)

   b) W.J. Hunt, P.J.Hay and W.A. Goddard, J. Chem. Phys. 57 738 (1972)

   c) V.A. Nicely and J.F. Harrison, J. Chem. Phys. 54 4363 (1971)

   d) R.J. Blint and W.A. Goddard, J. Chem. Phys. 57 5296 (1972)

   e) I. Røeggen, Int. J. Quantum Chem. 19 319 (1981)

   f) I. Røeggen, Int. J. Quantum Chem. 20 817 (1981)

4) H. Shull, J. Chem. Phys. 30 1405 (1959)

5) T. Arai, J. Chem. Phys. 33 95 (1960)

6) P.-O. Löwdin, J. Chem. Phys. 35 78 (1961)

7) a) P.G. Lykos and R.G. Parr, J. Chem. Phys. 24 1166 (1956)

   b) J.M. Parks and R.G. Parr, J. Chem. Phys. 28 335 (1958)

   c) R. McWeeny, Proc. Roy. Soc. (London) A253 242 (1959)

8) K.A. Brueckner and J.L. Gammel, Phys. Rev. 109 1023 (1958)

9) See, for example,

   a) K.A. Brueckner, in 'The Many-Body Problem; Grenoble Université, Ecole d'été de physique theorique, Les Houches', John Wiley and Sons : New York (1959)

   or

   b) D.J. Thouless, 'The Quantum Mechanics of Many-Body Systems', Academic Press : New York and London, 2'nd Edition (1972)

10) H.A. Bethe, Phys. Rev. 103 1353 (1956)

11) See, for example, M. Gell-Mann and K.A. Brueckner, Phys. Rev. 106 364 (1957)

12) O. Sinanoglu, Proc. Natl. Acad. Sci. U.S.A. <u>47</u> 1217 (1961)

13) For a general review of MET applied to electron correlation, see O. Sinanoglu and K.A. Brueckner, 'Three Approaches to Electron Correlation in Atoms', Yale University : New Haven (1970)

14) O. Sinanoglu, Rev. Mod. Phys. <u>35</u> 517 (1963)

15) O. Sinanoglu, J. Chem. Phys. <u>36</u> 706 (1962)

16) J. Goldstone, Proc. Roy. Soc. (London) <u>A239</u> 267 (1957)

17) See, for example, T.L. Hill, 'Statistical Mechanics: Principles and Selected Applications', McGraw-Hill Book Company Ltd. : New York (1956)

18) O. Sinanoglu, Adv. in Chem. Phys. <u>6</u> 315 (1964)

19) See, for example, J.P. Lowe, 'Quantum Chemistry', Academic Press : New York (1978)

20) O. Sinanoglu and D.F. Tuan, J. Chem. Phys. <u>38</u> 1740 (1963)

21) R.E. Stanton, J. Chem. Phys. <u>42</u> 2353 (1965)

22) G.K. Taylor and K.E. Banyard, Phys. Rev. <u>8A</u> 1157 (1973)

23) K.E. Banyard and G.K. Taylor, Phys. Rev. <u>10A</u> 1972 (1974)

24) A.W. Weiss, Phys. Rev. <u>122</u> 1826 (1961)

25) K.E. Banyard and M.M. Mashat, J. Chem. Phys. <u>67</u> 1505 (1977)

26) R.J. Boyd and J. Katriel, Int. J. Quant. Chem. <u>8</u> 255 (1974)

27) K.E. Banyard and R.J.Mobbs, J. Chem. Phys. <u>75</u> 3433 (1981)

28) R.J. Mobbs and K.E. Banyard, J. Chem. Phys. <u>78</u> 6106 (1983)

29) K.H. Al-Bayati, Ph.D. Thesis, 'Electron Correlation in the $(1s^2 2s)$ ^2S and $(1s^2 2p)$ ^2P States of the Lithium Isoelectronic Sequence in Position and Momentum Space', University of Leicester, 1984

30) See, for example, I.N. Levine, 'Quantum Chemistry', Allyn and Bacon, Inc. : Boston (1976)

31) P.A.M. Dirac, 'The Principles of Quantum Mechanics', Oxford University Press : Oxford, 4'th edition (1958)

32) A.W. Weiss, Astrophys. J. <u>138</u> 1262 (1963)

33) C.E. Reed, Ph.D. Thesis, 'Properties of Electron Momentum Distributions: A Study Of Correlation Effects in Some Two-Electron Systems and an Examination of Directional Compton Profiles for the Lithium Halides', University of Leicester (1980)

34) a) R.J. Boyd, Chem. Phys. Lett. <u>44</u> 363 (1976)

   b) A. Gupta and R.J. Boyd, J. Chem. Phys. <u>68</u> 1951 (1977)

35) J.C. Moore, Ph.D. Thesis, 'Electron Capture From Hydrogen Negative Ions and a Study of Electron Correlation in Momentum Space', University of Leicester (1978)